

Peripherally Functionalized Silane and Siloxane Scaffolds for the Assembly of Multi-Metallic Cages, Clusters and Supramolecules

A Thesis

Submitted in Partial Fulfilment of the Requirements

For the Degree of

Doctor of Philosophy

By

Mahesh S Deshmukh

ID: 20123157



Department of Chemistry

Indian Institute of Science Education and Research, Pune

2018

Dedicated to

Aai and Nana (my parents)
&
Lovely Two Brothers...



भारतीय विज्ञान शिक्षा एवं अनुसंधान संस्थान, पुणे

INDIAN INSTITUTE OF SCIENCE EDUCATION AND RESEARCH (IISER), PUNE

(An Autonomous Institution, Ministry of Human Resource Development, Govt. of India)

Dr. Homi Bhabha Road, Pune 411008.

Dr. R. Boomi Shankar

Associate Professor

Department of Chemistry,

IISER Pune

CERTIFICATE

Certified that the work incorporated in the thesis entitled “***Peripherally Functionalized Silane and Siloxane Scaffolds for the Assembly of Multi-Metallic Cages, Clusters and Supramolecules***” submitted by **Mr. Mahesh Sadashiv Deshmukh** was carried out by the candidate, under my supervision. The work presented here or any part of it has not been included in any other thesis submitted previously for the award of any degree or diploma from any other university or institution.

Date:

Place: Pune

Dr. R. Boomi Shankar

(Research Supervisor)



भारतीय विज्ञान शिक्षा एवं अनुसंधान संस्थान, पुणे

INDIAN INSTITUTE OF SCIENCE EDUCATION AND RESEARCH (IISER), PUNE

(An Autonomous Institution, Ministry of Human Resource Development, Govt. of India)

Dr. Homi Bhabha Road, Pune 411008.

DECLARATION

I declare that, this written submission represents my ideas in my own words and where other's ideas have been included; I have adequately cited and referenced the original sources. I also declare that I have adhered to all principles of academic honesty and integrity and have not misrepresented or fabricated or falsified any idea/data/fact/ source in my submission. I understand that violation of the above will be cause for disciplinary action by the Institute and can also evoke penal action from the sources which have thus not been properly cited or from whom proper permission has not been taken when needed.

Date:

Mr. Mahesh Sadashiv Deshmukh

Place: Pune

ID: 20123157

Acknowledgements

I would like to express my sincere gratitude to my thesis supervisor Dr. R. Boomi Shankar for his continuous support, guidance, motivation and immense knowledge during my six year tenure of Doctoral Research work. I am very thankful to him for believing in my abilities and always stood behind me in my failures and successes and helped me to achieve the goals. I revere his lessons on independent thinking, perfection of soft skills and many more in shaping up the researcher in me. Additionally, I acknowledge him for the training related to preparing and delivering the scientific presentation.

I am very thankful to Prof. K. N. Ganesh (Former Director, IISER-Pune) and Prof. Jayant B. Udgaonkar (Director, IISER-Pune) for providing excellent research facilities and an outstanding research ambiance. It is my privilege to be a part of Indian Institute of Science Education and Research (IISER), Pune.

I would like to acknowledge my sincere gratitude to my Research Advisory Committee (RAC) members Dr. Shabana Khan (IISER Pune) and Dr. Benudhar Punji (NCL-Pune) for their intellectual support, encouragement and valuable suggestions.

I would like to thank Prof. Avinash S. Kumbhar and Mr. Vishavanath Mane (SPPU Pune) for helping me with the water splitting experiments on my samples and valuable suggestions to improve the quality of my research work. I would like to thank Dr. Arun Venkatanathan and his student Mr. Rakesh Pant for their valuable suggestion and help in the TD-DFT calculations. I am also grateful to the Prof. Davide. M. Proserpio and Dr. Pavel N. Zolotarev (SCTMS), Samara University, Russia for their valuable suggestions and help in the analysis of topology of my compounds. I am very thankful to Dr. R. Vaidhyanathan for the help in PXRD analysis as well as to perform gas adsorption studies. I also thank Mr. Amod desai for performing gas adsorption studies.

I would also like to express my sincere gratitude to all the faculty members of the Department of Chemistry, IISER-Pune for their support and making a research friendly working atmosphere. I thank Dr. Umeshreddy Kacherki (Librarian) for support through library services. I would also like to acknowledge the help from the technical staff for their

support in accessing various instruments: Ms. Archana (SCXRD), Mr. Parven Nasa (SCXRD and PXRD), Mr. Prashant Kale (PXRD), Mr. Nilesh Dumbre (PXRD and SEM), Mr. Anil & Mr. Yatish (SEM), Ms. Swati M. Dixit (MALDI-TOF and CHN analysis), Ms. Swati (HRMS), Mr. Sandeep (HRMS), Mrs. Deeplai & Mr. N. Dalvi (NMR), Mr. Mahesh Jadhav (TGA), Mr. Suresh Prajapati (UG Chemistry Lab), Mr. Ganesh Dimbar (IR). I am also thankful to the entire IT department for their support. I thank the administrative department of IISER-Pune for their support, especially Col. (Retd.) G. Raja Sekhar (Registrar, IISER-Pune), Dr. V. S. Rao, Mr. Prabhash and Mr. Mayuresh. I pay my warm acknowledgement for the support from the staff of Dean Doctoral Studies Office, specially Ms. Dipali Dalvi and Mr. Tushar.

It's my pleasure to thank all my lab members. I thank the support and help provided by my seniors Dr. Arvind K. Gupta and Dr. Anant Kumar Srivastava. I am fortunate enough to share moments with Ashok, Vijayakanth, Rajasekar, Rishabh, Atul, Sravan, Sachin, Neetu, Meghamala, Swati and Anupriya; whose friendly discussions and support made this journey joyful and memorable. I do remember the cheerful moments shared with energetic and high-spirited juniors like Arun, Indra, and Saurabh (BS-MS alumini). I also thank the project students Tarun (NISER), Suchitra (IISER, Kolkata), Navya Sree (University of Hyderabad) who worked with me although for small duration but added much to my research experience. I thank you all again for all the timely help, discussions, sharing of knowledge and research experience.

I would also like to pay my gratitude to some of the seniors from other labs specially Dr. Gopalakrishna, Dr. Santosh Gadekar, Dr. Santosh Panchal, Dr. Kiran Reddy, Dr. Sanjog Nagarkar. I thank all of my IISER colleagues and friends for their support and help.

Thanks to all my friends outside the IISER Pune, Dr. Mahavir Naykode, Dr. Sachin Patil, Dr. Sujit Chavan, Dr. Dnyaneshawer Subhedar, Dr. Abhijit Chaudhary, and Mr. Sachin chitale, Mr. Sakaram Tayade, Mr. Vishavanath Mane, Mr. Sachin Shinde for shearing the ups/down of my life for the last six years.

No words can ever convey my sense of gratitude felt for my parents (my father; Mr. Sadashiv (Nana) Deshmukh, and mother; Mrs. Ranjana (aai) Deshmukh, older brother; Mr. Ganesh (dada) Deshmukh and younger brother; Umesh Deshmukh). It is due to their unconditional

trust, timely encouragement, endless patience and unstinting sacrifice. I am able to reach to this position. I would like to thank a special person to whom I am really grateful over the time for her unconditional love and caring.

I am thankful to University Grant Commission (UGC) for my research scholarships and requisite financial support during the course of Ph.D. Furthermore, I acknowledge American Chemical Society (ACS), Royal Society of Chemistry (RSC), Elsevier Science Ltd., John Wiley & Sons, Springer etc. for publishing the research articles produced during the course of my research as well as for providing the permission and to reprint the materials under copyright.

Finally I pray to almighty God whose blessings made me to complete the research work towards my Ph.D. degree.

Mahesh Sadashiv Deshmukh

Contents

Contents	I
Synopsis	Vii
Abbreviations	Xiii
Rights and Permissions	XV
List of Publications	XVi
Chapter 1: Introduction	1-30
1.1 Design of Coordination Compounds	3
1.2 Choice of Building Units (SBUs)	4
1.3 Organic Linker (Ligand)	5
1.4 Design of Silane and Siloxane-Containing Ligands	7
1.5 Organosilicon Containing Ligands	8
1.6 Siloxane Containing Ligands	11
1.6.1 Disiloxane containing ligands	12
1.6.2 Cyclic siloxanes	14
1.6.3 Stereoisomer of cyclic siloxane	14
1.7 Synthesis of Functionalized Cyclic Siloxanes	
1.7.1 Hydrolytic condensation of silane	16
1.7.2 Peripherally functionalization of siloxanes	17
(a) Hydrosilylation reaction	18
(b) Silylative coupling reaction	20
(c) Metathesis reaction	22
(d) Heck coupling reaction	23
1.8 Outline and Objective of the Thesis	24
1.9 References	26

Chapter 2: Thermochromic and Mechnochromic Luminescence Reversal in Iso-structural 2D-Coordination Polymers Based on Cu₆I₆ Clusters	31-56
2.1 Introduction	33
2.2 Experimental Section	34
2.2.1 General remarks	34
2.2.2 Syntheses	35
2.2.3 Crystallography	37
2.2.4 Lifetime measurements	38
2.2.5 DFT calculations	39
2.3 Result and Discussion	39
2.3.1 Syntheses	39
2.3.2 Crystal structures	40
2.3.3 Photo-physical properties	43
2.3.4 DFT calculations	49
2.4 Conclusion	52
2.5 References	53
Chapter 3: Stereochemically Distinct Cyclotetrasiloxanes Containing 3-Pyridyl Moieties and Their Functional Coordination Polymer	57-80
3.1 Introduction	59
3.2 Experimental Section	60
3.2.1 General remarks	60
3.2.2 Syntheses	60
3.2.3 Crystallography	64

3.2.4	Lifetime measurements	66
3.2.5	DFT calculations	66
3.3	Result and Discussion	66
3.3.1	Syntheses and spectra	66
3.3.2	Crystal structures	71
3.3.3	Photo-physical properties	76
3.4	Conclusion	77
3.5	References	78

Chapter 4

Section A:	A 3D Coordination Network Built from $\text{Cu}^{\text{II}}_4\text{Cl}_3(\text{H}_2\text{O})_2$ Linear Clusters and Tetra-Pyridyl Tetrahedral Silane Ligands: Reversible Iodine Uptake and Friedel-Crafts Alkylation Reactions	81-100
4A.1	Introduction	83
4A.2	Experimental Section	84
4A.2.1	General remarks	84
4A.2.2	Syntheses	84
4A.2.3	Crystallography	87
4A.3	Result and Discussion	88
4A.3.1	Syntheses	88
4A.3.2	Crystal structures	89
4A.3.3	Iodine uptake studies of 10	93
4A.3.4	Catalytic activities of 10 and 11	96
4A.4	Conclusion	97
4A.5	References	98

Section B: Solvent Dependent Copper Iodide Cluster MOFs and their Utility as a Catalyst for the Ullmann Coupling Reaction	101-116
4B.1 Introduction	103
4B.2 Experimental Section	105
4B.2.1 General remarks	105
4B.2.2 Synthesis	105
4B.2.3 Crystallography	106
4B.3 Results and Discussion	107
4B.3.1 Synthesis	107
4B.3.2 Crystal structure	107
4B.3.3 Catalytic studies of 12 and 13	111
4B.4 Conclusion	112
4B.5 References	113
Chapter 5: Light-driven Hydrogen Evolution from Water by a Tripodal Silane Based $\text{Co}^{\text{II}}\text{L}^1_8$ Octahedral Cage	117-132
5.1 Introduction	119
5.2 Experimental Section	120
5.2.1 Materials and characterization	120
5.2.2 Synthesis of cage 14	120
5.2.3 Crystallography	121
5.2.4 General procedure for light driven hydrogen Evolution	121
5.2.5 Electrochemical studies	122

5.3	Result and Discussion	123
5.3.1	Syntheses	123
5.3.2	Crystal structures	123
5.3.3	Electrochemical behaviour	125
5.3.4	Electro-catalytic hydrogen Evolution	127
5.3.5	Photocatalytic activity	128
5.4	Conclusion	130
5.5	References	131
Chapter 6:	Thesis Conclusion and Future Perspectives	133-136
Appendix		137-198

Synopsis

The thesis entitled “*Peripherally Functionalized Silane and Siloxane Scaffolds for the Assembly of Multi-Metallic Cages, Clusters and Supramolecules*” describes the design and synthesis of pyridine functionalized tetrahedral silane and cyclic siloxane backbone as a ligands for the construction of functional coordination materials and studies their structure, stereochemistry and reactivity as well as exploit them for various applications such as luminescence, adsorption, catalysis etc.

Chapter 1: Introduction

This chapter provides a brief introduction about the design and synthesis of coordination materials and the role of silicon centered ligands for the construction of new or existing coordination materials with specific properties. Further, this chapter describes the overview on silane and siloxane based ligands for the development of coordination assemblies with novel architectures and topologies. It describes various synthetic protocols involved in the synthesis of functionalized cyclic siloxane apart from the hydrolytic condensation of silane compounds. Further, it gives a description of the structures of stereoisomers exhibited by the cyclic tri- and tetrasiloxanes the peripheral functionalization of cyclic siloxanes containing Si-H/Si-vinyl bonds under the conditions of Hydrosilylation, Metathesis, Silylative and Heck coupling reaction. A brief discussion about the mechanism of these reactions and the drawbacks has been explained. Finally, the outline and objectives of the present thesis has been described starting the design of silane and cyclic siloxane based ligands having N-donor metal binding sites for obtaining functional coordination materials.

Chapter 2: Thermochromic and Mechanochromic Luminescence reversal in Isostructural 2D-Coordination Polymers Based on Cu₆I₆ Clusters

Two isostructural coordination polymer materials, namely, {[MeSi(3-Py)₃]₆(Cu₆I₆)}_n (**1**) and {[MeSi(3-Qy)₃]₆(Cu₆I₆)}_n (**2**), featuring Cu₆I₆ clusters were synthesized from tridentate arylsilane ligands of the type MeSi(3-Py)₃ (3-Py = 3-pyridyl) and MeSi(3-Qy)₃ (3-Qy = 3-quinolyl), respectively. While the coordination polymer **1** displays the usual thermochromism associated with traditional Cu₄I₄Py₄ clusters, the coordination polymer **2** shows ³XLCT/³MLCT emission due to the Cu₆I₆ cluster core at both 298 and 77 K, albeit with some marginal variations in its emission wavelengths. Interestingly, an unusual reversal in the

mechanochromic luminescent behavior was observed for these isostructural coordination polymers at 298 K wherein a pronounced blue-shifted high energy emission for **1** (from orange to yellowish-orange) and a red-shifted low-energy emission for **2** (from green to orange) were obtained upon grinding these samples. This is primarily due to the variations in their cuprophilic interactions as **1** displays shorter Cu...Cu distances (2.745(1) Å) in comparison with those present in **2** (3.148(0) Å). As a result, the ground sample of **2** exhibits a prominent red shift in luminescence owing to the reduction of its Cu...Cu distances to an unknown value closer to the sum of van der Waals radii between two Cu(I) atoms (2.80 Å). However, the blue-shifted emission in **1** is presumably attributed to the rise in its lowest unoccupied molecular orbital energy levels caused by changes in the secondary packing forces. Furthermore, the absorption and emission characteristics of **1** and **2** were substantiated by time dependent density functional theory calculations on their discrete-model compounds. In addition, the syntheses, reactivity studies, and photophysical properties of two one-dimensional coordination polymers, namely, {[MeSi(3-Qy)₃]₂(Cu₂I₂)}_n (**3**) and {[MeSi(3-Qy)₃](CuI)}_n (**4**), having dimeric Cu₂I₂ and monomeric CuI moieties, respectively, were examined (Figure 1).

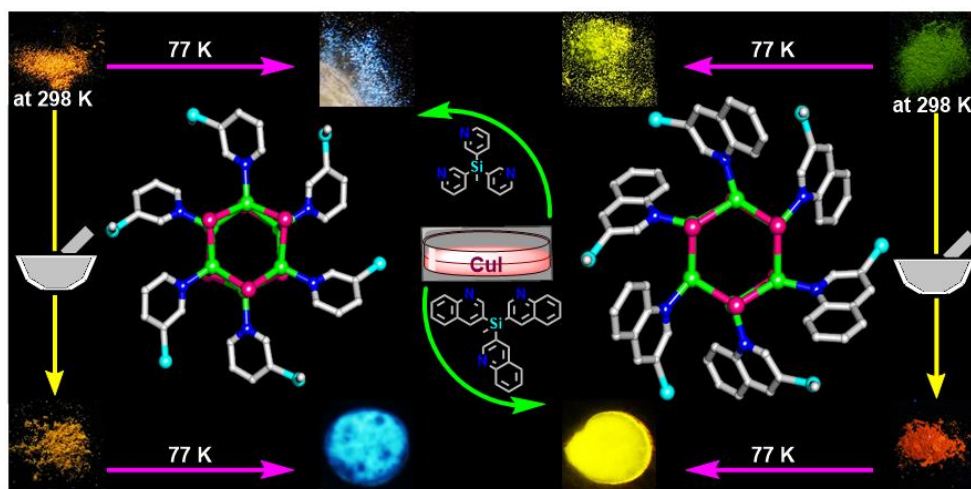


Figure 1: Thermo- and Mechano-chromic Luminescence reversal in Isostructural 2D-Coordination Polymers Based on Cu₆I₆ Clusters

Chapter 3: Stereochemically Distinct Cyclotetrasiloxanes Containing 3-Pyridyl Moieties and Their Functional Coordination Polymers

Synthesis of new cyclotetrasiloxane scaffolds containing peripherally functionalized 3-pyridyl moieties, [MeSiO(CH=CH3-Py)]₄ (L³) and [MeSiO(CH₂CH₂3-Py)]₄ (L⁴), and their reactivity studies with certain d¹⁰ metal ions are reported. The ligand L³ is obtained by the

Heck-coupling reaction of tetramethyl tetra vinyl tetrasiloxane (D_4^{vi}) and 3-bromopyridine in the presence of the Pd(0) catalysts. The as synthesized ligand L^3 shows the presence of three stereoisomers, *cis-trans-cis* (L^{3A}), *cis-cis-trans* (L^{3B}), and *all-trans* (L^{3C}), which are quantitatively separated by column chromatography. Subsequent reduction of L^{3A} , L^{3B} , and L^{3C} with triethylsilane in the presence of catalytic amounts of Pd/C leads to the formation of the ligands L^{4A} , L^{4B} , and L^{4C} with retention of stereochemistry due to the precursor moieties. Treatment of ZnI_2 with L^{3A} gives a one-dimensional coordination framework $[(L^{3A})_4(ZnI_2)_2]_\infty$, **5**. These 1D-chains are further connected by π - π stacking interactions between the pyridyl groups of the adjacent chains leading to the formation of a three-dimensional network with the topology of a **PtS** net. The reaction of silver nitrate with ligand L^{3B} gives a chain like one-dimensional cationic coordination polymer $\{[(L^{3B})_4Ag_2] \cdot 2NO_3 \cdot H_2O \cdot CH_3OH\}_\infty$, **6**, consisting of two different kinds of 32-membered macrocycles. Treatment of the *all-trans* ligand L^{4C} with copper (I) iodide salt results in the formation of a cubane-type Cu_4I_4 cluster MOF $[(L^{4C})_4Cu_4I_4]_\infty$, **7**, in a two-dimensional 4-connected uninodal **sql**/Shubnikov tetragonal plane net topology represented by the Schläfli symbol $\{4^4.6^2\}$. This MOF displays a thermochromic luminescence behavior due to Cu_4I_4 clusters showing an orange emission at 298 K and a blue emission at 77 K. The reaction of L^{3A} with $Cd(NO_3)_2 \cdot 6H_2O$ at RT gives an 2D polymeric sheet **8** of formula $\{[(L^{3A})(Cd(NO_3)_2)] \cdot THF\}_\infty$ having **sql** topology. Interestingly, treatment of L^{3A} with $Cd(NO_3)_2 \cdot 6H_2O$ and biphenyl dicarboxylate (bpdc) under solvothermal conditions gave a differed 2D-network $\{[(L^{3C})Cd_2(bpdc)_2] \cdot DMF\}_\infty$, **9**, in which a facile conversion of L^{3A} to L^{3C} has been observed (Figure 2).

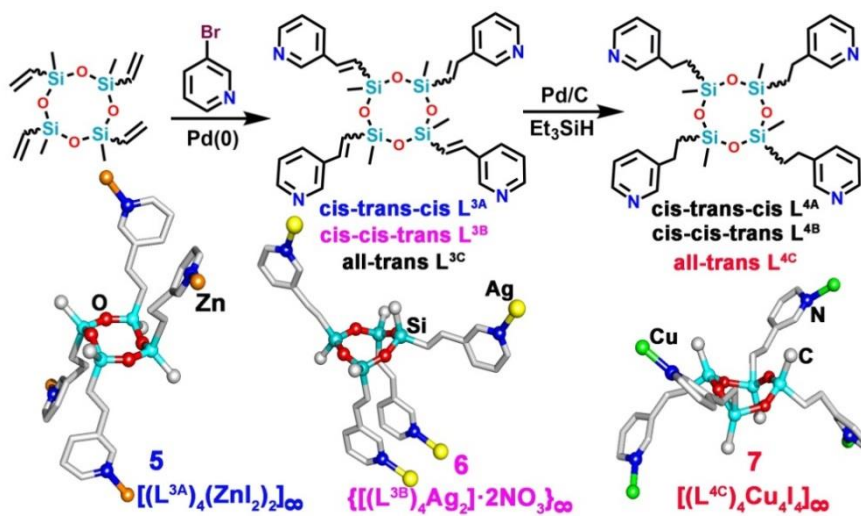


Figure 2: Stereochemically Distinct Cyclotetrasiloxanes Containing 3-Pyridyl Moieties and Their Functional Coordination Polymers

Chapter 4

Section 4A: A 3D Coordination Network Built from $\text{Cu}^{\text{II}}_4\text{Cl}_3(\text{H}_2\text{O})_2$ Linear Clusters and Tetrapyridyl Tetrahedral Silane Ligands: Reversible Iodine Uptake and Friedel–Crafts Alkylation Reactions

A novel three-dimensional coordination network **10** in a new 4,5,6-connected topology (4,5,6T115) built from linear $\text{Cu}^{\text{II}}_4\text{Cl}_3(\text{H}_2\text{O})_2$ clusters and tetrahedral tetrakis(3-pyridyl)vinylsilane ligands is reported. Utilizing a similar tetrahedral ligand, tetrakis(3-pyridyl)ethylsilane, a different framework **11** having $\text{Cu}^{\text{II}}_2\text{Cl}(\text{H}_2\text{O})_2$ clusters is obtained in **tcs** topology. The activated sample of **10** shows an excellent and reversible uptake of I_2 in solid as well as in solution phases owing to the presence of uncoordinated chloride ions and electron rich vinylic groups in it. The I_2 uptake studies on the anion-exchanged samples, of bromide, iodide, and nitrate ions, show a progressive decrease in the adsorption capacity with the sample containing uncoordinated Cl^- ion showing a maximum uptake of 48.5% and the one with the NO_3^- ions exhibiting the lowest uptake of 24.0%. These observations suggest that the halide counter ions interact better with I_2 in comparison with nitrate ions and the better I_2 uptake in the presence of Cl^- ions over the other two halides is due to its smaller size that offers a larger surface area for adsorption. Also, both these compounds were shown to be useful catalysts for the solvent-free syntheses of bis(indolyl)methanes via Friedel–Crafts alkylation reaction (Figure 3).

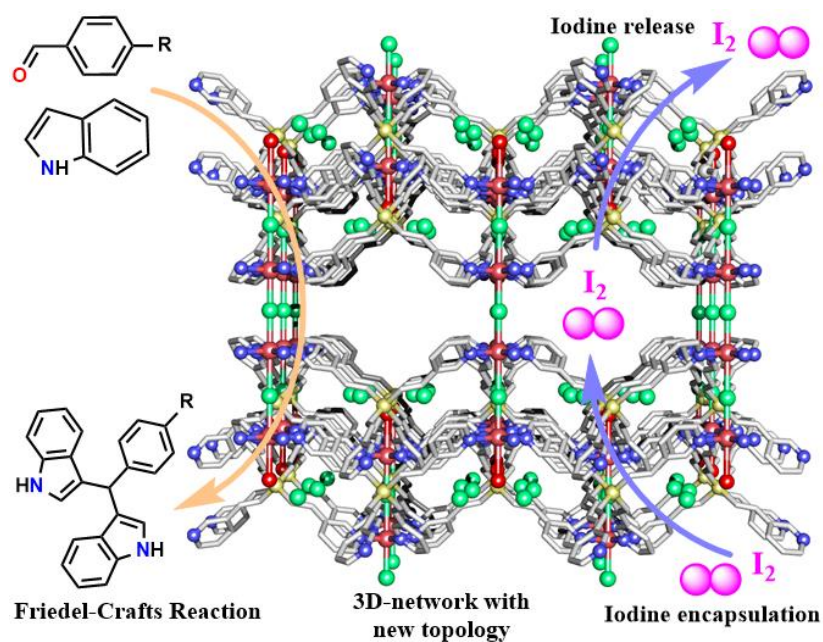


Figure 3: A 3D Coordination Network Built from $\text{Cu}^{\text{II}}_4\text{Cl}_3(\text{H}_2\text{O})_2$ Linear Clusters and Tetrapyridyl Tetrahedral Silane Ligands: Reversible Iodine Uptake and Friedel–Crafts Alkylation Reactions

Section 4B: Solvent Dependent Copper Iodide Cluster MOFs and their Utility as a Catalyst for the Ullmann Coupling Reaction

Extending the reactivity studies from the previous section, treatment of TPVS with copper (I) iodide gave two new cluster MOFs **12** {[TPVS](Cu₂I₂)} and **13**, {[TPVS](Cu₄I₄)}. The solvothermal reactions of CuI with TPVS in acetonitrile (ACN) at 90 °C gave an interpenetrated 3D-network **12** with a 4-connected uninodal **sql** topology consisting of a rhomboid shaped [Cu₂I₂] cluster which initially forms a 2D coordination network that further self-assembles into a 3D network **12** through interpenetration. However, the reaction of CuI in a solvent-mixture of acetonitrile (ACN) and tetrahydrofuran (THF) afforded a [Cu₄I₄] based 3D two fold interpenetrated MOF **13** with uninodal **sra** topology. The gas adsorption studies show that the porous nature of the MOF **12** as it adsorbs selectively CO₂ over the N₂. The CO₂ adsorption at 273 K exhibits type I behaviours with an uptake capacity of 25 cm³ g⁻¹ for the MOF **12** while the MOF **13** showed no uptake characteristics indicating its nonporous nature due to the filling of its void space by interpenetration. Both these MOFs were shown to be efficient catalysts for the Ullmann coupling reaction under slightly mild conditions comparison with certain other literature catalysts (Figure 4).

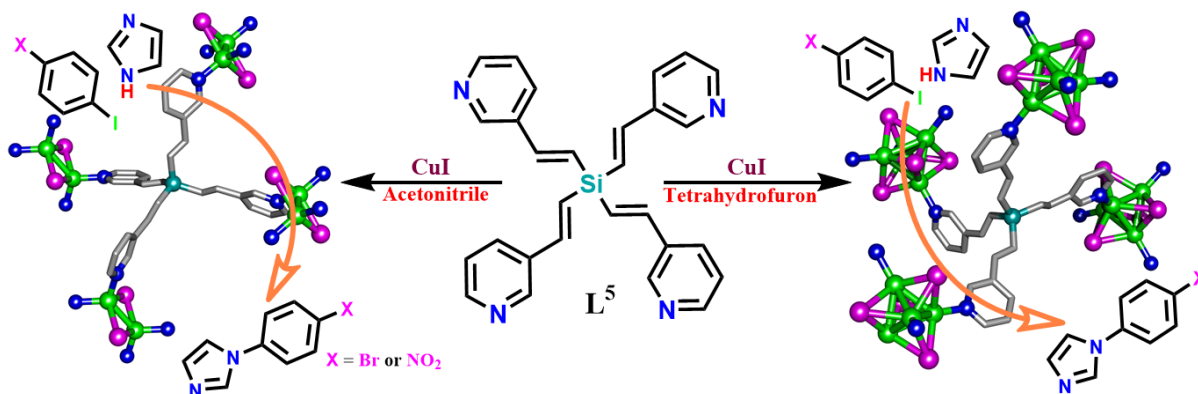


Figure 4: Solvent Dependent Copper Iodide Cluster MOFs and their Utility as a Catalyst for the Ullmann Coupling Reaction

Chapter 5: Light-driven Hydrogen Evolution from Water by a Tripodal Silane Based Co^{II}L₈¹ Octahedral Cage

Utilizing the tridentate arylsilane ligands MeSi(3-Py)₃ (described in the chapter 2), an octahedral cage assembly of composition [Co^{II}₆L₈¹Cl₆(H₂O)₆]Cl₆ has been synthesized in a single-step reaction. The electrochemical behavior of the cage in water exhibits the pH dependence of potential as well as catalytic current indicating the possible involvement of proton-coupled electron transfer in H₂ evolution. Electrocatalytic hydrogen evolution from an

aqueous buffered solution containing this cage gave a turnover frequency of 16 h^{-1} . Further, this cage assembly has been explored as a photocatalyst (blue light irradiation λ 469 nm) for the evolution of H_2 from water in the presence of $\text{Ru}(\text{bpy})_3^{2+}$ as a photosensitizer and ascorbic acid as a sacrificial electron donor. This catalytic reaction is found to be pseudo first order with a turnover frequency of 20.50 h^{-1} (Figure 5).

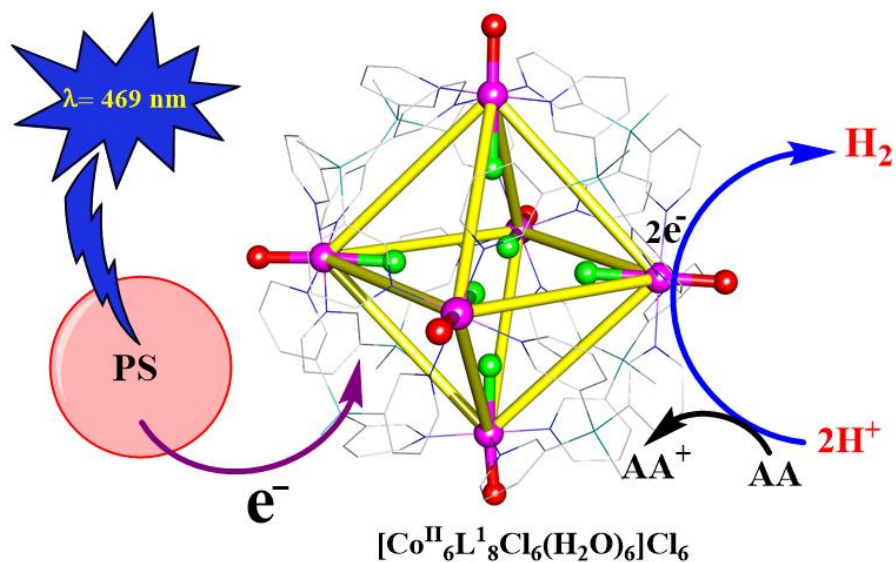


Figure 5: Light-driven Hydrogen Evolution from Water by a Tripodal Silane Based $\text{Co}^{\text{II}}_6\text{L}^1_8$ Octahedral Cage

Abbreviations

AA	Ascorbic Acid
Anal.	Analysis
bpy	2,2,bipyridine
Calcd.	Calculated
CCDC	Cambridge Crystallographic Data Center
DCM	Dichloromethane
DFT	Density Functional Theory
DMF	Dimethyl Formamide
DSC	Differential Scanning Calorimetry
ESI	Electron Spray Ionization
FTIR	Fourier Transform Infrared Spectroscopy
HRMS	High Resolution Mass Spectroscopy
LT	Low Temperature
MALDI-TOF	Matrix-Assisted Laser Desorption Ionization-Time of Flight
MeOH	Methanol
MeCN	Acetonitrile
mg	Milligram
min	Minutes
μl	Microliter
mmol	Millimoles
MOF	Metal-Organic Framework
NMR	Nuclear Magnetic Resonance
RT	Room Temperature
Py	Pyridyl
PXRD	Powder X-ray Diffraction
PS	Photosensitizer
SCXRD	Single Crystal X-ray Diffraction
TGA	Thermogravimetric Analysis
TPVS	Tetrakis-(3-pyridyl)vinylsilane
TPES	Tetrakis-(3-pyridyl)ethylsilane

Rights and Permissions

Chapter 2:

Reprinted (adapted) with permission from “*Inorg. Chem.* **2015**, *54*, 1337–1345”

© 2015 American Chemical Society

Chapter 3:

Reprinted (adapted) with permission from “*Inorg. Chem.* **2016**, *55*, 3098–3104”

© 2016 American Chemical Society

Chapter 4: Section A

Reprinted (adapted) with permission from “*Inorg. Chem.* **2017**, *56*,

11762–11767” © 2017 American Chemical Society

Chapter 5:

Reprinted (adapted) with permission from “*Inorg. Chem.* **2017**, *56*,

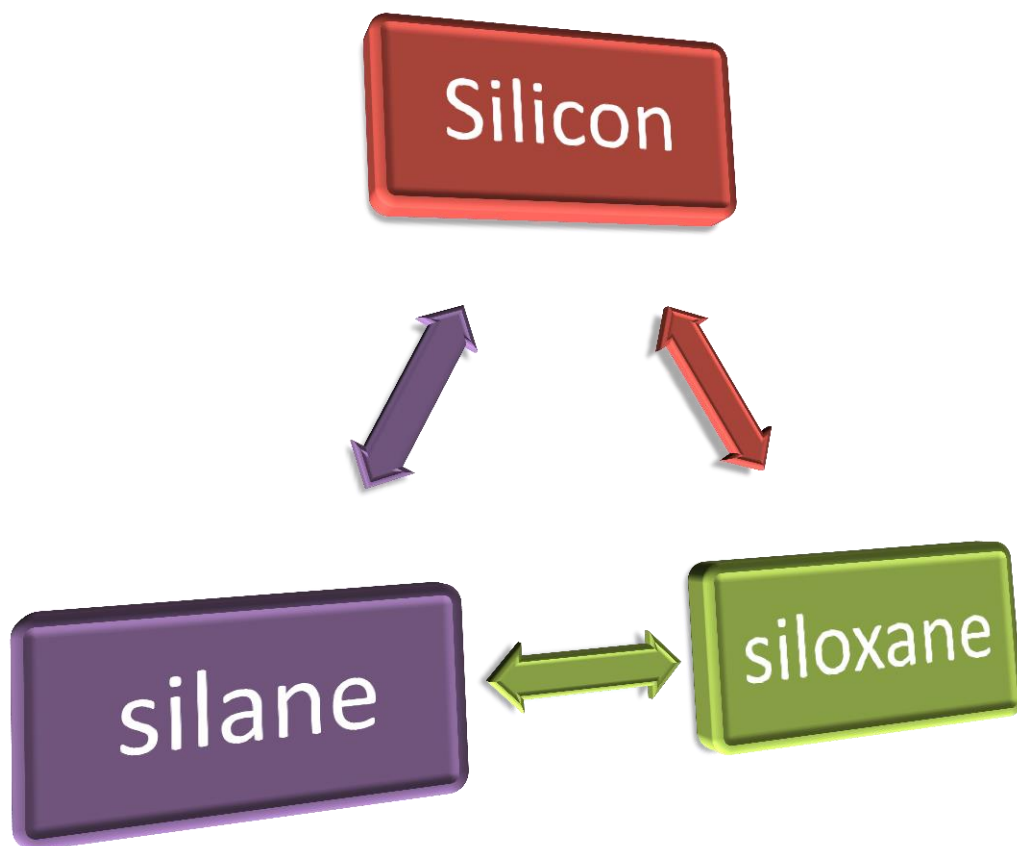
13286–13292” © 2017 American Chemical Society

Publications

1. Thermochromic and Mechanochromic Luminescence Umpolung in Isostructural Metal–Organic Frameworks Based on Cu_6I_6 Clusters
Mahesh S. Deshmukh, Ashok Yadav, Rakesh Pant, and Ramamoorthy Boomishankar
Inorg. Chem. **2015**, *50*, 1337–1345
2. Stereochemically Distinct Cyclotetrasiloxanes Containing 3-Pyridyl Moieties and their functional coordination polymers
Mahesh S. Deshmukh, T. Vijayakanth, and Ramamoorthy Boomishankar
Inorg. Chem. **2016**, *51*, 3098–3104
3. A Novel 3D Coordination Network Built from $\text{Cu}^{\text{II}}_4\text{Cl}_3(\text{H}_2\text{O})_2$ Linear Clusters and Tetra-pyridyl Tetrahedral Silane Ligand
Mahesh S. Deshmukh, Atul Chaudhary, Pavel N. Zolotarey, and Ramamoorthy Boomishankar
Inorg. Chem. **2017**, *56*, 11762–11767
4. Light-driven Hydrogen Evolution from Water by a Tripodal Silane Based $\text{Co}^{\text{II}}_6\text{L}^1_8$ Octahedral Cage
Mahesh S. Deshmukh, Vishwanath S. Mane, Avinash S. Kumbhar, and Ramamoorthy Boomishankar
Inorg. Chem. **2017**, *56*, 13286–13292
5. Solvent Dependent Copper Iodide Cluster MOFs and their Utility as a Catalyst for the Ullmann Coupling Reaction
Mahesh S. Deshmukh and Ramamoorthy Boomishankar
(Manuscript under preparation)

Chapter 1

INTRODUCTION



1.1 Design of Coordination compounds

The rational design and synthesis of functionalized coordination compounds with specific motifs have attracted considerable attention.¹⁻⁸ The motivations are not only due to their remarkable potential applications in luminescence,^{9,10} molecular separation,¹¹⁻¹³ molecular container,¹⁴ toxic materials adsorption,¹⁵ ion exchange,¹⁶ catalysis,^{17,18} molecular recognition,¹⁹ sensors²⁰ etc., but also their intriguing variety of architectures and topologies.²¹ Thus, various kinds of coordination compounds have been obtained with specific properties by careful choice of organic and inorganic units, following the pioneer work by Hoskins and Robson.²² In these coordination compounds, organic and inorganic units are linked to each other through the coordination bonds.

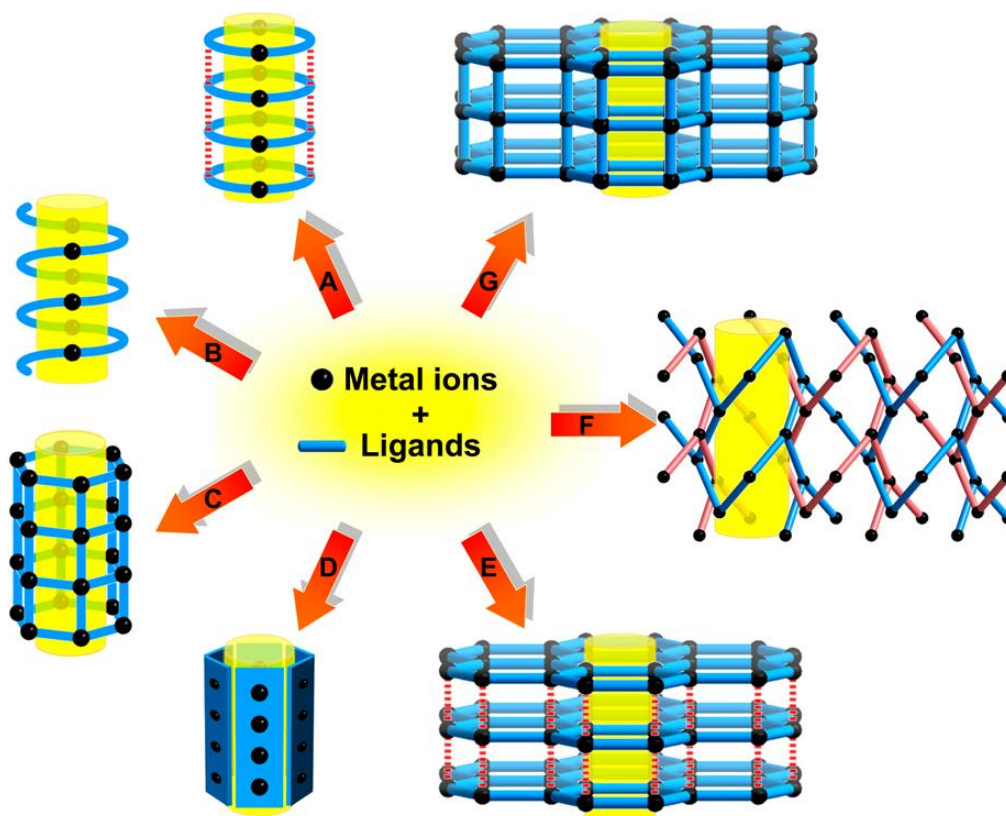


Figure 1.1: Schematic representation of construction principles of various channel architecture: (A) via columnar stacking of metal macrocycles, (B) via helical coordination polymers, (C) via 1D cylindrical coordination polymers, (D) via vertical arrays of 1D coordination polymers, (E) via stacking of 2D coordination polymers, (F) via interpenetration of wave 2D coordination polymers, and (G) via 3D coordination polymerization. (Adapted from “Jung et al. *Acc. Chem. Res.*, **2016**, *49*, 1835” with permission of the American Chemical Society)

Generally, the inorganic unit consists of metal ions or clusters which are often defined as secondary building units (SBUs)²³ whereas the organic unit, also known as ligand or linker or bridging unit, consists of carboxylates, heterocyclic (containing N, O, and S as donor atoms) compounds or other organic anions, such as sulfonate, phosphonate. Thus, it is possible to obtain coordination compounds with predetermined structure and topology by the careful design and choice of organic linkers as well as the metal ions or clusters with the fixed geometry (Figure 1.1).²⁴⁻²⁶ The nature and geometry of the metal ions along with the choice of organic linker/ligand plays a vital role to determine the structure and functional properties of the coordination compounds. However, other factors such as effect of temperature, solvent, concentration, and metal ions coordination environment can also affect the final structure of the coordination polymers.²⁷ Thus, one of the most difficult and important tasks is the design and synthesis of new tectonic linker/ligand with appropriately located binding sites for the construction of tailor-made coordination polymers.

1.2 Choice of Building Units (SBUs)

As earlier discussion, the choice and design of building units (organic and inorganic) are crucial to obtain well defined structure, topology and properties of the coordination compounds. These units act as nodes for the construct of coordination polymers. Thus, the structure and properties of the polymer can be tuned by proper selection of inorganic and organic nodes. For the construction of coordination polymers, usually, transition metal ions are used as nodes. However, almost all the metal ions di-, tri- and tetravalent, ranging from alkali metals to lanthanides have been utilized for the synthesis of coordination polymers. The coordination number of the metal ions are varied from the 2-7 depending on the metal ions and its oxidation state.² In some cases, polyatomic metal clusters have been obtained during the reaction and act as an inorganic node. The number of metal ions in the discrete cluster may vary from the 2-13 and are connected to each other in different directions via the organic linkers to form an extended networks in 1D, 2D or 3D architectures.²⁸ In addition to many metal containing SBUs, clusters based on copper iodide (CuI), such as a Cu_2I_2 rhomboid dimer, Cu_4I_4 cubane tetramer, and Cu_6I_6 hexagonal prisms are also well-known to form the building units for frameworks in presence of neutral ligands. This is due to their variety of coordination geometries for Cu(I) as well as potential bridging ability for I^- anion.³¹⁻³⁴ In some of the coordination polymers, instead of discrete metal clusters, infinite rod-like metal cluster chains connected by the organic linkers have been found. Such metal

cluster chains sometimes resemble to metal oxide nodes, as observed in certain coordination polymers having carboxylate linkers. (Figure 1.2).^{29,30}

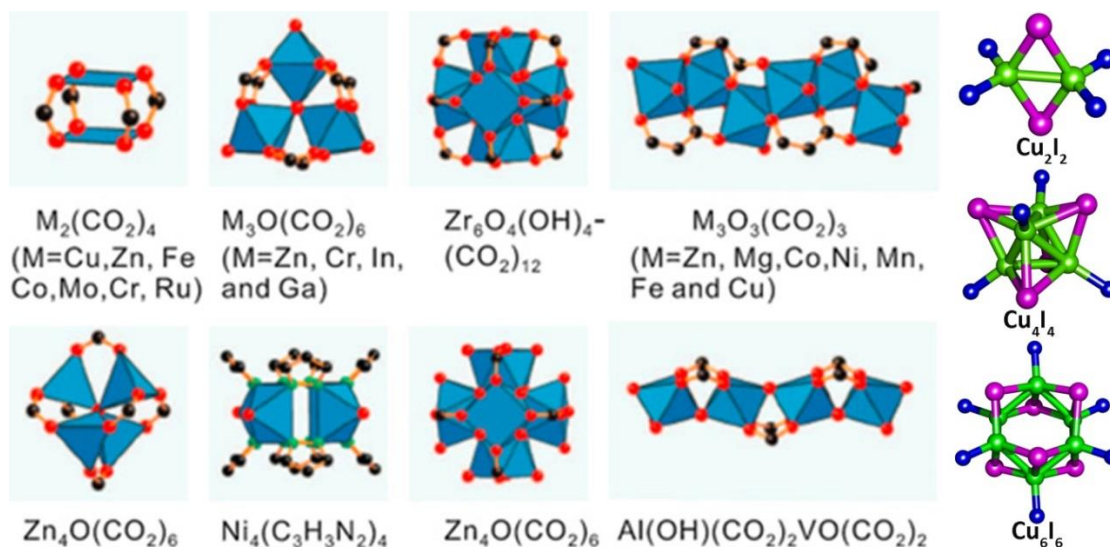


Figure 1.2: Representative examples of polyatomic Cluster/Chain present in coordination compounds (Adapted from “Wöll et al. *Coord. Chem. Rev.* **2016**, 307, 391” with permission of the Elsevier)

1.3 Organic Linker (Ligand)

The ligand is an ion or molecule that contains pendent binding groups which provides different possibilities of linkage for the inorganic nodes at regular intervals. These ligands are classified as a monodentate, bidentate or polydentate depending on the number of binding sites present on the ligand to bind the metal ions. The framework structure, stability, properties and novel topologies of the coordination compounds also depends on the angle of organic linkers.

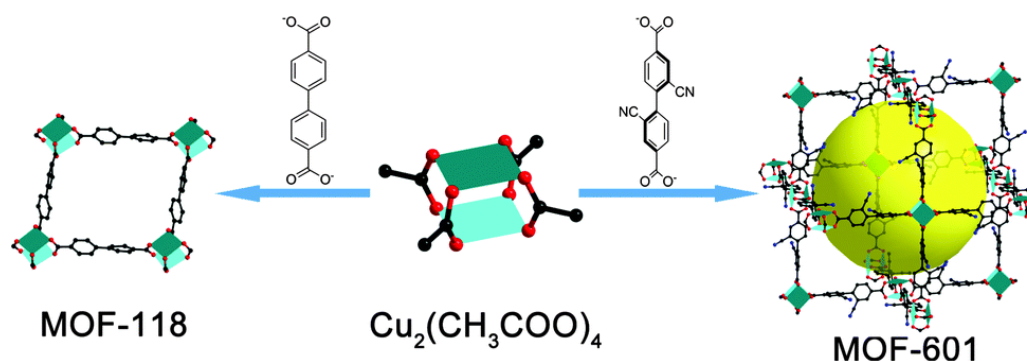


Figure 1.3: Examples of the dimensionality and topology of coordination polymer products dictated by the twisted angle of dicarboxylates (Adapted from “Zhou et al. *Chem. Soc. Rev.* **2014**, 43, 5561” with permission of the Royal Society of Chemistry)

Yaghi et al. have demonstrated that the structural dimensionality and topology of the frameworks can be tuned by utilizing the twist angle of linear carboxylate linker. For example, in the 4,4'-biphenyl dicarboxylate (*bpdc*), even though two phenyl rings are slightly twisted with respect to each other, the two carboxylate groups are orientated in an almost coplanar fashion. Thus, the reaction of *bpdc* with the copper acetate forms a 2D polymeric sheet with **sql** topology owing to the coplanar geometry of the copper acetate squares that are linked by *bpdc* ligands. However, when these copper acetate squares are linked by the substituted *bpdc* ligand 2,2'-dicyano-4,4'-biphenyl dicarboxylate (*cnbpdc*), a 3D-MOF with **nbo** topology is obtained due to twisting of the ligand which renders the two carboxylate-groups orthogonal to each other (Figure 1.3).³⁵ Thus, it is imperative that the design and selection of organic linker plays a very important role to obtain new materials.

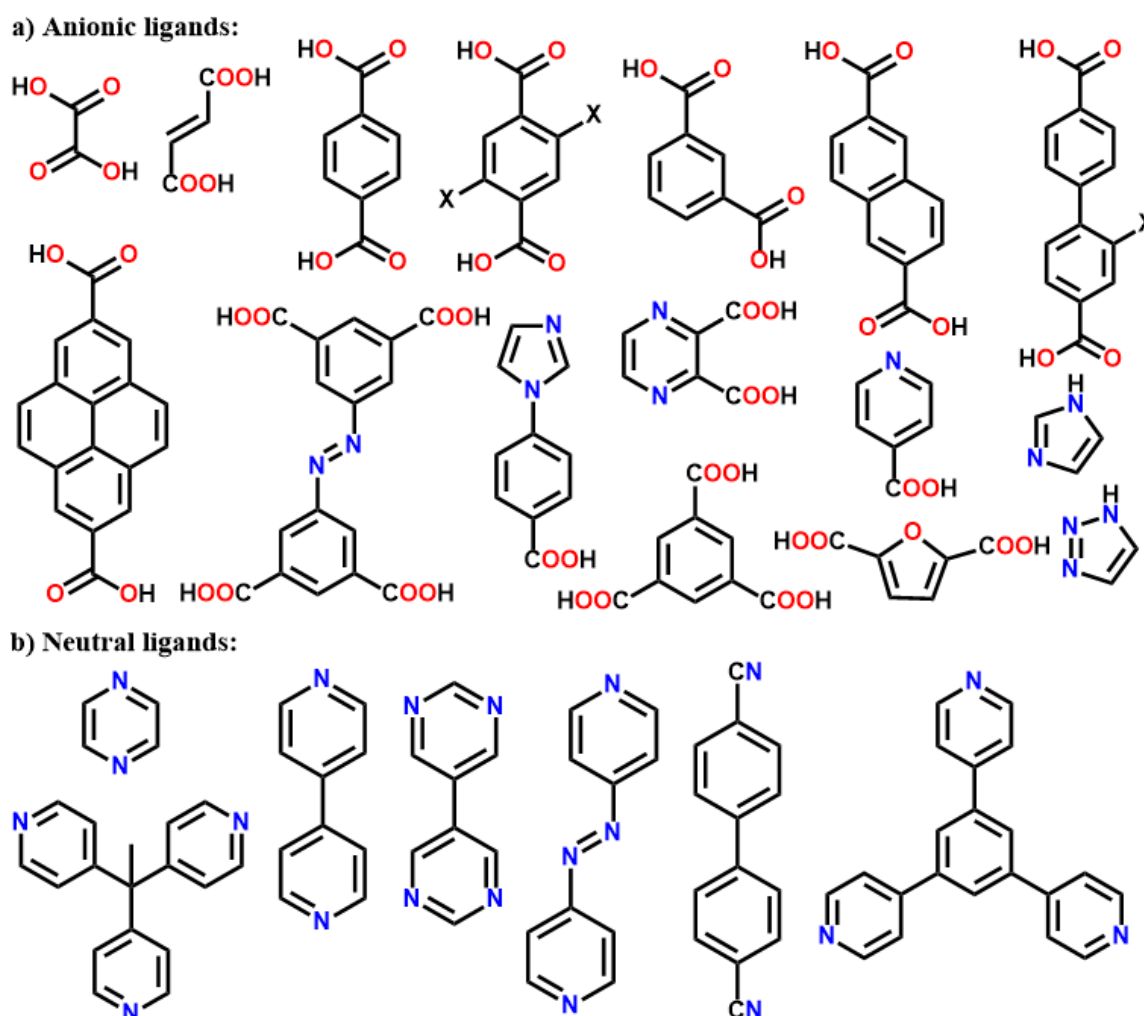


Figure 1.4: Representative examples of ligands used for the synthesis of coordination polymers.

Most commonly used linkers are neutral and anionic ligands. However, certain cationic

ligands such as 1,4-di(pyridin-4-yl)pyrazine-1,4-dium and [3,1':4',4":1",3'''-quaterpyridine]-1',1"-dium have also been used for the synthesis of coordination networks. The typical anionic linkers are aromatic/aliphatic, di-, tri, tetra-, and hexacarboxylate molecules (Figure 1.4a).³⁶ Non-symmetric ligands with a combination of anionic and neutral coordinating groups have been employed for the synthesis of coordination polymers. The neutral ligand mainly includes polytopic N-heterocycle containing functionalities like pyridyl, cyano, etc., with different spacer units (Figure 1.4b). Neutral ligands yield to the cationic framework with anions being located inside the pores or coordinates to the cationic metal centres in terminal or bridging fashion.

1.4 Design of Silane and Siloxane-Containing Ligands

In the literature various types of ligands have been reported for the construction of coordination polymers. However, use of tetrahedral ligands for the preparation of coordination polymers are not much explored because of the challenging synthetic procedure as well as low yields.⁶ Recently, design and synthesis of silicon-containing ligands for the construction of coordination polymers have been attracted considerable attention. This is due to the silicon-containing ligands possess characteristic properties like tetrahedral angle around Si atom ($\sim 109^\circ$), multidentate coordination, conformational nonrigidity, variable lengths and solubility.³⁷⁻⁴⁰ Thus, to overcome the synthetic problems of for obtaining tetrahedral ligands, Davies and Zhou et al. have synthesized some distinct silicon containing ligands for the construction of coordination polymers, where the introduction of silane containing ligand has largely simplified the process for preparing ligands with tetrahedral geometry.^{41,42} One of the advantages of having ligands with silicon centres is that they are more synthetically accessible than their carbon analogs and therefore it act as an promising candidate to obtain a series of linkers for the construction coordination polymers with easily modifiable chemical and structural properties. In addition, silicon containing ligands have longer bond length as compare to that of carbon analogue, so it increases the bond angle flexibility at the silicon and decrease the conformational rigidity which allows the construction of coordination polymers with novel topology and structural forms.³⁷⁻⁴⁴ Utilizing this strategy, Davies et al. have also demonstrated the influence of silicon-centric ligands on the structure and properties of the obtained coordination polymers. They have reported that switching of carbon with silicon in the structure gives a key difference regarding the orientation of the metal-connecting nodes within the frameworks.⁴⁵ The framework obtained

from the carbon based ligand reveals that all the nodes are coplanar and orientated in the [001] crystal plane whereas in the silicon based framework nodes are oriented alternatively and lie perpendicular to each other in either [110] or $[\bar{1}10]$ crystal planes (Figure 1.5). Thus, the framework obtained from the silicon based ligand shows an increase in the crystallographic 'a' and 'b' lattices and decrease in the 'c' lattice. As a result, it forms a large cavity within the framework with an increase in the porosity. So, inclusion of larger silicon atom increases the bond length from 1.54 Å (C-Ar) to 1.87 Å (Si-Ar) which allow the rotational freedom for the aryl group and thereby facilitating the metal nodes to adopt perpendicular alignments.

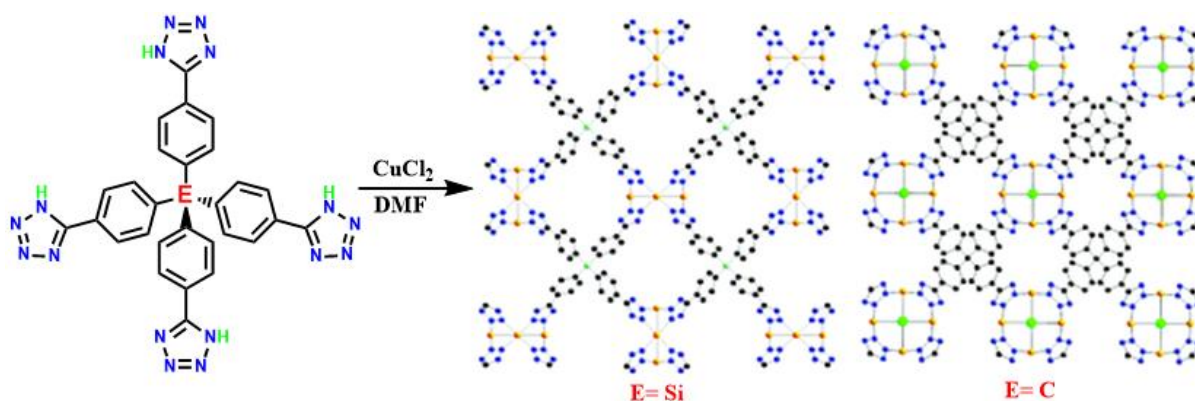


Figure 1.5: View of crystal structures obtained from silicon and carbon analogous tetrahedral ligand (Adapted from "Davies et al. Dalton Trans. 2013, 42, 13860" with permission of the Royal Society of Chemistry)

1.5 Organosilicon Containing Ligands

The compounds having silicon-carbon bond are known as organosilicon compound. The first example for the construction of coordination compounds based on the silicon centred ligands was reported by Tilley and Liu in 1997, where they have synthesized 3D MOFs with Ag(I) and Ti(IV) metal ions by utilizing tetrakis(4-cyanophenyl)silane ligand, which is similar to the carbon-based building block tetrakis(4-cyanophenyl)methane.^{46,47} Later on, in 1999, Stang et al. has synthesized bis(4-pyridyl)silanes to obtain self-assembled dinuclear platinum (II) and palladium (II) rhomboids.⁴⁸ Further, Jung et al. has synthesized numerous pyridine functionalized silane ligands to obtain various macrocycles and coordination polymers (Figure 1.6A).⁴⁹⁻⁵⁸ Recently, Lambert, Froba, and Zhou have synthesized carboxylate based silane ligands for the construction of 3D MOFs (Figure 1.6B and 1.6C).^{43,44,59,60} More recently, Davies and Lickiss have synthesized some novel pyridine and carboxylate based

silane ligands and utilized them to obtain interesting coordination polymers (Figure 1.6D and 1.6E).^{41,42,45,61,62} In addition to their coordination chemistry, there are some reports for the formation of 3D hydrogen-bonded assemblies based on the ligands $\text{Si}(p\text{-C}_6\text{H}_4\text{CO}_2\text{H})_4$ ⁶³ and $\text{Si}(p\text{-C}_6\text{H}_4\text{B}(\text{OH})_2)_4$ ⁶⁴. Yaghi and coworkers have obtained a 3D covalent organic framework by condensation of $\text{Si}(p\text{-C}_6\text{H}_4\text{B}(\text{OH})_2)_4$,⁶⁵ while Kaskel and coworkers have synthesized microporous polysilane materials through the lithiation of $\text{Si}(p\text{-C}_6\text{H}_4\text{Br})_4$ ⁶⁶ (Figure 1.7). Figure 1.8 and 1.9 has shown the silane ligands used for construction of coordination polymers.

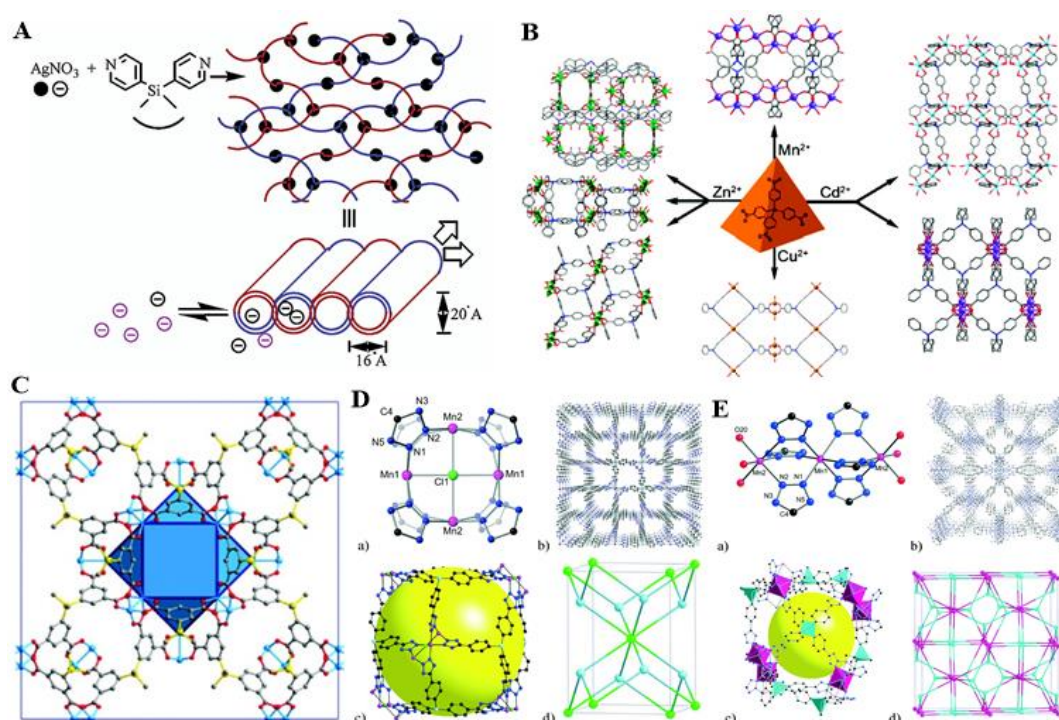


Figure 1.6: Some representative examples of MOFs based on silane containing ligands; (A) 2D sheet having 20-Å-thick interwoven nanotubes (Adapted from “Jung et al. *J. Am. Chem. Soc.*, **2002**, 124, 7906” with permission of the American Chemical Society), (B) Metal–Organic Frameworks Built from Rigid Tetrahedral $[\text{Si}(p\text{-C}_6\text{H}_4\text{CO}_2)_4]^{4-}$ Struts (Adapted from “Davies et al. *Cryst. Growth Des.*, **2010**, 10, 4571” with permission of the American Chemical Society), (C) Highly porous MOFs obtained from the 5,5’-(dimethylsilanediyl)diisophthalate and dicopper paddle wheel units (Adapted from “Fröba et al. *Inorg. Chem.*, **2009**, 48, 6559” with permission of the American Chemical Society), (D) and (E) Microporous MOFs built from rigid tetrahedral tetrakis(4-tetrazolylphenyl)silane (Adapted from “Davies et al. *CrystEngComm*, **2014**, 16, 8094” with permission of the Royal Society of Chemistry)

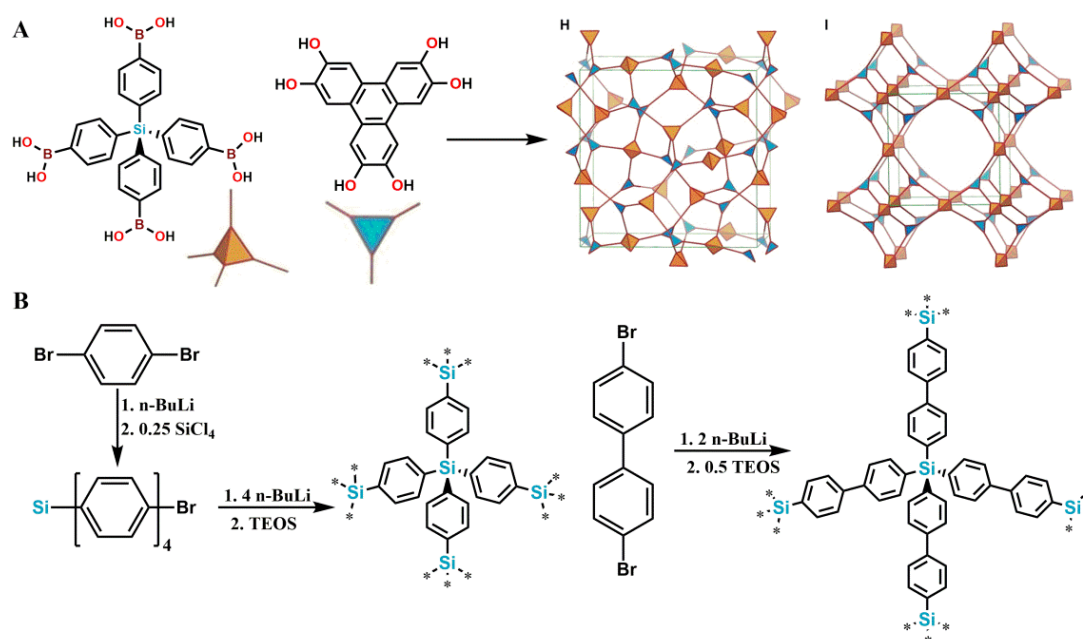


Figure 1.7: Representative condensation routes to 3D COFs; (A) 3D covalent organic framework obtained by condensation of $\text{Si}(\text{p-C}_6\text{H}_4\text{B}(\text{OH})_2)_4$ (Adapted from “Yaghi et al. *Science*, **2007**, 316, 268” with permission of the The American Association for the Advancement of Science), (B) Synthesis of microporous polysilane materials through the lithiation of $\text{Si}(\text{p-C}_6\text{H}_4\text{Br})_4$ (TEOS = Tetraethyl orthosilicate)

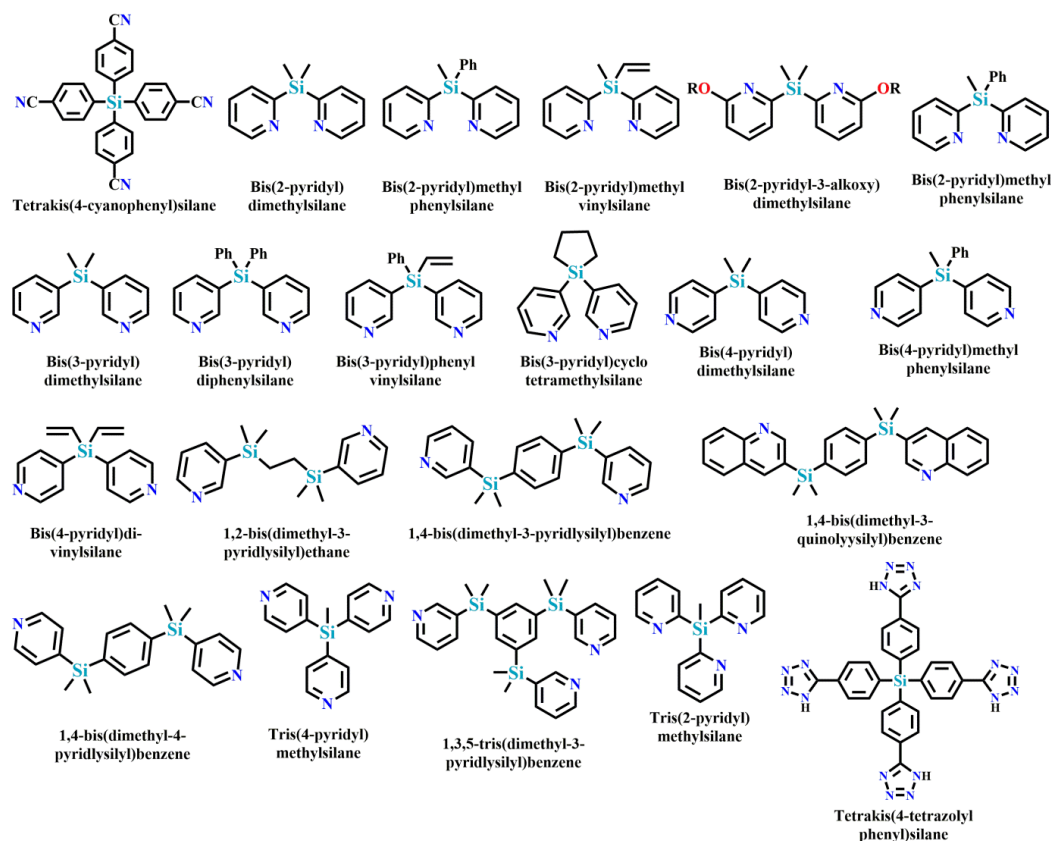


Figure 1.8: Representative examples of N-donor functionalized silane containing ligands

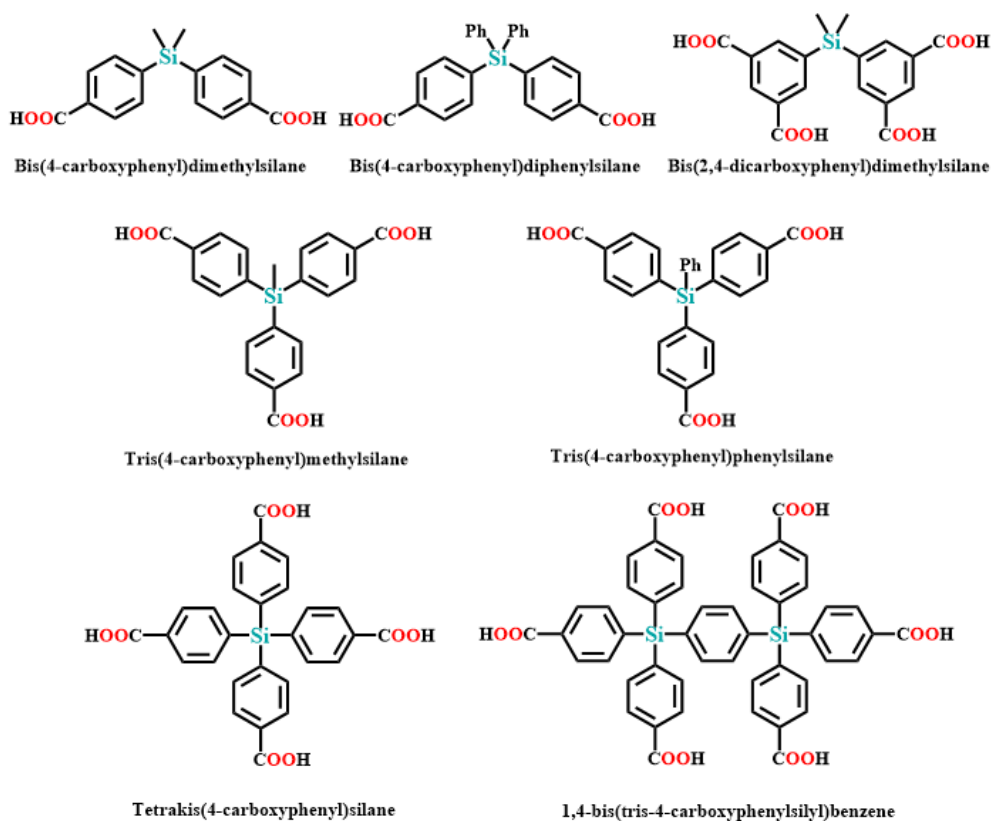


Figure 1.9: Representative examples of carboxylate-containing silane ligands

1.6 Siloxane Containing Ligands

The compound containing silicon-oxygen-silicon (Si–O–Si) linkages are known as siloxane compounds. The silicon atom can also be attached to different numbers of oxygen atoms and this dictates the naming and type of structure such as Silane: four functional groups attached to a silicon atom, and contains no Si–O–Si (siloxane) linkage ($R^1R^2R^3R^4Si$); Siloxane: these compounds are linear in nature consisting of Si–O–Si linkages $-(R'R''Si-O)_n-$; Silsesquioxane: these compounds have, on average one and a half oxygen atoms per silicon atom, and these materials can form interesting ladder, cage and network type polymers $-(R'Si-O_{1.5})_n-$; Silicates: these are hard, highly crosslinked materials, consisting of siloxane type linkages to each silicon atom $-(Si-O_2)_n-$. Another naming system, originally introduced by Hurd, and referred to as the GE (General Electric) system has been in common usage for many years. The silicon atom can be attached by one, two, three or four siloxane bonds; and the residual valencies (of the silicon atom) are taken up by three, two, one or zero methyl groups respectively. The symbols M (monofunctional), D (difunctional), T (trifunctional), and Q (tetrafunctional), respectively, are used to represent the silicon atom centres.

1.6.1 Disiloxane containing ligands

The use of siloxane (Si–O–Si) containing ligands for the construction of coordination materials are not much studied, though the siloxane motifs are widely employed in many classes of materials such as periodic mesoporous organosilica, zeolites, other porous materials and POSS hybrids.⁶⁷⁻⁷¹ The incorporation of well-separated metal binding sites (N, O or S) on the flexible siloxane backbones offers the possibility of synthesizing new zeolite-like materials with Si-O bonds, metal ions and organic spacer units. The choice or design of a siloxane backbone on which metal binding sites can be anchored is dictated to a large extent by the necessities of chemical stability, steric effects and ease of synthesis. The use of siloxane-based ligands for the construction of coordination polymers was first reported by Goodgame et al, where N-donor functionalized disiloxane ligands [${}^i\text{Pr}_2\text{SiO}(\text{CH}_2)_n{}^3\text{py}$] $_2\text{O}$, ($n = 0, 1$ or 3) were utilized for obtaining coordination assemblies with large-ring, chain or polymeric sheet structures (Figure 1.10A).³⁸

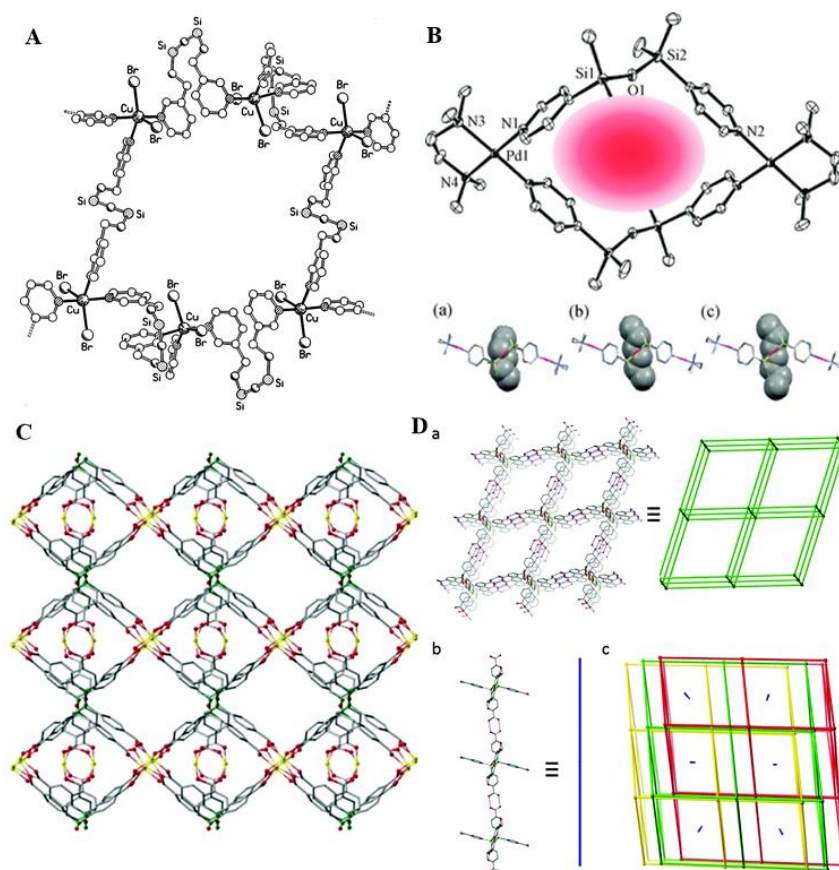


Figure 1.10: Some representative examples of MOFs based on siloxane backbones; (A) Polymeric structures having macrocycle obtained from copper (II) and siloxypyridine ligands (Adapted from “Williams et al. *Inorganica Chem. Acta*, **2001**, 324, 218” with permission of

the Elsevier), (B) Pseudorotaxane-type *n*-hydrocarbon container obtained from 3-bis(4-pyridyl)tetramethyldisiloxane and Pd(II) (Adapted from “Jung et al. Dalton Trans, 2011, 40, 8520” with permission of the Royal Society of Chemistry), (C) 3D MOFs obtained from Zn(II) and hexa(4-carboxyphenyl)disiloxane (Adapted from “Davies et al. Chem Commun., 2017, 53, 12524” with permission of the Royal Society of Chemistry), (D) H-Bonding of assembly of hexa(4-carboxyphenyl)disiloxane with *pcu* net having one-dimensional supramolecular polymeric chains (Adapted from “Davies et al. Chem Commun., 2017, 53, 12524” with permission of the Royal Society of Chemistry)

Interestingly it has been shown that moisture sensitive alkoxy silanes (Si-OR groups) can be used to support the pyridyl donors by incorporating bulky *i*Pr groups on the silicon atoms (example: $i\text{Pr}_2\text{Si-O}(\text{CH}_2)_n\text{py}$) which reduces the rate of hydrolysis and stabilize the alkoxy silane bonds in the neutral solution.^{37,39} Jung et al. have synthesized pyridyl functionalized di- or tri-siloxanes and employed them to obtain macrocycles and polymeric chains with silver and palladium ions (Figure 1.10B).⁷²⁻⁷⁴ More recently, Davies et al. have synthesized siloxane based octahedral hexa(4-carboxyphenyl)disiloxane ligand and applied them to obtain interesting 3D MOFs. In addition, the parent ligand hexa(4-carboxyphenyl)disiloxane itself shows an unusual triply interpenetrated hydrogen-bonded organic framework having 1D-chains of H-bonded guest solvates in its pore (Figure 1.10C and 1.10D).⁷⁵ Figure 1.11 has shown the outline of siloxane backbone ligands for the construction of coordination polymers.

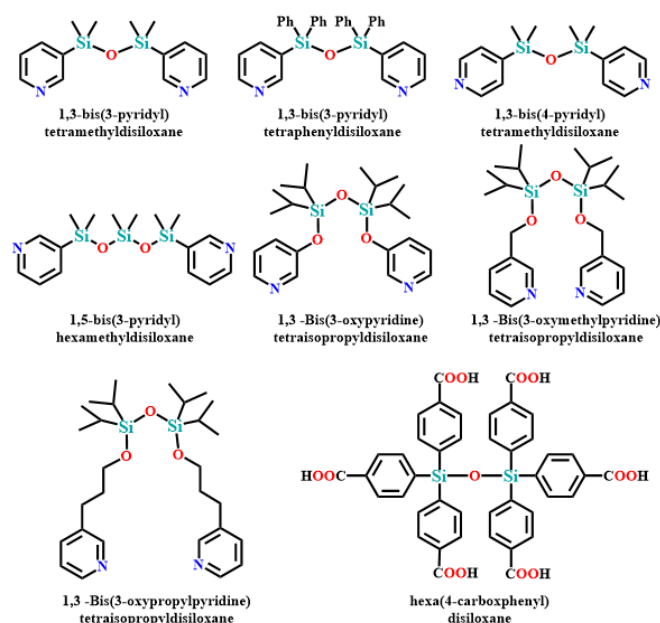


Figure 1.11: disiloxane containing ligands for the coordination polymers

1.6.2 Cyclic siloxanes

Cyclic siloxanes are well known raw materials for preparing cosmetics, silicones, dry-cleaning solvents, emulsifiers, skin cleaning agents, etc. Organo-functionalized polysiloxanes have been extensively used as basic silicone materials for the preparation of membranes, resins, coatings, liquid crystals, etc. Then unique features of these materials are due to the flexibility and strength of the Si-O bonds along with the propensity with which various functional groups can be anchored to the silicon atom.⁷⁶⁻⁷⁸ These functionalized cyclosiloxanes also act as fundamental starting materials for both cationic and anionic ring-opening polymerization or copolymerization to give the respective organofunctional silicone polymers such as polysiloxanes, siloxane-containing block-copolymers, etc.⁷⁶⁻⁷⁸ Recently, alkenyl functionalized (vinyl or aryl) cyclosiloxanes have been utilized as a core for the carbosilane dendrimers⁷⁹ or as synthetic reagents for organic compounds via palladium catalysed coupling (Hiyama coupling) reaction⁸⁰⁻⁸² and also as novel μ -donor ligands for transition metal complexes.⁸³⁻⁸⁷ However, currently, efforts have been given to the development of synthetic routes to incorporate metal binding sites on these flexible and hydrophobic polymeric supports.

1.6.3 Stereoisomer of cyclic siloxane

In the cyclic siloxane, each silicon atom has two substituents, so there is probability to have these substituents in one of the two possible spatial arrangements. During the formation of a cyclic siloxane three or more silane molecules arbitrarily interact with each other and when the ring is closed and the spatial orientations of the substituted groups on each of the silicon atoms is retained. Thus, once the ring is formed or closed the spatial orientation of substituted groups are adequately fixed. The cyclic ring can undergo normal vibrational and translation motions but unless the cyclic ring is cleaved by chemical and thermal methods, the orientation of the substituted groups remains unchanged. This randomness of the silane moieties during the formation of cyclic ring leads to the isomeric mixtures of cyclic siloxanes.¹⁰⁷ Therefore, there is a possibility for the formation of different types of stereoisomer during the formation of the cyclic siloxanes. In case of a trimer, there is possibility of two geometrical stereoisomers while in case of tetramer four geometrical stereoisomers are possible. For example, the trimethyltriphenylcyclotrisiloxane exhibits *cis-cis* and *cis-trans* isomer depending on the orientation of methyl and phenyl groups (Figure

1.14a). In the *cis-cis* isomer, all the phenyl groups are oriented on the axial position, as they lie on the same side of the siloxane ring while in case of *cis-trans* isomer, one of the phenyl groups is oriented on the equatorial position and two phenyl rings and one methyl group lie on the same side of the siloxane ring or vice versa. The tetramethyltetraphenylcyclotetrasiloxane exhibits four stereoisomers; *all-cis*, *cis-trans-cis*, *cis-cis-trans* and *all-trans* isomers (Figure 1.14b). In the *all-cis* isomer, all the phenyl rings are oriented on the axial position. In the *cis-trans-cis* isomer the phenyl groups on two neighboring silicon atoms are oriented on the axial positions, while remaining phenyl groups (on the two other neighbouring atoms) are oriented on the equatorial positions. In the *cis-cis-trans* isomer, phenyl groups on the three neighboring silicon atoms are oriented on the axial position while the fourth phenyl ring is located at the equatorial position. In *all-trans* isomer, the four phenyl groups are oriented at the axial and the equatorial positions alternatively.

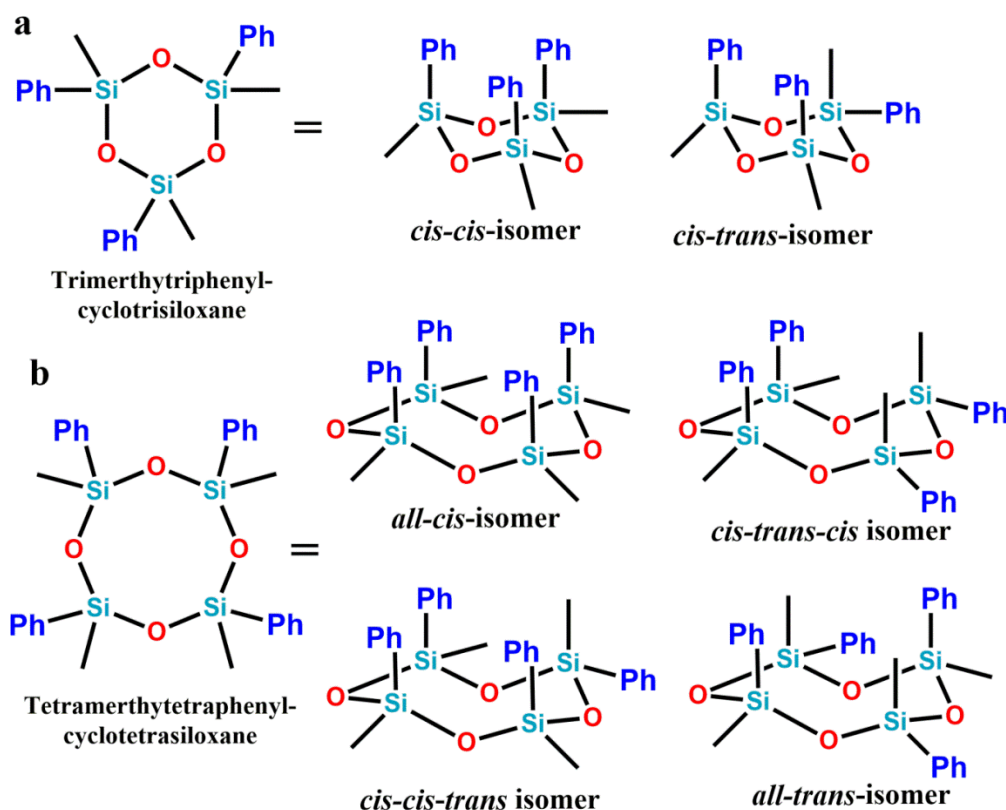


Figure 1.14: Representation of the stereoisomers for the cyclic tri- and tetrasiloxanes

1.7 Synthesis of Functionalized Cyclic Siloxanes

Among the cyclic siloxanes, cyclic tri- and tetrasiloxanes have been extensively studied for the assembling of multi-metallic cages and clusters. These cyclic siloxanes have been synthesized either by the hydrolytic condensation of silane compounds containing two

reactive groups and two functionalized organic groups⁸⁸ or by the chemical modification of molecular cyclosiloxanes, $[\text{RMeSiO}]_n$ ($n = 3-4$) having Si-vinyl/Si-H as reactive groups.⁸⁹

1.7.1 Hydrolytic condensation of silane

The one of the facile methods for the preparation of functionalized cyclic siloxane is to use monomeric silicon precursors having two reactive groups such as chloride, hydroxyl or alkoxy, which on the hydrolytic condensation in a controlled manner in presence of a base leading to the formation of the cyclotrisiloxane or cyclotetrasiloxane (Figure 1.12). By adopting this method the research groups of Unno, Shchegolikhina, and some others have synthesized a series of hydroxy functionalized cyclosiloxanes, $[\text{R}(\text{OH})\text{SiO}]_n$ ($n = 3-7$) and utilize them as ligand for the transition metal ions.⁹⁰⁻⁹⁸ The preferential formation of tri- or tetracyclosiloxane depends upon the ratio of ethanol to water as well as the bulkiness of the functional group. Usually, the ethanol to water ratio of 5:1 and smaller substituents on Si results in the formation of the tetrameric siloxane over trisiloxane.⁹⁷

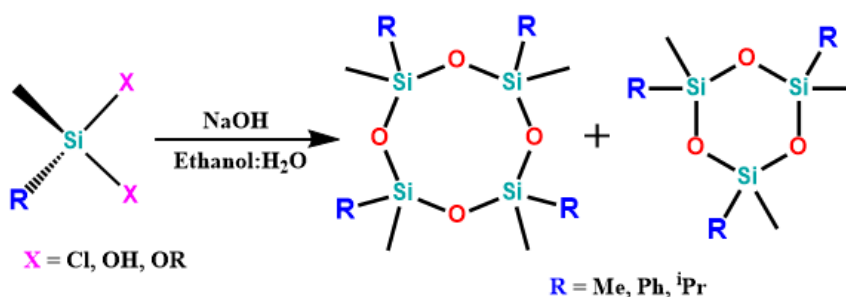


Figure 1.12: Synthesis of functionalized cyclic siloxane by hydrolytic condensation reaction.

In comparison with the cyclic tetra siloxane, synthesis of cyclic trisiloxanes are not much explored because of the high reactivity and ring strain in the trisiloxane ring. They have been regarded as reactive compounds, and thus these compounds have been isolated as stable functionalized cyclosiloxanes by the introduction of bulky groups on silicon atoms. Therefore, only few reports have been reported for the synthesis of cyclotrisiloxanetriols through the hydrolytic condensation of silane compounds. The first example for the synthesis of cyclic trisiloxane was reported by the Roesky and co-workers in 1996, where they have isolated the *cis-trans* isomer of cyclotrisiloxanetriol $[\text{Ar}(\text{Me}_3\text{Si})\text{NSi}(\text{OH})\text{O}]_3$ ($\text{Ar} = 2,6$ -dimethylphenyl), by utilizing bulky $\text{Ar}(\text{Me}_3\text{Si})\text{N}$ - group to stabilize the cyclosiloxane.⁹⁹ Subsequently in 2002, they have reported the preparation and crystal structure of *cis-cis* isomer of $[\text{Me}_3\text{SiCH}_2\text{Si}(\text{OH})\text{O}]_3$ (Figure 1.13a).¹⁰⁰ In 2000 and 2002, Fujita's group have isolated *cis-cis* isomer of $[\text{ArSi}(\text{OH})\text{O}]_3$ ($\text{Ar} = \text{phenyl, naphthyl, } m\text{-tolyl}$) by using the Pd(II)-

linked coordination cage as an hosts for these isomers (Figure 1.13b).^{101,102}

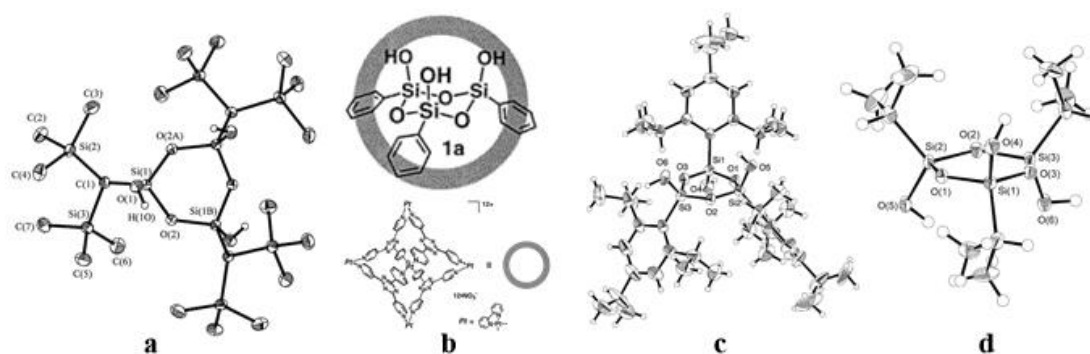


Figure 1.13: Crystal structure of cyclic trisiloxanes; (a) *cis-cis*-[Me₃SiCH₂]Si(OH)O₃ (Adapted from “Roesky et al. *Organometallics*, **2002**, *21*, 3671” with permission of the American Chemical Society), (b) *cis-cis*-[ArSi(OH)O]₃ (Adapted from “Fujita and Kusukawa et al. *J. Am. Chem. Soc.*, **2000**, *122*, 6311” with permission of the American Chemical Society), (c) *cis-trans*-[TipSi(OH)O]₃ and (d) *cis-trans*-[^{*i*}PrSi(OH)O]₃ (Adapted from “Unno et al. *J. Organomet. Chem.*, **2003**, *686*, 175 and *Organometallics*, **2004**, *23*, 6221” with permission of the American Chemical Society).

Recently, Unno et al. have reported the structure of *cis-trans* isomer of [TipSi(OH)O]₃ (Tip = 2,4,6-triisopropylphenyl) (Figure 1.13c) and [^{*i*}PrSi(OH)O]₃ where the cyclotrisiloxane is stabilized by the relatively small substituents (Figure 1.13d).^{103,104} Brown and Vogt have synthesized the first cyclic tetrasiloxane in 1965, where they have reported 1,3,5,7-tetrahydroxy-1,3,5,7-tetraphenylcyclotetrasiloxane and 1,3,5,7-tetrahydroxy-1,3,5,7-tetracyclohexylcyclotetrasiloxane which were obtained by the hydrolytic condensation of trichlorophenylsilane and trichlorocyclohexylsilane, respectively.^{105,106} Later on, Unno, Pizzotti, Feher, and Shchegolkhina have synthesized a series of cyclic tetrasiloxane by single or multistep reaction from the corresponding silane compounds.⁹⁰⁻⁹⁸ The cyclic siloxane obtained by using hydrolytic condensation method exhibits multiple stereoisomers; cyclic trisiloxane exists in two isomeric structures (*cis-cis* and *cis-trans* isomer) while the cyclic tetrasiloxane exists as four different isomers (*all-cis*, *cis-trans-cis*, *cis-cis-trans* and *all-trans* isomers).

1.7.2 Peripherally functionalized siloxanes

This is one of the widely accepted approach to synthesize functionalized cyclic siloxane through the chemical modification of molecular cyclosiloxanes bearing Si-H/Si-vinyl groups via hydrosilylation, metathesis, silylating coupling and Heck reactions.

a) **Hydrosilylation reaction:** The hydrosilylation reaction is one of the most important catalytic reaction for the synthesis of various organosilicon compounds. The hydrosilylation reaction proceeds via the addition of silicon hydrides to the multiple carbon-carbon bonds using a metal catalyst and Lewis acid or radical initiator (Figure 1.15).¹⁰⁸ This reaction widely utilized in the industry to obtain various silicone polymers such as rubbers, oils, and resins as well as some silane coupling agents. This reaction can also used to obtain various organosilicon agents that are utilized in fine chemical synthesis for cross-coupling reaction, stereospecific oxidation etc.¹⁰⁹⁻¹¹²

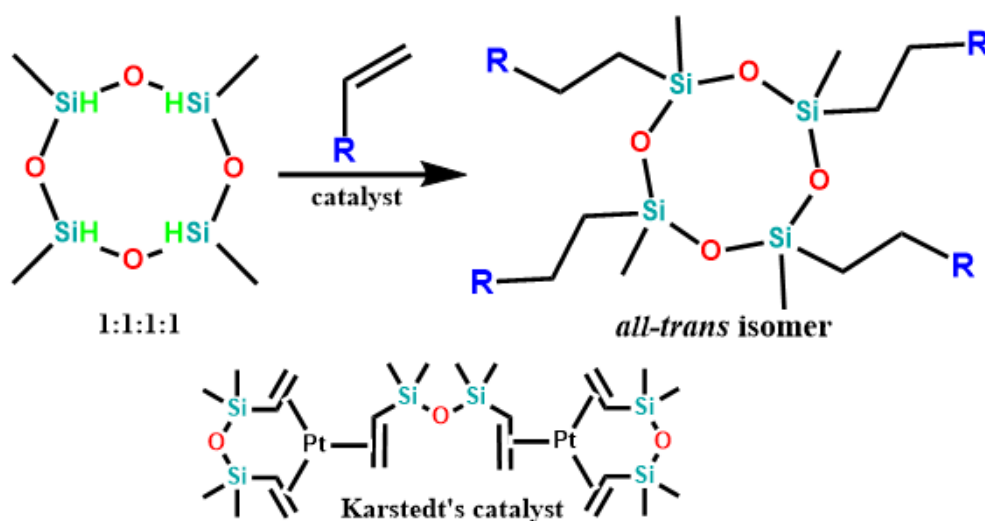


Figure 1.15: Synthesis of functionalized cyclo-tetrasiloxane by hydrosilylation reaction

The first article on the hydrosilylation reaction for synthesis of organosilane compounds was reported by the Sommer in 1947, in which they have shown that the reaction of 1-octene with trichlorosilane in the presence of peroxide as an catalyst. The reaction proceeded via free-radical mechanism but the selectivity was very low.¹¹³ Later on, in the late 1950s, Speier et al. have improved the selectivity to a large extent by utilizing the hexachloroplatinic acid [H₂PtCl₆]·H₂O as an homogeneous transition metal catalyst also known as Speier's catalyst.¹¹⁴ The important breakthrough in the hydrosilylation reaction has been made in 1973 after the development of platinum (0) catalyst by the Karstedt group. The Karstedt's catalyst contains a platinum (0) has been satbilized by the vinyl-siloxane ligands (Figure 1.15). By utilizing this catalyst the selectivity and activity of the reaction has been improved drastically. As a result, this process has been extensively used in the silicone chemistry, for example, the synthesis of various commodities including pressure-sensitive adhesives, lubricating oils, paper release coatings, and liquid injection molding products, etc. The mechanism for the hydrosilation reaction was proposed by Chalk and Harrod in 1965 via oxidative addition and

reductive elimination process. The reaction proceeds by the oxidative addition of silane compounds to a metal alkene complex $[\text{Pt}(0)]$ followed by migrative insertion of alkene in to the metal hydride bond (M-H) and the resulting metal(silyl)(alkyl) complex undergoes reductive elimination with the formation of Si-C bond with regeneration of the catalyst (metal-alkene complex) in the presence of excess alkene (Figure 1.16).¹¹⁵

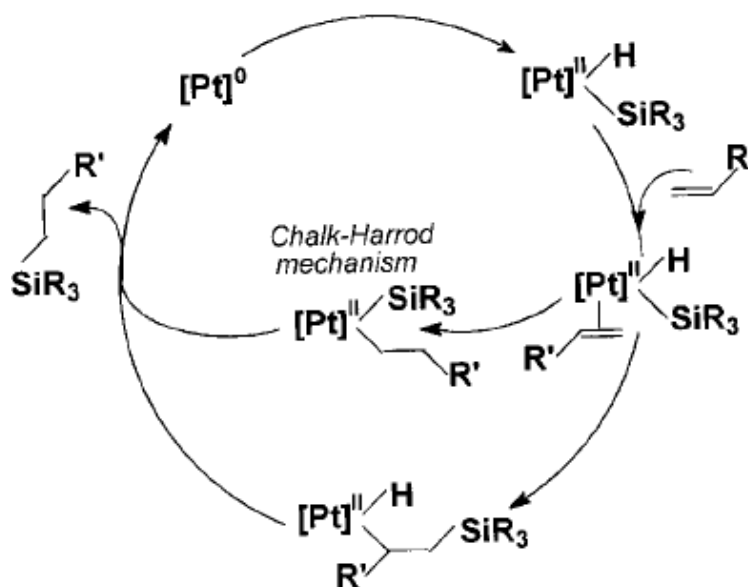


Figure 1.16: Hydrosilylation reaction mechanism (Adapted from “Marciniec et al. *Appl. Organometal. Chem.* **2000**, *14*, 527” with permission of the John Wiley & Sons, Ltd)

By adopting this method, Cuadrado and coworker have synthesized a series of siloxane cages containing peripheral ferrocene groups. Utilizing the cyclic siloxanes or silsesquioxanes as cores, they were able to construct polyferrocenyl dendrimers, polymers, POSS-containing twenty-four ferrocenyl groups (Figure 1.17) in presence of Karstedt’s catalyst.¹¹⁶⁻¹²⁰ However, Despite the high utility in industry, Platinum catalyzed hydrosilylation reactions suffered from some drawbacks. For example, hydrosilylation of olefins is often accompanied by some side reactions, such as hydrogenation of olefins, dehydrogenative silylation, isomerization of olefins, olefin oligomerization and redistribution of hydrosilanes (Figure 1.18).¹²¹ These side reactions cause a significant reduction in the yield of the final product. Also, to remove these impurities additional processes were required, which could cause the deleterious effects on the properties or quality of the final product.

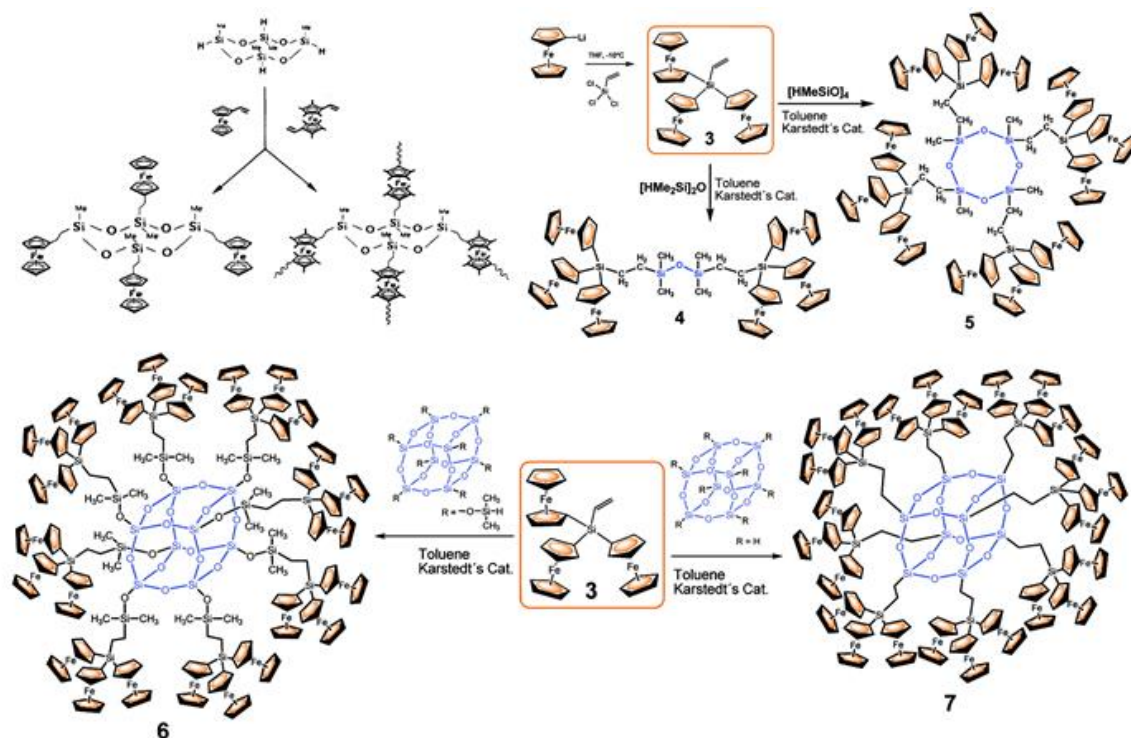


Figure 1.17: Representative examples of peripherally functionalized ferrocene moieties with cyclic siloxanes and POSS (Adapted from “Cuadrado et al. *Organometallics* **1995**, *14*, 2618 and *Organometallics*, **2012**, *31*, 3248” with permission of the American Chemical Society).

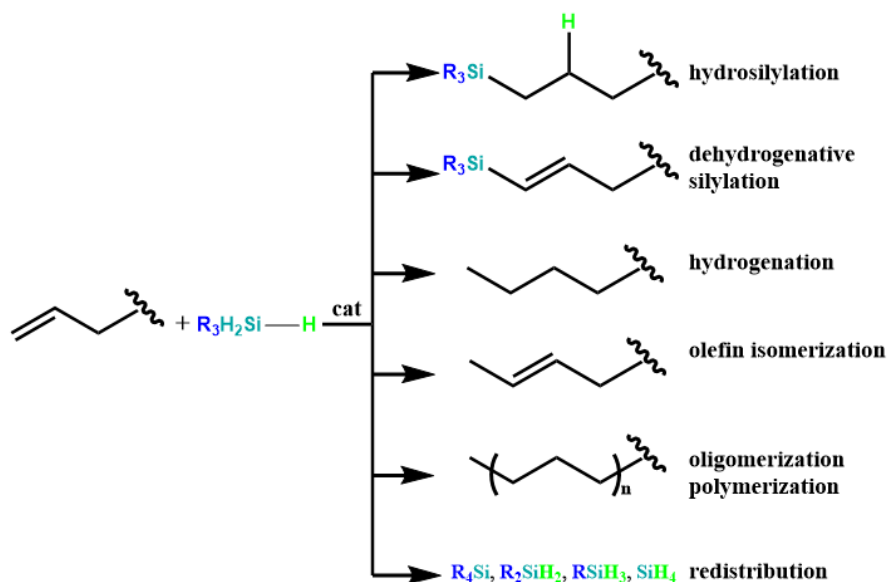


Figure 1.18: Reaction of an olefin with hydrosilane in the presence of a catalyst

b) Silylative coupling reaction: The silylative coupling also known as trans-silylative reaction in which reaction of vinyl-substituted organosilicons with the olefins take place in the presence of transition-metal catalyst. This reaction proceeds through the cleavage of the

sp^2 hybridized carbon-hydrogen bond ($=C-H$) of the olefin and the carbon-silicon bond ($C-Si$) of vinyl silane (Figure 1.19).¹²²

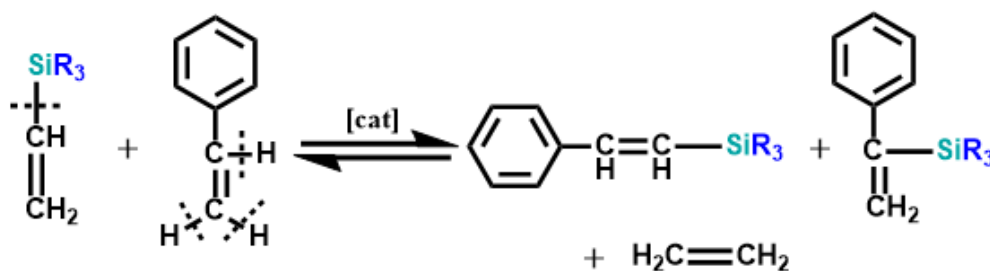


Figure 1.19: Silylative coupling routes

These reactions were catalyzed by various transition metal complexes such as Ru,^{123,124} Rh,^{125,126} Ir,¹²⁷ Co¹²⁸ via metal hydride ($M-H$) or metal silicon ($M-Si$) bonds (initially present or generated in situ) during the catalytic reactions. In 1984, Marciniec et al. has discovered the silylative coupling reaction.¹³¹ The mechanism for this reaction has been proposed by Wakatsuki et al.¹²² for the Ru-complexes which was further modified by Marciniec group and applied it for other metal complexes such as Rh, Co and Ir. This reaction occurs by the insertion of vinylsilane into the metal hydride ($M-H$) bond followed by the β -Si transfer to the metal centre with the formation of metal silicon ($M-Si$) species and elimination of ethylene molecules. Then the insertion of substituted alkene followed by the β -H transfer to the metal centre with the elimination of substituted vinylsilane and regenerated catalyst for the next cycle (Figure 1.20).^{129,130}

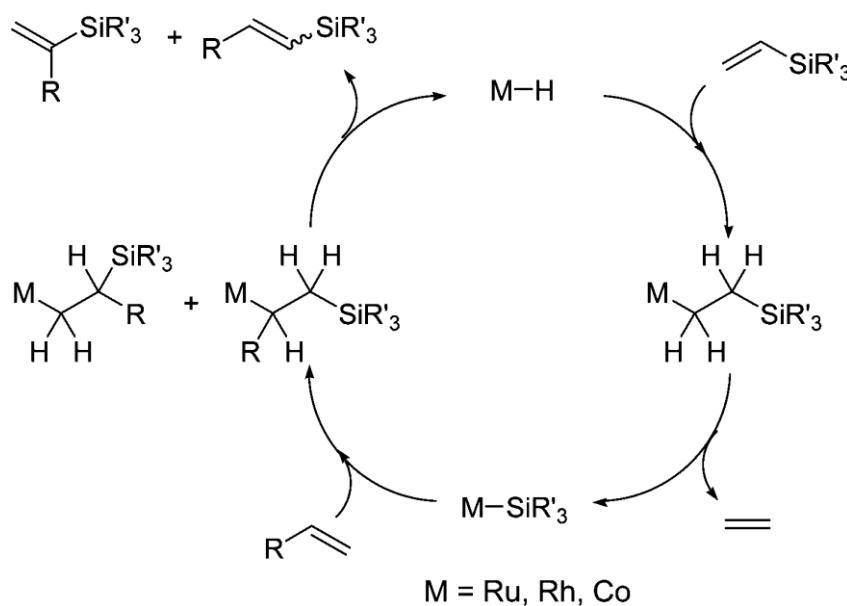


Figure 1.20: General mechanism for the silylative coupling reaction

Generally, ruthenium (II) complexes such as $[\text{Ru}(\text{H})(\text{Cl})(\text{CO})(\text{PCy}_3)_2]$ and $[\text{Ru}(\text{H})(\text{Cl})(\text{CO})(\text{PPh}_3)_3]$ containing hydride and phosphine as ligands act as most efficient and selective catalysts for this reaction. By utilizing this catalyst various functionalized olefins containing nitrogen and aryl groups, (e.g., substituted styrenes, N-vinyl amides, N-vinyl carbazole), have been catalyzed most effectively and selectively. In addition, this reaction has been successfully applied for the functionalization of organosilicon compounds containing multivinyl groups such as cyclosilazanes and cyclosiloxanes,¹³² silsesquioxanes and spherosilicates¹³³⁻¹³⁶ as well as to the modification of vinyl-substituted polysiloxanes in the presence of ruthenium complexes as catalysts.¹³⁷

c) Metathesis reaction: Metathesis reaction involves the exchange of substituents between different types of olefins in the presence of Grubbs or Schrock type of catalysts. Both metathesis and silylative coupling reactions lead to the same product, but differ mechanistically. Metathesis reaction occurs by the cleavage of a C=C bond whereas silylative coupling reaction occurs via a carbon silicon (=C–Si) and carbon hydrogen (=C–H) bond cleavage (Figure 1.21).^{138,139}

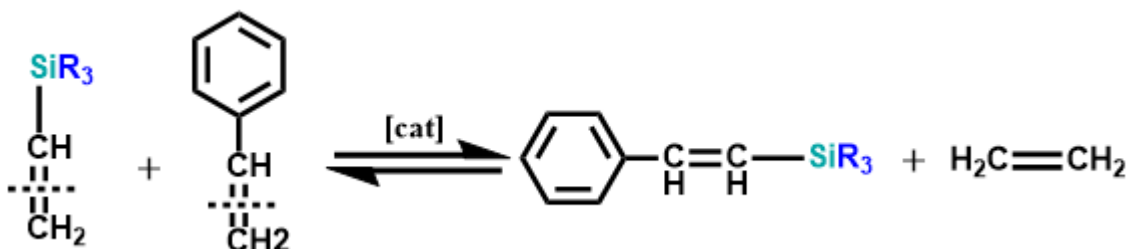


Figure 1.21: Metathesis coupling routes

Metathesis reactions were catalysed by well-defined alkylidene complexes of Ru, Mo, and W through the carbene mechanism.¹⁴⁰ The use of metathesis reaction for the functionalization of vinyl substituted siloxane has been demonstrated by the Marciniak and Feher groups in presence of Grubbs' and Schrock's catalyst. Marciniak group has utilized first generation Grubbs', second generation Grubbs' and Hoveyda Grubbs' catalysts for the functionalization of vinyltrialkoxysilanes, vinyltris(trimethylsiloxy)silane, trichlorovinylsilanes and vinyl silicon compounds containing electron withdrawing groups with various olefins.¹⁴¹⁻¹⁴⁴ Metathesis reaction has been catalysed efficiently for various derivatives of vinyl silicon but it is quite inactive for the alkyl substituted vinyl silane compounds. The mechanism of metathesis reaction was first proposed by Herisson and Chauvin. The reaction proceeds via a [2+2] cycloaddition reaction of an alkene to a alkylidene moieties of catalyst to form

intermediate metallacyclobutane which undergo cyloelimination to give either the original alkene or a new alkene and an alkylidene complex (Figure 1.22).¹⁴⁵

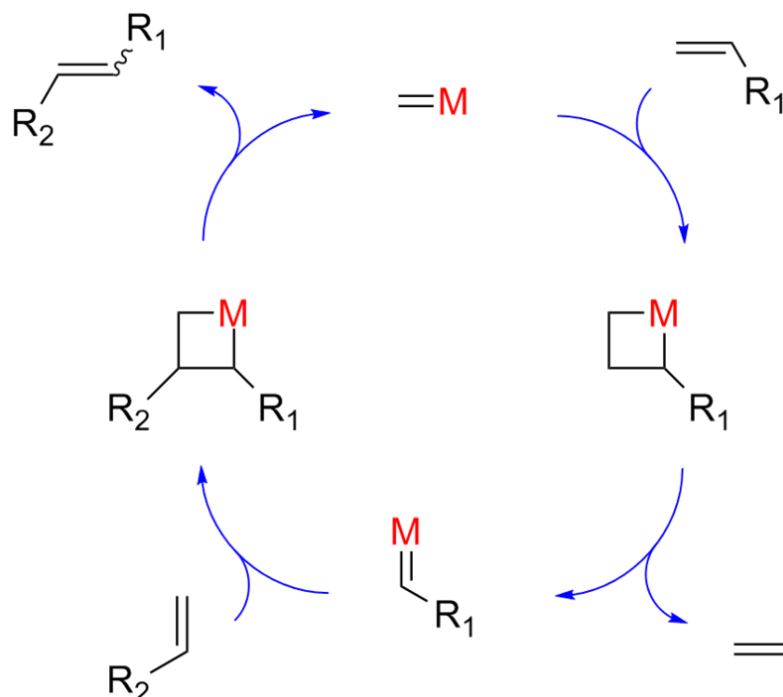


Figure 1.22: General mechanism for the metathesis reaction

d) Heck coupling reaction: The Heck coupling reaction is a cross-coupling reaction of aryl halides with an alkene to make substituted alkene by utilizing palladium (0) as a catalyst (Figure 1.23). This reaction is extensively used for the synthesis substituted dienes; olefins and various types of unsaturated compounds including processed that run on the industrial scales.¹⁴⁶⁻¹⁴⁹ It is also used to obtain conjugated polymer systems and nanocomposite materials which is applied in optoelectronics.^{150,151}

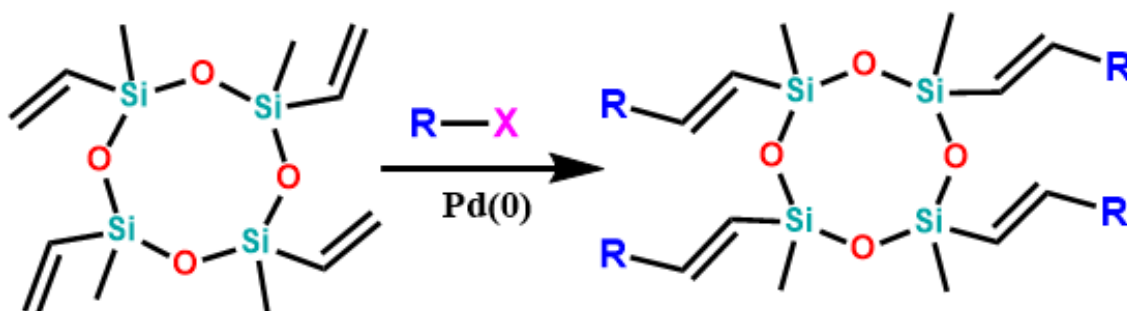


Figure 1.23: Synthetic routes for the Heck Coupling Reaction

The mechanism of the Heck coupling reaction was proposed via oxidative addition and β -hydride elimination process. The reaction proceeds by the oxidative addition of aryl halide to

the palladium (0) metal which producing a very reactive organo-palladium(II) halide complex followed by the syn-addition of olefin in between palladium carbon bond. Then follows torsional strain relieving rotation to the trans isomer and resulting complex undergoes a β -hydride transfer to the palladium by eliminating hydridopalladium halide and forming the substituted vinylsilane product. Finally, hydridopalladium halide product decomposes into palladium and hydrogen halide in the presence of base, which is then available to go through another reaction cycle (Figure 1.24).¹⁵²

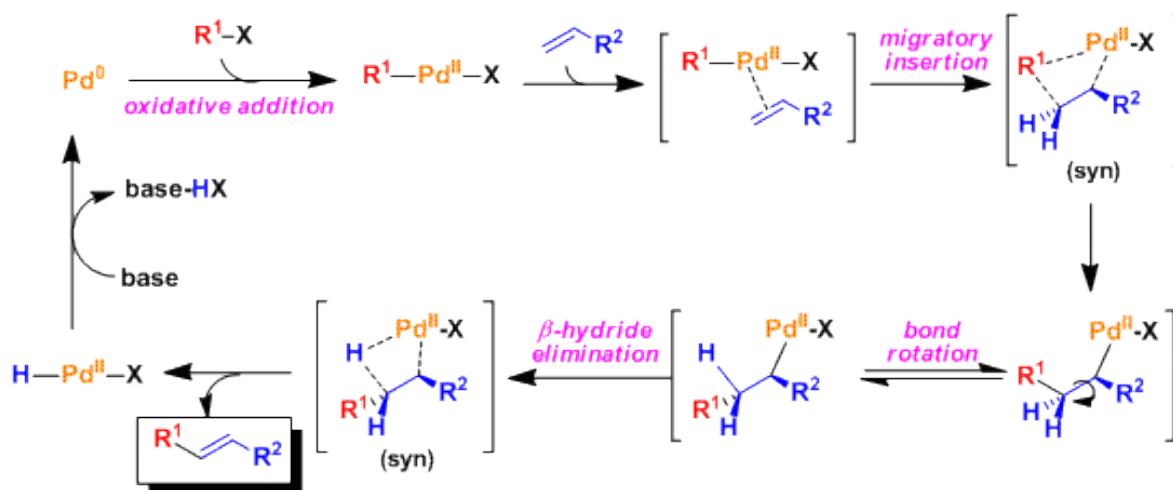


Figure 1.24: General mechanism for the Heck coupling reaction

Currently, incorporation of arylolefinyl moieties on the organosilicon polymer backbones or oligomers in the primary or side chains have received considerable attention due to the potential applications, as materials in personal care as gloss ingredients, polymers for nonlinear optics and light emitting devices, resulting from the presence of p-conjugated moieties. Recently, use of Heck coupling reaction for the functionalization of cyclic siloxane in good yields has been demonstrated by the Stanczyk group in the presence of various palladium salts as catalysts.¹⁵³ Thus, the Heck coupling reaction was found to be an efficient alternative route to the silylating and cross-metathesis reaction for the functionalization of silicon.

1.8 Outline and Objective of the Thesis

All these above mentioned discussions have shown that design and synthesis of ligands plays a vital role for obtaining molecular materials with predetermined structures or properties. As seen earlier, N-donor functionalized ligands with tetrahedral geometry is not much studied for the construction of coordination compounds due to the complicated synthetic procedures and the low yields. Employing a silicon backbone offers an alternative approach to overcome

the problem associated with synthetic methods, for the construction of coordination polymers with tetrahedral ligands. Despite the recent reports on the silane and siloxane based ligands for the construction of MOFs, there is a broad scope to develop new ligands based on rigid and flexible backbone of silane and siloxane scaffolds and study their structure, stereochemistry as well as explore their utility to obtain functional coordination polymers for applications in the areas of adsorption, luminescence and catalysis.

In this regard, this thesis demonstrates the systematic synthesis of a series of peripheral pyridyl functionalized tri- and tetrapodal silane and cyclotetrasiloxane ligands/scaffolds in acyclic and cyclic topologies to obtain different coordination polymers and study their structure, stereochemistry and reactivity as well as exploit them for various applications such as luminescence, catalysis, and chemical adsorption. The second chapter will discuss the synthesis of two new iso-structural coordination polymers featuring Cu_6I_6 clusters supported by tridentate arylsilane ligand and study their thermochromic and mechanochromic luminescence umpolung behavior. The third chapter demonstrates the synthesis of new cyclotetrasiloxane scaffolds containing peripherally functionalized 3-pyridyl moieties by using Heck Coupling reaction and establish the stereochemistry of these ligands with the proton and silicon NMR and also from the Single crystal X-ray analysis of their respective complexes. In chapter four, synthesis of a rigid and a flexible tetrahedral tetra-pyridyl silane ligands will be discussed along with their utility for obtaining charge-separated Cu(II) containing 3D coordination networks having unique linear $\text{Cu}^{\text{II}}_4\text{Cl}_3(\text{H}_2\text{O})_2$ and $\text{Cu}^{\text{II}}_4\text{Cl}_3(\text{H}_2\text{O})_2$ clusters. These coordination networks were shown to exhibit a reversible iodine uptake and act as Lewis acidic heterogeneous catalysts for Friedel-Crafts alkylation reactions under solvent-free conditions. By using the same rigid silane ligand, two solvent dependent copper iodide cluster MOFs have been synthesized which were further utilized as catalysts for Ullmann coupling reaction. Synthesis of a self-assembled octahedral cobalt (II) cage, based on a tris(3-pyridyl) methylsilane ligand and its utility as a homogeneous catalyst for the electro- and photocatalytic hydrogen evolution from the water will be described in fifth chapter.

Thus present thesis aims:

1. To synthesize new N-donor functionalized tri- or tetrapodal silane ligand and study their structure as well as coordination chemistry with different transition metal ions.

2. To synthesize pyridine functionalized stereochemically distinct cyclotetrasiloxanes and study their coordination chemistry with transition metal ions.
3. Use of these transition metal complexes for the various properties of practical application such as luminescence, adsorption, and catalysis.

1.9 References:

- (1) Farha, O. K.; Hupp, J. T. *Acc. Chem. Res.* **2010**, *43*, 1166-1175.
- (2) Kitagawa, S.; Kitaura, R.; Noro, S. I. *Angew. Chem. Int. Ed.* **2004**, *43*, 2334-2375.
- (3) Zhou, H.-C.; Long, J. R.; Yaghi, O. M. *Chem. Rev.* **2012**, *112*, 673-674.
- (4) Tranchemontagne, D. J.; Park, K. S.; Furukawa, H.; Eckert, J.; Knobler, C. B.; Yaghi, O. M. *J. Phys. Chem. C* **2012**, *116*, 13143-13151.
- (5) Zhang, J.-P.; Zhang, Y.-B.; Lin, J.-B.; Chen, X.-M. *Chem. Rev.* **2011**, *112*, 1001-1033.
- (6) Qiu, S.; Zhu, G. *Coord. Chem. Rev.* **2009**, *253*, 2891-2911.
- (7) Férey, G. *Chem. Soc. Rev.* **2008**, *37*, 191-214.
- (8) Jiang, H.-L.; Xu, Q. *Chem. Commun.* **2011**, *47*, 3351-3370.
- (9) Cui, Y.; Yue, Y.; Qian, G.; Chen, B. *Chem. Rev.* **2011**, *112*, 1126-1162.
- (10) Shan, X.-c.; Jiang, F.-l.; Yuan, D.-q.; Zhang, H.-b.; Wu, M.-y.; Chen, L.; Wei, J.; Zhang, S.-q.; Pan, J.; Hong, M.-c. *Chem. Sci.* **2013**, *4*, 1484-1489.
- (11) Liu, Q.-K.; Ma, J.-P.; Dong, Y.-B. *J. Am. Chem. Soc.* **2010**, *132*, 7005-7017.
- (12) Sun, J.-K.; Ji, M.; Chen, C.; Wang, W.-G.; Wang, P.; Chen, R.-P.; Zhang, J. *Chem. Commun.* **2013**, *49*, 1624-1626.
- (13) Li, J.-R.; Kuppler, R. J.; Zhou, H.-C. *Chem. Soc. Rev.* **2009**, *38*, 1477-1504.
- (14) Cram, D. J. *Nature* **1992**, *356*, 29-36.
- (15) Khan, N. A.; Hasan, Z.; Jung, S. H. *J. Haz. Mat.* **2013**, *244*, 444-456.
- (16) Kuppler, R. J.; Timmons, D. J.; Fang, Q.-R.; Li, J.-R.; Makal, T. A.; Young, M. D.; Yuan, D.; Zhao, D.; Zhuang, W.; Zhou, H.-C. *Coord. Chem. Rev.* **2009**, *253*, 3042-3066.
- (17) Song, J.; Luo, Z.; Britt, D. K.; Furukawa, H.; Yaghi, O. M.; Hardcastle, K. I.; Hill, C. L. *J. Am. Chem. Soc.* **2011**, *133*, 16839-16846.
- (18) Wu, C.-D.; Hu, A.; Zhang, L.; Lin, W. *J. Am. Chem. Soc.* **2005**, *127*, 8940-8941.
- (19) Chen, B.; Xiang, S.; Qian, G. *Acc. Chem. Res.* **2010**, *43*, 1115-1124.
- (20) Kreno, L. E.; Leong, K.; Farha, O. K.; Allendorf, M.; Van Deyne, R. P.; Hupp, J. T. *Chem. Rev.* **2012**, *112*, 1105-1125.
- (21) O'Keeffe, M.; Yaghi, O. M. *Chem. Rev.* **2012**, *112*, 675-702.
- (22) Hoskins, B. F.; Robson, R. *J. Am. Chem. Soc.* **1990**, *112*, 1546-1554.
- (23) Eddaoudi, M.; Moler, D. B.; Li, H.; Chen, B.; Reineke, T. M.; O'Keeffe, M.; Yaghi, O. M. *Acc. Chem. Res.* **2001**, *34*, 319-330.
- (24) Zhao, D.; Timmons, D. J.; Yuan, D.; Zhou, H.-C. *Acc. Chem. Res.* **2011**, *44*, 123-133.
- (25) Paz, F. A. A.; Klinowski, J.; Vilela, S. M.; Tome, J. P.; Cavaleiro, J. A. S.; Rocha, J. *Chem. Soc. Rev.* **2012**, *41*, 1088-1110.
- (26) Noh, T. H.; Jung, O.-S. *Acc. Chem. Res.* **2016**, *49*, 1835-1843.
- (27) Luo, L.; Chen, K.; Liu, Q.; Lu, Y.; Okamura, T.-a.; Lv, G.-C.; Zhao, Y.; Sun, W.-Y. *Cryst. Growth Des.* **2013**, *13*, 2312-2321.

- (28) Tranchemontagne, D. J.; Mendoza-Cortés, J. L.; O’Keeffe, M.; Yaghi, O. M. *Chem. Soc. Rev.* **2009**, *38*, 1257-1283.
- (29) Loiseau, T.; Serre, C.; Huguenard, C.; Fink, G.; Taulelle, F.; Henry, M.; Bataille, T.; Férey, G. *Chem.-Eur. J.* **2004**, *10*, 1373-1382.
- (30) Volkringer, C.; Meddouri, M.; Loiseau, T.; Guillou, N.; Marrot, J.; Férey, G.; Haouas, M.; Taulelle, F.; Audebrand, N.; Latroche, M. *Inorg. Chem.* **2008**, *47*, 11892-11901.
- (31) Peng, R.; Li, M.; Li, D. *Coord. Chem. Rev.* **2010**, *254*, 1-18.
- (32) Hu, S.; Zhang, Z.-M.; Meng, Z.-S.; Lin, Z.-J.; Tong, M.-L. *CrystEngComm* **2010**, *12*, 4378-4385.
- (33) Prajapati, R. K.; Verma, S. *Inorg. Chem.* **2011**, *50*, 3180-3182.
- (34) Yang, X.-J.; Li, H.-X.; Xu, Z.-L.; Li, H.-Y.; Ren, Z.-G.; Lang, J.-P. *CrystEngComm* **2012**, *14*, 1641-1652.
- (35) Furukawa, H.; Kim, J.; Ockwig, N. W.; O’Keeffe, M.; Yaghi, O. M. *J. Am. Chem. Soc.* **2008**, *130*, 11650-11661.
- (36) Lu, W.; Wei, Z.; Gu, Z.-Y.; Liu, T.-F.; Park, J.; Park, J.; Tian, J.; Zhang, M.; Zhang, Q.; Gentle III, T.; Bosch, M.; Zhou, H.-C. *Chem. Soc. Rev.* **2014**, *43*, 5561-5593.
- (37) Fereday, A.; Goodgame, D. M.; Lickiss, P. D.; Rooke, S. J.; White, A. J.; Williams, D. J. *Inorg. Chem. Commun.* **2002**, *5*, 805-807.
- (38) Goodgame, D. M.; Lickiss, P. D.; Rooke, S. J.; White, A. J. P.; Williams, D. J. *Inorganica Chim. Acta* **2001**, *324*, 218-231.
- (39) Goodgame, D. M.; Lickiss, P. D.; Rooke, S. J.; White, A. J. P.; Williams, D. J. *Inorganica chim. acta* **2003**, *343*, 61-73.
- (40) Goodgame, D. M.; Kealey, S.; Lickiss, P. D.; White, A. J. P. *J. Mol. Struct.* **2008**, *890*, 232-239.
- (41) Davies, R. P.; Less, R. J.; Lickiss, P. D.; Robertson, K.; White, A. J. P. *Cryst. Growth Des.* **2010**, *10*, 4571-4581.
- (42) Davies, R. P.; Less, R. J.; Lickiss, P. D.; Robertson, K.; White, A. J. P. *Inorg. Chem.* **2008**, *47*, 9958-9964.
- (43) Lambert, J. B.; Liu, Z.; Liu, C. *Organometallics* **2008**, *27*, 1464-1469.
- (44) Wenzel, S. E.; Fischer, M.; Hoffmann, F.; Fröba, M. *Inorg. Chem.* **2009**, *48*, 6559-6565.
- (45) Timokhin, I.; Torres, J. B.; White, A. J. P.; Lickiss, P. D.; Pettinari, C.; Davies, R. P. *Dalton Trans.* **2013**, *42*, 13806-13808.
- (46) Liu, F.-Q.; Tilley, T. D. *Inorg. Chem.* **1997**, *36*, 5090-5096.
- (47) Liu, F.-Q.; Liu, F.-Q.; Tilley, T. D. *Chem. Commun.* **1998**, *0*, 103-104.
- (48) Schmitz, M.; Leininger, S.; Fan, J.; Arif, A. M.; Stang, P. J. *Organometallics* **1999**, *18*, 4817-4824.
- (49) Lee, Y.-A.; Kim, S.-A.; Jung, S.-M.; Jung, O.-S.; Oh, Y.-H. *Bull. Korean Chem. Soc.* **2004**, *25*, 581-583.
- (50) Cha, M.-S.; Park, B.-I.; Kang, H.-J.; Yoo, K.-H.; Jung, O.-S. *Bull. Korean Chem. Soc.* **2007**, *28*, 1057-1059.
- (51) Na, Y.-M.; Kang, H.-J.; Hong, J.; Jung, O.-S. *Bull. Korean Chem. Soc.* **2008**, *29*, 2361-2364.
- (52) Na, Y.-M.; Noh, T.-H.; Ha, B.-J.; Hong, J.-K.; Jung, O.-S. *Bull. Korean Chem. Soc.* **2009**, *30*, 573-576.
- (53) Lee, S.; Lee, H.; Jung, O.-S. *Dalton Trans.* **2017**, *46*, 5843-5847.
- (54) Na, Y. M.; Noh, T. H.; Chun, I. S.; Lee, Y.-A.; Hong, J.; Jung, O.-S. *Inorg. Chem.* **2008**, *47*, 1391-1396.
- (55) Lee, J. W.; Kim, E. A.; Kim, Y. J.; Lee, Y.-A.; Pak, Y.; Jung, O.-S. *Inorg. Chem.* **2005**, *44*, 3151-3155.
- (56) Kim, H.; Lee, H.; Noh, T. H.; Hong, J.; Jung, O.-S. *Inorganica Chim. Acta* **2016**, *443*,

51-56.

- (57) Jung, O.-S.; Kim, Y. J.; Kim, K. M.; Lee, Y.-A. *J. Am. Chem. Soc.* **2002**, *124*, 7906-7907.
- (58) Ryu, M.; Lee, Y.-A.; Jung, O.-S. *J. Mol. Struct.* **2017**, *1144*, 415-420.
- (59) Liu, Z.; Stern, C. L.; Lambert, J. B. *Organometallics* **2008**, *28*, 84-93.
- (60) Zhang, M.; Chen, Y.-P.; Zhou, H.-C. *CrystEngComm* **2013**, *15*, 9544-9552.
- (61) Davies, R. P.; Lickiss, P. D.; Robertson, K.; White, A. J. P. *CrystEngComm* **2012**, *14*, 758-760.
- (62) Timokhin, I.; White, A. J. P.; Lickiss, P. D.; Pettinari, C.; Davies, R. P. *CrystEngComm* **2014**, *16*, 8094-8097.
- (63) Lambert, J. B.; Zhao, Y.; Stern, C. L. *J. Phys. Org. Chem.* **1997**, *10*, 229-232.
- (64) Fournier, J.-H.; Maris, T.; Wuest, J. D.; Guo, W.; Galoppini, E. *J. Am. Chem. Soc.* **2003**, *125*, 1002-1006.
- (65) El-Kaderi, H. M.; Hunt, J. R.; Mendoza-Cortés, J. L.; Côté, A. P.; Taylor, R. E.; O'Keeffe, M.; Yaghi, O. M. *Science* **2007**, *316*, 268-272.
- (66) Rose, M.; Böhlmann, W.; Sabo, M.; Kaskel, S. *Chem. Commun.* **2008**, *0*, 2462-2464.
- (67) Eliášová, P.; Opanasenko, M.; Wheatley, P. S.; Shamzhy, M.; Mazur, M.; Nachtigall, P.; Roth, W. J.; Morris, R. E.; Čejka, J. *Chem. Soc. Rev.* **2015**, *44*, 7177-7206.
- (68) Van Der Voort, P.; Esquivel, D.; De Canck, E.; Goethals, F.; Van Driessche, I.; Romero-Salguero, F. J. *Chem. Soc. Rev.* **2013**, *42*, 3913-3955.
- (69) Croissant, J. G.; Cattoën, X.; Man, M. W. C.; Durand, J.-O.; Khashab, N. M. *Nanoscale* **2015**, *7*, 20318-20334.
- (70) Cordes, D. B.; Lickiss, P. D.; Rataboul, F. *Chem. Rev.* **2010**, *110*, 2081-2173.
- (71) Zhou, H.; Li, J.; Chua, M. H.; Yan, H.; Ye, Q.; Song, J.; Lin, T. T.; Tang, B. Z.; Xu, J. *Chem. Commun.* **2016**, *52*, 12478-12481.
- (72) Lee, Y.-A.; Yoo, K. H.; Park, K.-M.; Jung, O.-S. *Bull. Korean Chem. Soc.* **2002**, *23*, 1839-1841.
- (73) Park, B.-I.; Kim, Y.-J.; Lee, Y.-A.; Park, K.-M.; Jung, O.-S. *Bull. Korean Chem. Soc.* **2004**, *25*, 1969-1972.
- (74) Ahn, J.; Kim, S. M.; Noh, T. H.; Jung, O.-S. *Dalton Trans.* **2011**, *40*, 8520-8522.
- (75) Delmas, L. C.; Horton, P. N.; White, A. J. P.; Coles, S. J.; Lickiss, P. D.; Davies, R. P. *Chem. Commun.* **2017**, *53*, 12524-12527.
- (76) Dvornic, P.; Jones, R.; Ando, W.; Chojnowski, J. *Jones, RG* **2000**, 185-212.
- (77) Magnus, P. J. Wiley and Sons: New York. **2000**
- (78) Kendrick, T.; Parbhoo, B.; White, J. **1989**, 1289-1361.
- (79) Kim, C.; Park, J. *J. Organomet. Chem.* **2001**, *629*, 194-200.
- (80) Denmark, S. E.; Wang, Z. *Org. Lett.* **2001**, *3*, 1073-1076.
- (81) Denmark, S. E.; Wang, Z. *J. Organomet. Chem.* **2001**, *624*, 372-375.
- (82) Mori, A.; Suguro, M. *Synlett* **2001**, *2001*, 0845-0847.
- (83) Maciejewski, H.; Kubicki, M.; Marciniak, B.; Sydor, A. *Polyhedron* **2002**, *21*, 1261-1265.
- (84) Hitchcock, P. B.; Lappert, M. F.; Maciejewski, H. *J. Organomet. Chem.* **2000**, *605*, 221-225.
- (85) Chandra, G.; Lo, P. Y.; Hitchcock, P. B.; Lappert, M. F. *Organometallics* **1987**, *6*, 191-192.
- (86) Harrod, J. F.; Shaver, A.; Tucka, A. *Organometallics* **1985**, *4*, 2166-2170.
- (87) Rybinskaya, M. I.; Rybin, L. V.; Pogrebnyak, A. A.; Nurtdinova, G. V.; Yur'ev, V. P. *J. Organomet. Chem.* **1981**, *217*, 373-383.
- (88) Kinoshita, S.; Watase, S.; Matsukawa, K.; Kaneko, Y. *J. Am. Chem. Soc.* **2015**, *137*, 5061-5065.

- (89) Alonso, B.; González, B.; García, B.; Ramírez-Oliva, E.; Zamora, M.; Casado, C. M.; Cuadrado, I. *J. Organomet. Chem.* **2001**, *637*, 642-652.
- (90) Unno, M.; Chang, S.; Matsumoto, H. *Bull. Chem. Soc. Jap.* **2005**, *78*, 1105-1109.
- (91) Unno, M.; Kawaguchi, Y.; Kishimoto, Y.; Matsumoto, H. *J. Am. Chem. Soc.* **2005**, *127*, 2256-2263.
- (92) Ito, R.; Kakihana, Y.; Kawakami, Y. *Chem. Lett.* **2009**, *38*, 364-365.
- (93) Feher, F. J.; Schwab, J. J.; Soulivong, D.; Ziller, J. W. *Main Group Chem.* **1997**, *2*, 123-132.
- (94) Pozdnyakova, Y. A.; Lyssenko, K. A.; Korlyukov, A. A.; Blagodatskikh, I. V.; Auner, N.; Katsoulis, D.; Shchegolikhina, O. I. *Eur. J. Inorg. Chem.* **2004**, *2004*, 1253-1261.
- (95) Ronchi, M.; Pizzotti, M.; Biroli, A. O.; Macchi, P.; Lucenti, E.; Zucchi, C. *J. Organomet. Chem.* **2007**, *692*, 1788-1798.
- (96) Shchegolikhina, O. I.; Pozdnyakova, Y. A.; Chetverikov, A.; Peregudov, A.; Buzin, M.; Matukhina, E. *Rus. Chem. Bull.* **2007**, *56*, 83-90.
- (97) Pozdnyakova, Y. A.; Korlyukov, A. A.; Kononova, E. G.; Lyssenko, K. A.; Peregudov, A. S.; Shchegolikhina, O. I. *Inorg. Chem.* **2009**, *49*, 572-577.
- (98) Shchegolikhina, O. I.; Pozdnyakova, Y. A.; Molodtsova, Y. A.; Korkin, S. D.; Bukalov, S. S.; Leites, L. A.; Lyssenko, K. A.; Peregudov, A. S.; Auner, N.; Katsoulis, D. E. *Inorg. Chem.* **2002**, *41*, 6892-6904.
- (99) Murugavel, R.; Böttcher, P.; Voigt, A.; Walawalkar, M. G.; Roesky, H. W.; Parisini, E.; Teichert, M.; Noltemeyer, M. *Chem. Commun.* **1996**, 2417-2418.
- (100) Ackerhans, C.; Roesky, H. W.; Labahn, T.; Magull, J. *Organometallics* **2002**, *21*, 3671-3674.
- (101) Yoshizawa, M.; Kusukawa, T.; Fujita, M.; Yamaguchi, K. *J. Am. Chem. Soc.* **2000**, *122*, 6311-6312.
- (102) Yoshizawa, M.; Kusukawa, T.; Fujita, M.; Sakamoto, S.; Yamaguchi, K. *J. Am. Chem. Soc.* **2001**, *123*, 10454-10459.
- (103) Unno, M.; Tanaka, T.; Matsumoto, H. *J. Organomet. Chem.* **2003**, *686*, 175-182.
- (104) Unno, M.; Kishimoto, Y.; Matsumoto, H. *Organometallics* **2004**, *23*, 6221-6224.
- (105) Brown Jr, J. F. *J. Am. Chem. Soc.* **1965**, *87*, 4317-4324.
- (106) Brown Jr, J. F.; Vogt Jr, L. H. *J. Am. Chem. Soc.* **1965**, *87*, 4313-4317.
- (107) Mann, T.; Haley, J.; Lacey, D. *J. Mat. Chem.* **1999**, *9*, 353-360.
- (108) Lewis, L. N.; Stein, J.; Gao, Y.; Colborn, R. E.; Hutchins, G. *Platinum Metals Rev.* **1997**, *41*, 66-75.
- (109) Tamao, K.; Ishida, N.; Tanaka, T.; Kumada, M. *Organometallics* **1983**, *2*, 1694-1696.
- (110) Fleming, I.; Henning, R.; Plaut, H. *J. Chem. Soc. Chem. Commun.* **1984**, 29-31.
- (111) Hatanaka, Y.; Hiyama, T. *J. Org. Chem.* **1988**, *53*, 918-920.
- (112) Denmark, S. E.; Regens, C. S. *Acc. Chem. Res.* **2008**, *41*, 1486-1499.
- (113) Sommer, L.; Pietrusza, E.; Whitmore, F. *J. Am. Chem. Soc.* **1947**, *69*, 188-188.
- (114) Speier, J. L.; Webster, J. A.; Barnes, G. H. *J. Am. Chem. Soc.* **1957**, *79*, 974-979.
- (115) Chalk, A. J.; Harrod, J. *J. Am. Chem. Soc.* **1965**, *87*, 16-21.
- (116) Casado, C. M.; Cuadrado, I.; Moran, M.; Alonso, B.; Lobete, F.; Losada, J. *Organometallics* **1995**, *14*, 2618-2620.
- (117) Bruña, S.; Nieto, D.; González-Vadillo, A. M.; Perles, J.; Cuadrado, I. *Organometallics* **2012**, *31*, 3248-3258.
- (118) Blasco, C.; Bruña, S.; Cuadrado, I.; Delgado, E.; Hernández, E. *Organometallics* **2012**, *31*, 2715-2719.
- (119) Moran, M.; Casado, C. M.; Cuadrado, I.; Losada, J. *Organometallics* **1993**, *12*, 4327-4333.
- (120) Casado, C. M.; Cuadrado, I.; Morán, M.; Alonso, B.; Barranco, M.; Losada, J. *Appl.*

Organometal. Chem. **1999**, *13*, 245–259.

(121) Nakajima, Y.; Shimada, S. *RSC Adv.* **2015**, *5*, 20603-20616.

(122) Marciniak, B.; Waehner, J.; Pawluc, P.; Kubicki, M. *J. Mol. Cat. A: Chem.* **2007**, *265*, 25-31.

(123) Wakatsuki, Y.; Yamazaki, H.; Nakano, M.; Yamamoto, Y. *J. Chem. Soc. Chem. Commun.* **1991**, 703-704.

(124) Marciniak, B. *Coord. Chem. Rev.* **2005**, *249*, 2374-2390.

(125) Marciniak, B.; Walczuk-Guściora, E.; Pietraszuk, C. *Organometallics* **2001**, *20*, 3423-3428.

(126) Marciniak, B.; Walczuk-Guściora, E.; Błazejewska-Chadyniak, P. *J. Mol. Cat. A: Chem.* **2000**, *160*, 165-171.

(127) Marciniak, B.; Kownacki, I.; Kubicki, M. *Organometallics* **2002**, *21*, 3263-3270.

(128) Marciniak, B.; Kownacki, I.; Chadyniak, D. *Inorg. Chem. Commun.* **1999**, *2*, 581-583.

(129) Marciniak, B.; Kujawa, M.; Pietraszuk, C. *Organometallics* **2000**, *19*, 1677-1681.

(130) Marciniak, B.; Kujawa, M.; Pietraszuk, C. *New J. Chem.* **2000**, *24*, 671-675.

(132) Marciniak, B.; Guliński, J. *J. Organomet. Chem.* **1984**, *266*, c19-c21.

(133) Itami, Y.; Marciniak, B.; Kubicki, M. *Organometallics* **2003**, *22*, 3717-3722.

(133) Waehner, J.; Marciniak, B.; Pawluc, P. *Eur. J. Inorg. Chem.* **2007**, *2007*, 2975-2980.

(134) Itami, Y.; Marciniak, B.; Kubicki, M. *Chem.-Eur. J.* **2004**, *10*, 1239-1248.

(135) Żak, P.; Pietraszuk, C.; Marciniak, B.; Spólnik, G.; Danikiewicz, W. *Adv. Synt. Cat.* **2009**, *351*, 2675-2682.

(136) Żak, P.; Dudzic, B.; Kubicki, M.; Marciniak, B. *Chem.-Eur. J.* **2014**, *20*, 9387-9393.

(137) Żak, P.; Skrobańska, M.; Pietraszuk, C.; Marciniak, B. *J. Organomet. Chem.* **2009**, *694*, 1903-1906.

(138) Marciniak, B. *Appl. Organomet. Chem.* **2000**, *14*, 527-538.

(139) Marciniak, B.; Pietraszuk, C.; Kujawa, M. *J. Mol. Cat. A: Chem.* **1998**, *133*, 41-49.

(140) Grubbs, R. H.; O'Leary, D. J. John Wiley & Sons: 2015.

(141) Pietraszuk, C.; Marciniak, B.; Fischer, H. *Organometallics* **2000**, *19*, 913-917.

(142) Pietraszuk, C.; Fischer, H.; Kujawa, M.; Marciniak, B. *Tetrahedron Lett.* **2001**, *42*, 1175-1178.

(143) Pietraszuk, C.; Marciniak, B.; Fischer, H. *Tetrahedron Lett.* **2003**, *44*, 7121-7124.

(144) Pietraszuk, C.; Fischer, H.; Rogalski, S.; Marciniak, B. *J. Organomet. Chem.* **2005**, *690*, 5912-5921.

(145) Grubbs, R. H.; Burk, P. L.; Carr, D. D. *J. Am. Chem. Soc.*, **1975**, *97*, 3265–3267

(146) Denmark, S. E.; Kobayashi, T. *J. Org. Chem.* **2003**, *68*, 5153-5159.

(147) Trzeciak, A. M.; Ziółkowski, J. *J. Coord. Chem. Rev.* **2005**, *249*, 2308-2322.

(148) Oestreich, M. John Wiley & Sons: 2009.

(149) Sellinger, A.; Tamaki, R.; Laine, R. M.; Ueno, K.; Tanabe, H.; Williams, E.; Jabbour, G. E. *Chem. Commun.* **2005**, 3700-3702.

(150) Deluge, M.; Cai, C. *Langmuir* **2005**, *21*, 1917-1922.

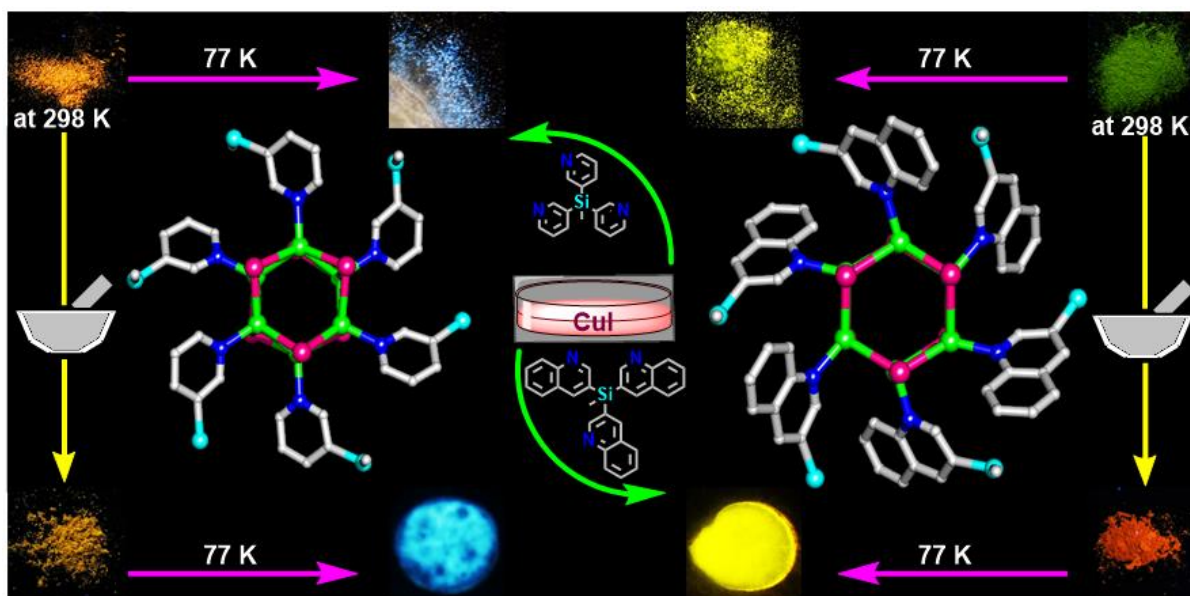
(151) Yamamoto, T.; Asao, T.; Fukumoto, H. *Polymer* **2004**, *45*, 8085-8089.

(152) Heck, R. F.; Nolley Jr, J. *J. Org. Chem.* **1972**, *37*, 2320-2322.

(153) Czech, A.; Ganicz, T.; Noskowska, M.; Stańczyk, W. A.; Szeląg, A. *J. Organomet. Chem.* **2009**, *694*, 3386-3389.

Chapter 2

THERMOCHROMIC AND MECHNOCHROMIC LUMINESCENCE REVERSAL IN ISO-STRUCTURAL 2D-COORDINATION POLYMERS BASED ON Cu_6I_6 CLUSTERS



2.1 Introduction

Luminescent coordination compounds have received immense attention in materials science due to their wide-spread applications in detection and sensing, labeling and opto-electronic display devices.¹ Metal complexes that exhibit stimuli-responsive luminescent properties are attractive from the stand point of fundamental understanding and practical applications.² Noteworthy examples include the polynuclear complexes of Pt(II), Au(I) and Cu(I) ions which are shown to exhibit distinct photophysical properties in response to various external stimuli.³ Thus, they display thermochromism, acidochromism, vapochromism and mechanochromism (also called as piezochromism or tribochromism) in response to the stimuli effects of temperature, pH, solvent vapor and mechanical grinding, respectively.⁴ Such dynamic materials find functional applications such as temperature and pressure sensors, actuators and damage detectors etc.⁵ Donor stabilized Poly-nuclear clusters of copper (I) halides, particularly copper (I) iodide (CuI), moieties are an important family of compounds in this category.⁶ Over the years, these CuI assemblies were obtained in discrete clusters, cages and in some cases infinite metal-organic framework (MOF) structures and shown to exhibit stimuli-responsive multiple emissions derived from their energetically distinct triplet states.⁷ For example, the well-known cubane type Cu₄I₄(Py)₄ (Py = pyridyl) cluster shows two unique triplet emissions at room temperature (298 K) and at low temperature (77 K). Thus at 298 K, it displays a low energy (LE) cluster-centred (³CC) triplet emission at 580 nm ($\lambda_{\text{ex}} = 380 \text{ nm}$) consisting of a mixture of iodide to copper charge transfer (³XMCT) and metal d \rightarrow s,p transitions.^{7e} At 77 K, this band disappears and a new high energy (HE) band at 438 nm ($\lambda_{\text{ex}} = 365 \text{ nm}$) characteristic of iodide to ligand charge transfer (³XLCT) and metal to ligand charge transfer (³MLCT) transitions was obtained. In another report, the Cu₄I₄(PPh₂(CH₂CH=CH₂)₄) cluster, supported by the phosphine ligand, was shown to exhibit both thermochromism and mechanochromism in which the LE ³CC emission was found to be red-shifted by 50 nm upon mechanical grinding.⁸ Although the stimuli-responsive behavior of CuI clusters (especially of thermochromism) is fairly studied through various examples, their emission shifts, color and shift direction are still unpredictable.⁹ In fact, only a limited number of reports are available for the mechanochromic and/or multi-stimuli responsive photo-physical behavior of CuI based clusters and MOFs.¹⁰ MOF materials consisting of CuI clusters and organic linkers are an interesting class of compounds as these clusters can not only give rigidity to the framework but also can impart the desired photo-

physical properties to it.¹¹ Hence in an effort to synthesize and systematically investigate the multi-stimuli responsive behavior of CuI coordination polymers, we set out to employ the CuI salt in reaction with multi-site coordinating ligands based on organo-silicon scaffolds. Herein, I report the synthesis and photo-physical properties of two iso-structural hexameric CuI cluster coordination polymers **1**, {[MeSi(3-Py)₃]₆(Cu₆I₆)}_n and **2**, {[MeSi(3-Qy)₃]₆(Cu₆I₆)}_n starting from the N-donor functionalized tridentate aryl-silane ligands MeSi(3-Py)₃, L¹ and MeSi(3-Qy)₃, L². Use of a main-group element such as silicon as the central atom aids in obtaining identical ligand topologies for various donor functionalities and subsequently has led to the isolation of iso-structural CuI coordination polymers for a systematic investigation of their optical properties. While the coordination polymer **1** displays the usual thermochromism associated with Cu₄I₄Py₄ clusters, the coordination polymer **2** shows only the ³XLCT/³MLCT-emission due to the Cu₆I₆ cluster core at both 298 and 77 K. More interestingly, an unusual mechanochromic emission behavior was observed for these coordination polymers wherein a pronounced blue-shifted HE emission for **1** and red-shifted LE emission for **2** was obtained upon mechanical grinding. To the best of our knowledge, this is the first observation for a mechanochromic luminescence umpolung in iso-structural CuI clusters mediated by variations in cuprophilic interactions. In addition, synthesis and photo-physical properties of two 1D-coordination polymers containing dimeric Cu₂I₂ and monomeric CuI moieties were discussed in this chapter.

2.2 Experimental Section

2.2.1 General remarks

All manipulations were performed under dry atmosphere in standard Schlenk-glassware. CuI, MeSiCl₃, n-BuLi (2.0 M in hexane), 3-bromopyridine and 3-bromoquinoline were purchased from Aldrich and used as received. NMR spectra were recorded on a 400 MHz Jeol FT spectrometer (¹H-NMR: 400 MHz, ¹³C{¹H}-NMR: 100 MHz, ²⁹Si-NMR: 80 MHz) at room temperature using SiMe₄ as external standards. The powder X-ray diffraction data were obtained from a Bruker-D8 Advance diffractometer. Elemental analyses were performed on a Vario-EL cube elemental analyser. FT-IR spectra were taken on a Perkin-Elmer spectrophotometer. The absorption studies were done by a Perkin-Elmer Lambda 45 UV-Visible spectrophotometer; emission and lifetime spectra were recorded on a SPEX Fluorolog HORIBA JOBIN VYON spectrophotometer with a double-grating 0.22 m SPEX 1680

monochromator and a 450W Xe lamp as the excitation source. The excitation and emission spectra of the complexes were corrected at instrumental function. Thermogravimetric analysis (TGA) data was obtained in Perkin-Elmer STA 1000 instrument.

2.2.2 Syntheses

2.2.2.1 Synthesis of ligand MeSi(3-Py)₃ (L¹): To a stirred solution of 3-bromopyridine (9.48 g, 60 mmol) in dry diethylether (80 mL) was added drop wise n-Butyllithium (33 ml 2M, 66 mmol) at -78 °C and the mixture was stirred for 1 h to obtain a yellow suspension. Methyltrichlorosilane (2.98 g, 20 mmol) was added to this suspension at -78 °C under nitrogen atmosphere. The reaction mixture was slowly brought back to room temperature and kept stirring for 12 h. The resulting reaction mixture was diluted with diethyl ether (50 mL) and extracted with distilled water (2 X 100 mL). The organic phase was washed with brine solution (2 X 50 mL), dried over Na₂SO₄ and concentrated to yield 4.8 g of clear yellow-red oily product. The crude product was purified through column chromatography using 60% ethyl acetate in hexane to give 3.6 g of L¹ as a white solid (65%). ¹H NMR (400 MHz, CDCl₃): δ = 0.92 (s, 3H), 7.29 (m, 3H), 7.74 (dt, *J*₁ = 8.0 Hz, *J*₂ = 2.0 Hz, 3H), 8.64 (m, 3H), 8.65 (m, 3H) ppm. ¹³C{¹H}-NMR (100 MHz, CDCl₃): δ 3.92, 123.65, 129.10, 142.73, 151.30, 155.28. ²⁹Si NMR (80 MHz, CDCl₃, Me₄Si): δ -12.21 ppm. MALDI-TOF = 300.0945 [M+Na]⁺ (Expected 300.0933). FT-IR data in powdered sample (cm⁻¹): 1573, 15557, 1474, 1399, 1333, 1258, 1223, 1124, 1027, 813, 717. Anal. calcd. for C₁₆H₁₅N₃Si: C, 69.28; H, 5.45; N, 15.15. Found: C, 69.26; H, 5.47; N, 15.18. Melting point 92.

2.2.2.2 Synthesis of ligand MeSi(3-Qy)₃ (L²): To a stirred solution of 3-bromoquinoline (6.24g, 30 mmol) in dry diethylether (80 mL) was added drop wise n-Butyllithium (17 ml 2M, 34 mmol) at -78 °C and the mixture was stirred for 1 h to obtain a brown suspension. Methyltrichlorosilane (1.49 g, 10 mmol) was added to this suspension at -78 °C under nitrogen atmosphere. The reaction mixture was slowly brought back to room temperature and kept stirring for 12 h. The resulting reaction mixture was diluted with diethyl ether (50 mL) and extracted with distilled water (2 X 100mL). The organic phase was washed with brine solution (2 X 50mL), dried over Na₂SO₄ and concentrated to yield 3.8 g of clear yellow-red oily product. The crude product was purified through column chromatography using 30% ethyl acetate in hexane to give 3.0 g of L² as a yellow-colored oily liquid (70%). ¹H NMR (400 MHz, CDCl₃): δ = 1.19 (s, 3H), 7.56 (m, 3H), 7.75 (m, 3H), 7.78 (m, 3H), 8.14 (d, *J* = 8.0

Hz, 3H), 8.33 (m, 3H), 9.06 (d, $J = 4.0$ Hz 3H) ppm. $^{13}\text{C}\{^1\text{H}\}$ -NMR (100 MHz, CDCl_3): δ 3.39, 126.25, 127.39, 127.71, 128.14, 128.30, 129.50, 130.50, 144.95, 148.80, 153.24. ^{29}Si NMR (80 MHz, CDCl_3 , Me_4Si): δ -11.38 ppm. MALDI-TOF = 450.1235 $[\text{M}+\text{Na}]^+$ (Expected 450.14). FT-IR data in powdered sample (cm^{-1}): 1718, 1700, 1577, 1570, 1559, 1544, 1541, 1534, 1527, 1522, 1500, 1280, 1108, 789. Anal. calcd. for $\text{C}_{16}\text{H}_{15}\text{N}_3\text{Si}$: C, 78.65; H, 4.95; N, 9.83. Found: C, 78.67; H, 4.93; N, 9.80.

2.2.2.3 Synthesis of compound $\{[\text{MeSi}(\mathbf{3}\text{-Py})_3]_6(\text{Cu}_6\text{I}_6)\}_n$ (1): To a solution of \mathbf{L}^1 (20 mg, 0.07 mmol) in DCM (1 mL) kept in a screw-capped vial was added a solution of CuI (41 mg, 0.22 mmol) in acetonitrile (2 mL) with the immediate formation of a yellow precipitate. Then DMF (1 mL) was added to this precipitate and heated at 120 °C under solvothermal condition for 36 h. The resultant solution was slowly cooled to room temperature (at the rate of 0.1 °C per minute) to yield colourless crystals of **1**. Yield: 40 mg (65% based on Cu). FT-IR data in KBr pellet (cm^{-1}): 1581, 1559, 1473, 1396, 1334, 1254, 1227, 1194, 1047, 1029, 810, 790, 744, 703. Anal. calcd. for $\text{C}_{32}\text{H}_{30}\text{Cu}_6\text{I}_6\text{N}_6\text{Si}_2$: C, 22.64; H, 1.78; N, 4.95. Found: C, 22.68; H, 1.75; N, 4.93.

2.2.2.4 Synthesis of Compound $\{[\text{MeSi}(\mathbf{3}\text{-Qy})_3]_6(\text{Cu}_6\text{I}_6)\}_n$ (2): To a solution of \mathbf{L}^2 (20 mg, 0.046 mmol) in DCM (1 mL) kept in a screw-capped vial was added a solution of CuI (27 mg, 0.14 mmol) in acetonitrile (2 mL) with the immediate formation of a yellow precipitate. Then DMF (1 mL) was added to this precipitate and heated at 120 °C under solvothermal condition for 36 h. The resultant solution was slowly cooled to room temperature (at the rate of 0.1 °C per minute) to yield yellowish-green colored crystals of **2**. Yield: 30 mg (65 % based on Cu). FT-IR data in KBr pellet (cm^{-1}): 1616, 1571, 1490, 1375, 1349, 1263, 1193, 1099, 1021, 909, 862, 750, 656. Anal. calcd. for $\text{C}_{56}\text{H}_{42}\text{Cu}_6\text{I}_6\text{N}_6\text{Si}_2$: C, 33.67; H, 2.12; N, 4.21. Found: C, 33.65; H, 2.15; N, 4.25.

2.2.2.5 Synthesis of compound $\{[\text{MeSi}(\mathbf{3}\text{-Qy})_3]_2(\text{Cu}_2\text{I}_2)\}_n$ (3): To a solution of \mathbf{L}^2 (20 mg, 0.046 mmol) in DCM (1 mL) kept in a screw-capped vial was added a solution of CuI (8.7 mg, 0.046 mmol) in acetonitrile (5 mL) with the immediate formation of a yellow precipitate. Then DMF (1 mL) was added to this precipitate and stirred for 12 h at room temperature. The cloudy solution was filtered and the filtrate was concentrated to approximately 2 mL of volume. Reddish orange crystals of **3** were isolated from this solution after 5 days. Yield: 9.5 mg (30 % based on Cu) FT-IR data in KBr pellet (cm^{-1}): 1706, 1675, 1617, 1570, 1491, 1381,

1349, 1262, 1219, 1150, 1098, 1086, 973, 973, 868, 750, 730, 659. Anal. calcd. for C₃₁H₂₈CuIN₄OSi: C, 53.87; H, 4.08; N, 8.11. Found: C, 53.90; H, 4.07; N, 8.13.

2.2.2.6 Synthesis of compound {[MeSi(3-Qy)₃](CuI)}_n (4): To a solution of **L**² (20 mg, 0.046 mmol) in DCM (1 mL) kept in a screw-capped vial was added a solution of CuI (8.7 mg, 0.046 mmol) in acetonitrile (5 mL) with the immediate formation of a yellow precipitate. Then DMF (1 mL) was added to this precipitate and was heated at 120 °C under solvothermal condition for 36 h. The resultant solution was slowly cooled to room temperature (at the rate of 0.1 °C per minute) to yield red-colored crystals of **4**. Yield: 21 mg (75 % based on Cu) FT-IR data in KBr pellet (cm⁻¹): 1706, 1654, 1617, 1570, 1507, 1492, 1374, 1351, 1103, 1103, 1019, 866, 790, 758, 656. Anal. calcd. for C₂₈H₂₁CuIN₃Si: C, 54.46; H, 3.43; N, 6.80. Found: C, 54.45; H, 3.41; N, 6.83.

Synthesis of 2 from 3 (or 4): To a suspension of **3** (10 mg, 0.014 mmol) or **4** (10 mg, 0.016 mmol) in DMF (2 mL), a solution of CuI (6.7 mg, 0.035 mmol) in acetonitrile (1 mL) was added and the resulting mixture was heated at 120 °C under hydrothermal condition for 36 hours. The resultant solutions were slowly cooled to room temperature (at the rate of 0.1 °C per minute) to yield yellowish-green coloured crystals of **2**. Yield: 20 % (5.7 mg).

Synthesis of 4 from 2: To a suspension of **2** (10 mg, 0.005 mmol) in DMF (2 mL), a solution of **L**² (4.27 mg, 0.01 mmol) in DCM (1 mL) was added and the resulting mixture was heated at 120 °C under solvothermal condition for 36 hours. The resultant solutions were slowly cooled to room temperature (at the rate of 0.1 °C per minute) to yield red-coloured crystals of **4**. Yield: 20 % (2.8 mg).

Similarly, quantitative conversion of **3** to **4** and **4** to **3** can be achieved by treating their 2 mL DMF suspensions at 120 and 90 °C, respectively, under solvothermal conditions.

2.2.3 Crystallography

Reflections were collected on a Bruker Smart Apex Duo diffractometer at 100 K using MoK α radiation ($\lambda = 0.71073 \text{ \AA}$) Structures were refined by full-matrix least-squares against F² using all data (SHELX).¹² Crystallographic data for all these compounds are listed in (Table 2.1 and Appendix A2.1). All non-hydrogen atoms were refined anisotropically if not stated otherwise. Hydrogen atoms were constrained in geometric positions to their parent atoms. Some of the aromatic carbon atoms in the structure **3** had slightly bad ellipsoids and hence

were refined with equal anisotropic displacement parameters or partial isotropic refinements.

2.2.4 Lifetime measurements

The luminescent lifetime of L¹, L², **1**, **2**, **3** and **4** were measured at room temperature (289 K) as well as low temperature (77K). The room-temperature phosphorescence decay profiles were fitted to bi- or triexponential curves. The 77 K phosphorescence decay profiles were fitted to monoexponential equations. In all the cases the lifetimes were fitted by using the DAS software. Throughout the manuscript, the lifetimes of bi- or triexponential curves were discussed only with respect to the highest lifetimes for the sake of simplicity.

*Table 2.1: Details of crystallographic data collection and structure refinements for L¹, **1** at 100K, **1** at 298K, **2** at 100K, **2** at 298K, **3** and **4**.*

Compound	L ¹	1 at 100 K	1 at 298 K	2 at 100 K
Chemical formula	C ₁₆ H ₁₅ N ₃ Si	C ₃₂ H ₃₀ Cu ₆ I ₆ N ₆ Si ₂	C ₃₂ H ₃₀ Cu ₆ I ₆ N ₆ Si ₂	C ₅₆ H ₄₂ Cu ₆ I ₆ N ₆ Si ₂
Formula weight	277.40	1697.44	1697.44	1997.77
Temperature	100(2)K	100(2)K	296(2) K	100(2) K
Crystal system	Trigonal	Trigonal	Trigonal	Trigonal
Space group	R-3	R-3c	R-3c	R-3
a (Å); α (°)	13.664(4); 90°	13.310(2); 90°.	13.292(11); 90°.	13.032(2); 90°.
b (Å); β (°)	13.664(4); 90°	13.310(2); 90°.	13.292(11); 90°.	13.032(2); 90°.
c (Å); γ (°)	13.849(4); 120°	41.548(7); 120°.	41.760(4); 120°.	30.206(5); 120°.
V (Å ³); Z	2239.2(15); 4	6375(2) ; 6	6394(5) ; 6	4442.6(15); 3
ρ (calc.) mg m ⁻³	1.234	2.653	2.645	2.240
μ(Mo K _α) mm ⁻¹	0.151	7.397	7.374	5.326
2θ _{max} (°)	56	50	50	56
R(int)	0.0536	0.0553	0.1704	0.0426
Completeness to θ	99.9 %	99.8 %	99.6 %	99.9 %
Data / param.	1248/62	1780/80	1799 / 80	2468 / 116
GOF	1.044	1.049	0.999	1.012
R1 [F>4σ(F)]	0.0795	0.0151	0.0440	0.0486
wR2 (all data)	0.2485	0.0330	0.1046	0.0528
max. peak/hole (e.Å ⁻³)	1.009/-0.544	1.740/-1.681	0.776 /-0.933	0.918/-0.550
Compound	2 at 298 K	3	4	
Chemical formula	C ₅₆ H ₄₂ Cu ₆ I ₆ N ₆ Si ₂	C ₃₁ H ₂₈ CuIN ₄ OSi	C ₂₈ H ₂₁ CuIN ₃ Si	
Formula weight	1997.77	691.10	618.01	
Temperature	296(2) K	100(2) K	100(2) K	
Crystal system	Trigonal	Triclinic	Monoclinic	
Space group	R-3	P-1	P21/n	
a (Å); α (°)	13.076(2); 90°.	10.087(4); 112.29(10)°.	10.668(18); 90°.	
b (Å); β (°)	13.076(2); 90°.	11.412(4); 95.69(9)°.	17.828(3); 92.88(4)°.	
c (Å); γ (°)	30.416(5); 120°.	14.137(6); 99.29(9)°.	13.673(3); 90°.	
V (Å ³); Z	4503.8(16); 3	1462.9(9); 2	2597.1(8); 4	
ρ (calc.) mg m ⁻³	2.210	1.569	1.581	
μ(Mo K _α) mm ⁻¹	5.253	1.874	2.097	
2θ _{max} (°)	62	50	56	
R(int)	0.0924	0.1803	0.0782	
Completeness to θ	99.9 %	96.5 %	99.6 %	
Data / param.	3263 / 116	5105 / 18/355	6422 / 96/308	
GOF	1.000	0.986	1.015	
R1 [F>4σ(F)]	0.0357	0.0556	0.0352	
wR2 (all data)	0.0858	0.1802	0.0841	
max. peak/hole (e.Å ⁻³)	0.818/-1.272	1.778/-2.105	1.556/-1.021	

2.2.5 DFT calculations

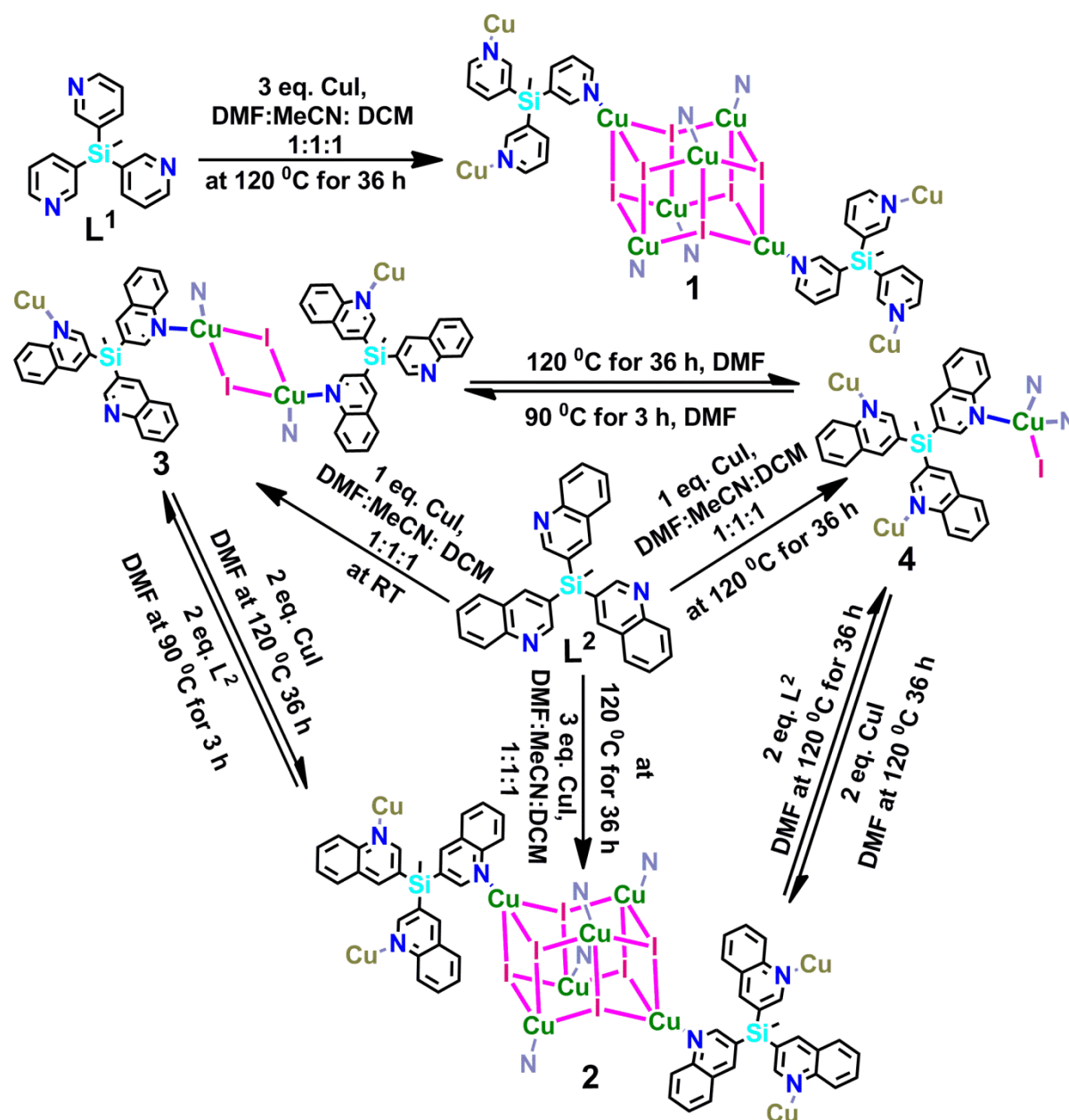
The density functional theory (DFT) calculations have been performed by using Gaussian 09 program package.¹³ The B3LYP exchange-correlation functional was used throughout for all calculations.¹⁴ A combination of basis sets i.e., 6-31g(d) for C, H, N, and Si, and LANL2DZGEN for Cu and I atoms,¹⁵ respectively, were used for the discrete model compounds {[MeSiH₂(3-Py)]₆(Cu₆I₆)} (**1a**) and {[MeSiH₂(3-Qy)]₆(Cu₆I₆)} (**2a**) to obtain the geometry optimization and TDDFT calculations for the excitation energies. The calculated absorption spectra and related MO contributions were obtained from the TDDFT output file and *gausssum* 2.2.6.1.¹⁶ The theoretical emission wavelengths of **1a** and **2a** were derived by single point energy calculations on the optimized triplets as the energy difference between the lowest energy triplet state and its corresponding singlet state.

2.3 Result and Discussion

2.3.1 Syntheses

The precursor ligands L¹ and L² were prepared from the reaction of 3-bromopyridine and 3-bromoquinoline with ⁿBuLi followed by MeSiCl₃, respectively. The ligands were characterized by ²⁹Si NMR, mass spectroscopy, emission spectra and crystallography in case of L¹ (Appendix A2.1-A2.5). Crystals of the cluster coordination polymers **1** and **2** were obtained by the respective reaction of L¹ and L² with 3 equivalents of copper (I) iodide at 120 °C under solvothermal conditions. SC-XRD analysis revealed that both **1** and **2** were obtained as 2D-assemblies consisting of iso-structural hexameric Cu₆I₆ clusters. Use of lower equivalents of the metal salt (CuI) in reaction with L² gave 1D-assemblies having smaller cluster motifs. Thus the 1:1 reaction of L² and CuI at room temperature (RT) and under solvothermal conditions lead to the formation of 1D coordination polymers {[MeSi(3-Qy)₃]₂(Cu₂I₂)}_n **3** and {[MeSi(3-Qy)₃](CuI)}_n **4**, respectively. In fact, **3** is the only compound at RT for all the three stoichiometries. Interestingly, treatment of **3** and **4** with added equivalents of CuI gave rise to the 2D-coordination polymers **2**. Similarly, by increasing the ligand stoichiometry in **2**, clean products of **3** and **4** can be obtained under solvothermal conditions at different temperatures. However, the reaction of L¹ and CuI in all the three stoichiometries at RT as well as under solvothermal conditions results only in the hexameric coordination polymers **1** (scheme 2.1). TGA data shows that coordination polymers **1** and **2** exhibit stabilities above 300 °C; while **3** and **4** starts to decompose around 115 and 210 °C,

respectively (Appendix A2.6).



Scheme 2.1: Reaction schemes and conditions for the formation of the CuI cluster coordination polymers 1-4.

2.3.2 Crystal structures

The molecular structures of **1** and **2** were solved in hexagonal space groups $R\bar{3}c$ and $R\bar{3}$, respectively (Figures 2.1a and 2.1b, Appendix A2.7 and A2.8). The asymmetric unit in both of them consists of one Cu(I) ion, one iodide ion and one third of the ligand moiety. The molecular core of **1** and **2** consists of a hexameric Cu_6I_6 cluster in which each I^- ion acts as a

μ_3 -bridging unit. The Cu(I) ions are located in a tetrahedral coordination consisting of three I^- contacts and one aryl silane N-donor contact. While the Cu_6I_6 clusters, surrounded by the six tripodal ligand segments, act as six-connected nodes, the tridentate silane ligands act as three-connected nodes and associate with three hexameric clusters. The cumulative effect of these interactions is the formation of a 2D-hexagonal sheet structure with the topology of a 'gra' net (Figure 2.1c).¹⁷ The adjacent sheets in **1** are further connected by moderately stronger $\pi\cdots\pi$ interactions (4.105(1) Å) between the 3-Py moieties in addition to a slightly longer intra-sheet $\pi\cdots\pi$ interactions (4.136(0) Å) (Appendix A2.9). Further, a moderate intra-sheet C-H $\cdots\pi$ interactions have been found in **1** (d: 3.467(0) Å, \angle : 133.64°). However, such interactions are very weak in **2** as it exhibits a longer intra-sheet $\pi\cdots\pi$ stacking (4.436(1) Å) between the 3-Qy moieties and the shortest C-H $\cdots\pi$ distance observed in it is at a distance of 4.208(1) Å (Appendix A2.10-A2.12). The unit cell packing diagrams in **1** and **2** reveal the presence of a densely packed structure with almost no void space present in both of them. Although **2** is slightly porous compared to **1**, the measured contact surface and the solvent accessible volumes of $\sim 205 \text{ \AA}^3$ (4.5 % of unit-cell volume) and $\sim 12 \text{ \AA}^3$ (< 1% of unit cell volume), respectively, are very small to accommodate any guest solvent in its solid state packing.

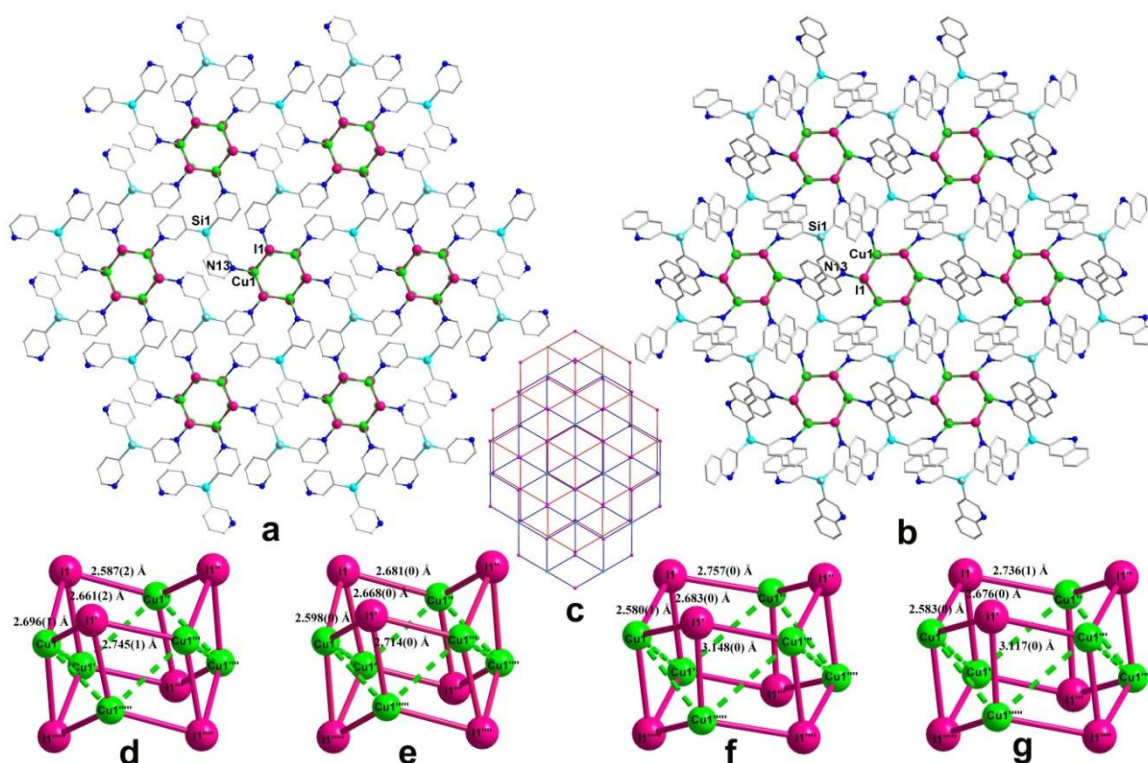


Figure 2.1: (a) Molecular structures of the hexagonal coordination polymers (a) **1** and (b) **2**. (c) Topological view of the hexameric sheets in **1** and **2**. View of the Cu_6I_6 core and the Cu...Cu and Cu-I contact distances in **1** at (d) 298 and (e) 100 K and in **2** at (f) 298 and (g) 100 K.

The crystal structures of **3**·2DMF and **4** were obtained in the triclinic, P-1 and monoclinic, $P2_1/n$ space groups, respectively (Figure 2.2 and 2.3, Appendix A2.13-A2.15). The molecular structure of **3** consists of a dimeric Cu_2I_2 core and two bridging ligand scaffolds of L^2 on either sides of it. The ligand L^2 in **3** acts as a bidentate cisoidal ligand (with respect to the Si-Me group) and connects the adjacent Cu_2I_2 segments leading to the formation of a 1D-chain polymer. The third 3-Qy moiety is non-coordinating and remains above and below the 1D-polymer.

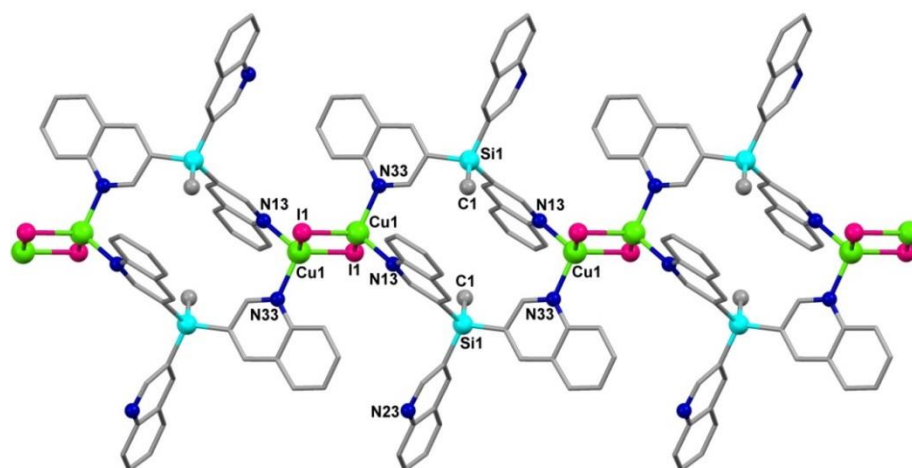


Figure 2.2: Molecular structure of the 1D-coordination polymers **3**

The core structure in **4** consists of a monomeric CuI motif connected by the three N-donor sites of the Ligand L^2 . The Cu(I) atoms are bonded to the three 3-Qy segments originating from three different ligands and one terminal iodide ion. Each ligand is attached to three Cu(I) centers in a pseudo C_3 -symmetric fashion and help the molecule to propagate in a 1D-polymeric structure.

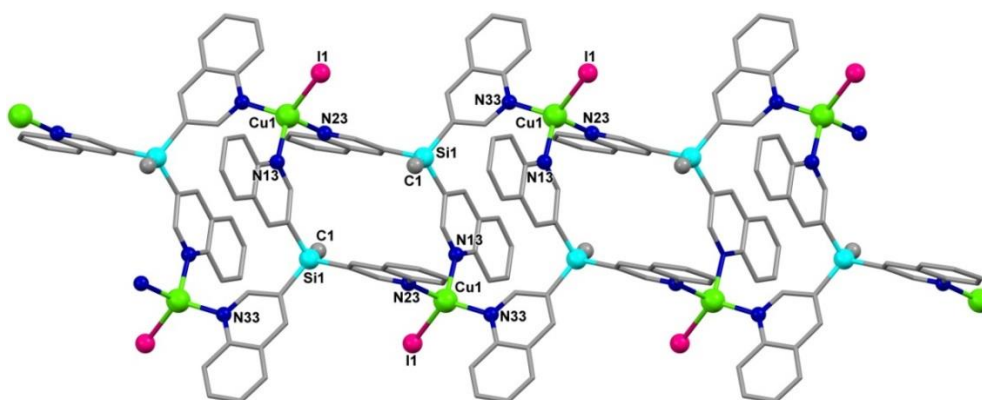


Figure 2.3: Molecular structure of the 1D-coordination polymers **4**.

2.3.3 Photo-physical properties

The respective crystals of **1** and **2** are white and pale-green solids at ambient temperature, which under UV excitation shows orange and green colored emissions (Figures 2.4a, 2.4b, 2.4g and 2.4h). Upon cooling to 77 K, the coordination polymer **1** shows a bluish emission while the coordination polymer **2** shows an intense-yellow emission in the solid state (Figures 2.4c and 2.4i). The original emission colours of **1** and **2** can be recovered again within 2 minutes upon gradually warming the sample to room-temperature indicating a completely reversible thermochromic luminescence in both of them.

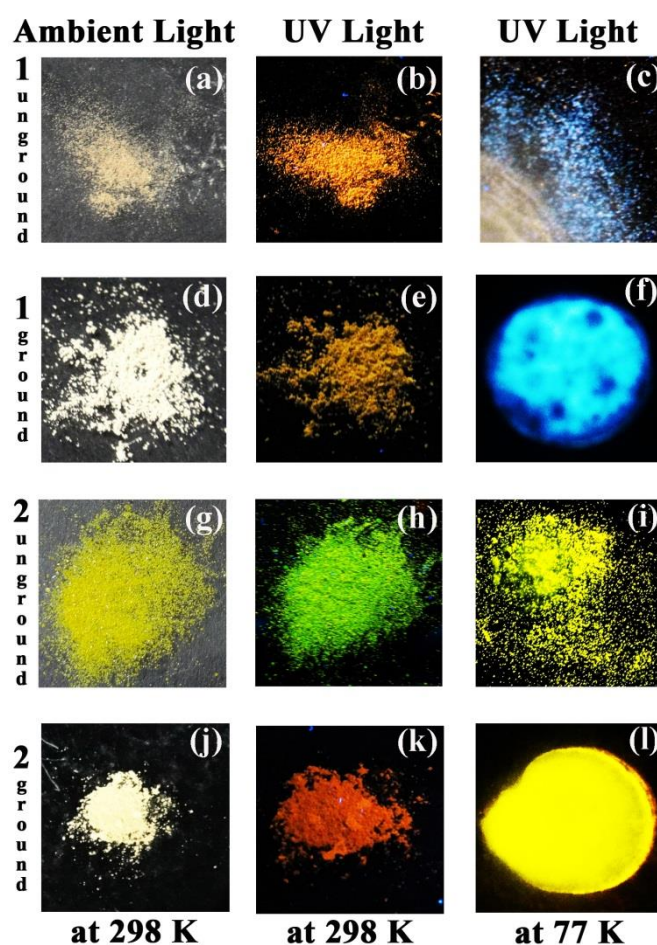


Figure 2.4: Solid State emission colors of various samples of **1** and **2** under ambient light and UV-lamp (irradiated at 365 nm)

To understand these phenomena further, the excitation and emission spectra of **1** and **2** were recorded in the solid state and the corresponding results are summarized in Table 2.2. At 298 K, the emission spectrum of **1** displays an intense LE emission band centered at 611 nm along with a weak HE band at 478 nm ($\lambda_{\text{ex}} = 395$ nm, Appendix A2.16). This LE band is in

agreement with the orange emission observed at room temperature, which can be attributed to the “cluster-centered” (^3CC) emission band characteristic of the traditional $\text{Cu}_4\text{I}_4\text{L}_4$ clusters. While at 77 K the HE band at 478 nm ($\lambda_{\text{ex}} = 375$ nm) is prominently observed with the concomitant quenching of the ^3CC -LE band (Figure 2.5). This HE band is attributed to the $^3\text{XLCT}/^3\text{MLCT}$ transitions similar to those observed for the cubane type $\text{Cu}_4\text{I}_4\text{L}_4$ clusters. The decay measurements in **1** at 298 and 77 K gave the life time (τ_{em}) values of 1.1 and 57 μs , respectively (Figure 2.6).

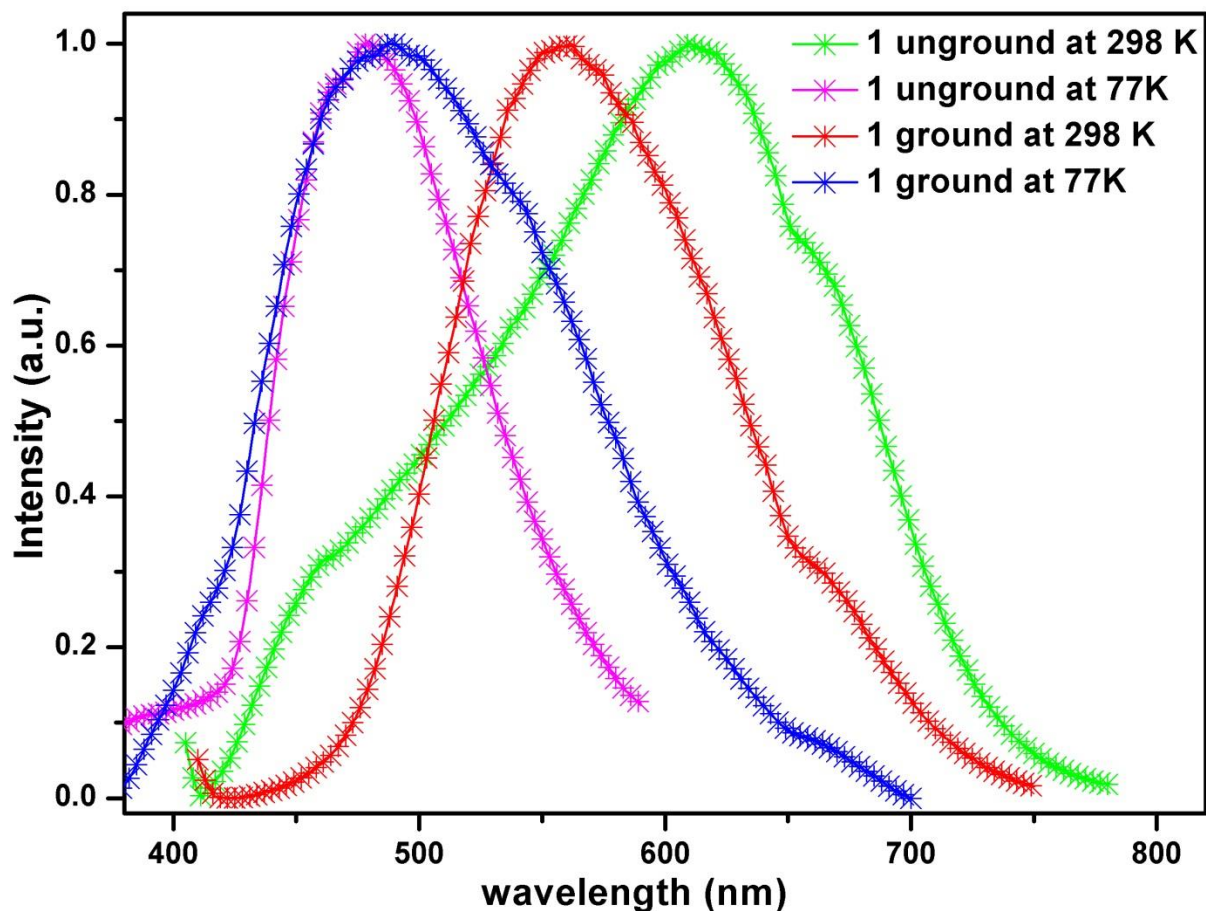


Figure 2.5: Solid-state photoluminescence spectra of **1** in unground and ground states at 298 and 77 K

The emission spectrum of **2** displays a single broad emission band centred at 535 nm ($\lambda_{\text{ex}} = 395$ nm, Appendix A2.17) at 298 K which is red shifted to 566 nm at 77 K (Figure 2.7). Although both **1** and **2** are iso-structural, the emission maxima in them differ by a large factor owing to the disparate Cu-Cu distances present in these two compounds. Thus at 298 K, the observed Cu...Cu distances in **1** and **2** are 2.745(1) and 3.148(0) Å, respectively (the van der Waals radii of Cu(I) is 2.80 Å). These values were found to be marginally lowered at 100 K:

2.714(0) Å in **1** and 3.117(0) Å in **2**. Thus, the origin of the emission signatures in **2** at both 298 and 77 K can be attributed to the ³XLCT/³MLCT transitions and not to the ³CC-transitions, as the Cu...Cu distances in it exceeds 2.80 Å. Though it is rare, there are some examples in literature such as Cu₄I₄(PPh₃)₄ and Cu₄I₄(2-(C₆H₅)₂CH-C₅H₄N)₄ where the ³XLCT/³MLCT transitions are found to occur at room temperature.^{18,7c} Also from the DFT analyses of the ligands and the coordination polymers (vide supra), which shows the presence of low-lying π* orbitals for L² and **2** (because of their conjugated QY rings), it is apparent that **2** can exhibit ³XLCT/³MLCT transitions predominantly. Hence it is clear that the higher wavelength ³CC-emission in **1** in comparison with lower wavelength ³XLCT/³MLCT transition in **2** is due to the shorter Cu...Cu distances present in **1**.^{19,7e} However, upon lowering the temperature to 77 K the emission band in **2** is marginally red shifted as observed by a slight decrease in its Cu...Cu distances. The measured decay values in **2** showed that the life time (τ_{em}) increases from 0.2 μs to 55 μs as the temperature is switched from 298 K to 77 K (Figure 2.6). The photo-physical studies on the 1D-coordination polymers **3** and **4** show no thermochromic behaviour that is associated with the 2D-coordination polymers **1** and **2** (Appendix A2.18 and A2.19). Thus, the observed ³CC-emission bands at 645 and 615 nm in the 298 K luminescence spectra of **3** and **4**, respectively, remained unaltered at 77 K as well (Table 2.2).

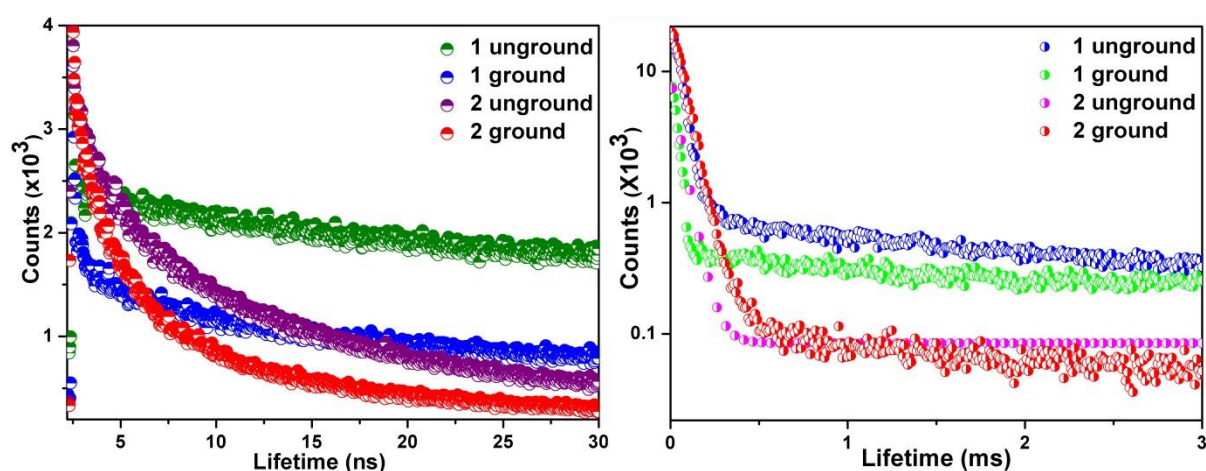


Figure 2.6: Solid-state phosphorescence decay profiles of **1** and **2** in unground and ground states at 298 K (a) and at 77 K (b)

Apart from the thermochromic behaviour, the coordination polymers of **1** and **2** exhibits interesting mechnochromic luminescence properties. Upon grinding the sample of **1** in a mortar, the orange emission of **1** was found to be diminished with a dull yellowish-orange

emission under the UV-lamp (Figures 2.4d and 2.4e). Interestingly, a drastic change of color from green to orange was observed under the UV-lamp for **2** during the mechanical grinding (Appendix A2.20). However, no appreciable color changes were observed for both **1** and **2** under ambient light (Figures 2.4j and 2.4k). The excitation spectra of the respective unground and ground samples of **1** and **2** are closely matching and indicate only minor variations due to temperature or mechanical grinding (Appendix A2.16 and A2.17). When, the ground samples were treated with 0.5 mL of DMF or DCM (heating at 50 °C or sonication) and dried, the original colors of the samples were recovered. This dynamic behaviour of colors was observed for three grinding and solvent recovery cycles confirming the existence of mechanochromism in both of them. In order to understand whether the mechanical grinding has caused any structural fluctuations, the powder X-ray diffraction (PXRD) analysis was performed for the coordination polymers **1** and **2** in various states. The PXRD data of the as-synthesized coordination polymers exhibit well-defined peaks which are in good agreement with the simulated peaks from the single crystal X-ray data. In contrast, the PXRD of the ground samples of **1** and **2** indicate structural changes in the crushed state when compared to the unit-cell parameters obtained from single-crystal data (Appendix Table A2.2).

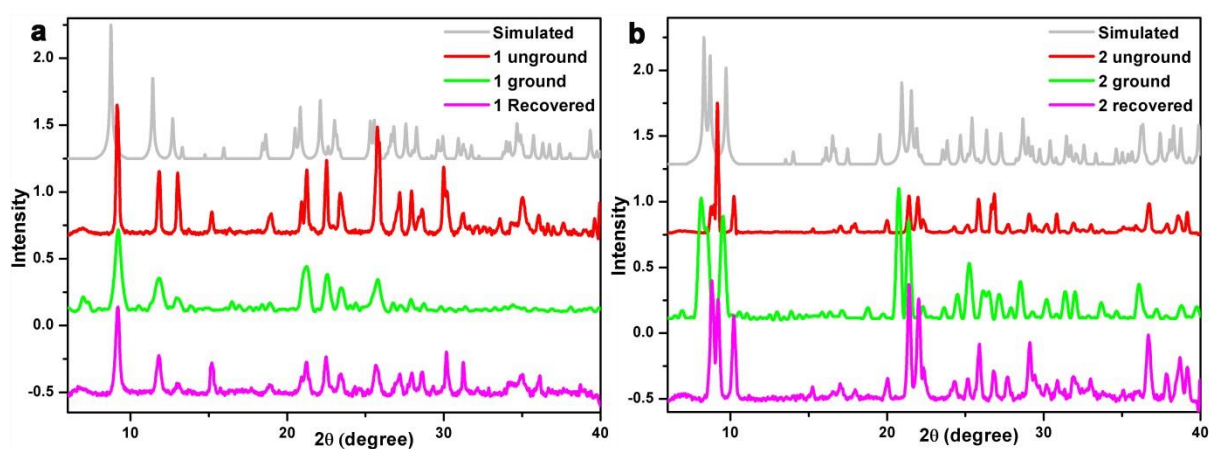
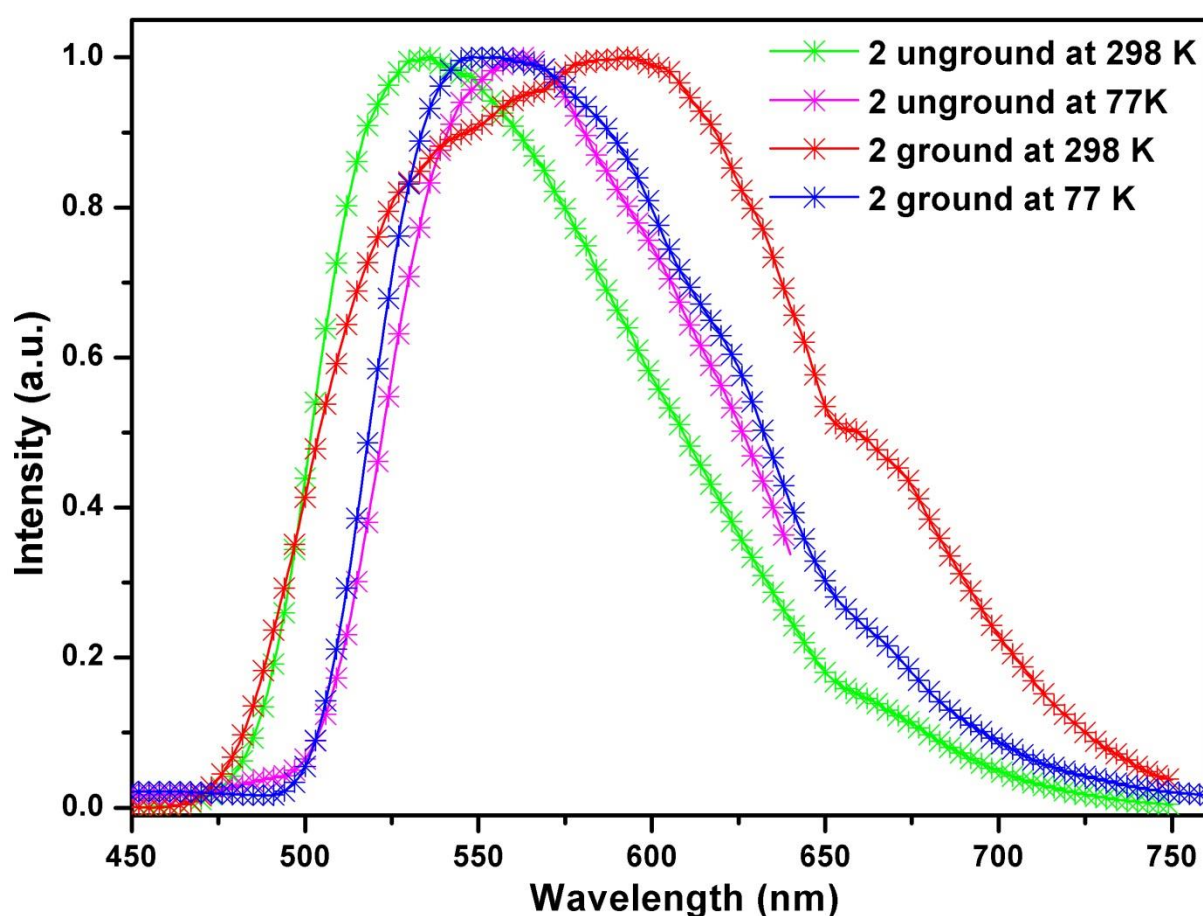


Figure 2.8: PXRD profiles of unground, ground and recovered samples of **1** (a) and **2** (b) at 298 K.

A noteworthy feature was the change in cell parameters along all three axes in the crushed form. This could suggest a slipping of the layers with simultaneous increase or decrease in the inter-layer distances. However, solvent treatment (as described above) has shown to recover the PXRD patterns due to the pristine samples of **1** and **2** (Figure 2.8). Concurrent with these observations, the luminescence band of the ground sample of **1** was found to be

blue shifted to 561 nm (611 nm for the unground sample), while that of the ground sample of **2** was found to be red shifted to 594 nm (535 nm in the unground state). These changes in emission colors accompanied with large Stoke's shifts confirm the presence of mechanochromism in both of them. Furthermore, the ground sample of **1** exhibits thermochromism and gives rise to the emission due to the $^3\text{XLCT}/^3\text{MLCT}$ transitions at 489 nm upon lowering the temperature to 77 K proving that the Cu_6I_6 core of **1** was not destroyed during mechanical grinding. The luminescence lifetime values of 1.2 and 34 μs obtained for the ground sample of **1** at both 298 and 77 K, respectively, are slightly lower than that of the unground sample of **1** (Figure 2.6).



*Figure 2.7: Solid-state photoluminescence spectra of **2** in unground and ground states at 298 and 77 K*

Interestingly the ground sample of **2** exhibits a normal thermochromism (77 K) as that of **1** and gives rise to a new blue shifted luminescence at 548 nm, matching closely with that of the unground sample at 77 K. The decay measurements on $\mathbf{2}_{\text{ground}}$ gave lifetime values of 0.14 μs and 75 μs at 298 and 77 K, respectively (Figure 2.6). These observations suggest that

cuprophilic interactions play a crucial role as the emission bands for the unground and ground samples of **2** at 298 K originate from different triplet states. Thus, grinding the sample of **2** have presumably caused a pronounced change in the Cu...Cu distances as observed from the large positive Stoke's shift. Recently, Perruchas and co-workers have shown from the solid state ⁶⁵Cu NMR data that mechanical grinding significantly modifies the Cu(I) environment in the local structure of a cubane type Cu₄I₄ cluster leading to the contraction of its Cu...Cu contacts.²⁰ Previous DFT calculations on Cu₄I₄ derivatives indicate that the Cu-Cu interactions in the ground state (HOMO) are nonbonding in character, while the excited state (LUMO) predominantly has the Cu-Cu bonding character.^{21,7b,7e} Hence, the origin of the new LE band in **2**_{ground} at 594 nm is due to the ³CC- transitions caused by the shortening of the Cu...Cu distances by mechanical grinding, while **2**_{unground} shows ³XLCT/³MLCT transitions at 298 K. However, at 77 K the ³XLCT/³MLCT transition is seemingly prevalent in both the ground and unground samples of **2** resulting in a yellow emission around 550 nm in both cases. Whereas, the Cu...Cu distances observed in **1**_{unground} (at both 298 K and 77 K) are already below the sum of Cu(I)-Cu(I) van der Waals radii and hence any shortening of the Cu...Cu distances due to mechanical grinding has little influence in further stabilizing its ³CC-excited states. A similar observation can be obtained from the 1D-coordination polymers **3**, with the Cu...Cu distance of 2.754(9) Å in the unground state, displaying no change in its emission maxima (645 nm) upon mechanical grinding. Thus, these observations strongly suggest that the possibility of mechanochromism in these Cu₆I₆ clusters, and may be in other neutral polynuclear Cu_xI_x clusters,^{8,20} is favoured if the Cu...Cu contacts are above the Cu(I) van der Waals radius. However, unlike **2** and other CuI clusters reported before where the emission bands are red shifted after mechanical grinding, there is a blue shift in emission for the coordination polymer **1**. This could presumably be attributed to the raise in the energy level(s) of the LUMO(s) (reduced delocalization of charge) caused by changes in its secondary packing forces such as π...π and C-H... π interactions.²²

Furthermore, the photo-physical characteristics of these 2D-coordination polymers were probed by UV-Visible spectroscopy and DFT calculations. The solid-state diffuse reflectance (DR) spectra of **1** and **2** show two prominent bands for each of these two compounds: around 310 and 395 nm for compound **1** and 310 and 495 nm for the compound **2** (Appendix A2.21). As with most cubane type Cu₄I₄L₄ clusters, the origin of the first high-energy bands are due to ligand π → π* transitions, while the second low-energy bands are due to the cluster based

¹XLCT/¹MLCT transitions. A similar trend has been observed when the absorption spectra of these compounds were recorded in DCM suspensions, albeit the presence of multiple absorption shoulders in the ¹XLCT region for the coordination polymer **2** (Appendix A2.22 and A2.23).

Table 2.2. Photoluminescence data of compounds used in this study

Complex	Temp./K	$\lambda_{\text{ex}}/\text{nm}$	$\lambda_{\text{em}}/\text{nm}$	τ_{em}			
1 _{unground}	298	395	611	0.16 μs			
				1.3 ns			
				1.1 μs			
1 _{ground}	77	375	478	57 μs			
				298	395	561	0.02 μs
				77			1.2 μs
2 _{unground}	298	395	535	1.2 ns			
				77	375	489	34 μs
				298			0.03 μs
2 _{ground}	77	325	566	0.2 μs			
				298	395	594	1.2 ns
							77
3	298	390	645	0.03 μs			
				77	325	548	1.6 ns
				298			75 μs
4	298	390	615	0.03 μs			
				77	390	645	1.4 ns
				298			58 μs
L ¹	298	310	405	0.8 ns			
				77	390	615	4.9 ns
				298			58 μs
L ²	298	310	395	0.8 ns			
				77	310	395	3.4 ns
				298			1.8 ns
	77	310	395, 495	0.2 μs			

2.3.4 DFT calculations

To substantiate these observations, preliminary theoretical calculations were performed on the discrete model compounds **1a** and **2a**. The atomic coordinates from the crystal structures of **1** and **2** were taken for these calculations and then were optimized for the gas phase geometries. A detailed examination of the frontier orbitals on the optimized structures of **1a** and **2a** indicate that the majority of the highest occupied molecular orbitals (**Hs**) were located on the cluster core (up to **H-53** for **1a** and **H-33** for **2a**) featuring the iodine (5p) and copper (3d) orbitals, while most of the lowest unoccupied molecular orbitals (**Ls**) comprise of the

ligand π^* orbitals (up to L+11 for **1a** and L+11 for **2a**). It is interesting to note that the first few LUMO orbitals in **1a** feature isodensity surfaces on all the six Py chromophores, while in **2a** these are located mostly on a single Qy chromophore. The energy separation between the H and L orbitals in **1a** and **2a** are found to be 3.74 and 3.02 eV, respectively (Figure 2.9).

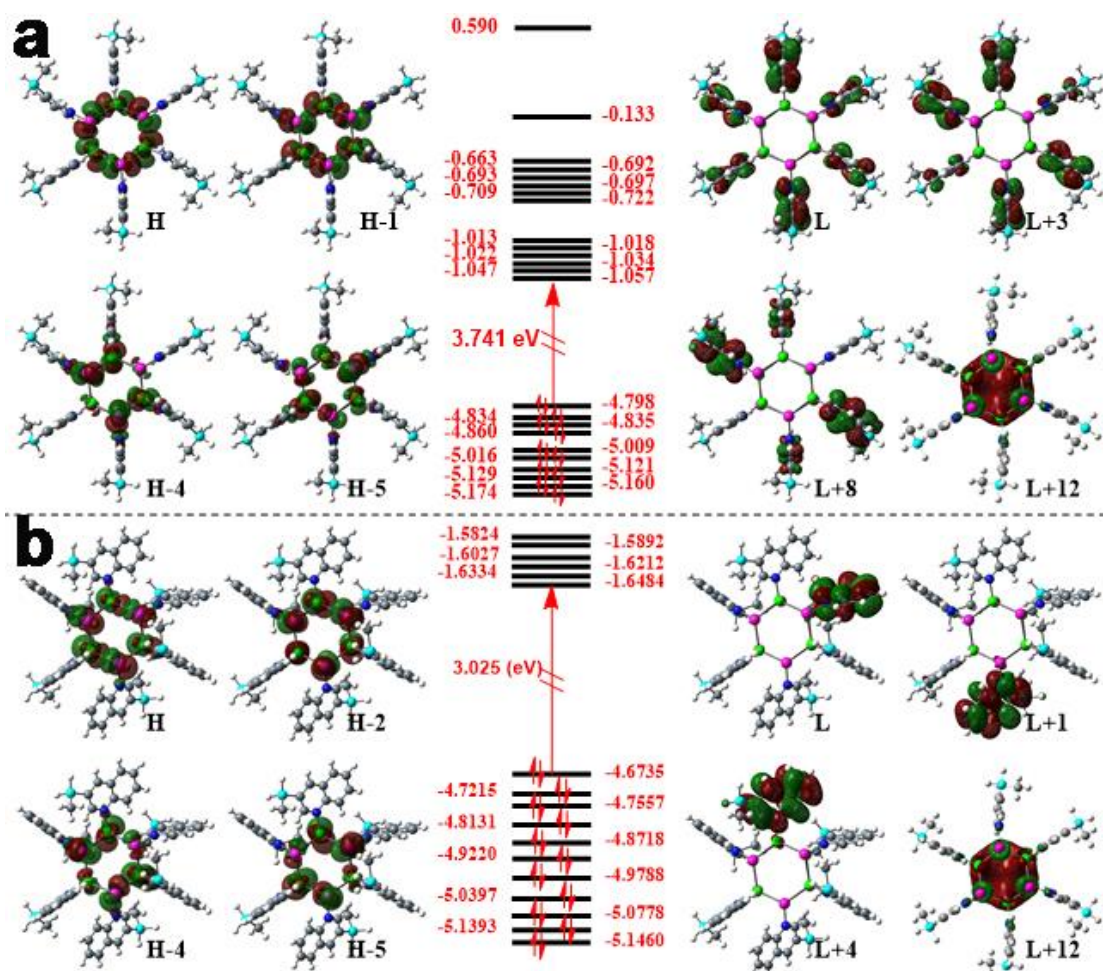


Figure 2.9: DFT derived surface diagrams and energies (in eV) of some relevant molecular orbitals at the S_0 optimized geometry for **1a** (a) and **2a** (b).

The optical properties of the discrete model compounds **1a** and **2a** were further examined by TDDFT calculations and the first 50 transitions were computed. Thus for **1a**, prominent transitions were found between 352 and 348 nm with major contributions from H-1 \rightarrow L+10 ($f = 0.018$), H \rightarrow L+8 ($f = 0.017$), H-5 \rightarrow L+3 ($f = 0.014$), H \rightarrow L+9 ($f = 0.013$) and H-6 \rightarrow L ($f = 0.01$) transitions (Appendix, Table A2.3). These transitions are closely comparable to the observed $^1\text{XLCT}/^1\text{MLCT}$ band centered at 350 nm in DR spectrum of **1**. Interestingly for **2a**, a wide-range of bands were found to occur between 500 and 425 nm with major

contributions from $\mathbf{H} \rightarrow \mathbf{L}+1$ ($f = 0.003$), $\mathbf{H}-1 \rightarrow \mathbf{L}$ ($f = 0.0035$), $\mathbf{H} \rightarrow \mathbf{L}$ ($f = 0.0035$), $\mathbf{H}-2 \rightarrow \mathbf{L}+1$ ($f = 0.0051$), $\mathbf{H}-2 \rightarrow \mathbf{L}+4$ ($f = 0.0065$), $\mathbf{H}-4 \rightarrow \mathbf{L}+4$ ($f = 0.0065$) and $\mathbf{H}-5 \rightarrow \mathbf{L}+5$ ($f = 0.005$) transitions (Appendix, Table A2.4, $f =$ oscillator strength). Many of these theoretically predicted transitions closely match with the prominent absorption bands at 478, 460 and 420 nm in the experimental UV-Visible spectrum of **2** in DCM suspensions. The additional bands at 382 and 525 nm in the solution (DCM suspension) emission spectrum of **2** have not been assigned with any transitions as these regions were not covered in the first 50 TDDFT computed transitions. In order to understand the multiple emission properties of **1** and **2**, triplet state optimizations were performed on **1a** and **2a** by following the approach by De Angelis and co-workers.^{19b} Promotion of an electron in the ligand based π^* LUMO in the S_0 state gives rise to one of the triplet states T_2 . The molecular orbitals of **1a** and **2a** in this state closely match with their corresponding S_0 optimized state except that the Cu...Cu distances in them have significantly elongated in the T_2 state (Appendix, Table A2.5 and A2.6). The emission wavelength from this state, as the adiabatic $S_0 \rightarrow T_2$ gap, can be computed by a single point calculation (Figure 2.10).

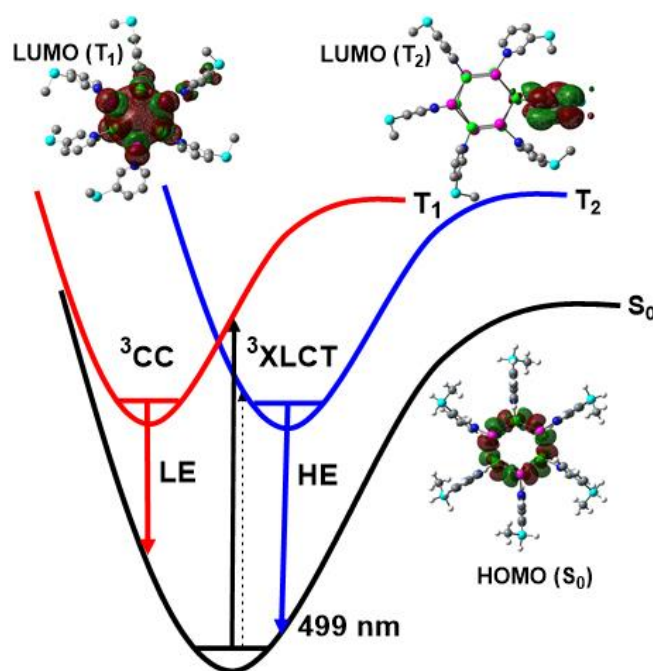


Figure 2.10: Simplified energy level diagram of **1a** cluster. Note that the $S_0 \rightarrow T_1$ gap has not been calculated as the cluster based LUMO could not be lowered below $L+2$ level

Thus for **1a** and **2a** these values were computed to be 499 and 578 nm, respectively, matching closely with the observed 77 K emission bands of **1** (478 nm) and **2** (565 nm) corresponding

to ³XLCT/³MLCT transitions. The other triplet state T₁, which corresponds to the promotion of an electron in the cluster based L+12 of the singlet ground state S₀. In order to access this T₁ state we performed separate optimization processes by progressively reducing Cu...Cu distances in the starting geometry. Thus for **1a**, the cluster based LUMO is lowered from L+12 to L+5 and L+2 upon reducing the Cu...Cu distances from ~2.75 Å (singlet optimized) to 2.65 (also 2.60 and 2.55 Å) and 2.50 Å, respectively. However, we were unable to bring this to the desired lowest level of L even at a distance of 2.50 Å which precludes the computation of the observed 298K ³CC-emission wavelength of **1**.

2.4 Conclusion

In conclusion, by adopting a similar ligand backbone two iso-structural coordination materials featuring Cu₆I₆ clusters have been synthesized and studied for their stimuli-responsive photo-physical properties. In spite of their iso-structural architectures, the coordination polymer **2** exhibits a pronounced mechchromic behavior compared to **1** showing a drastic change of emission color from green to intense-orange. This is attributed to contraction of its Cu...Cu distances to an unknown value closer towards the sum of Cu(I) van der Waals radii. This observation was further substantiated by the emission properties of the 1D-coordination polymer **3** (Cu...Cu distance: 2.741(9) Å) in which no change in emission color was observed upon mechanical grinding. However, the coordination polymer **1**, featuring shorter Cu...Cu contacts (below 2.80 Å), exhibits a slightly blue-shifted emission upon mechanical grinding due to changes in secondary packing forces caused by change in unit-cell parameters. Furthermore, interesting thermochromic behavior has been observed for both **1** and **2** in the ground and unground states as the temperature is lowered to 77 K. The present work demonstrates that CuI containing cluster coordination polymers can display the multi-stimuli responsive photo-physical behaviors that are associated with certain discrete Cu_xI_x clusters. Also, it has been shown that by bringing subtle variations in the ligand backbone it is possible to tune the cuprophilic interactions in iso-structural CuI-coordination polymers and thereby their photo-functional behavior can be altered. Stimuli-responsive coordination polymers featuring CuI cores are a class of smart photo-active materials and have the potential utility in modern opto-electronic devices.

2.5 References

- (1) (a) Pang, J.; Marcotte, E. J. P.; Seward, C.; Brown, R. S.; Wang, S. *Angew. Chem., Int. Ed.* **2001**, *40*, 4042-4045; (b) Keefe, M. H.; Benkstein, K. D.; Hupp, J. T. *Coord. Chem. Rev.* **2000**, *205*, 201-228; (c) Fernández-Moreira, V.; Thorp-Greenwood, F. L.; Coogan, M. P. *Chem. Commun.* **2010**, *46*, 186-202; (d) McLaurin, E. J.; Vlaskin, V. A.; Gamelin, D. R. *J. Am. Chem. Soc.* **2011**, *133*, 14978-14980; (e) Cui, Y.; Xu, H.; Yue, Y.; Guo, Z.; Yu, J.; Chen, Z.; Gao, J.; Yang, Y.; Qian, G.; Chen, B. *J. Am. Chem. Soc.* **2012**, *134*, 3979-3982; (f) Uchiyama, S.; Kawai, N.; de Silva, A. P.; Iwai, K. *J. Am. Chem. Soc.* **2004**, *126*, 3032-3033.
- (2) (a) Wojtecki, R. J.; Meador, M. A.; Rowan, S. J. *Nat. Mater.* **2011**, *10*, 14-27; (b) Sagara, Y.; Kato, T. *Nat. Chem.* **2009**, *1*, 605-610; (c) Schneider, H. J.; Tianjun, L.; Lomadze, N. *Angew. Chem., Int. Ed.* **2003**, *42*, 3544-3546; (d) Ikeda, T.; Mamiya, J. i.; Yu, Y. *Angew. Chem., Int. Ed.* **2007**, *46*, 506-528.
- (3) (a) Huang, L.-M.; Tu, G.-M.; Chi, Y.; Hung, W.-Y.; Song, Y.-C.; Tseng, M.-R.; Chou, P.-T.; Lee, G.-H.; Wong, K.-T.; Cheng, S.-H. *J. Mater. Chem. C* **2013**, *1*, 7582-7592; (b) Choi, S. J.; Kuwabara, J.; Nishimura, Y.; Arai, T.; Kanbara, T. *Chem. Lett.* **2012**, *41*, 65-67; (c) Ni, J.; Zhang, X.; Wu, Y. H.; Zhang, L. Y.; Chen, Z. N. *Chem.-Eur. J.* **2011**, *17*, 1171-1183; (d) Abe, T.; Itakura, T.; Ikeda, N.; Shinozaki, K. *Dalton Trans.* **2009**, 711-715; (e) Kozhevnikov, V. N.; Donnio, B.; Bruce, D. W. *Angew. Chem., Int. Ed.* **2008**, *47*, 6286-6289; (f) Catalano, V. J.; Horner, S. J. *Inorg. Chem.* **2003**, *42*, 8430-8438; (g) Schneider, J.; Lee, Y.-A.; Pérez, J.; Brennessel, W. W.; Flaschenriem, C.; Eisenberg, R. *Inorg. Chem.* **2008**, *47*, 957-968; (h) Ito, H.; Saito, T.; Oshima, N.; Kitamura, N.; Ishizaka, S.; Hinatsu, Y.; Wakeshima, M.; Kato, M.; Tsuge, K.; Sawamura, M. *J. Am. Chem. Soc.* **2008**, *130*, 10044-10045; (i) Lee, Y.-A.; Eisenberg, R. *J. Am. Chem. Soc.* **2003**, *125*, 7778-7779; (j) Laguna, A.; Lasanta, T.; López-de-Luzuriaga, J. M.; Monge, M.; Naumov, P. e.; Olmos, M. E. *J. Am. Chem. Soc.* **2009**, *132*, 456-457; (k) Zhang, J.-X.; He, J.; Yin, Y.-G.; Hu, M.-H.; Li, D.; Huang, X.-C. *Inorg. Chem.* **2008**, *47*, 3471-3473; (l) Dias, H. R.; Diyabalanage, H. V.; Rawashdeh-Omary, M. A.; Franzman, M. A.; Omary, M. A. *J. Am. Chem. Soc.* **2003**, *125*, 12072-12073.
- (4) (a) Malwitz, M. A.; Lim, S. H.; White-Morris, R. L.; Pham, D. M.; Olmstead, M. M.; Balch, A. L. *J. Am. Chem. Soc.* **2012**, *134*, 10885-10893; (b) Lefebvre, J.; Batchelor, R. J.; Leznoff, D. B. *J. Am. Chem. Soc.* **2004**, *126*, 16117-16125; (c) Ni, J.; Zhang, L.-Y.; Wen, H.-M.; Chen, Z.-N. *Chem. Commun.* **2009**, 3801-3803; (d) Wadas, T. J.; Wang, Q.-M.; Kim, Y.-

j.; Flaschenreim, C.; Blanton, T. N.; Eisenberg, R. *J. Am. Chem. Soc.* **2004**, *126*, 16841-16849; (e) Mínguez Espallargas, G.; Brammer, L.; van de Streek, J.; Shankland, K.; Florence, A. J.; Adams, H. *J. Am. Chem. Soc.* **2006**, *128*, 9584-9585; (f) Zhang, X.; Chi, Z.; Zhang, Y.; Liu, S.; Xu, J. *J. Mater. Chem. C* **2013**, *1*, 3376-3390; (g) Shan, X.-c.; Jiang, F.-l.; Yuan, D.-q.; Zhang, H.-b.; Wu, M.-y.; Chen, L.; Wei, J.; Zhang, S.-q.; Pan, J.; Hong, M.-c. *Chem. Sci.* **2013**, *4*, 1484-1489.

(5) (a) Baleizao, C.; Nagl, S.; Schäferling, M.; Berberan-Santos, M. N.; Wolfbeis, O. S. *Anal. Chem.* **2008**, *80*, 6449-6457; (b) Wang, X.-d.; Wolfbeis, O. S.; Meier, R. *J. Chem. Soc. Rev.* **2013**, *42*, 7834-7869; (c) Nagura, K.; Saito, S.; Yusa, H.; Yamawaki, H.; Fujihisa, H.; Sato, H.; Shimoikeda, Y.; Yamaguchi, S. *J. Am. Chem. Soc.* **2013**, *135*, 10322-10325; (d) Sage, I.; Badcock, R.; Humberstone, L.; Geddes, N.; Kemp, M.; Bourhill, G. *Smart materials and structures* **1999**, *8*, 504; (e) Sage, I.; Bourhill, G. *J. Mater. Chem.* **2001**, *11*, 231-245.

(6) Ford, P. C.; Cariati, E.; Bourassa, J. *Chem. Rev.* **1999**, *99*, 3625-3648 and references therein.

(7) (a) Ford, P. C.; Vogler, A. *Acc. Chem. Res.* **1993**, *26*, 220-226; (b) Ford, P. C. *Coord. Chem. Rev.* **1994**, *132*, 129-140; (c) Vitale, M.; Palke, W. E.; Ford, P. C. *J. Chem. Phys.* **1992**, *96*, 8329-8336; (d) Xie, H.; Kinoshita, I.; Karasawa, T.; Kimura, K.; Nishioka, T.; Akai, I.; Kanemoto, K. *J. Chem. Phys. B* **2005**, *109*, 9339-9345; (e) Kyle, K. R.; Ryu, C. K.; Ford, P. C.; DiBenedetto, J. A. *J. Am. Chem. Soc.* **1991**, *113*, 2954-2965; (f) Yadav, A.; Srivastava, A. K.; Balamurugan, A.; Boomishankar, R. *Dalton Trans.* **2014**, *43*, 8166-8169; (g) Sun, D.; Yuan, S.; Wang, H.; Lu, H.-F.; Feng, S.-Y.; Sun, D.-F. *Chem. Commun.* **2013**, *49*, 6152-6154; (h) Perruchas, S.; Desboeufs, N.; Maron, S. b.; Le Goff, X. F.; Fargues, A.; Garcia, A.; Gacoin, T.; Boilot, J.-P. *Inorg. Chem.* **2011**, *51*, 794-798.

(8) Perruchas, S.; Goff, X. F. L.; Maron, S.; Maurin, I.; Guillen, F.; Garcia, A.; Gacoin, T.; Boilot, J.-P. *J. Am. Chem. Soc.* **2010**, *132*, 10967-10969.

(9) (a) Wong, F. H.; Banks, D. S.; Abu-Arish, A.; Fradin, C. *J. Am. Chem. Soc.* **2007**, *129*, 10302-10303; (b) Peng, H.; Stich, M. I.; Yu, J.; Sun, L. n.; Fischer, L. H.; Wolfbeis, O. S. *Adv. Mater.* **2010**, *22*, 716-719; (c) Feng, J.; Tian, K.; Hu, D.; Wang, S.; Li, S.; Zeng, Y.; Li, Y.; Yang, G. *Angew. Chem., Int. Ed.* **2011**, *50*, 8072-8076.

(10) (a) Shan, X.-C.; Zhang, H.-B.; Chen, L.; Wu, M.-Y.; Jiang, F.-L.; Hong, M.-C. *Cryst.*

Growth Des. **2013**, *13*, 1377-1381; (b) Balch, A. L. *Angew. Chem., Int. Ed.* **2009**, *48*, 2641-2644; (c) Shan, X.-C.; Jiang, F.-L.; Chen, L.; Wu, M.-Y.; Pan, J.; Wan, X.-Y.; Hong, M.-C. *J. Mater. Chem. C* **2013**, *1*, 4339-4349.

(11) (a) Gu, X.; Xue, D. *Inorg. Chem.* **2007**, *46*, 5349-5353; (b) Kitagawa, H.; Ozawa, Y.; Toriumi, K. *Chem. Commun.* **2010**, *46*, 6302-6304; (c) Li, M.; Li, Z.; Li, D. *Chem. Commun.* **2008**, 3390-3392; (d) Tzeng, B.-C.; Chang, T.-Y. *Cryst. Growth Des.* **2009**, *9*, 5343-5350; (e) Wang, F.; Yu, R.-M.; Wu, X.-Y.; Lu, C.-Z. *Inorg. Chem. Commun.* **2012**, *19*, 70-72.

(12) Sheldrick, G. M. *Acta Crystallogr.* **2008**, *A64*, 112-122.

(13) Frisch, M. J.; Trucks, G. W.; Schlegel, H. B.; Scuseria, G. E.;

Robb, M. A.; Cheeseman, J. R.; Scalmani, G.; Barone, V.; Mennucci, B.; Petersson, G. A.; Nakatsuji, H.; Caricato, M.; Li, X.; Hratchian, H. P.; Izmaylov, A. F.; Bloino, J.; Zheng, G.; Sonnenberg, J. L.; Hada, M.; Ehara, M.; Toyota, K.; Fukuda, R.; Hasegawa, J.; Ishida, M.; Nakajima, T.; Honda, Y.; Kitao, O.; Nakai, H.; Vreven, T.; Montgomery, J. A.; Jr., Peralta, J. E.; Ogliaro, F.; Bearpark, M.; Heyd, J. J.; Brothers, E.; Kudin, K. N.; Staroverov, V. N.; Keith, T.; Kobayashi, R.; Normand, J.; Raghavachari, K.; Rendell, A.; Burant, J. C.; Iyengar, S. S.; Tomasi, J.; Cossi, M.; Rega, N.; Millam, J. M.; Klene, M.; Knox, J. E.; Cross, J. B.; Bakken, V.; Adamo, C.; Jaramillo, J.; Gomperts, R.; Stratmann, R. E.; Yazyev, O.; Austin, A. J.; Cammi, R.; Pomelli, C.; Ochterski, J. W.; Martin, R. L.; Morokuma, K.; Zakrzewski, V. G.; Voth, G. A.; Salvador, P.; Dannenberg, J. J.; Dapprich, S.; Daniels, A. D.; Gaussian 09, Revision C.01 Gaussian, Inc.: Wallingford, CT, **2013**.

(14) Becke, A. D. *J. chem. phys.* **1993**, *98*, 5648-5652.

(15) Hay, P. J.; Wadt, W. R. *J. chem. phys.* **1985**, *82*, 270-280.

(16) O'boyle, N. M.; Tenderholt, A. L.; Langner, K. M. *J. comput. chem.* **2008**, *29*, 839-845.

(17) (a) O'Keeffe, M.; Yaghi, O. M. *Chem. Rev.* **2012**, *112*, 675-702; (b) Blatov, V. A.; Shevchenko, A. P.; Proserpio, D. M. *Cryst. Growth Des.* **2014**, *14*, 3576-3586; (c) Blatov, V.; Shevchenko, A.; Serezhkin, V.; Korchagin, D. <http://www.topos.ssu.samara.ru.>

(18) (a) Ryu, C. K.; Vitale, M.; Ford, P. C. *Inorg. Chem.* **1993**, *32*, 869-874; (b) Perruchas, S.; Tard, C.; Le Goff, X. F.; Fargues, A.; Garcia, A.; Kahlal, S.; Saillard, J.-Y.; Gacoin, T.;

Boilot, J.-P. *Inorg. Chem.* **2011**, *50*, 10682-10692; (c) Kyle, K. R.; Ford, P. C. *J. Am. Chem. Soc.* **1989**, *111*, 5005-5006.

(19) (a) Kim, T. H.; Shin, Y. W.; Jung, J. H.; Kim, J. S.; Kim, J. *Angew. Chem., Int. Ed.* **2008**, *47*, 685-688; (b) De Angelis, F.; Fantacci, S.; Sgamellotti, A.; Cariati, E.; Ugo, R.; Ford, P. C. *Inorg. Chem.* **2006**, *45*, 10576-10584.

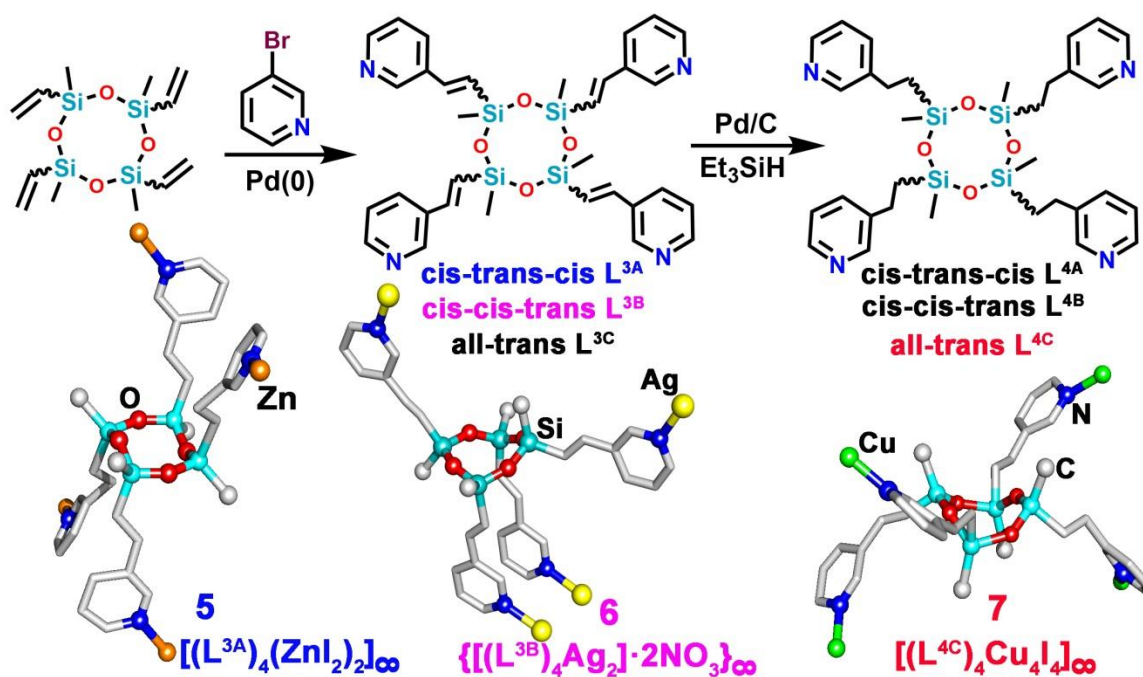
(20) Benito, Q.; Le Goff, X. F.; Maron, S. b.; Fargues, A.; Garcia, A.; Martineau, C.; Taulelle, F.; Kahlal, S.; Gacoin, T.; Boilot, J.-P. *J. Am. Chem. Soc.* **2014**, *136*, 11311-11320.

(21) (a) Vitale, M.; Ryu, C. K.; Palke, W. E.; Ford, P. C. *Inorg. Chem.* **1994**, *33*, 561-566; (b) Vega, A.; Saillard, J.-Y. *Inorg. Chem.* **2004**, *43*, 4012-4018; (c) Mealli, C.; Godinho, S. S.; Calhorda, M. J. *Organometallics* **2001**, *20*, 1734.

(22) (a) Chung, J. W.; You, Y.; Huh, H. S.; An, B.-K.; Yoon, S.-J.; Kim, S. H.; Lee, S. W.; Park, S. Y. *J. Am. Chem. Soc.* **2009**, *131*, 8163-8172; (b) Mizukami, S.; Houjou, H.; Sugaya, K.; Koyama, E.; Tokuhisa, H.; Sasaki, T.; Kanosato, M. *Chem. Mater.* **2005**, *17*, 50-56; (c) Crenshaw, B. R.; Weder, C. *Chem. Mater.* **2003**, *15*, 4717-4724; (d) Tzeng, B. C.; Chang, T. Y.; Sheu, H. S. *Chem.- Eur. J.* **2010**, *16*, 9990-9993; (e) Kojima, M.; Taguchi, H.; Tsuchimoto, M.; Nakajima, K. *Coord. Chem. Rev.* **2003**, *237*, 183-196.

Chapter 3

STEREOCHEMICALLY DISTINCT CYCLOTETRASILOXANES CONTAINING 3-PYRIDYL MOIETIES AND THEIR FUNCTIONAL COORDINATION POLYMERS



3.1 Introduction

The design and synthesis of new materials based on peripherally functionalized siloxanes have received considerable attention in materials science.¹ This is primarily due to the similarities of the cyclic and cage siloxanes as small-molecule mimics for the silica-containing surfaces which exhibit diverse properties and functional behavior.²⁻⁴ One of the hallmark properties of the silica surfaces is the ability to host various metal ions on their surface for applications in heterogeneous catalysis and materials development.⁵ Thus, it would be interesting to mimic the structural and functional behavior of metallated silica surfaces by preparing metal complexes of peripherally functionalized cyclic and cage siloxanes. Also, metal complexes of such higher siloxanes would give enormous molecular level and structural insights for metal-containing surfaces and hybrid motifs containing metal-organic materials and silica surfaces. However, owing to the difficulties associated with obtaining crystalline solids, use of these scaffolds as ligand platforms/templates in building metal-containing assemblies has been limited to a very small number of systems such as the ones synthesized from silicon bound hydroxyl functionalities,⁶ a Ni(0) complex supported by the Si-bound vinyl groups, $[(\text{Ni}(\text{P}\{\text{C}_6\text{H}_4\text{Me}_4\}_3)_2\{\mu\text{-CH}_2=\text{CH}(\text{Me})\text{Si}(\mu\text{-O})\}_4)]$,⁷ and a Pt(II) complex of a mono-terpyridyl functionalized polyhedral oligomeric silsesquioxane (POSS).⁸ Apart from these, metal complexes of peripherally functionalized siloxane based ligands have been mostly restricted only to a simple disiloxane backbone. For instance, some interesting metal complexes of pyridyl group tethered disiloxanes and metalladisiloxanes with π -systems and azo functionalities as additional donors are known in the literature.⁹ In addition, cyclosiloxanes exist as a mixture of two or more stereoisomers complicating the quantitative purification and isolation of the obtained metal complexes.¹⁰ For example, the tetrahydroxy cyclotetrasiloxane $[\text{Pr}(\text{OH})\text{SiO}]_4$ is a stochastic mixture of four different isomers in *all-cis*, *all-trans*, *cis-trans-cis* and *cis-cis-trans* geometries.¹¹ In spite of these issues, we set out to employ peripherally functionalized cyclotetrasiloxane motif as anchor for obtaining multinuclear metal complexes and frameworks since it emulates as a medium-sized building block for polymeric siloxanes and can provide better control during metalation reactions in comparison with the fully functionalized octameric POSS.¹²

Herein, I report the synthesis, separation and conversion of the stereoisomers of 3-pyridyl functionalized cyclotetrasiloxane ligands, $[\text{MeSiO}(\text{CH}=\text{CH}3\text{-Py})]_4$ (L^3) and $[\text{MeSiO}(\text{CH}_2\text{CH}_23\text{-Py})]_4$ (L^4). Three isomers have been isolated for each of these ligands in

cis-trans-cis (L^{3A} and L^{4A}), *cis-cis-trans* (L^{3B} and L^{4B}), and *all-trans* (L^{3C} and L^{4C}) geometries (scheme 3.1). The existence of these isomers has been probed by ^1H , ^{13}C , and ^{29}Si NMR spectroscopy. Further, their stereochemistry has been unambiguously confirmed by the single crystal X-ray analysis of some of their corresponding complexes **5**, $[(L^{3A})(\text{ZnI}_2)_2]_\infty$, **6**, $\{[(L^{3B})\text{Ag}_2] \cdot 2\text{NO}_3 \cdot \text{H}_2\text{O} \cdot \text{CH}_3\text{OH}\}_\infty$, **7**, $[(L^{4C})\text{Cu}_4\text{I}_4]_\infty$ and **8**, $\{[(L^{3A})(\text{Cd}(\text{NO}_3)_2) \cdot \text{THF}]\}_\infty$. Interestingly, the conversion of *cis-trans-cis* to *all-trans* isomer has been obtained by the reaction of *cis-trans-cis* isomer (L^{3A}) with $\text{Cd}(\text{NO}_3)_2 \cdot 4\text{H}_2\text{O}$ and biphenyl-4,4'-dicarboxylic acid (bpdc-2H) under solvothermal conditions which gave a 2D-coordination polymer **9**, $\{[(L^{3C})\text{Cd}_2(\text{bpdc})_2] \cdot \text{DMF}\}_\infty$ with change in the stereochemical configuration of ligands to all trans isomer. Separation of stereoisomers of cyclosiloxanes is a challenging task and the metal complexes reported based on these ligands is the first instance, to the best of our knowledge, where topologically unique coordination polymers have been isolated from stereochemically distinct cyclosiloxane scaffolds.

3.2 Experimental Section

3.2.1 General remarks

All manipulations were performed under a dry atmosphere in standard Schlenk-glassware. 2,4,6,8-Tetramethyl-2,4,6,8-tetravinyl-cyclotetrasiloxane (D_4^{Vi}), 3-bromopyridine, Bis(tert-butylphosphine)palladium(0) ($\text{Pd}[\text{t-Bu}_3\text{P}]_2$), CuI , ZnI_2 , AgNO_3 and $\text{Cd}(\text{NO}_3)_2 \cdot 4\text{H}_2\text{O}$ were purchased from Aldrich and used as received. NMR spectra were recorded on a 400 MHz Bruker FT spectrometer (^1H -NMR: 400 MHz, $^{13}\text{C}\{^1\text{H}\}$ -NMR: 100 MHz, ^{29}Si -NMR: 80 MHz) at room temperature using SiMe_4 as external standards. FT-IR spectra were taken on a Perkin-Elmer spectrophotometer. Thermal gravimetric analysis (TGA) data were obtained from a PerkinElmer STA-6000 thermogravimetric analyzer. The differential scanning calorimetric (DSC) data were recorded on a TA Instruments Q20 model instrument. The absorption and emission studies were done by a Perkin-Elmer Lambda 45 UV-Visible spectrophotometer and SPEX Fluorolog HORIBA JOBIN VYON fluorescence spectrophotometer with a double-grating 0.22 m SPEX 1680 monochromator and a 450W Xe lamp as the excitation source. The excitation and emission spectra of the complexes were corrected at the instrumental function.

3.2.2 Syntheses

3.2.2.1 Synthesis of ligand [MeSiO(CH=CH3-Py)]₄ (L³): 3-Bromopyridine (7.18 g 44 mmol) and D₄^{Vi} (3.92 g, 11 mmol) were kept under nitrogen in a 250 ml two neck round bottom flask, equipped with magnetic stirrer and reflux condenser. The flask was purged with nitrogen for 15 min at room temperature, and then 15 ml of triethylamine and Pd[t-Bu₃P]₂ (20 mg, 0.1 mmol) were added. The reaction mixture was then stirred at 90 °C for 96 h. After cooling to room temperature, hexane (50 ml) was added and the mixture was washed with water in a separating funnel. The organic layer was separated, filtered through celite and evaporated in vacuum, to yield 60% of the crude L³ as a yellowish-brown oily compound. The crude mixture was purified by column chromatography using tetrahydrofuran and chloroform (20:80) as eluent which gave three stereoisomers of L³, namely the *cis-trans-cis* L^{3A}, *cis-cis-trans* L^{3B} and *all-trans* L^{3C}, in the respective 35, 60 and 5% compositions.

L^{3A}: ¹H NMR (400 MHz, CDCl₃): δ = 8.63 (s, 4H), 8.50 (d, *J* = 4.0 Hz, 4H), 7.73 (d, *J* = 8.0 Hz, 4H), 7.24 (dd, *J*₁ = 4.0 Hz, *J*₂ = 4.0 Hz, 4H), 7.09 (d, *J* = 20.0 Hz, 4H), 6.46 (d, *J* = 20.0 Hz, 4H), 0.37 (s, 12H) ppm. ¹³C{¹H}-NMR (100 MHz, CDCl₃): δ -0.26, 123.52, 127.67, 132.90, 133.04, 142.64, 148.74, 149.56. ²⁹Si NMR (80 MHz, CDCl₃, Me₄Si): δ -31.22 (s, 4Si) ppm MALDI-TOF *m/z* = 675.1517 [M+Na] (Expected 675.17). FT-IR data in powdered sample (cm⁻¹): 2961, 2926, 2853, 1609, 1566, 1474, 1411, 1384, 1261, 1207, 1065, 824, 781, 704. Anal. Calcd for C₃₂H₃₆N₄O₄Si₄: C, 58.86; H, 5.56; N, 8.58. Found: C, 58.65; H, 5.75; N, 8.45.

L^{3B}: ¹H NMR (400 MHz, CDCl₃): δ = 8.71 (s, 1H), 8.57 (m, 4H), 8.49 (m, 3H), 7.83 (d, *J* = 8.0 Hz, 1H), 7.66 (m, 3H), 7.32 (m, 1H), 7.20 (m, 3H), 7.09 (m, 4H), 6.46 (m, 4H), 0.37, (s, 3H) 0.38, (s, 3H) 0.40 (s, 6H) ppm. ¹³C{¹H}-NMR (100 MHz, CDCl₃): δ -0.32, -0.16, 123.50, 127.63, 127.69, 132.80, 132.69, 133.02, 148.68, 148.80, 149.51. ²⁹Si NMR (80 MHz, CDCl₃, Me₄Si): δ -31.26, (s, 1Si), -31.14, (s, 2Si) -31.07 (s, 1Si) ppm MALDI-TOF *m/z* = 653.2097 [M+H] (Expected 654.01). FT-IR data in powdered sample (cm⁻¹): 2961, 2926, 2853, 1609, 1566, 1474, 1411, 1384, 1261, 1207, 1065, 824, 781, 704. Anal. Calcd for C₃₂H₃₆N₄O₄Si₄: C, 58.86; H, 5.56; N, 8.58. Found: C, 58.59; H, 5.64; N, 8.40.

L^{3C}: ¹H NMR (400 MHz, CDCl₃): δ = 8.53 (s, 4H), 8.48 (s, 4H), 7.58 (d, *J* = 8.0 Hz, 4H), 7.16 (d, *J* = 4.0 Hz, 4H), 7.06 (d, *J* = 20.0 Hz, 4H), 6.44 (d, *J* = 20.0 Hz, 4H), 0.42 (s, 12H) ppm. ¹³C{¹H}-NMR (100 MHz, CDCl₃): δ -0.26, 123.52, 127.67, 132.90, 133.04, 142.64, 148.74, 149.56. ²⁹Si NMR (80 MHz, CDCl₃, Me₄Si): δ -31.20 (s, 4Si) ppm MALDI-TOF *m/z*

= 675.2520 [M+Na] (Expected 675.17). FT-IR data in powdered sample (cm^{-1}): 2961, 2926, 2853, 1609, 1566, 1474, 1411, 1384, 1261, 1207, 1065, 824, 781, 704. Anal. Calcd for $\text{C}_{32}\text{H}_{36}\text{N}_4\text{O}_4\text{Si}_4$: C, 58.86; H, 5.56; N, 8.58. Found: C, 58.55; H, 5.65; N, 8.55.

3.2.2.2 Synthesis of ligand $[\text{MeSiO}(\text{CH}_2\text{CH}_2\text{3-Py})_4 (\text{L}^4)$: To a stirred mixture of the ligand L^3 ($\text{L}^{3\text{A}}$ or $\text{L}^{3\text{B}}$ or $\text{L}^{3\text{C}}$) (0.25 g, 0.38 mmol) and 10% palladium on carbon (2.5 mg) in MeOH (5-10 mL) taken in a two-necked round bottom flask at room temperature under inert atmosphere, triethylsilane (1.8 g, 15 mmol) was added drop-wise from a pressure-equalizing funnel. When the reaction was complete (TLC), the mixture was filtered through celite and the solvent was removed in vacuo. The product was purified by using a short silica gel column to yield the respective products of L^4 .

$\text{L}^{4\text{A}}$: ^1H NMR (400 MHz, CDCl_3): δ = 8.47 (s, 4H), 8.44 (d, J = 1.2 Hz, 4H), 7.51 (d, J = 8.0 Hz, 4H), 7.21 (m, 4H), 2.69 (t, J = 8.0 Hz, 8H), 0.93 (t, J_1 = 8.0 Hz, J_2 = 8.0 Hz, 8H), 0.14 (s, 12H) ppm. $^{13}\text{C}\{^1\text{H}\}$ -NMR (100 MHz, CDCl_3): δ -0.57, 18.55, 26.32, 123.32, 135.18, 139.41, 147.26, 149.46. ^{29}Si NMR (80 MHz, CDCl_3 , Me_4Si): δ -20.43 ppm. MALDI-TOF m/z = 683.2113 [M+Na] (Expected 683.23). FT-IR data in powdered sample (cm^{-1}): 2960, 2925, 2915, 1478, 1424, 1383, 1261, 1186, 1080, 1027, 796, 714. Anal. Calcd for $\text{C}_{32}\text{H}_{44}\text{N}_4\text{O}_4\text{Si}_4$: C, 58.14; H, 6.71; N, 8.48. Found: C, 58.44; H, 6.59; N, 8.49.

$\text{L}^{4\text{B}}$: ^1H NMR (400 MHz, CDCl_3): δ = 8.43 (s, 4H), 8.40 (d, J = 1.2 Hz, 4H), 7.49 (m, 4H), 7.18 (m, 4H), 2.66 (t, J_1 = 4.0 Hz, J_2 = 4.0 Hz, 8H), 0.90 (m, 8H) 0.12 (s, 12H) ppm. $^{13}\text{C}\{^1\text{H}\}$ -NMR (100 MHz, CDCl_3): δ -0.57, -0.54, -0.47, 18.57, 26.32, 123.32, 135.21, 139.37, 139.47, 147.23, 149.39. ^{29}Si NMR (80 MHz, CDCl_3 , Me_4Si): δ -20.70 (s, 1Si) -20.46 (s, 2Si), -20.36 (s, 1Si) ppm. MALDI-TOF m/z = 661.2346 [M+H] (Expected 661.25). FT-IR data in powdered sample (cm^{-1}): 2960, 2925, 2915, 1478, 1424, 1383, 1261, 1186, 1080, 1027, 796, 714. Anal. Calcd for $\text{C}_{32}\text{H}_{44}\text{N}_4\text{O}_4\text{Si}_4$: C, 58.14; H, 6.75; N, 8.48. Found: C, 58.35; H, 6.69; N, 8.54.

$\text{L}^{4\text{C}}$: ^1H NMR (400 MHz, CDCl_3): δ = 8.40 (s, 4H), 8.35 (s, 4H), 7.72 (m, 4H), 7.36 (m, 4H), 2.75 (t, J_1 = 8.0 Hz, J_2 = 12.0 Hz, 8H), 0.96 (t, J = 8.0 Hz, J = 12.0 Hz, 8H), 0.15 (s, 12H) ppm. $^{13}\text{C}\{^1\text{H}\}$ -NMR (100 MHz, CDCl_3): δ -0.57, 18.55, 26.32, 123.32, 135.18, 139.41, 147.26, 149.46. ^{29}Si NMR (80 MHz, CDCl_3 , Me_4Si): δ -20.43 ppm. MALDI-TOF m/z = 661.2403 [M+H] (Expected 611.25). FT-IR data in powdered sample (cm^{-1}): 2960, 2925, 2915, 1478, 1424, 1383, 1261, 1186, 1080, 1027, 796, 714. Anal. Calcd for $\text{C}_{32}\text{H}_{44}\text{N}_4\text{O}_4\text{Si}_4$:

C, 58.14; H, 6.71; N, 8.48. Found: C, 58.40; H, 6.75; N, 8.45.

3.2.2.3 Synthesis of compound $[(L^{3A})(ZnI_2)_2]_\infty$ (5): To a solution of L^{3A} (10 mg, 0.015 mmol) in THF (1 ml), kept in a 10 cm long glass tube, was slowly layered a methanolic solution of ZnI_2 (10 mg, 0.031 mmol). The layered solutions in the tube were kept at room temperature for 2 day to get colorless crystals of **5** (Yield 30%). FT-IR data in powdered sample (cm^{-1}): 2956, 2924, 1605, 1581, 1482, 1432, 1262, 1193, 1135, 1062, 799, 700, 655. Anal. Calcd for $C_{32}H_{36}Zn_2I_4N_4O_4Si_4$: C, 29.76; H, 2.81; N, 4.34. Found: C, 29.65; H, 2.73; N, 4.40.

3.2.2.4 Synthesis of compound $\{[(L^{3B})Ag_2] \cdot 2NO_3 \cdot H_2O \cdot CH_3OH\}_\infty$ (6): To a solution of L^{3B} (12 mg, 0.018 mmol) in DCM (3 mL), kept in a 10 cm long glass tube, toluene (1mL) was added followed by a careful layering of a solution of $AgNO_3$ (6 mg, 0.036 mmol) in water (3 mL). The resulting slightly cloudy solution was kept in dark for crystallization. Colorless crystals were obtained after 4 days (Yield 25 %). FT-IR data in powdered sample (cm^{-1}): 2955, 2922, 1598, 1478, 1427, 1261, 1192, 1086, 1033, 853, 795, 702, 649. Calcd for $C_{33}H_{42}Ag_2N_6O_{12}Si_4$: C, 38.01; H, 4.06; N, 8.06. Found: C, 38.35; H, 3.95; N, 8.20.

3.2.2.5 Synthesis of compound $[(L^{4C})Cu_4I_4]_\infty$ (7): To a solution of L^{2C} (10 mg, 0.015 mmol) in DCM (1 ml), kept in 10 cm long glass tube, was slowly layered CuI solution in acetonitrile (10 mg, 0.06 mmol). The layered solutions in the tube were kept at room temperature for 7 days to get colorless crystals of **7** (Yield 10%). FT-IR data in powdered sample (cm^{-1}): 2955, 2922, 1598, 1478, 1427, 1261, 1192, 1086, 1033, 853, 795, 702, 649. Anal. Calcd for $C_{32}H_{44}Cu_4I_4N_4O_4Si_4$: C, 27.01; H, 3.12; N, 3.94. Found: C, 27.15; H, 3.20; N, 3.79.

3.2.2.6 Synthesis of compound $\{[(L^{3A})(Cd(NO_3))] \cdot THF\}_\infty$ (8): To a solution of L^{3A} (10 mg, 0.015 mmol) in THF (2 ml), kept in a 10 cm long glass tube, was slowly layered a methanolic solution of $Cd(NO_3)_2 \cdot 4H_2O$ (4.7 mg, 0.015 mmol). The layered solutions in the tube were kept at room temperature for 5 day to get colorless crystals of **8** (Yield 35%). FT-IR data in powdered sample (cm^{-1}): 2959, 2914, 1595, 1591, 1502, 1492, 1282, 1213, 1095, 1102, 800, 695, 555. Anal. Calcd for $C_{37}H_{48}CdN_6O_{12}Si_4$: C, 44.73; H, 4.87; N, 8.46. Found: C, 44.69; H, 4.85; N, 8.49.

3.2.2.7 Synthesis of compound $\{[(L^{3C})(Cd_2(bpdc)_2) \cdot DMF\}_\infty$ (9): To a solution of L^{3A} (10 mg, 0.015 mmol) in MeOH (1 mL), kept in a screw-capped vial, was added a solution of a

$\text{Cd}(\text{NO}_3)_2 \cdot 4\text{H}_2\text{O}$ (9.4 mg, 0.03 mmol) in methanol (2 mL) and bpdc (7.2 mg, 0.03 mmol) in DMF (2ml) with the immediate formation of a white precipitate. This was heated at 90 °C under the solvothermal condition for 36 h. The resultant solution was slowly cooled to room temperature (at the rate of 0.1 °C per minute) to obtain colourless crystals of **9** (Yield 45%). FT-IR data in powdered sample (cm^{-1}): 2966, 2944, 1615, 1571, 1492, 1452, 1292, 1173, 1155, 1022, 809, 685, 645. Anal. Calcd for $\text{C}_{63}\text{H}_{59}\text{Cd}_2\text{N}_5\text{O}_{13}\text{Si}_4$: C, 52.87; H, 4.15; N, 4.89. Found: C, 52.90; H, 4.13; N, 4.87.

3.2.3 Crystallography

Reflections were collected on a Bruker Smart Apex Duo diffractometer at 100 K using $\text{MoK}\alpha$ radiation ($\lambda = 0.71073 \text{ \AA}$) for **6**, **7**, **8** and **9**. For **5**, the data was collected on a Bruker D8 Venture fitted with a microfocus detector at 100 K using $\text{MoK}\alpha$ radiation ($\lambda = 0.71073 \text{ \AA}$). Structures were refined by full matrix least squares against F^2 using all data (SHELX).^{13a} Crystallographic data for all these compounds are listed in (Table 3.1 and Appendix, Table A3.1). All non-hydrogen atoms were refined anisotropically if not stated otherwise. Hydrogen atoms were constrained in geometric positions to their parent atoms. Crystals of **5**, **6**, **8** and **9** were weakly diffracting at higher angles and hence a $2\theta = 50^\circ$ cut-off was applied. Owing to the weak diffraction data and partially opaque nature of the crystals, the C and N atoms of the pyridyl vinyl groups in **6** were refined isotropically. Only one of the two nitrate groups in **6** was located; the other nitrate group was disordered with solvate groups and hence has been removed by the squeeze routine of the Platon program. The TGA of **6** showed a 5% weight loss up to 110 °C corresponding to one molecule of water and one molecule of methanol (Appendix, A3.1). The tetrasiloxane ring and one of the vinyl carbons in all the four vinyl pyridyl moieties in **5** were disordered over two positions and hence were freely refined using the SAME/SADI restraints. The Zn bound iodine atoms in **5** were disordered over three positions and refined by the SUMP command. Crystals of **7** were very poor in quality, and we could just manage to solve the structure of the compound. The data were very weak and of poor quality as indicated by high $R(\text{int})$ and $R(\text{sigma})$ values. We have refined the structure with truncated data (1A) because of the low resolution of the reflection pattern. We have also tried several lower symmetry space groups; none of them gave a considerable improvement. For example, in the Pc space group the siloxane ring shifts away slightly of what would be the 2-fold axis of $P2/c$. There were also difference peaks in regions where one would not expect them. This may be due to non-merohedral twinning. But on the whole, we believe the

disorder of the ligand in **7** is intrinsic in nature owing to the flexibility of the siloxane ring and the ethyl pyridyl side chains favoring more than one conformation for the ligand without affecting the coordination geometry. This becomes apparent when one looks at the thermal parameters, which become larger the farther the atoms are to the center of the ligand and reach a maximum at the siloxane ring. Because there were a large number of domains, it was impossible to refine a meaningful model of the disorder.

Table 3.1: Details of crystallographic data collection and structure refinements for 5, 6, 7, 8 and 9

Compound	5	6	7
Chemical formula	C ₃₂ H ₃₆ I ₄ N ₄ O ₄ Si ₄ Zn ₂	C ₄₅ H ₅₀ Ag ₄ N ₈ O ₆ Si ₈	C ₃₂ H ₄₄ Cu ₄ I ₄ N ₄ O ₄ Si ₄
Formula weight	1291.35	1526.03	1422.83
Temperature	100(2)K	100(2)K	100(2) K
Crystal system	Monoclinic	Triclinic	Monoclinic
Space group	C2/c	P-1	P2/c
a (Å); α (°)	14.0420(10); 90°.	8.797(3); 82.26°	16.29(3); 90°.
b (Å); β (°)	26.3107(19); 105.55(3) °.	13.654(4); 83.83°	11.09(2); 109.86(3) °.
c (Å); γ (°)	16.8170(10); 90°.	18.420(5); 73.828°	16.96(3); 90°.
V (Å ³); Z	5985.8(7); 4	2093.2(10); 2	2880(9); 2
ρ (calc.) mg m ⁻³	1.433	2.421	1.641
μ(Mo K _α) mm ⁻¹	2.972	2.272	3.714
2θ _{max} (°)	50.052	50.054	41.64
R(int)	0.1728	0.1318	0.4341
Completeness to θ	97.2 %	97.0 %	99.3 %
Data / param.	5269/260	7370/295	2997 / 127
GOF	1.031	1.238	1.306
R1 [F>4σ(F)]	0.0935	0.0993	0.1559
wR2 (all data)	0.3360	0.4473	0.4703
max. peak/hole (e.Å ⁻³)	0.875/-0.602	1.896/-1.931	2.598 /-1.001
Compound	8	9	
Chemical formula	C ₃₂ H ₃₆ N ₆ O ₁₀ Si ₄ Cd	C ₆₀ H ₅₆ I ₄ N ₄ O ₁₂ Si ₄ Cd ₂	
Formula weight	766.08	1362.10	
Temperature	100(2)K	100(2)K	
Crystal system	Monoclinic	Triclinic	
Space group	P2(1)/n	P-1	
a (Å); α (°)	17.63(2); 67.24(3)°.	14.45(6); 65.23(8)°.	
b (Å); β (°)	18.33(2); 62.48(3) °.	15.30(6); 106.9(9) °.	
c (Å); γ (°)	16.8170(10); 74.08(3)°.	18.79(7); 105.4(9)°.	
V (Å ³); Z	4825.8(7); 4	3725.8(7); 4	
ρ (calc.) mg m ⁻³	2.782	1.196	
μ(Mo K _α) mm ⁻¹	1.071	0.678	
2θ _{max} (°)	54.44	50.054	
R(int)	0.9559	0.1127	
Completeness to θ	98.3	99.9	
Data / param.	23890/1128	133304/739	
GOF	0.741	1.335	
R1 [F>4σ(F)]	0.1016	0.1175	
wR2 (all data)	0.51	0.3987	
max. peak/hole (e.Å ⁻³)	0.65/-1.39	3.27/-1.244	

Nevertheless, all connectivity patterns of the molecule were unambiguously established in the

crystal structure of **7**. However, owing to its high R-factor (about 15%) the bond-lengths and bond-angles in it have to be dealt with caution. In addition, all the C and N atoms in **7** were refined isotropically due to poor diffraction data. The diffuse solvent molecules in compound **9** could not be modeled appropriately. Hence, these were treated as diffuse contributions to the overall scattering and removed by the SQUEEZE/PLATON for a better refinement data.^{13b}

3.2.4 Lifetime measurements

The luminescent lifetime of **7** was measured at room temperature (298 K) as well as low temperature (77 K). The room-temperature phosphorescence decay profiles were fitted to bi- or triexponential curves. The 77 K phosphorescence decay profiles were fitted to monoexponential equations. In all the cases the lifetimes were fitted by using the DAS software. Throughout the manuscript, the lifetimes of bi- or triexponential curves were discussed only with respect to the highest lifetimes for the sake of simplicity.

3.2.5 DFT calculations

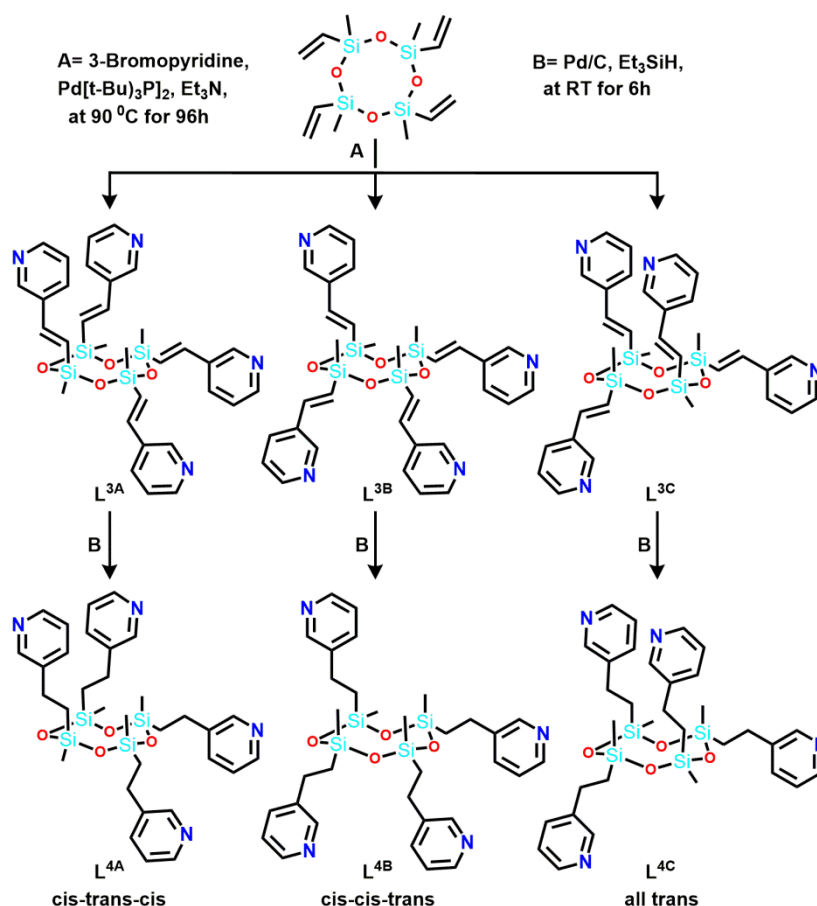
The density functional theory (DFT) calculations for the stereoisomers of L^3 and L^4 were performed using Gaussian 09 program package.¹⁴ The B3LYP exchange-correlation functional was used throughout for all calculations along with 6-31g(d,p) basis sets.¹⁵ The stereogeometry of the ligand isomers was prefixed, and their energies were optimized during the calculations.

3.3 Result and Discussion

3.3.1 Syntheses and spectra

The ligand L^3 was synthesized from the reaction of precursor tetramer D_4^{vi} with 3-bromopyridine in the presence of $Pd[t-Bu_3P]_2$ catalyst and triethylamine as base. The progress of the reaction was monitored by 1H -NMR with the change in chemical shift of the Si-bound vinyl protons from 5.80–6.10 ppm for D_4^{vi} to around 6.45 and 7.29 ppm for L^3 . The crude product was purified by column chromatography using tetrahydrofuran and dichloromethane (20:80) as eluent which gave three stereoisomers of L^3 , namely the *cis-trans-cis* L^{3A} , *cis-cis-trans* L^{3B} and *all-trans* L^{3C} , in the respective 35, 60 and 5% compositions.¹⁶ Although there are several methods available for obtaining peripherally

modified cyclotetrasiloxanes, the Heck coupling reaction was found to be successful in this case exhibiting an excellent functional group tolerance and good stereochemical separation.¹⁷ It is noteworthy to mention that a single cyclic tetrasiloxane containing propylammonium trifluoromethanesulfonate and methyl side groups in *cis-trans-cis* geometry has been recently synthesized from the hydrolytic condensation of 3-aminopropyldiethoxymethylsilane.¹⁸



Scheme 3.1: Reaction schemes and conditions for synthesis of L^3 and L^4

The ²⁹Si NMR spectrum of L^{3A} gave a single peak at -31.2 ppm indicating that all the four Si atoms are equivalent in the *cis-trans-cis* geometry. Similarly, the Si-bound methyl groups gave a single resonance in the ¹H and ¹³C NMR spectrum at 0.37 and -0.26 ppm, respectively. The signals due to all the four vinyl moieties and pyridyl groups in L^{3A} were also found to be equivalent. The vinyl groups gave two doublets at 6.46 and 7.09 ppm; the pyridyl groups gave four signals centered at 7.24, 7.73, 8.50 and 8.63 ppm. In contrast, the *cis-cis-trans* isomer L^{3B} showed three unique environments for the four Si atoms in it. In L^{3B} , The methyl groups present on Si1, Si2 and Si3 are located at the equatorial positions whereas that of Si4 is located at the axial position. As a result, Si1, Si3, and Si4 possess chemically different

environments, and Si2 has an equivalent environment as that of Si1 (Appendix, A3.3). Thus, the major peak at -31.1 ppm in the ^{29}Si NMR spectrum of L^{3B} corresponds to the Si1 and Si2 atoms with its two neighboring Si-Me groups located in the mixed axial-equatorial environment. The lower intensity peak at -31.0 ppm corresponds to Si3, which contains an equatorial methyl group (as that of Si1), with both of its neighboring Si-Me groups at equatorial positions. The Fourth silicon atom, Si4, having an axially located methyl group and two neighboring equatorially directed Si-Me groups is in the totally different environment and gave rise to a signal somewhat shifted at -31.3 ppm.

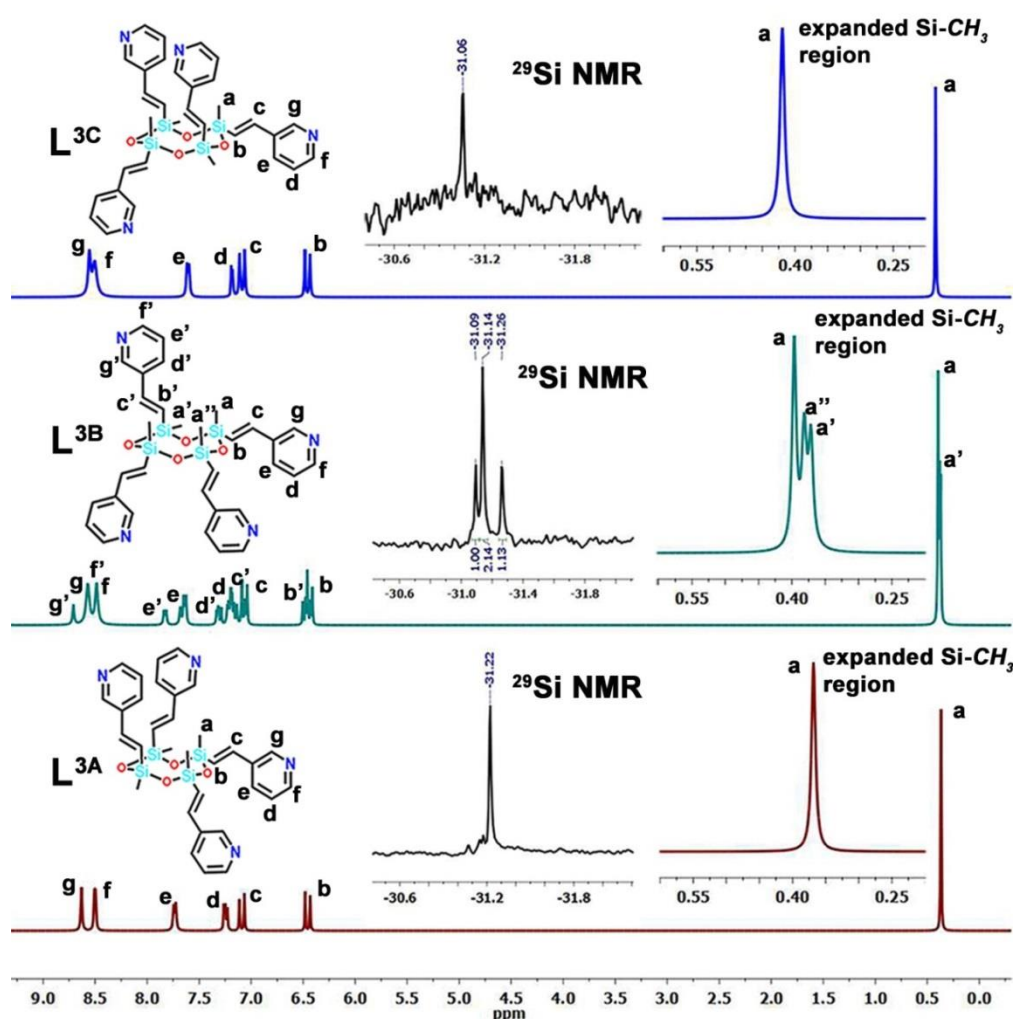


Figure 3.1: ^1H and ^{29}Si (inset) NMR spectra of the ligand L^{3A} – L^{3C}

Similarly, it showed three peaks at 0.37, 0.38 and 0.40 ppm (in 1:1:2 ratio) in ^1H NMR and two peaks at -0.31 and -0.16 ppm in ^{13}C NMR for the Si-Me groups. The vinyl protons in L^{1B} gave a set of two doublets in the 1:3 ratios at 6.46 and 7.09 ppm. Similarly, the pyridyl

groups, owing to their two unique conformations, displayed two sets of four chemical shift values in 3:1 ratio in the range between 7.21–8.72 ppm. The ligand L^{3C} showed similar ^{29}Si and ^1H NMR spectra as that of L^{3A} with marginal changes in the chemical shift values. The ^{29}Si NMR spectrum of L^{3C} gave a single peak at -31.1 ppm and the silicon bound methyl groups observed as a single resonance at 0.42 ppm in the ^1H NMR spectrum (Figure 3.1, and Appendix, A3.2-A3.9). However, these isomers were distinguished from their R_f values (0.56, 0.34 and 0.12 for L^{3A} , L^{3B} , and L^{3C} , respectively, after two runs in DCM: THF (80:20) mixture) on TLC strips.

In order to obtain more flexible ligands based on the tetrasiloxane platform, all the three isomers of L^3 (L^{3A} , L^{3B} , and L^{3C}) were individually subjected to the reduction reaction of the vinylic bonds utilizing triethylsilane as reducing agent.¹⁹ As observed before the ^{29}Si NMR spectra of both L^{4A} and L^{4C} exhibit single resonances (at -20.4 ppm) owing to similar environments for all the four Si-atom. Whereas, three different signals were observed in the ratio of 1:2:1 for L^{4B} (at -20.7, -20.5 and -20.4 ppm), signifying the retention of its *cis-cis-trans* geometry. Similarly, the ^1H NMR spectra of L^{4A} and L^{4C} showed single resonances for the methyl protons at 0.14 and 0.15 ppm respectively, while L^{4B} exhibits two overlapping peaks at 0.12 ppm. The ^{13}C NMR spectrum of L^{4B} gave three peaks at -0.57, -0.54 and -0.47 ppm for methyl carbons, whereas L^{4A} showed a single peak at -0.52 ppm. The protons due to the orthogonally attached ethyl pyridyl groups in all three isomers exhibit similar peak patterns due to the flexible nature of these side arms (Figure 3.2, and Appendix, A3.10-A3.17). Furthermore, all these ligands were subjected to thermogravimetric (TGA) and differential scanning calorimetric (DSC) analysis to understand their thermal behavior (Appendix, A3.18-A3.25). The TGA profiles indicate that the decomposition temperature of these ligands varies between 120 and 190 °C. In both L^3 and L^4 series, the all-trans isomer (L^{3C} and L^{4C}) exhibit lower stabilities, with the respective decomposition values of 120 and 150 °C, in comparison with the other two isomers. Also, from the DSC profiles, it can be observed that the stereochemical isomers of both L^3 and L^4 exhibit distinct crystallization and/or melting temperatures below 0 °C (Appendix, Table A3.2).

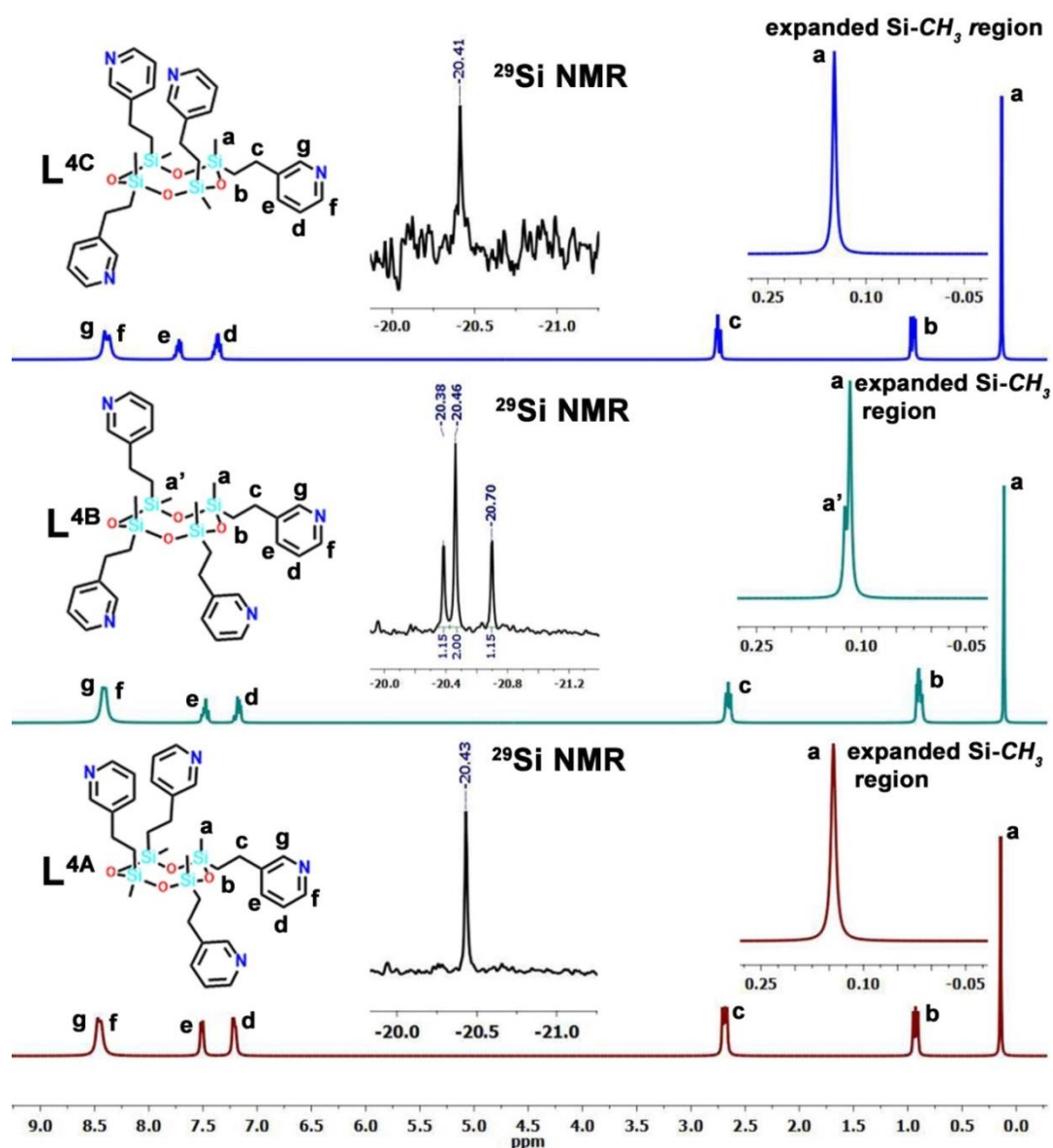


Figure 3.2: ^1H and ^{29}Si (inset) NMR spectra of the ligands L^{4A} – L^{4C}

Further, the metallation reactions of all these ligands were tested with several metal salts, especially those of certain d^{10} metal ions. The reaction of ZnI_2 with L^{3A} in 2:1 ratio at room temperature in methanol medium gave a white colored solid. Layering a methanolic solution of ZnI_2 on to a THF solution of L^{3A} gave single crystals of **5**. The SCXRD analysis of **5** showed the formation of the one-dimensional coordination polymeric structure of composition $[(L^{3A})(\text{ZnI}_2)_2]_\infty$. The reaction of L^{3B} (in DCM) and AgNO_3 (in water) in layering method yielded the cationic one-dimensional coordination polymer **6** of formula $\{[(L^{3B})\text{Ag}_2] \cdot 2\text{NO}_3 \cdot \text{H}_2\text{O} \cdot \text{CH}_3\text{OH}\}_\infty$. An interesting two-dimensional cubane-type Cu_4I_4 cluster coordination polymer **7** of formula $[(L^{4C})\text{Cu}_4\text{I}_4]_\infty$ was crystallized from layering the MeCN

solution of CuI to a DCM solution of L^{4C} . However, treatment of CuI with any of the ligands of the L^4 family in MeCN/DCM medium gave rise to almost identical solids **7a**. Due to the amorphous nature of the bulk samples of **7a**, the PXRD profiles of **7** and **7a** could not be matched. Individual investigation of the photo-physical properties of all these solids showed almost identical thermochromic behavior typical of cubane-type Cu_4I_4 clusters and emission characteristics (vide supra). Also, both **7** and **7a** gave comparable TGA profiles indicating close structural similarities between them (Appendix, A3.26). This may be attributed to the flexibility of the ligand L^4 , which includes the conformation of the siloxane ring and the configuration of its side chains. Due to the multitude of degrees of freedom, there may be more than one configuration of the ligand L^2 that can support the same coordination geometry with respect to the Cu_4I_4 cluster. The reaction of $Cd(NO_3)_2 \cdot 4H_2O$ (in MeOH) with L^{3A} (in THF) at room temperature gave a two-dimensional coordination polymer **8** of composition $[(L^{3A})(Cd(NO_3)_2 \cdot THF)]_\infty$. In an attempt to obtain a more open framework structure, the loosely bound nitrate ions on Cd(II) were replaced with various organic linkers. Thus, treatment of L^{3A} with $Cd(NO_3)_2 \cdot 4H_2O$ and bpdc-2H under solothermal conditions (mixture of MeOH and DMF) gave a new two dimensional coordination polymer **9** of composition $\{[(L^{3C})(Cd_2(bpdc)_2) \cdot DMF]\}_\infty$ in which the configuration of siloxane ligand is changed to the all trans isomer of L^{3C} .

3.3.2 Crystal structures

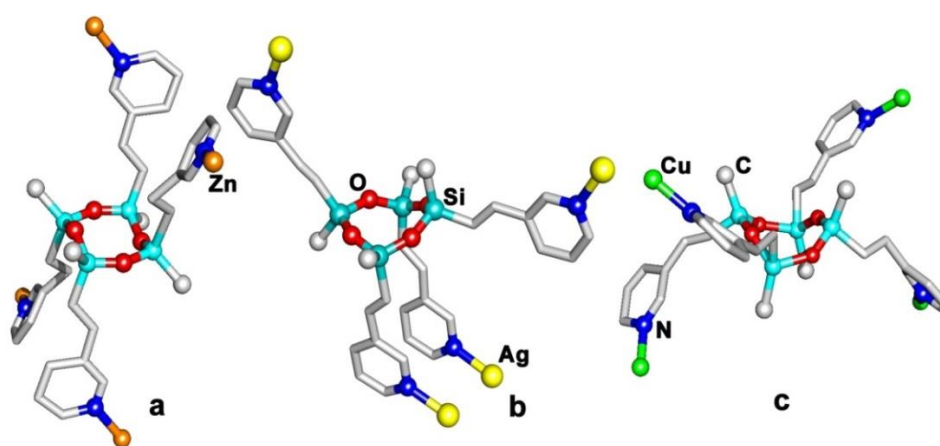


Figure 3.3: Closer view of the geometry of cyclotetrasiloxane motifs in **5**, **6** and **7**. (a) Chair conformation of L^{3A} in **5**; (b) boat-chair conformation of L^{3B} in **6**; (c) distorted boat conformation of L^{4C} in **7**. In the figure color represent as silicon; cyan, oxygen; red, carbon; light gray, nitrogen; blue, zinc; orange, silver; yellow, and copper; green.

All the obtained tetrasiloxane ligands (L^{3A} , L^{3B} , L^{3C} , L^{4A} , L^{4B} and L^{4C}) are colorless oily liquids. DFT (B3LYP-6-31g(d,p)) level energy optimizations show that all the stereoisomers of L^3 possess similar energetics (Appendix, A3.27). However, the stereo-conformations of these ligands can be gleaned from the crystal structure analysis of the metal complexes **5**, **6** and **7** that are derived from some of these ligands (Figure 3.3).

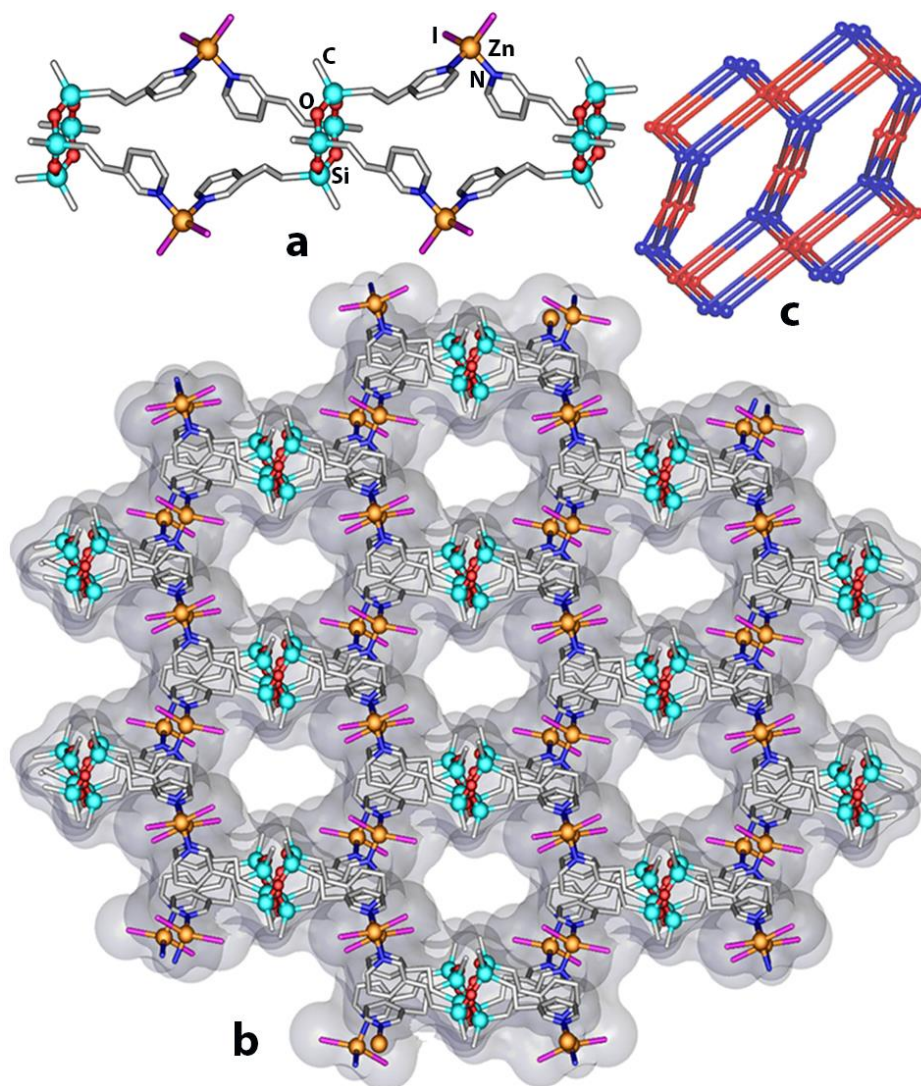


Figure 3.4: (a) Molecular structure of the 1D-coordination polymer **5** and (c) the PtS topology of the supramolecular network in it; blue color represents ligand as node and red color a node created by pyridinyl ring through π - π interactions. (b) Surface overlay view of the packing diagram of **5**.

The crystal structure of the Zn(II) complex **5** was obtained in the monoclinic space group C2/c (Figure 3.4a). Two of the four vinyl pyridyl moieties of the tetrasiloxane ligand are located at the axial positions while the remaining two are at the equatorial positions. The

tetrasiloxane backbone exhibits a chair conformation in which two of the four Si-bound methyl groups are located at the axial positions and the remaining two are at the equatorial positions confirming the *cis-trans-cis* geometry for L^{3A} in **5** (Figure 3.3a). The coordination environment around the Zn(II) ion can be described as distorted tetrahedral consisting of two terminal Γ ion and two N-donor sites from two different tetrasiloxane ligands L^{3A} . The four peripherally-attached pyridyl groups of L^{3A} are coordinated with four ZnI_2 units, two on one side and two on the other side of the Si_4O_4 ring, leading to the formation of a one-dimensional ribbon-like structure. The individual 1D-chains are made-up of 28-membered macrocycles that are fused to each other on either side of the tetrasiloxane scaffold. The 1D-chains of the adjacent layers are aligned perpendicular to each other and linked via two distinct π - π interactions (3.610 Å and 3.917 Å) of the pyridyl groups (Appendix, A3.28). The net effect of these π - π interactions is the formation of a supramolecular 3D-structure (Figure 3.4b). TOPOS analysis gave the topology of a PtS net represented by the Schläfli symbol $\{4^2.8^4\}$ (Figure 3.4c).²⁰ The 3D-packing structure of **5** reveals the presence of 1D-channels and the void volume (excluding the disordered atoms) calculated by Mercury software is 1618.14 Å³ which amounts to 27 % of the unit-cell volume. The gas adsorption analysis reveals a non-porous structure for **5**. This is primarily attributed to the disordered nature of the tetrasiloxane and the vinylic C-atoms (Appendix, A3.29) which takes-up a considerable amount of the void space present in **5**.

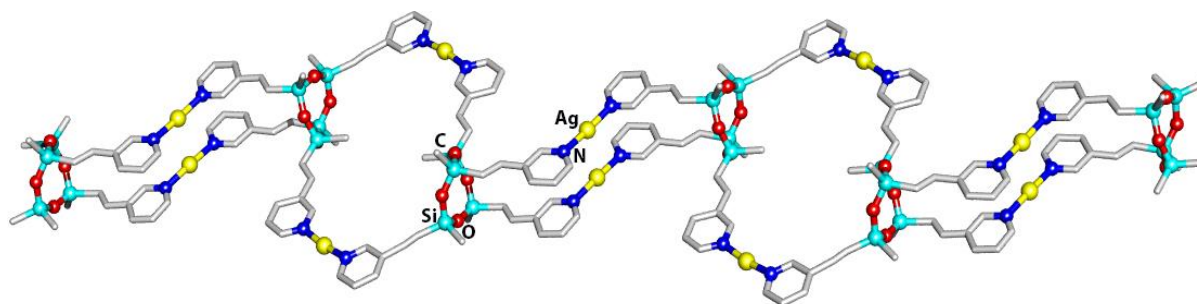


Figure 3.5: Molecular structure of the 1D-coordination polymer **6**.

The crystal structure of **6** was solved in the triclinic space group *P-1* (Figure 3.5). The siloxane ring displays a boat-chair conformation in which three of the four vinyl pyridyl moieties in **6** are located at equatorial positions while the fourth one is oriented in the axial position. The coordination environment around the Ag(I) atom consist of two N-donor sites from two different L^{3B} fragments (Figure 3.3b). As a result, the molecule propagates into a one-dimensional polymeric structure with two distinct 32-membered Ag_2L_2 -type macrocycles

featuring alternately arranged wider- and narrower-ring segments. While, the wider 32 membered macrocycle is formed by the participation of one axial and one equatorial pyridyl segments from each of the two L^{3B} fragments, the remaining two equatorial pyridyl segments from the narrow-spaced macrocycles.

The molecular structure of **7** was solved in monoclinic space groups P2/c (Figure 3.6a). The tetrameric Si-O ring exhibits a distorted boat shape. The four ethyl pyridyl moieties take up the equatorial positions and are located alternately above and below the Si_4O_4 ring (Figure 3.6c). The molecular core consist of a cubane-type Cu_4I_4 cluster in which each I^- ion acts as a μ^3 -bridging ligand and the Cu(I) ions are located in a tetrahedral coordination consisting of three I^- contacts and one pyridyl N-donor coordination from L^{4C} (Figure 3.6b). In return, each ligand is bonded to four Cu_4I_4 clusters. Thus both the ligands and the Cu_4I_4 clusters in **7** act as four connected nodes resulting in the formation of a two-dimensional metal-organic framework structure. TOPOS analysis gave a 4-connected uninodal sql/Shubnikov tetragonal plane net represented by the Schläfli symbol $\{4^4.6^2\}$ for **7** (Figure 3.6c).²⁰ The repeating unit of 2D assembly in **7** consists of 34-membered Cu_4L_2 macrocycles.

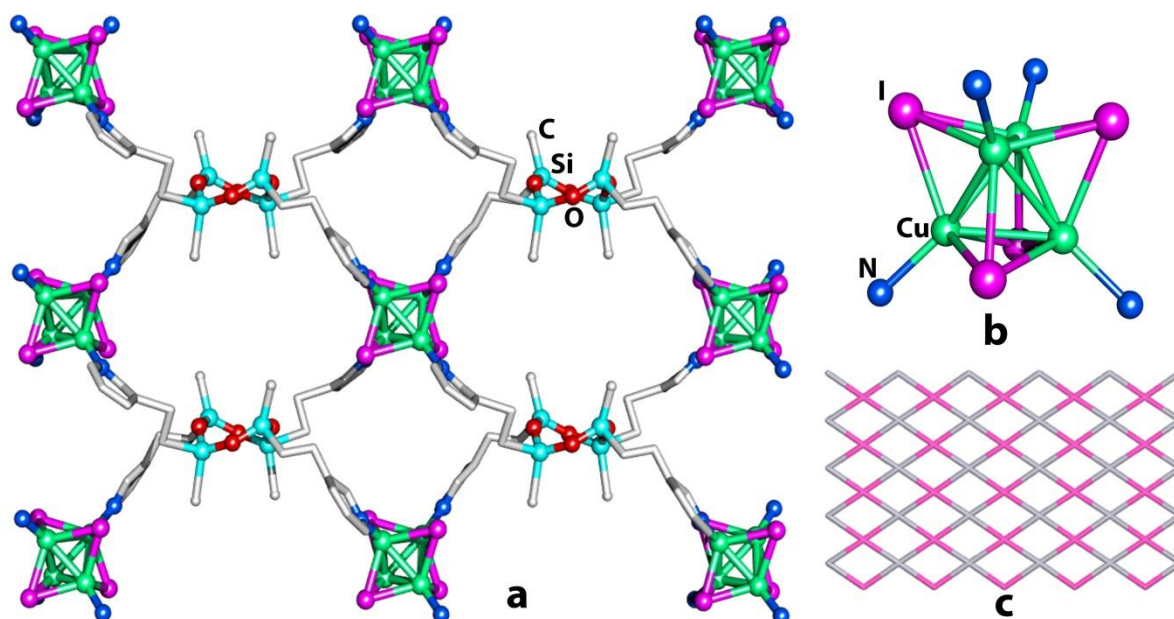


Figure 3.6: (a) Molecular structure of the 2D-coordination polymer **7** and (b) view of its Cu_4I_4 core. (c) View of the network topology in **7**; blue color represents ligand as a node and red color Cu_4I_4 as a node.

The molecular structure of **8** was solved in monoclinic space group P2(1)/n (Figure 3.7). The structural analysis reveals that the tetrameric siloxane ring exhibits a chair conformation in

which two of the four vinyl pyridyl moieties are located at the axial positions while the remaining two are oriented in the equatorial position confirming the *cis-trans-cis* geometry for L^{3A} in **8** (Figure 3.7b). The coordination environment around the Cd(II) ion has an octahedral geometry consists of four N-donor sites from the four different L^{3A} fragments at the equatorial plane and two oxygen atoms from the two different nitrate ions at apical position (Figure 3.3b). In return, each ligand is bonded to the four different Cd(II) ions. Thus both the ligands and the Cd(II) ions in **7** act as four connected nodes resulting in the formation of a two-dimensional polymeric sheet. TOPOS analysis gave a 4-connected uninodal sql/Shubnikov tetragonal plane net represented by the Schläfli symbol $\{4^4.6^2\}$ for **8** (Figure 3.7c).²⁰

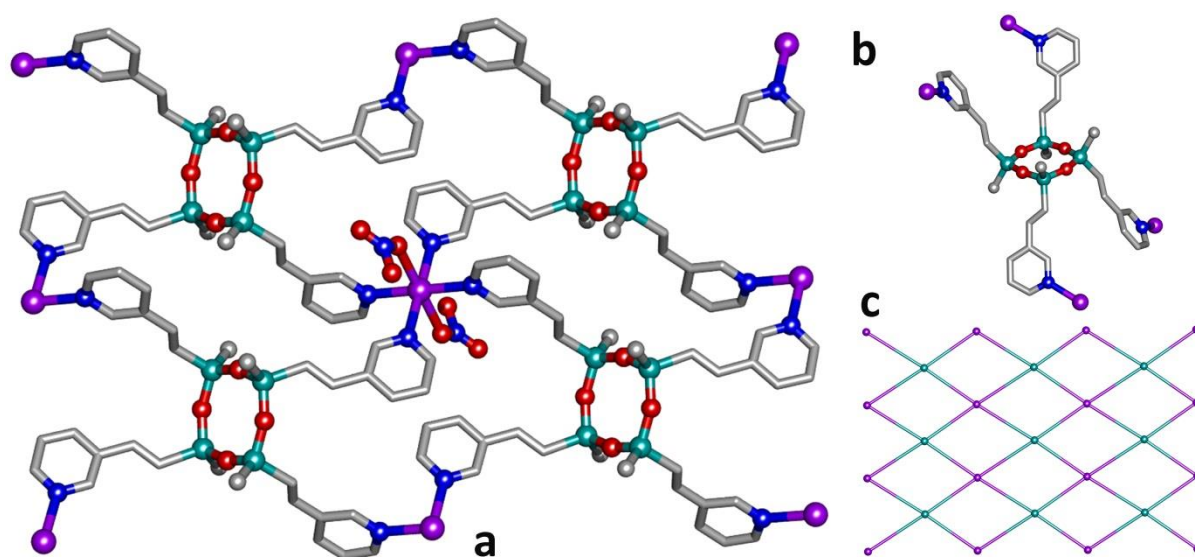


Figure 3.7: a) Molecular structure of the 2D-coordination polymer **8** and (b) view of the L^{3A} ligand in the **8**. (c) View of the network topology in **8**; cyan color represents ligand as a node and purple color metal ion as a node.

The molecular structure of **9** was solved in triclinic space group P-1 (Figure 3.8). The asymmetric unit of **9** contains two Cd(II) ions, two bpdc anions, one tetrasiloxane ligand and one DMF solvate. The Cd(II) ion is coordinated with two carboxylate groups of different bpdc ligands in which one carboxylate group acts as a bidentate ligands, and one as a monodentate bridging and bidentate chelating ligand. The Cd(II) atoms were bridged by one of the oxygen of carboxylate ligands to form an binuclear cluster with a Cd...Cd separation of 3.816(3) Å. The coordination environment around the Cd(II) is pentagonal bipyramidal consisting of five oxygen from the three bpdc ligand at equatorial plane and two N-donor

coordination from two different siloxane ligands at the apical position. Each binuclear cluster binds with four different bpdc ligands to form a 2D layered network with a 4-connected uninodal **sql** topology (Figure 3.8c). The tetrameric siloxane ring exhibits a boat shaped conformation in which the four vinyl pyridyl moieties take up the equatorial positions and are located alternately above and below the Si₄O₄ ring confirming the *all-trans* geometry for L^{3C} in **9** (Figure 3.8b). It observed that during the reaction the *cis-trans-cis* isomer has been converted to the *all-trans* isomer of the siloxane ligand caps the adjacent binuclear Cd(II) clusters alternatively above and below the 2D polymeric sheet formed by the Cd-bpdc units providing the see-saw shaped structure for the 2D-network (Figure 3.8d).

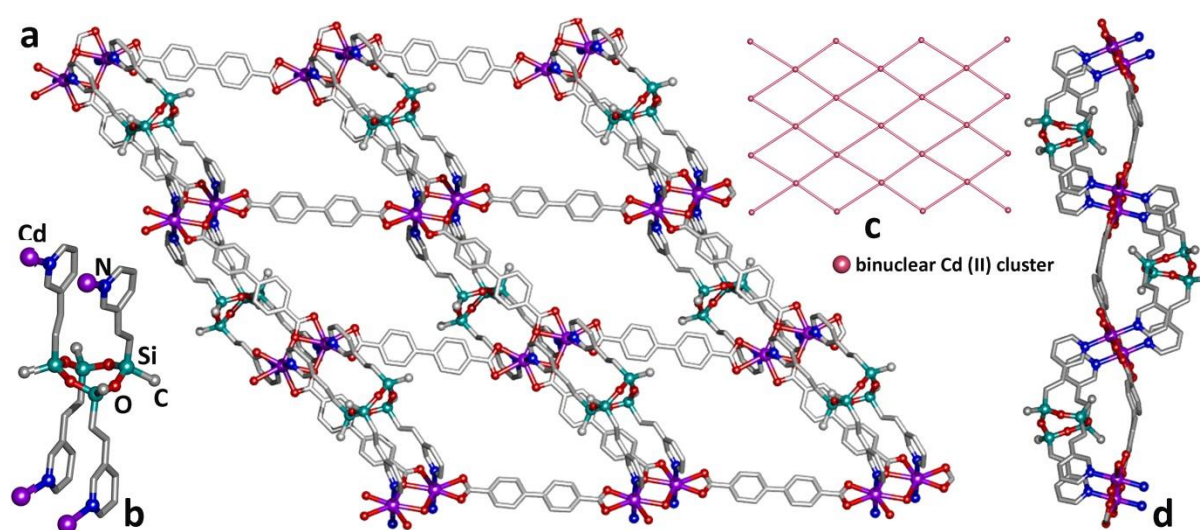


Figure 3.8: a) Molecular structure of the 2D-coordination polymer **9** and (b) view of the L^{3A} ligand in the **9**. (c) View of the network topology in **9** (d) View of siloxane ligands around 2D polymeric sheet.

3.3.3 Photo-physical properties

The compound **7a** is a white powder at ambient temperature and light (Figure 3.7a). Under UV excitation at 298 K, the compound **7a** shows an intense orange emission while cooling to 77 K shows an intense blue emission. Interestingly, the original emission color of **7a** can be recovered again within 2 minutes upon gradually warming the sample to room temperature indicating a completely reversible thermochromic luminescence (Figure 3.7b and 3.7c). To understand these phenomena, the excitation and emission spectra of **7a** were recorded in the solid state, and the corresponding results are summarized in Table A3.3 (Appendix). At 298 K, the emission spectrum of **7a** displays a single broad low energy (LE) emission band centered at 595 nm ($\lambda_{\text{exc}} = 375$ nm). This is in agreement with the intense orange emission

observed at room temperature, which can be attributed to the “cluster-centered” (^3CC) emission consisting of a mixture of iodide to copper charge transfer ($^3\text{XMCT}$) and metal $d \rightarrow s,p$ transitions. While at 77 K a new high energy (HE) band appears at 447 nm ($\lambda_{\text{ex}} = 375$ nm), with the concomitant quenching of the $^3\text{CC-LE}$ band (Figure 3.7). This HE band is attributed to the iodide to ligand charge transfer and metal to ligand charge transfer ($^3\text{XLCT}/^3\text{MLCT}$) transitions. These observed triplet-emission bands are characteristic of the copper iodide clusters and are closely comparable with those reported for traditional $\text{Cu}_4\text{I}_4\text{Py}_4$ clusters.²¹ The decay measurements in **7a** at 298 and 77 K gave the lifetime (τ_{em}) values of 1.1 and 162 μs , respectively (Appendix, A3.30- A3.32). It is interesting to note that the retention of thermochromism due to the Cu_4I_4 core in the cluster coordination polymer **7** is one among the rare instance since such thermochromic behavior is found to be absent in several infinite frameworks based on these clusters.²²

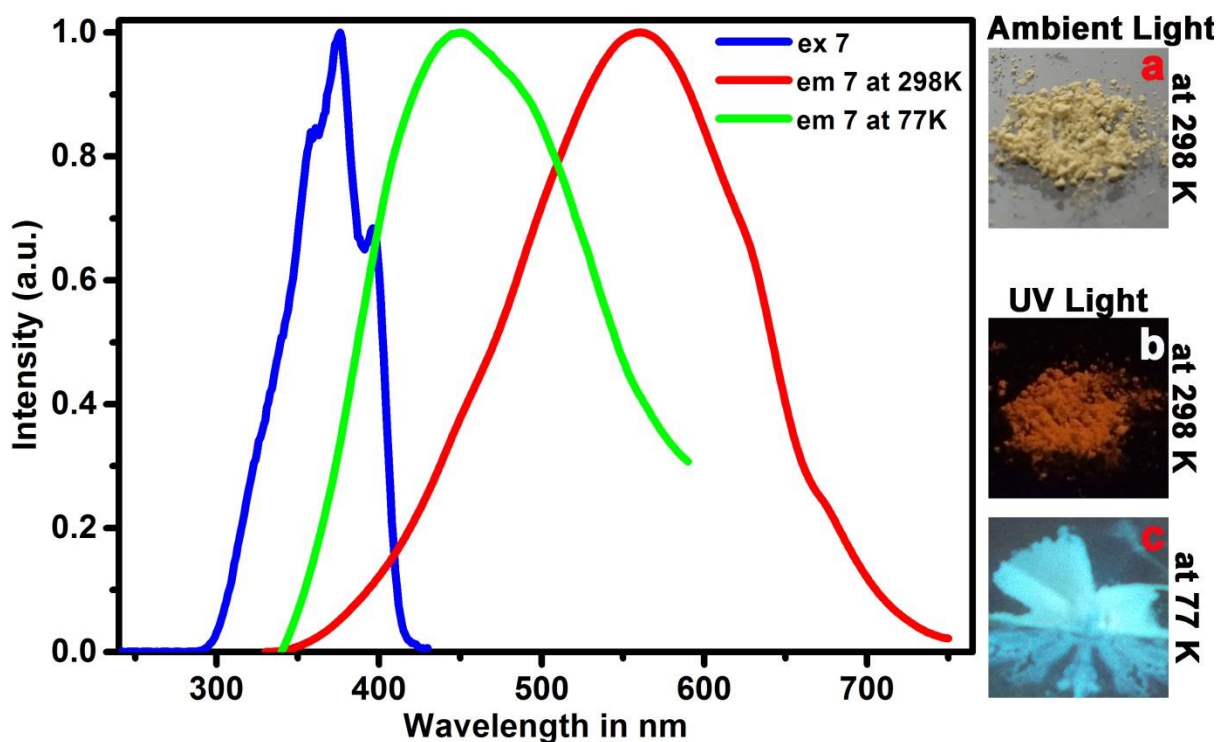


Figure 3.7: Excitation (*ex.*) and emission (*em.*) spectra of **7a** in the solid state and its emission colors at ambient and UV light.

3.4 Conclusion

In conclusion, this work demonstrates that Pd(0) catalyzed Heck coupling reaction offers a facile route for obtaining pyridyl-functionalized cyclosiloxanes, and a new family of tetra-

pyridyl substituted cyclotetrasiloxanes tethered by vinyl and ethyl spacers has been synthesized for the first time. Among the four known isomers of cyclotetrasiloxane scaffolds, three isomers, *cis-trans-cis*, *cis-cis-trans*, and *all-trans*, have been identified and isolated in quantitative yields for these 3-pyridyl-functionalized tetramers. The stereochemistry of these ligands has been established with the help of ^1H and ^{29}Si NMR studies and from the crystal structures derived from the metallation of some of these ligands. The emission spectra and the luminescent decay profiles recorded on **7a** reveal interesting thermochromic behavior for the 2D-coordination polymer **7**. Along with this, a conversion of *cis-trans-cis* to *all-trans* isomer has also been observed under the solvothermal reaction conditions. Further studies are aimed at synthesizing new families of cyclotetrasiloxanes containing various metal-coordinating groups by utilizing this Heck-coupling approach. These ligands owing to their inherent conformational flexibility can be utilized to rationally design dynamically-switchable functional framework materials.

3.5 References

- (1) Cordes, D. B.; Lickiss, P. D.; Rataboul, F. *Chem. Rev.* **2010**, *110* (4), 2081-2173; b) Chandrasekhar, V.; Boomishankar, R.; Nagendran, S. *Chem. Rev.* **2004**, *104*, 5847-5910.
- (2) (a) Bolis, V.; Busco, C.; Aina, V.; Morterra, C.; Ugliengo, P. *J. Phys. Chem. C* **2008**, *112*, 16879-16892; (b) Dong, A.; Zhang, Q.; Wang, T.; Wang, W.; Liu, F.; Gao, G. *J. Phys. Chem. C* **2010**, *114*, 17298-17303; (c) Rimola, A.; Costa, D.; Sodupe, M.; Lambert, J.-F.; Ugliengo, P. *Chem. Rev.* **2013**, *113*, 4216-4313; (d) Feher, F. J.; Budzichowski, T. A.; Rahimian, K.; Ziller, J. W. *J. Am. Chem. Soc.* **1992**, *114*, 3859-3866.
- (3) (a) Ledin, P. A.; Tkachenko, I. M.; Xu, W.; Choi, I.; Shevchenko, V. V.; Tsukruk, V. V. *Langmuir* **2014**, *30*, 8856-8865; (b) Sanchez, C.; Lebeau, B.; Chaput, F.; Boilot, J.-P. in *Functional Hybrid Materials*, Romero P. G. and Sanchez, C. (eds) Wiley Weinheim, 2003, pp.122-168; (c) Miniewicz, A.; Girones, J.; Karpinski, P.; Mossety-Leszczak, B.; Galina, H.; Dutkiewicz, M. *J. Mater. Chem. C* **2014**, *2*, 432-440.
- (4) (a) Silicon-Containing Polymers, Jones R.G.; Ando W.; Chojnowski J. Kluwer Academic Publishers, Dordrecht **2000**; (b) Brook, M. A. Silicon in Organic, Organometallic and polymer Chemistry: J. Wiley **2000**; (c) Lewis, L.; Stein, J.; Smith, K.; Messmer, R.; Legrand, D.; Scott, R.; Marciniak, B.; Chojnowski, J. *Prog. Organosilicon Chem. Gordon & Breach, Amsterdam* **1995**, 263; (d) Stevens, C. *Int. J. Cosm. Sci.* **1998**, *20*, 296-304.
- (5) (a) Alkordi, M. H.; Liu, Y.; Larsen, R. W.; Eubank, J. F.; Eddaoudi, M. *J. Am. Chem. Soc.* **2008**, *130*, 12639-12641; (b) Kuwahara, Y.; Maki, K.; Matsumura, Y.; Kamegawa, T.; Mori, K.; Yamashita, H. *J. Phys. Chem. C* **2009**, *113*, 1552-1559; (c) Daniel, M. C.; Astruc, D. *Chem. Rev.* **2004**, *104*, 293-346.
- (6) (a) Ronchi, M.; Pizzotti, M.; Biroli, A. O.; Macchi, P.; Lucenti, E.; Zucchi, C. *J. Organomet. Chem.* **2007**, *692*, 1788-1798; (b) Shchegolikhina, O.; Pozdniakova, Y.; Antipin, M.; Katsoulis, D.; Auner, N.; Herrschaft, B. *Organometallics* **2000**, *19*, 1077-1082; (c) Murugavel, R.; Voigt, A.; Walawalkar, M. G.; Roesky, H. W. *Chem. Rev.* **1996**, *96*, 2205-

2236.

(7) (a) Hitchcock, P. B.; Lappert, M. F.; Maciejewski, H. *J. Organomet. Chem.* **2000**, *605*, 221-225; (b) Maciejewski, H.; Kubicki, M.; Marciniak, B.; Sydor, A. *Polyhedron* **2002**, *21*, 1261-1265.

(8) Au-Yeung, H.-L.; Leung, S. Y. L.; Tam, A. Y. Y.; Yam, V. W. W. *J. Am. Chem. Soc.* **2014**, *136*, 17910-17913; (b) Köytepe, S.; Demirel, M. H.; Gültek, A.; Seçkin, T. *Polym. Int.* **2014**, *63*, 778-787; (c) Goodgame, D. M.; Kealey, S.; Lickiss, P. D.; White, A. J. P. *J. Mol. Struct.* **2008**, *890*, 232-239

(9) (a) Goodgame, D. M. L.; Lickiss, P. D.; Menzer, S.; Rooke, S. J.; Williams, D. J. *J. Organomet. Chem.* **2000**, *593*, 161-166; (b) Goodgame, D. M. L.; Lickiss, P. D.; Rooke, S. J.; White, A. J. P.; Williams, D. J. *Inorg. Chim. Acta* **2001**, *324*, 218-231; (c) Fereday, A.; Goodgame, D. M. L.; Lickiss, P. D.; Rooke, S. J.; White, A. J. P.; Williams, D. J. *Inorg. Chem. Commun.* **2002**, *5* (10), 805-807; (d) Goodgame, D. M.; Lickiss, P. D.; Rooke, S. J.; White, A. J. P.; Williams, D. J. *Inorg. Chim. Acta* **2003**, *343*, 61-73; (e) Čas, D.; Hurkes, N.; Spirk, S.; Belaj, F.; Bruhn, C.; Rechberger, G. N.; Pietschnig, R. *Dalton Trans.* **2015**, *44*, 12818-12823; (f) Pietschnig, R.; Merz, K. *Organometallics* **2004**, *23*, 1373-1377; (g) Kakiage, K.; Nakada, Y.; Kogure, T.; Yamamura, M.; Kyomen, T.; Unno, M.; Hanaya, M. *Silicon Chem.* **2008**, *3* (6), 303-305.

(10) Mann, T.; Haley, J.; Lacey, D. *J. Mater. Chem.* **1999**, *9*, 353-360.

(11) Unno, M.; Kawaguchi, Y.; Kishimoto, Y.; Matsumoto, H. *J. Am. Chem. Soc.* **2005**, *127*, 2256-2263.

(12) (a) Lichtenhan, J. D.; Otonari, Y. A.; Carr, M. J., *Macromolecules* **1995**, *28*, 8435-8437; (b) Trastoy, B.; Pérez-Ojeda, M. E.; Sastre, R.; Chiara, J. L. *Chem. Eur. J.* **2010**, *16*, 3833-3841; (c) Shockey, E. G.; Bolf, A. G.; Jones, P. F.; Schwab, J. J.; Chaffee, K. P.; Haddad, T. S.; Lichtenhan, J. D., *Appl. Organometal. Chem.* **1999**, *13*, 311-327; (d) Lichtenhan, J. D.; Schwab, J. J.; An, Y.-Z.; Reinerth, W.; Feher, F. J., *Patents*: **2005.US**

(13) (a) Sheldrick, G. M. *Acta Crystallogr.* **2008**, *A64*, 112-122; (b) Spek, A. L. *Acta Cryst.* **2015**, *C71*, 9-18.

(14) Frisch, M. J.; Trucks, G. W.; Schlegel, H. B.; Scuseria, G. E.; Robb, M. A.; Cheeseman, J. R.; Scalmani, G.; Barone, V.; Mennucci, B.; Petersson, G. A.; Nakatsuji, H.; Caricato, M.; Li, X.; Hratchian, H. P.; Izmaylov, A. F.; Bloino, J.; Zheng, G.; Sonnenberg, J. L.; Hada, M.; Ehara, M.; Toyota, K.; Fukuda, R.; Hasegawa, J.; Ishida, M.; Nakajima, T.; Honda, Y.; Kitao, O.; Nakai, H.; Vreven, T.; Montgomery, J. A., Jr.; Peralta, J. E.; Ogliaro, F.; Bearpark, M.; Heyd, J. J.; Brothers, E.; Kudin, K. N.; Staroverov, V. N.; Keith, T.; Kobayashi, R.; Normand, J.; Raghavachari, K.; Rendell, A.; Burant, J. C.; Iyengar, S. S.; Tomasi, J.; Cossi, M.; Rega, N.; Millam, J. M.; Klene, M.; Knox, J. E.; Cross, J. B.; Bakken, V.; Adamo, C.; Jaramillo, J.; Gomperts, R.; Stratmann, R. E.; Yazyev, O.; Austin, A. J.; Cammi, R.; Pomelli, C.; Ochterski, J. W.; Martin, R. L.; Morokuma, K.; Zakrzewski, V. G.; Voth, G. A.; Salvador, P.; Dannenberg, J. J.; Dapprich, S.; Daniels, A. D.; Gaussian 09, Revision C.01 Gaussian, Inc.: Wallingford, CT, **2013**.

(15) Becke, A. D. *J. Chem. Phys.* **1993**, *98*, 5648-5652.

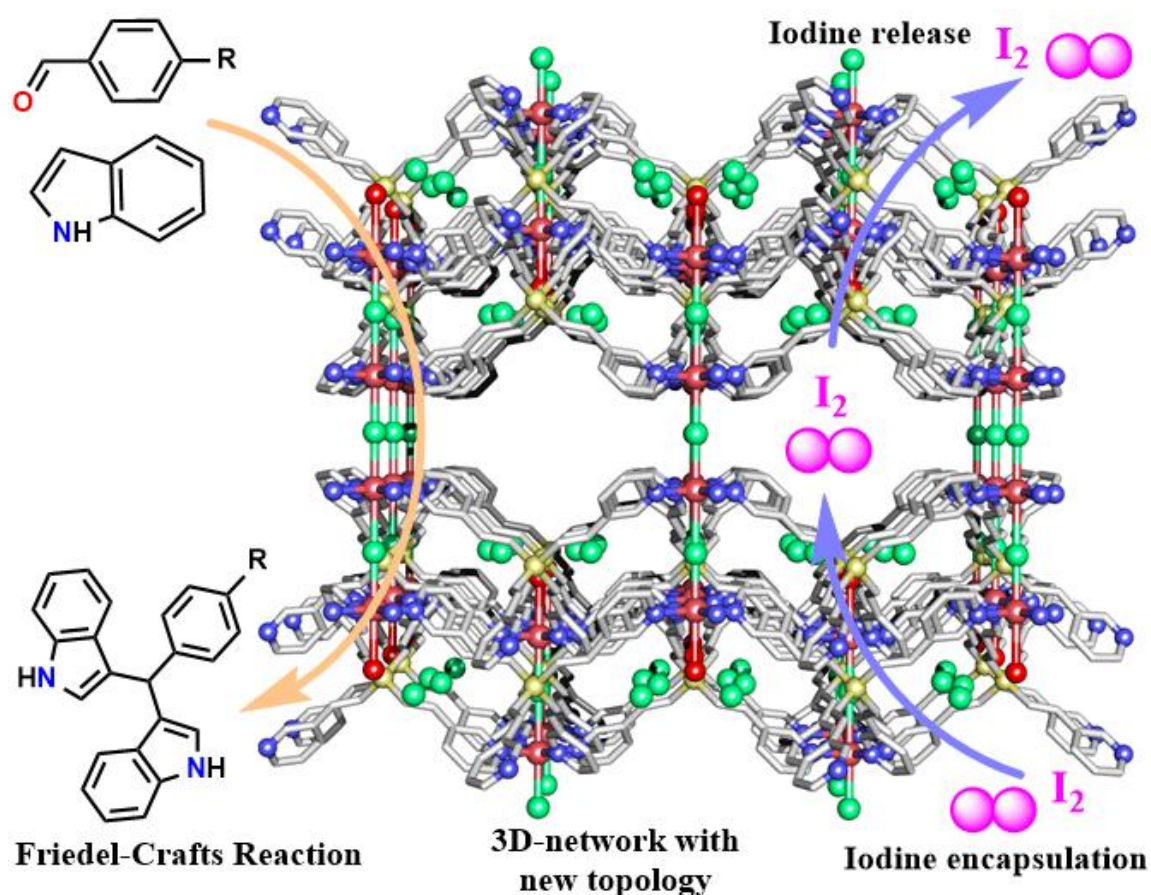
(16) The ^{29}Si NMR spectrum of commercial D_4^{Vi} (95% pure) gives three major peaks at 32.42, 32.44 and 32.52 ppm in the ratio of 1:2:1 similar to those observed for the *cis-cis-trans* isomer L^{1B} . A small hump around 32.42 may be attributed to some other (presumably *cis-trans-cis*) isomer. A single broad peak in both HPLC and GC analysis of D_4^{Vi} further confirms this observation. Similarly, crystal structure of a Ni(0) complex reported in 7a supports the existence of the *cis-trans-cis* isomer (Figures S35-S37, Supporting Information). However, the formation of three different isomers in *cis-trans-cis*, *cis-cis-trans*, and *all-trans* conformation for L^{1} shows a change in isomeric ratio during the reaction.

(17) (a) Paulasaari, J. K.; Weber, W. P. *Macromolecules*, **1999**, *32*, 6574-6577; (b) Ronchi,

- M.; Pizzotti, M.; Biroli, A. O.; Macchi, P.; Lucenti, E.; Zucchi, C. *J. Organomet. Chem.*, **2007**, *692*, 1788-1798; (c) Lewis, L. N.; Sy, K. G.; Bryant Jr, G. L.; Donahue, P. E. *Organometallics*, **1991**, *10*, 3750-3759; (d) Marciniec, B. *Acc. Chem. Res.*, **2007**, *40*, 943-952; (e) Fürstner, A. *Angew. Chem.Int. Ed.*, **2000**, *39*, 3012-3043; (f) Czech, A.; Ganicz, T.; Noskowska, M.; Stańczyk, W. A.; Szelać, A. *J. Organomet. Chem.*, **2009**, *694*, 3386-3389.
- (18) Kinoshita, S.; Watase, S.; Matsukawa, K.; Kaneko, Y. *J. Am. Chem. Soc.* **2015**, *137*, 5061-5065.
- (19) Mandal, P. K.; McMurray, J. S. *J. org. chem.* **2007**, *72*, 6599-6601.
- (20) (a) Blatov, V. A.; Shevchenko, A. P.; Proserpio, D. M. *Cryst. Growth Des.*, **2014**, *14*, 3576-3586; (b) Blatov, V.; Shevchenko, A.; Serezhkin, V. *J. Appl. Crystallogr.*, **2000**, *33*, 1193-1193; (c) Blatov, V.; Shevchenko, A.; Serezhkin, V.; Korchagin, D. <http://www.topos.ssu.samara.ru>.
- (21) (a) Kyle, K. R.; Ryu, C. K.; Ford, P. C.; DiBenedetto, J. A. *J. Am. Chem. Soc.* **1991**, *113*, 2954-2965; (b) Ford, P. C.; Cariati, E.; Bourassa, J. *Chem. Rev.* **1999**, *99*, 3625-3648.; (c) Deshmukh, M. S.; Yadav, A.; Pant, R.; Boomishankar, R. *Inorg. Chem.* **2015**, *54*, 1337-1345; (d) Thébault, F.; Barnett, S. A.; Blake, A. J.; Wilson, C.; Champness, N. R.; Schröder, M. *Inorg. Chem.* **2006**, *45*, 6179-6187.
- (22) Siddiqui, M. M.; Mague, J. T.; Balakrishna, M. S. *Inorg. Chem.*, **2015**, *54*, 6063-6065.

Chapter 4: Section A

A 3D COORDINATION NETWORK BUILT FROM $\text{Cu}^{\text{II}}_4\text{Cl}_3(\text{H}_2\text{O})_2$ LINEAR CLUSTERS AND TETRA-PYRIDYL TETRAHEDRAL SILANE LIGANDS: REVERSIBLE IODINE UPTAKE AND FRIEDEL-CRAFTS ALKYLATION REACTIONS



4A.1 Introduction

Design and synthesis of three-dimensional coordination networks has received immense attention because of their fascinating structures and perceived potential in the development of materials for adsorbents, catalysis, sensors, molecular sieving, luminescence and drug delivery, etc.¹⁻⁴ These frameworks are typically constructed from the combination of metal ions or clusters of metal ions with multidentate organic ligands.⁵⁻⁷ The availability of numerous organic ligands of various geometries and functionalities has allowed the rational design of porous coordination polymers with specific structure and properties.⁸⁻¹⁰ The discovery of structures with new and novel topologies is important from the stand point of understanding the fundamental correlation among the framework structure, stability, porosity and interpenetration.¹¹⁻¹² Therefore, considerable efforts have been devoted towards the preparation of new ligands and their effects in the assembly of coordination polymers with new and rare topologies. Use of rigid tetrahedral linkers for constructing metal-organic frameworks (MOFs) is an attractive approach to synthesize novel materials that exhibit intriguing topologies and functional behaviour.¹³⁻²² However, many of such MOFs suffer from the complicated ligand synthesis,¹³⁻¹⁵ limited porosity,^{16,17} and undesired interpenetration.^{13,18} Davies and Zhou et al., have prepared MOFs based on some novel silicon-centered ligands,^{17,19,23-26} where the introduction of the silane backbone has largely simplified the process of preparing tetrahedral ligands. Inspired by the utility of polytopic ligand such as tetrakis(carboxyphenyl)silane for the synthesis of porous MOFs,^{15,17,19,22} we paid attention to obtain new ligands based on organosilane scaffolds. Especially, we aim to synthesize pyridyl functionalized silane ligands, owing to the challenges associated with the synthesis of rigid tetrahedral ligands with this functionality.^{27,28} Herein, I report the synthesis of a new ligand tetrakis-(3-pyridyl)vinylsilane (**TPVS or L⁵**) starting from tetra-vinylsilane and 3-Bromopyridine via the Heck Coupling reaction. Subsequent reduction of the vinylic double bonds in **TPVS** resulted in the formation of another ligand tetrakis-(3-pyridyl)ethylsilane (**TPES or L⁶**). Further, I show that these ligands are excellent building blocks for constructing framework solids by preparing two new cationic coordination networks for Cu(II) ions. Treatment of the rigid **TPVS** ligand with $\text{CuCl}_2 \cdot 2\text{H}_2\text{O}$ gave a 3D coordination network **10** of formula $[\text{Cu}_4\text{Cl}_3(\text{TPVS})_4(\text{H}_2\text{O})_2] \cdot \text{Cl}_5 \cdot \text{DMF} \cdot \text{MeOH}$ which contains an unusual $\text{Cu}_4\text{Cl}_3(\text{H}_2\text{O})_2$ tetranuclear cluster as the secondary building unit (SBU).

Whereas, the flexible ligand TPES under similar reaction conditions formed a different 3D framework **11** of formula $[\text{Cu}_2\text{Cl}(\text{TPES})_2(\text{H}_2\text{O})_2] \cdot \text{Cl}_3 \cdot 2\text{MeOH}$ having shorter $\text{Cu}_2\text{Cl}(\text{H}_2\text{O})_2$ linear clusters as the SBUs. Due to the presence of uncoordinated chloride ions in their pores and the electron rich ligand vinyl moieties (in the case of **10**) which provide the sites of interaction, I explored the utility of these MOFs for iodine encapsulation. These studies showed a high reversible uptake of I_2 for **10**. Also, the presence of polynuclear Lewis acidic Cu(II) clusters in **10** and **11** prompted us to investigate the use of these solids as catalysts. Thus, we employed both **10** and **11** for the Friedel-Crafts alkylation reaction for the efficient syntheses of bis(indolyl)methanes, an important class of heterocyclic compounds for their biological activity.

4A.2 Experimental Section

4A.2.1 General remarks

All manipulations were performed under a dry atmosphere in standard Schlenk-glassware. Tetravinylsilane, 3-bromopyridine, $\text{Pd}[\text{t-Bu}_3\text{P}]_2$ and $\text{CuCl}_2 \cdot 2\text{H}_2\text{O}$ were purchased from Aldrich and used as received. NMR spectra were recorded on a 400 MHz Bruker FT spectrometer (^1H -NMR: 400 MHz, $^{13}\text{C}\{^1\text{H}\}$ -NMR: 100 MHz, ^{29}Si -NMR: 80 MHz) at room temperature using SiMe_4 as external standards. FT-IR spectra were taken on a Perkin-Elmer spectrophotometer. The absorption studies were done by a Perkin-Elmer Lambda 45 UV-Visible spectrophotometer. Thermogravimetric analysis (TGA) data was obtained in Perkin-Elmer STA 1000 instrument. The powder X-ray diffraction (PXRD) data were obtained from a Bruker-D8 Advance diffractometer. The morphology and elemental mapping data were recorded using Zeiss Ultra Plus Field-emission Scanning Electron Microscope (FESEM) and Energy dispersive X-ray spectroscopy (EDXS), respectively. Gas-adsorption measurements were performed using a BELSORP-max instrument. Elemental analyses were performed on a Vario-EL cube elemental analyzer.

4A.2.2 Syntheses

4A.2.2.1 Synthesis of ligand $\text{Si}(\text{CH}=\text{CH}_3\text{-Py})_4$ (TPVS or L^5): 3-Bromopyridine (7.18 g, 44 mmol) and tetravinyl silane (1.5 g, 11 mmol) was kept under nitrogen in a 250 ml two neck round bottom flask, equipped with magnetic stirrer and reflux condenser. The flask was purged with nitrogen for 15 min at room temperature and then 15 ml of triethylamine and

$\text{Pd}[\text{t-Bu}_3\text{P}]_2$ (20 mg, 0.1 mmol) were added. The reaction mixture was then stirred at 90 °C for 96 h. After cooling to room temperature, hexane (50ml) was added and the mixture was washed with water in a separating funnel. The organic layer was separated, filtered through celite and evaporated in vacuum, to get crude TPVS as yellowish-brown solid. The crude mixture was purified by column chromatography using ethyl acetate as eluent which gave 3.42 g (70 % yield) of pure ligand TPVS. ^1H NMR (400 MHz, CDCl_3): δ = 8.75 (s, 1H), 8.57 (d, J = 4.0 Hz, 1H), 7.88 (d, J = 8.0 Hz, 1H), 7.34(m, 1H), 7.16 (d, J = 20.0 Hz, 1H), 6.76 (d, J = 20.0 Hz, 1H) ppm. $^{13}\text{C}\{^1\text{H}\}$ -NMR (100 MHz, CDCl_3): δ 123.6, 125.2, 133.1, 145.1, 148.8, 149.7. ^{29}Si NMR (80 MHz, CDCl_3 , Me_4Si): δ -24.6 (s, 1Si) ppm MALDI-TOF m/z = 445.1517 [M+H] (Expected 445.18). FT-IR data in powdered sample (cm^{-1}):3347, 3262, 2378, 1646, 1410, 1235, 1027, 990, 776, 697, 1065. Anal. calcd. for $\text{C}_{28}\text{H}_{24}\text{N}_4\text{Si}$: C, 75.64; H, 5.44; N, 12.60. Found: C, 75.68; H, 5.49; N, 12.63. Melting Point 152.

4A.2.2.2 Synthesis of ligand $\text{Si}(\text{CH}_2\text{CH}_2\text{3-Py})_4$ (TPES or L^6): To a stirred mixture of the ligand TPVS (0.25g, 0.38 mmol) and 10% Pd-C (2.5mg) in MeOH (5-10 mL) taken in a two-necked round bottom flask at room temperature under an inert atmosphere, triethylsilane (1.8 g, 15 mmol) was added drop-wise from a pressure-equalizing funnel. When the reaction was complete (TLC), the mixture was filtered through celite and the solvent was removed under vacuum. The product was purified by using a short silica gel column to yield the respective products of TPES. ^1H NMR (400 MHz, CDCl_3): δ = 8.51 (s, 2H), 7.52 (d, J = 8.0 Hz, 1H), 7.26 (s, 1H), 2.68 (t, J = 8.0 Hz, 2H) 1.05 (t, J = 8.0 Hz, 2H) ppm. $^{13}\text{C}\{^1\text{H}\}$ -NMR (100 MHz, CDCl_3): δ -14.0, 27.2, 123.5, 153.1, 147.5, 149.3. ^{29}Si NMR (80 MHz, CDCl_3 , Me_4Si): δ 4.0 ppm. MALDI-TOF m/z = 453.123 [M+H] (Expected 453.68). FT-IR data in powdered sample (cm^{-1}):3029, 2923, 2378, 1664, 1476, 1420, 1317, 1129, 1026, 998, 832, 708. Anal. calcd. for $\text{C}_{28}\text{H}_{32}\text{N}_4\text{Si}$: C, 74.29; H, 7.13; N, 12.38. Found: C, 74.25; H, 7.19; N, 12.42.

4A.2.2.3 Synthesis of compound $[\text{Cu}_4\text{Cl}_3(\text{TPVS})_4(\text{H}_2\text{O})_2]\cdot\text{Cl}_5\cdot\text{DMF}\cdot\text{MeOH}$ (10): To a solution of TPVS (20 mg, 0.045 mmol) in methanol (1 mL) kept in a screw-capped vial was added a solution of $\text{CuCl}_2\cdot 2\text{H}_2\text{O}$ (7.75 mg, 0.045 mmol) in methanol (2 mL) with the immediate formation of a green precipitate. DMF (1 mL) was added to this precipitate to get a clear green solution and was subsequently heated at 90 °C under the solvothermal condition for 36 h. The resultant solution was slowly cooled to room temperature (at the rate of 0.1 °C

per minute) to obtain clear solution which on slow evaporation at room temperature yields blue crystals of **10** (Yield 60 %). FT-IR data in powdered sample (cm^{-1}): 3860, 3740, 3642, 3516, 3227, 2901, 2627, 2467, 2186, 1961, 1741, 1607, 1515, 1106, 989, 850, 797. Anal. calcd. for $\text{C}_{35}\text{H}_{38}\text{Cl}_2\text{CuN}_5\text{O}_{2.5}\text{Si}$: C, 58.53; H, 8.10; N, 10.12. Found: C, 58.58; H, 8.15; N, 10.16.

4A.2.2.4 Synthesis of compound $[\text{Cu}_2\text{Cl}(\text{TPES})_2(\text{H}_2\text{O})_2]\cdot\text{Cl}_3\cdot 2\text{MeOH}$ (11**):** To a solution of TPES (20 mg, 0.045 mmol) in methanol (1 mL) kept in a screw-capped vial was added a solution of $\text{CuCl}_2\cdot 2\text{H}_2\text{O}$ (7.75 mg, 0.045 mmol) in methanol (2 mL) with the immediate formation of a green precipitate. DMF (1 mL) was added to this precipitate to get a clear green solution and was subsequently heated at 90 °C under the solvothermal condition for 36 h. The resultant solution was slowly cooled to room temperature (at the rate of 0.1 °C per minute) to obtain clear solution which on slow evaporation at room temperature yields blue crystals of **11** (Yield 65%). FT-IR data in powdered sample (cm^{-1}): 3858, 3823, 3644, 2932, 2310, 1962, 1843, 1746, 1674, 1546, 1231, 1091, 985, 746. Anal. calcd. for $\text{C}_{29}\text{H}_{33}\text{Cl}_2\text{CuN}_4\text{OSi}$: C, 54.75; H, 5.86; N, 8.81. Found: C, 54.80; H, 5.90; N, 8.75.

4A.2.2.5 $\text{I}_2\subset\mathbf{10}$: The activated powder of **10** (**10''**) was placed in a screw-capped vessel filled with I_2 vapor at 350 K. The uptake of iodine was monitored gravimetrically which showed an almost saturated loading of about 45% iodine in 10 h. The TGA analysis of the fully-loaded sample (exposed to 15h I_2 vapor) showed a loading amount of 48.5 wt %.

4A.2.2.6 Monitoring the Gravimetric uptake of iodine: An activated powder of **10** (**10''**, 10 mg) was placed in a pre-weighed vial under a sealed atmosphere of I_2 and then heated at 70 °C. The sample vessel was removed from heating after every 30 minute period, cooled to room temperature, allowed the extra adsorbed iodine vapour to escape and the weight of the sample was measured. The gain in weight was monitored each time and it is observed that the adsorption capacity of **10''** was relatively very quick for the first 10 h period. After 15 h, there is no further uptake of iodine suggesting that the **10''** is saturated. A similar gravimetric I_2 uptake experiment was performed at room temperature. In this case, the saturation point was attained after 2 days.

4A.2.2.7 Gravimetric release of iodine: The 10 mg of $\text{I}_2\subset\mathbf{10}$ was placed in a pre-weighed vial and heated at open atmosphere at 100 °C. The gradual decrease in weight was recorded

over a period.

4A.2.3 Crystallography

Reflections were collected on a Bruker Smart Apex Duo diffractometer at 100 K using MoK α radiation ($\lambda = 0.71073 \text{ \AA}$). Structures were refined by full-matrix least-squares against F^2 using all data (SHELX).^{29a} Crystallographic data for all these compounds are listed in (Table 4A.1 and Appendix, A4A.1). All non-hydrogen atoms were refined anisotropically if not stated otherwise. Hydrogen atoms were constrained in geometric positions to their parent atoms. The diffuse solvent molecules in compound **10** and **11** could not be modeled appropriately. Hence, these were treated as diffuse contributions to the overall scattering and removed by the SQUEEZE/PLATON for a better refinement data.^{29b}

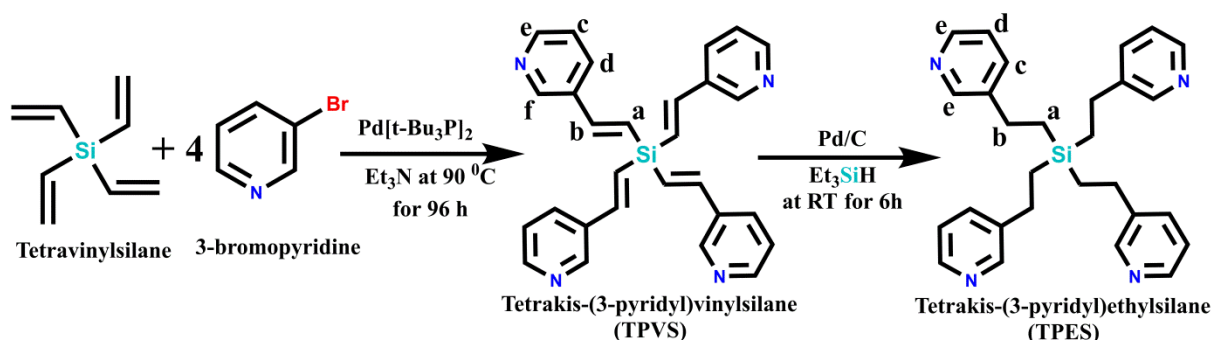
Table 4A.1: Details of crystallographic data collection and structure refinements for TPVS, 10 and 11

Compound	TPVS	10	11
Chemical formula	C ₂₈ H ₂₄ N ₄ Si	C ₁₁₂ H ₉₆ Cl ₈ Cu ₄ N ₁₆ O ₂ Si ₄	C ₃₆ H ₆₄ Cl ₄ Cu ₂ N ₈ O ₂ Si ₂
Formula weight	444.16	2348.16	1206.12
Temperature	100(2)K	100(2)K	100(2) K
Crystal system	Tetragonal	Tetragonal	Tetragonal
Space group	I-4	I4/m	I4/m
a (Å); α (°)	13.906(2); 90°	14.508(5); 90°	14.104(9); 90°
b (Å); β (°)	13.906(2); 90°	14.508(5); 90°	14.104(9); 90°
c (Å); γ (°)	5.8587(11); 90°	34.921(14); 90°	19.100(12); 90°
V (Å ³); Z	1133.0(4); 16	7350(6); 8	3800(6); 28
ρ (calc.) mg m ⁻³	1.303	1.061	1.054
μ (Mo K α) mm ⁻¹	0.128	0.792	0.768
2 θ_{\max} (°)	50.048	48.80	50.054
R(int)	0.0758	0.10939	0.1265
Completeness to θ	98.6 %	99.9 %	99.9 %
Data / param.	993/75	4699/173	1745 / 92
GOF	1.144	0.971	1.075
R1 [F > 4 σ (F)]	0.0520	0.0496	0.0607
wR2 (all data)	0.13960	0.1627	0.2061
max. peak/hole (e.Å ⁻³)	0.505/-0.441	0.953/-0.505	1.508 /-0.521

4A.2.4 Catalytic properties of 10 and 11

4A.2.4.1 General catalytic procedure for Friedel-Crafts alkylation of indole: A mixture of benzaldehyde (106.1 mg, 1 mmol) and indole (234.3 mg, 2 mmol) in the presence of the MOF (**10** or **11**) catalyst (5 mg, 5% wt) was stirred at room temperature for 4 h (monitored by TLC). After this period dichloromethane (2 mL) was added to the reaction mixture and the catalyst was recovered by filtration. The product of bis(indolyl)methane was extracted by

evaporating the solvent and subsequently purified by column chromatography on silica gel ($\text{CH}_2\text{Cl}_2/\text{petroleum ether} = 1 : 1$) to provide target product as a white solid (yield, 92 %). ^1H NMR (400 MHz, CDCl_3): $\delta = 7.91$ (s, 2H), 7.33 (m, 6H), 7.20 (t, 2H), 7.17 (dd, 1H), 7.14 (t, 2H), 6.99 (t, 2H), 6.63 (dd, 2H), 5.88 (s, 1H). ^{13}C NMR (100 MHz, CDCl_3) $\delta = 144.1, 136.8, 128.8, 128.3, 127.2, 126.2, 123.7, 122.0, 120.0, 119.3, 111.3, 40.3$. MS-EI, m/z, Anal. Calcd: 321.14, Exp: 321.13 (M+H).



Scheme 4A.1: Schematic diagram for the preparation of the silane ligands

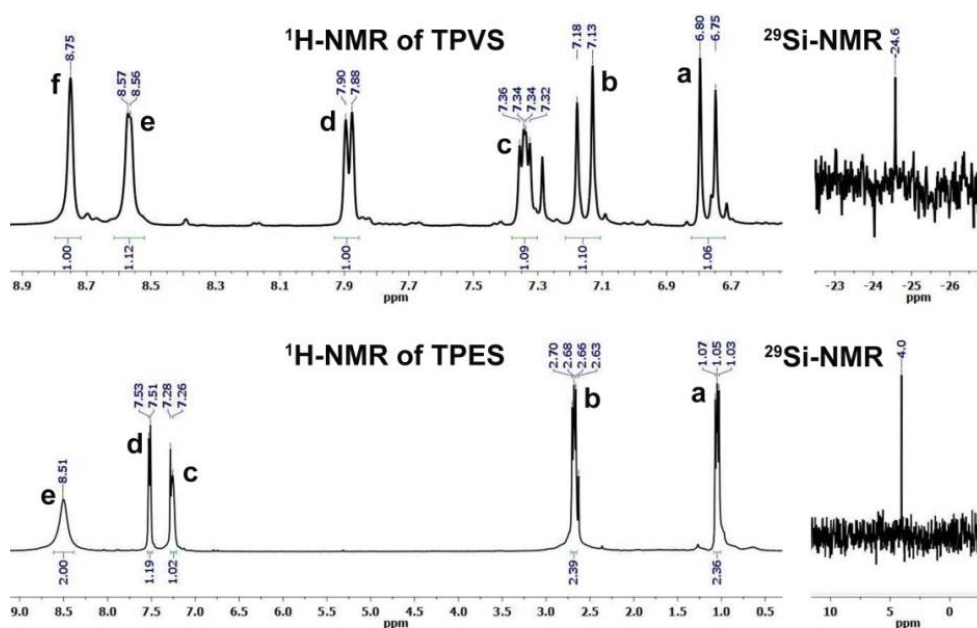


Figure 4A.1: ^1H and ^{29}Si NMR spectra of TPVS and TPES ligand

4A.3 Result and Discussion

4A.3.1 Syntheses

The rigid ligand TPVS was synthesized from the reaction of tetravinylsilane with 3-

bromopyridine in the presence of $\text{Pd}[\text{t-Bu}_3\text{P}]_2$ catalyst and triethylamine as a base, similar to the procedure we developed for the synthesis of tetra-vinylpyridyl tetrasiloxanes.³⁰ The flexible ligand **TPES** was subsequently obtained by the reduction of vinylic bonds in **TPVS** by using triethylsilane as reducing agent and Pd/C as the catalyst (Scheme 4A.1). The ligands were characterized by ^{29}Si , ^1H and ^{13}C NMR, mass spectroscopy and by single crystal X-ray diffraction analysis in the case of **TPVS** (Figures 4A.1 and Appendix, A4A.1-A4A.7). The single crystals of **10** and **11** as their solvate adducts were obtained by the respective reaction of **TPVS** and **TPES** with $\text{CuCl}_2 \cdot 2\text{H}_2\text{O}$ in mixed dimethylformamide (DMF) and methanol solvents under solvothermal conditions at 90°C for 36h followed by slow evaporation of the solvents at room temperature.

4A.3.2 Crystal structures

The SCXRD analysis revealed that both **10** and **11** were crystallized in the tetragonal space group $I4/m$ as their solvate adducts (Table 4A.1 and Appendix, A4A.1). The structural investigations showed the formation of intricate framework structures with 3D-network topologies (Figure 4A.2). The molecular framework in **10** consists of an unusual tetranuclear $\text{Cu}_4\text{Cl}_3(\text{H}_2\text{O})_2$ linear cluster as an SBU and the tetrahedral **TPVS** ligands as linkers. The molecular structure of **11** consists again of a cationic 3D framework build-up of the dinuclear $\text{Cu}_2\text{Cl}(\text{H}_2\text{O})_2$ clusters as SBUs and the stacked **TPES** as linkers.

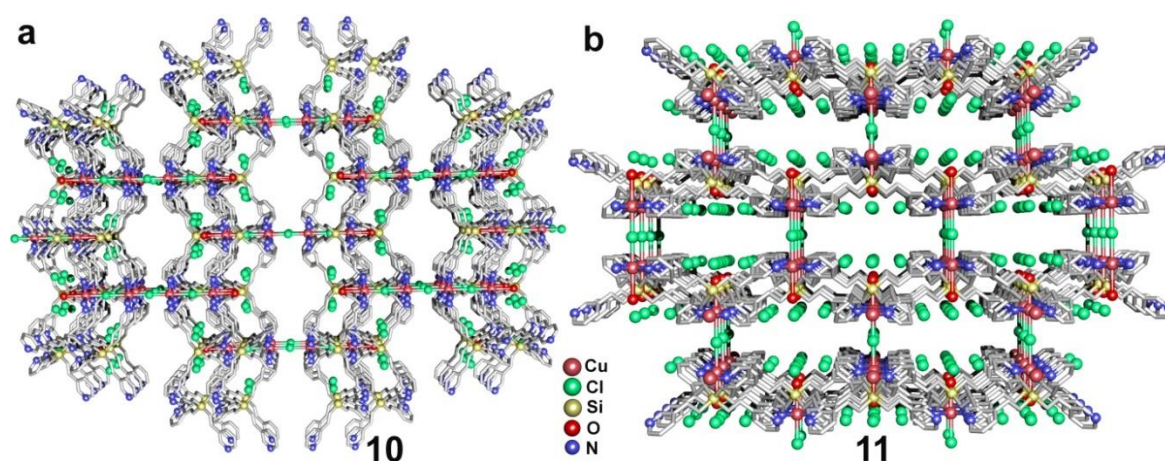


Figure 4A.2: View of the cationic 3D-networks in **10** (a) and **11** (b)

Each $\text{Cu}(\text{II})$ ions in **10** and **11** were attached to four different ligands. While the tetranuclear cluster in **8** is connected to sixteen unique pyridyl groups (Figure 4A.3b), the dinuclear

cluster in **11** is attached to eight pyridyl groups (Figure 4A.4b). In return, each TPVS and TPES ligands are four connected and are attached to Cu(II) atoms that belong to four different linear clusters (Figure 4A.3a and 4A.4a, respectively). All the Cu(II) sites in **10** and **11** are located in an octahedral environment in which the ring N-atoms of the pyridyl ligands form the square plane. In **10**, the outer Cu(II) atoms contain one terminal aqua ligand and one μ_2 -bridging Cl^- ion at the apical positions.

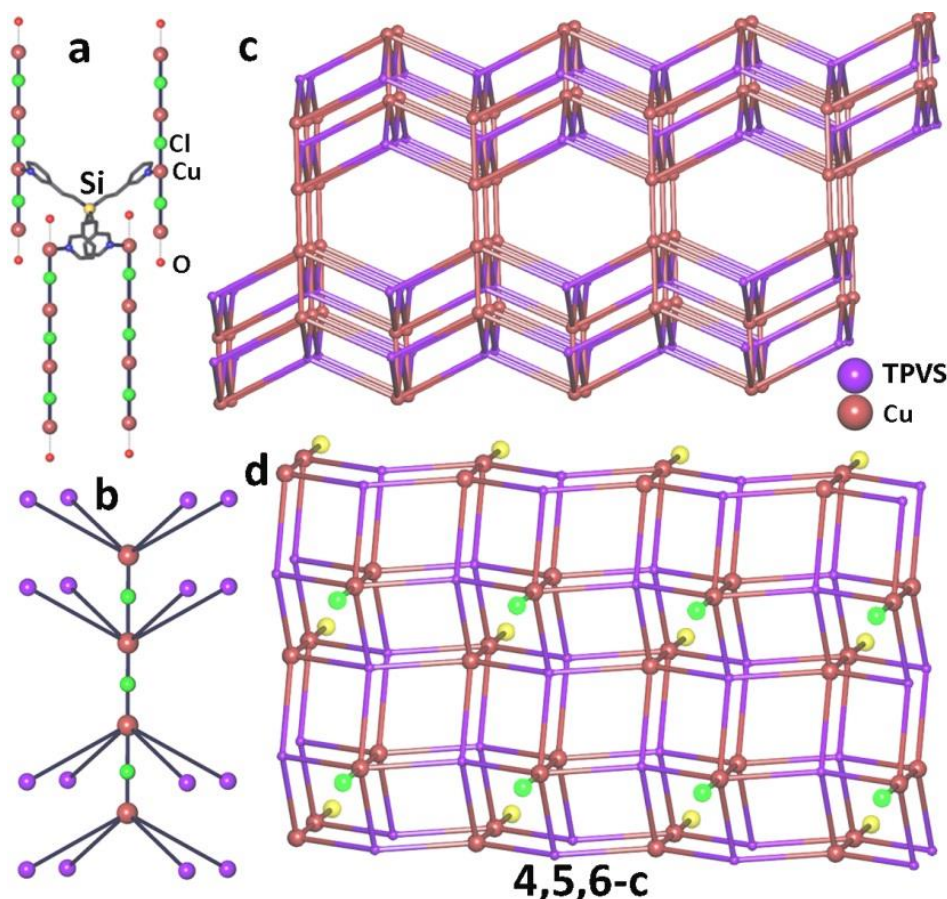


Figure 4A.3: Topological representation of **10** showing (a) the arrangement of the $\text{Cu}_4\text{Cl}_3(\text{H}_2\text{O})_2$ clusters around TPVS ligand; (b) the arrangement of the TPVS ligands around the $\text{Cu}_4\text{Cl}_3(\text{H}_2\text{O})_2$ cluster (hydrogen atoms omitted for clarity); (c) the underlying trinodal 4,5,6-c net (4,5,6T115) in **1** and (d) its similarity with tcs topology via the connection of the second μ_2 -chloride bridges represented by green and yellow spheres that can superimpose onto each other to form the double-layered aggregates.

Whereas, the internal Cu(II) atoms contain only μ_2 - Cl^- ions at their apex (Appendix, A4A.8). In **11**, both the Cu(II) atoms have an octahedral N_4ClO environment in which the bridging

chloride ions and the terminal aqua ligands were located at the apical positions (Appendix A4A.9). The void volumes of **10** and **11** were calculated by excluding the solvate molecules by using the Mercury program.³¹ The computed solvent accessible volumes in **10** and **11** were found to be 30.7 % (2252.74 Å³) and 22.6% (846.16 Å³), respectively, of the total unit cell volumes. The topological description of the crystal structures was carried out in ToposPro program using several simplification procedures in which the metal atoms remain intact, but ligands are represented by their center of mass, keeping the connectivity of the ligand with its neighbors.^{32,33} The standard simplification procedure resulted in 4,5,6-coordinated trinodal net (4,5,6-c) with a new topology in **10** represented by the symbol 4,5,6T115 (Figure 4A.3c) and 4,5-coordinated (4,5-c) **tcs** net in **11** (Figure 4A.4c). The ligands are always 4-connected and the copper atoms are 5 and 6-coordinated nodes in these nets.

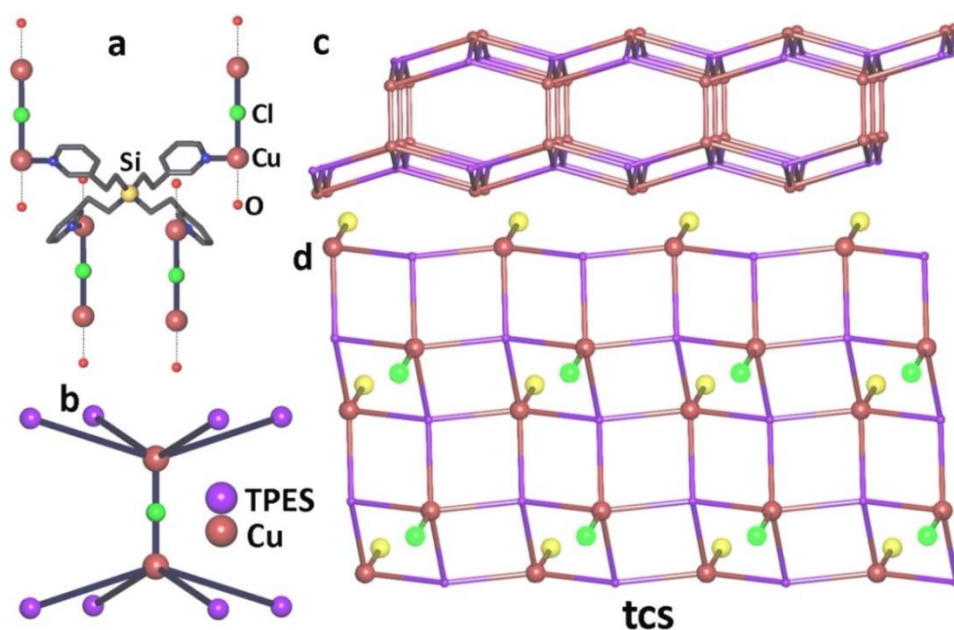


Figure 4A.4: Topological representation of **11** showing (a) the arrangement of the $\text{Cu}_2\text{Cl}(\text{H}_2\text{O})_2$ clusters around **TPES** ligand and (b) **TPES** ligands around the $\text{Cu}_2\text{Cl}(\text{H}_2\text{O})_2$ cluster (hydrogen atoms omitted for clarity); (c) the underlying binodal 4,5-c net of **tcs** topology and (d) the view of its single layer with **sql** topology. Green and yellow spheres represent the μ_2 -chloride ligands that superimpose onto each other to form the **tcs** network.

It is interesting to compare the structural topologies present in **10** and **11**. The **tcs** topology in **10** (Figure 4A.4c) is formed by the stacking of two **sql** layers (simple square-layers) onto each other. These layers are connected by the μ_2 -chloride ligands (green and yellow spheres)

in such a way that green squares are superimposed on the yellow ones (Figure 4A.4d). In **10**, the **sql** layers are doubled (Figure 4A.3d) and further connected by another μ_2 -chloride ligand leading to a hitherto unknown topology for the trinodal 4,5,6-c network (Figure 4A.3c). Nevertheless, the standard structural representation is unable to unveil the clear interrelation between the two MOFs fully. More meaningful representation can be obtained by considering the whole linear clusters as a single node or building blocks and the four connected ligands (**TPVS** and **TPES**) as another node. This arrangement results in the connection of $\text{Cu}_4\text{Cl}_3(\text{H}_2\text{O})_2$ clusters with sixteen **TPVS** ligands and $\text{Cu}_2\text{Cl}(\text{H}_2\text{O})_2$ clusters coordinated with eight **TPES** ligands in the structures of **10** and **11**, respectively. This representation leads to a new highly coordinated binodal 4,16-c net in **10** represented by the symbol 4,16T9 and to the well-known 4,8-c binodal net of the **flu** topological type in **11** (Figure 4A.5). A detailed search through the CSD for linear and finite copper-halogen chains using the ToposPro revealed that the structure of **10** is the only one that contains such a long linear Cu_4Cl_3 copper cluster as building units that are joined by ligands into the 3D framework. There is one instance of the resemblance of **11** for the OQIRAI structure with a rod-type Cu_2I_3 cluster. Other 3D frameworks comprise square Cu_4Cl cores with μ_4 -chloride ions.³⁴⁻³⁶

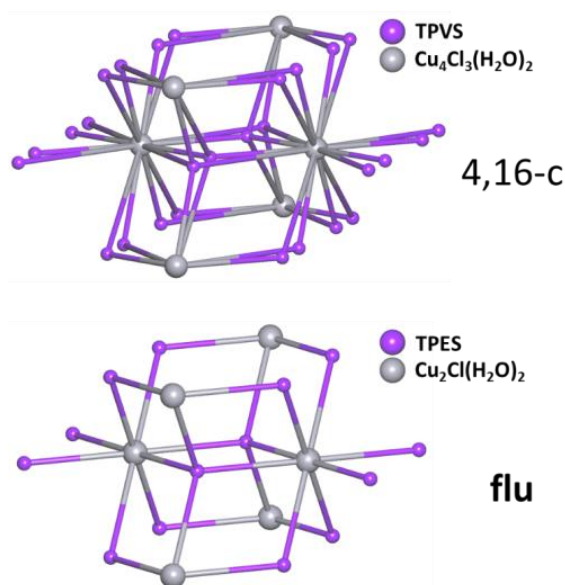


Figure 4A.5: Representation of structure **10** (top) that characterizes the connection mode of copper clusters and organic ligands **TPVS** as single nodes in a new 4,16-c topology represented by 4,16T9 and **11** (bottom) **TPES** as single nodes in the 4,8-c **flu** topology. This shows an intrinsic relationship between the two structures from a topological point of view

4A.3.3 Iodine uptake studies of **10**

The guest free samples of **10** and **11** were obtained by evacuating the solvents present in their pores. Before evacuation, the high boiling DMF solvate in **10** was exchanged with MeOH by soaking the crystals in methanol. From the PXRD analysis, it is apparent that **10** retain its crystallinity and framework integrity even after removal of the pore solvents. However, compound **11** was found to lose its crystallinity after removal of its methanol solvates (Appendix, A4A.10 and A4A.11). Further, TGA analysis of **10**, **10'** (MeOH exchanged) and **10''** (evacuated) showed that the solvent exchange route could achieve full evacuation. The variable temperature PXRD and TGA analyses show that the framework is stable up to 250 °C. The PXRD data obtained on the samples of **10** show that all the prominent diffraction peaks in **10'** and **10''** can be matched with those present in as made **10** (Appendix, A4A.12 and A4A.13). Owing to the presence of vinylic double bonds and polar Cl^- ions, we checked the gas adsorption and I_2 uptake behavior of **10** (Appendix, A4A.14). Thus, when **10''** was exposed to iodine vapor in a screw-capped vial at 70 °C, the color of the sample changed progressively from green to brown within one hour. A saturated iodine loading of about 45.2% was reached within ten hours to generate the I_2 loaded MOF **10** ($\text{I}_2 \subset \mathbf{10}$). The TGA plot of $\text{I}_2 \subset \mathbf{10}$ gave an I_2 content of around 48.5% indicated by a sharp weight loss at 100 °C (Figures 4A.6a and 4A.6b). Further, the iodine uptake of **10** was investigated in solution by soaking **10''** (50 mg) in the 0.03M ethanol (3 ml) solution of I_2 . The apparent uptake of I_2 was confirmed by the fading of the dark brown color of the I_2 solution to pale red with a concomitant increase in the intensity of color for the powdered sample of **10** (Appendix, A4A.15a). Notably, the I_2 uptake of **10** was found to be reversible both in solution and in the solid-state. When a solid sample of $\text{I}_2 \subset \mathbf{10}$ was heated at 100 °C for ten hours, 87% of the encapsulated iodine was completely removed, and **10''** was regenerated upon subsequent evacuation under vacuum. From the TGA and PXRD analysis, the retention of crystallinity and structural integrity of **10** during the reversible I_2 loading and unloading processes can be confirmed (Figure 4A.6c and Appendix, A4A.16). Similarly, the I_2 desorption in solution can be observed when the sample of $\text{I}_2 \subset \mathbf{10}$ is immersed in neat ethanol. Monitoring the I_2 release profile by UV-Visible spectroscopy indicates that the onset of I_2 release takes place as soon as $\text{I}_2 \subset \mathbf{10}$ comes into contact with ethanol. A gradual increase in the release profile can be observed as the time progresses and intensity of the I_2 absorption saturates in 2 h (Figures

4A.6d and Appendix, A4A.15b).

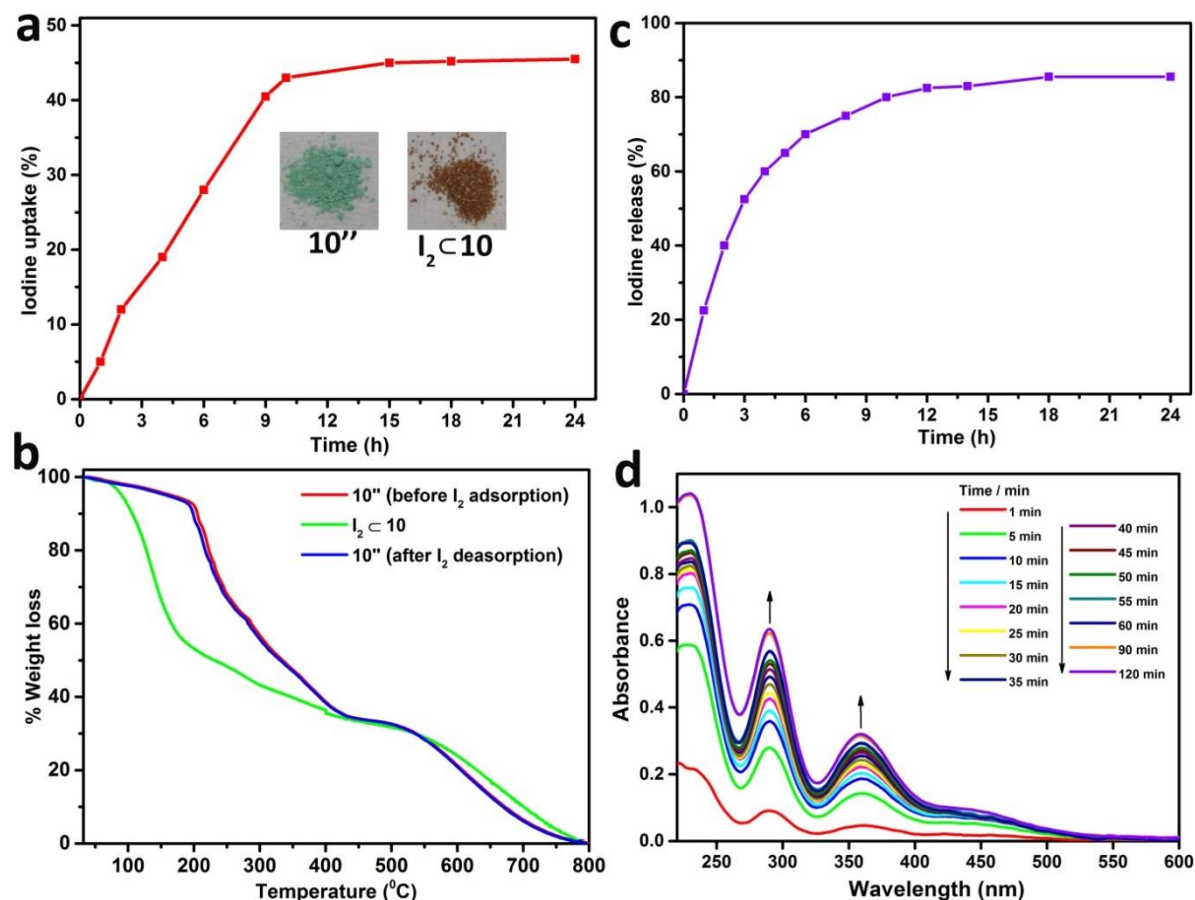


Figure 4A.6: (a) Gravimetric uptake of I_2 by **10** and (b) the I_2 release profile of $\text{I}_2 \subset 10$ in the solid-state. Insets show changes in sample colour before and after I_2 uptake. (c) TGA profiles showing a reversible I_2 uptake by **10**. (d) UV-visible spectral evolution showing the release of iodine from $\text{I}_2 \subset 10$ in ethanol.

To understand the role of uncoordinated chloride ions for the uptake of I_2 in **10**, we exchanged the Cl^- ions with other ones such as nitrate, bromide and iodide ions. The well ground crystalline powders of **10** were separately suspended in the 1M aqueous solution of NaNO_3 , KBr and NaI for the exchange studies. After three days, the exchanged samples were washed with distilled water several times and then dried under vacuum. The exchange products were analyzed by IR, PXRD and TGA methods which showed these compounds exhibit excellent stability in water. The PXRD of the exchanged samples shows similar patterns to that of **10** indicating that the basic framework remains unchanged upon anion exchange (Figure 4A.7a). In the IR spectra of the nitrate exchanged sample a new peak at

1311 cm^{-1} appeared due to the N-O symmetric stretching vibrations of the nitrate ion (Appendix, A4A.17). Scanning electron microscope (SEM) and energy-dispersive X-ray spectrometry (EDX) were performed to investigate the surface state of the samples. The SEM images showed that the morphology of **10** remains unaffected in all the anion exchanged samples (Appendix, A4A.18). The EDX results reveal that the relative atomic ratios of Cu, Si and C on the surface of all the anion-exchanged samples are mostly identical to that of **10**. These results indicate that no surface decomposition has occurred during the exchange process. Furthermore, the quantitative presence of Br^- and I^- ions were identified from the EDX profiles (Appendix, A4A.19-A4A.22). In the nitrate exchanged sample, the atomic ratio of Cl^- ion decreased considerably with a concomitant increase in the oxygen ratio. These observations were supported by the SEM-element mappings which gave a clear evidence for the exchange of anions in all these cases (Appendix, A4A.23-A4A.26).

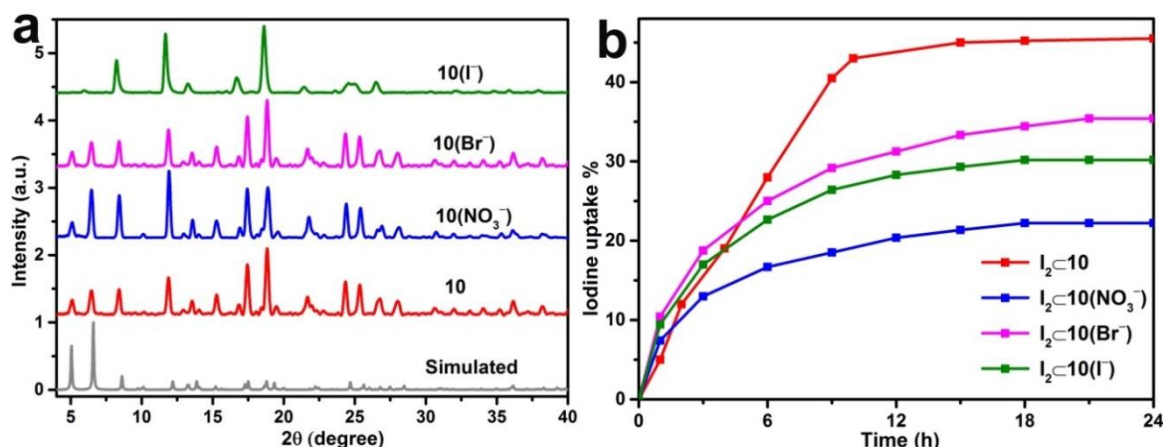


Figure 7: Comparisons of anion-exchanged samples of **10** (a) PXRD patterns and (b) Gravimetric uptake of I_2 .

To explore their anion-dependent I_2 adsorption properties, these exchanged compounds were exposed to Iodine vapors in a closed vial at $70\text{ }^\circ\text{C}$ for twelve hours. The TGA plot of the NO_3^- exchanged sample showed a considerable decrease of I_2 uptake from 48.5 to 24.0 %, while the Br^- and I^- exchanged compounds showed a marginally lower uptake of 37.7 and 32.0 %, respectively. These observations were consistent with their corresponding gravimetric uptake profiles (Figures 4A.7b and Appendix, A4A.27-A4A.30). These observations suggest that presence of halides counter ions has a clear influence on the iodine uptake characteristics of **10** which are found to interact better with I_2 in comparison with

nitrate ion. The better I₂ uptake of **10** in the presence of Cl⁻ ions over the other two halides can be attributed to its smaller size resulting in a larger surface area for adsorption. Known examples of MOFs with high I₂ affinity utilizes organic ligands featuring π -conjugated backbone and electron-pair donors (both neutral and anionic) groups such as pyridyl, alcohol, ether and amine functionalities.³⁷⁻³⁹ All these functional groups can interact with I₂ via stable charge-transfer complexation or halogen bond formation and thereby facilitate the increased adsorption of I₂. Furthermore, the reversible capture of I₂ by **10** has implications for addressing some important societal problems such as trapping radioactive isotope of ¹²⁹I from nuclear wastes and release of clinically useful ¹³¹I isotope for cancer therapy.⁴⁰⁻⁴²

4A.3.4 Catalytic activities of **10 and **11****

Finally, the compounds **10** and **11** were employed for the Cu(II) catalyzed synthesis of bis(indolyl)methanes by indole Friedel-Crafts alkylation under solvent-free conditions. Thus, the treatment of substituted benzaldehydes with indole in the 1:2 ratio in the presence of the catalysts (5 wt. % of **10** or **11**) at room-temperature afforded the corresponding bis(indolyl)methanes in quantitative yields; 75-90 % in case of **10** and 50-80% in the case of **11** in the isolated form (Figure 4A.8 and Appendix, Table A4A.2). Remarkably, the compounds **10** and **11** can be reused for five times without any significant loss in their catalytic activity (Appendix, Table A4A.3). The comparison of the PXRD patterns before and after the second and fifth catalytic cycle (recovered after removing the organic compounds in DCM) demonstrated that the crystallinity of the MOFs (**10** and **11**) is retained during these catalytic reactions. Also, it is observed that the catalysts are stable after the second catalytic cycle, but it starts to degrade slowly after the fifth cycle (Appendix, A4A.31 and A4A.32). Furthermore, to determine whether the surface or the inner pores of the MOF acts as the site of the catalytic activity, we studied the size-dependent catalytic activity of **10**. For that, the powdered solid of **10** was centrifuged (at 7540 RPM) in methanol for seven minutes, and the smaller particles of size less than 300 μ m were recovered from the supernatant part and dried. The catalytic studies revealed the smaller particles show a sizable decrease in the catalytic activity (20 % yield) in comparison with that of the larger ones (74 % yield) for the *p*-nitro benzaldehyde substrate. This indicates that the catalytic reaction takes place on the surface of these MOFs via the displacement of the weakly bound axial aqua ligands at the Cu(II) sites. Although the catalytic efficiency of **10** is expected to increase upon removal of

the axial aqua ligands, such studies were not performed due to the loss of crystallinity (Appendix, A4A.10) during the high-temperature activation process.

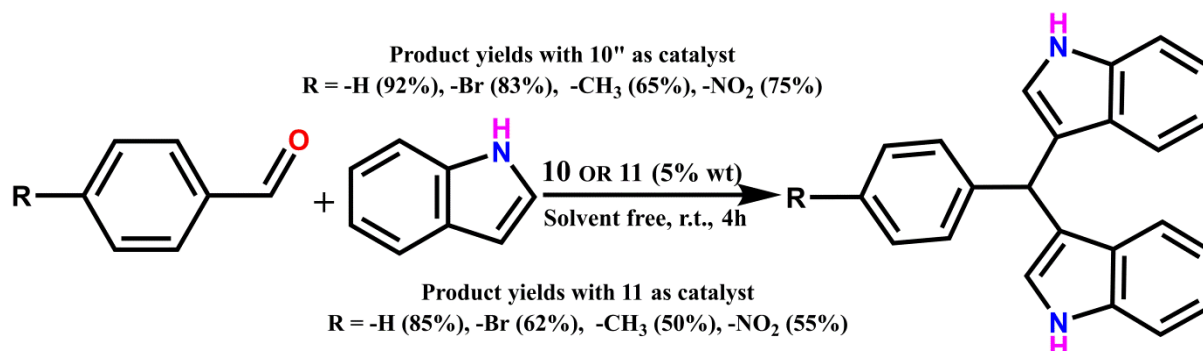


Figure 4A.8: Solvent free Friedel-Crafts alkylation of indole with benzaldehydes by **10** and **12**

To our knowledge, there are only two examples related to the heterogeneous catalytic indole Friedel-Crafts alkylation tandem reactions have so far been reported.^{43,44} These reported reactions were catalyzed by porous aluminosilicate materials and by triphenylphosphine-m-sulfonate salts to generate the corresponding Friedel-Crafts alkylation products in 91 and 75 % yields, respectively. However, these reactions require high temperatures and involve toxic species such as CBr_4 as additives. The compounds **10** and **11** have other advantages as they can catalyze these reactions at room temperature and importantly could offer a considerably clean synthetic approach as they require no additional organic solvents for this reaction.

4A.4 Conclusion

In conclusion, I have reported a simple synthetic protocol for preparing two tetrahedral tetra-pyridyl ligands utilizing an organosilane scaffold. These ligands feature rigid vinyl and flexible ethyl spacers in their backbone. The ligands were employed in reaction with CuCl_2 to obtain two novel 3D coordination networks having unique linear $\text{Cu}_4\text{Cl}_3(\text{H}_2\text{O})_2$ and $\text{Cu}_2\text{Cl}(\text{H}_2\text{O})_2$ clusters as secondary building units. A search of the CSD shows that the Cu_4Cl_3 motif of **10** is the longest building unit among copper halide clusters leading to the formation of a 4,5,6-c connected net with a new topology 4,5,6T115. The complex **10** (in the activated state) shows very good uptake and release of I_2 adsorption capacity in both vapor and solution phases. The I_2 adsorption studies of the anion-exchanged samples of **10** show better uptake characteristics for the sample containing Cl^- ions due to its better interaction and the

availability of larger surface area. Furthermore, these frameworks were found to be good catalysts for Friedel-Crafts alkylation reactions. Size-dependent catalytic activity of **10** shows a better activity for bigger-sized particles which indicates that the catalytically active sites are located on the surface of the MOF. The present work shows that organosilane backbones offer an excellent platform for obtaining framework materials in 3D-topologies. This strategy can be further utilized in future for obtaining MOFs with unique structures and functionalities.

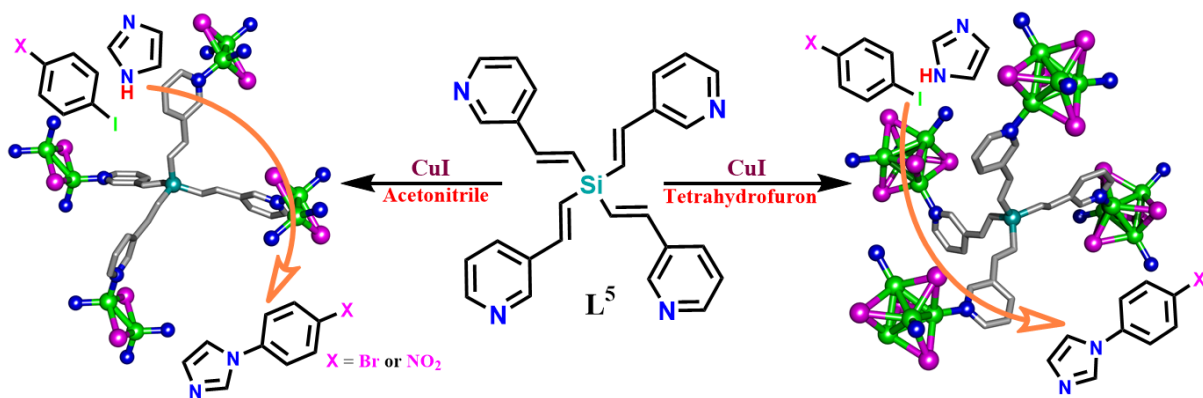
4A.5 References

- (1) Zhou, H.-C.; Long, J. R.; Yaghi, O. M. *Chem. Rev.* **2012**, *112*, 673-674.
- (2) Sumida, K.; Rogow, D. L.; Mason, J. A.; McDonald, T. M.; Bloch, E. D.; Herm, Z. R.; Bae, T.-H.; Long, J. R. *Chem. Rev.* **2011**, *112*, 724-781.
- (3) Liu, J.; Chen, L.; Cui, H.; Zhang, J.; Zhang, L.; Su, C.-Y. *Chem. Soc. Rev.* **2014**, *43*, 6011-6061.
- (4) Hu, Z.; Deibert, B. J.; Li, J. *Chem. Soc. Rev.* **2014**, *43*, 5815-5840.
- (5) Férey, G. *Chem. Soc. Rev.* **2008**, *37*, 191-214.
- (6) Kitagawa, S.; Kitaura, R.; Noro, S. I. *Angew. Chem. Intern. Ed.* **2004**, *43*, 2334-2375.
- (7) Deshmukh, M. S.; Yadav, A.; Pant, R.; Boomishankar, R. *Inorg. Chem.* **2015**, *54*, 1337-1354.
- (8) Lu, W.; Wei, Z.; Gu, Z.-Y.; Liu, T.-F.; Park, J.; Park, J.; Tian, J.; Zhang, M.; Zhang, Q.; Gentle III, T. *Chem. Soc. Rev.* **2014**, *43*, 5561-5193.
- (9) Paz, F. A. A.; Klinowski, J.; Vilela, S. M.; Tome, J. P.; Cavaleiro, J. A.; Rocha, J. *Chem. Soc. Rev.* **2012**, *41*, 1088-1110.
- (10) Zhao, D.; Timmons, D. J.; Yuan, D.; Zhou, H.-C. *Acc. Chem. Res.* **2010**, *44*, 123-133.
- (11) Blatov, V. A.; Carlucci, L.; Ciani, G.; Proserpio, D. M. *CrystEngComm.* **2004**, *6*, 377-395.
- (12) Li, M.; Li, D.; O'Keeffe, M.; Yaghi, O. M. *Chem. Rev.* **2013**, *114*, 1343-1370.
- (13) Liu, D.; Wu, H.; Wang, S.; Xie, Z.; Li, J.; Lin, W. *Chem. Sci.* **2012**, *3*, 3032-3037.
- (14) Tan, C.; Yang, S.; Champness, N. R.; Lin, X.; Blake, A. J.; Lewis, W.; Schröder, M. *Chem. Commun.* **2011**, *47*, 4487-4489.
- (15) Qiu, S.; Zhu, G. *Coord. Chem. Rev.* **2009**, *253*, 2891-2911.
- (16) Kim, J.; Chen, B.; Reineke, T. M.; Li, H.; Eddaoudi, M.; Moler, D. B.; O'Keeffe, M.; Yaghi, O. M. *J. Am. Chem. Soc.* **2001**, *123*, 8239-8247.
- (17) Chun, H.; Kim, D.; Dybtsev, D. N.; Kim, K. *Angew. Chem.Int. Ed.* **2004**, *43*, 5138-5175.
- (18) Wen, L.; Cheng, P.; Lin, W. *Chem. Commun.* **2012**, *48*, 2846-2848.
- (19) Davies, R. P.; Less, R. J.; Lickiss, P. D.; Robertson, K.; White, A. J. P. *Inorg. Chem.*, **2008**, *47*, 9958-9964.
- (20) Davies, R. P.; Less, R. J.; Lickiss, P. D.; Robertson, K.; White, A. J. P. *Cryst. Growth. Des.* **2010**, *10*, 4571-4581.
- (21) Dincă, M.; Dailly, A.; Long, J. R. *Chem. Eur. J.* **2008**, *14*, 10280-10285.
- (22) Lambert, J. B.; Liu, Z.; Liu, C. *Organometallics*, **2008**, *27*, 1464-1469.
- (23) Davies, R. P.; Lickiss, P. D.; Robertson, K.; White, A. J. P. *CrystEngComm* **2012**, *14*, 758-760.
- (24) Timokhin, I.; Torres, J. B.; White, A. J. P.; Lickiss, P. D.; Pettinari, C.; Davies, R. P. *Dalton Trans.* **2013**, *42*, 13806-13808.

- (25) Timokhin, I.; White, A. J. P.; Lickiss, P. D.; Pettinari, C.; Davies, R. P. *CrystEngComm* **2014**, *16*, 8094-8097.
- (26) Zhang, M.; Chen, Y.-P.; Zhou, H.-C. *CrystEngComm* **2013**, *15*, 9544-9552.
- (27) Matsumoto, K.; Kannami, M.; Inokuchi, D.; Kurata, H.; Kawase, T.; Oda, M. *Org. Lett.* **2007**, *9*, 2903-2906.
- (28) Peedikakkal, A. M. P.; Peh, C. S. Y.; Koh, L. L.; Vittal, J. J. *Inorg. Chem.* **2010**, *49*, 6775-6777.
- (29) (a) Sheldrick, G. M. *Acta Crystallogr.*, **2008**, *A64*, 112-122; (b) Spek, A. L. *Acta Cryst.* **2015**, *C71*, 9-18.
- (30) Deshmukh, M. S.; Vijayakanth, T.; Boomishankar, R. *Inorg. Chem.* **2016**, *55*, 3098-3104.
- (31) Macrae, C. F.; Edgington, P. R.; McCabe, P.; Pidcock, E.; Shields, G. P.; Taylor, R.; Towler, M.; Streek, J.V.D. *J. Appl. Crystallogr.* **2006**, *39*, 453-457.
- (32) Blatov, V. A.; Shevchenko, A. P.; Proserpio, D. M. *Cryst. Growth Des.* **2014**, *14*, 3576-3586; (Blatov, V.; Shevchenko, A.; Serezhkin, V.; Korchagin, D. <http://www.topos.ssu.samara.ru>).
- (33) Alexandrov, E. V.; Blatov, V. A.; Kochetkov, A. V.; Proserpio, D. M. *CrystEngComm* **2011**, *13*, 3947-3958.
- (34) Fu, J.; Li, H.; Mu, Y.; Hou, H.; Fan, Y. *Chem. Commun.* **2011**, *47*, 5271-5273.
- (35) Dincă, M.; Dailly, A.; Tsay, C.; Long, J. R. *Inorg. Chem.* **2008**, *47*, 11-13.
- (36) Gong, Y.-N.; Meng, M.; Zhong, D.-C.; Huang, Y.-L.; Jiang, L.; Lu, T.-B. *Chem. Commun.* **2012**, *48*, 12002-12004.
- (37) Zeng, M.-H.; Wang, Q.-X.; Tan, Y.-X.; Hu, S.; Zhao, H.-X.; Long, L.-S.; Kurmoo, M. *J. Am. Chem. Soc.*, **2010**, *132*, 2561-2563.
- (38) Yin, Z.; Wang, Q.-X.; Zeng, M.-H. *J. Am. Chem. Soc.* **2012**, *134*, 4857-4863.
- (39) Sava, D. F.; Rodriguez, M. A.; Chapman, K. W.; Chupas, P. J.; Greathouse, J. A.; Crozier, P. S.; Nenoff, T. M. *J. Am. Chem. Soc.* **2011**, *133*, 12398-12401.
- (40) Arıcı, M. r.; Yeşilel, O. Z.; Taş, M.; Demiral, H. *Inorg. Chem.*, **2015**, *54*, 11283-11291.
- (41) Bo, A.; Sarina, S.; Zheng, Z.; Yang, D.; Liu, H.; Zhu, H. *J. Haz. Mat.* **2013**, *246*, 199-205.
- (42) Sava, D. F.; Chapman, K. W.; Rodriguez, M. A.; Greathouse, J. A.; Crozier, P. S.; Zhao, H.; Chupas, P. J.; Nenoff, T. M. *Chem. Mater.* **2013**, *25*, 2591-2596.
- (43) Huo, C.; Sun, C.; Wang, C.; Jia, X.; Chang, W. *ACS Sustainable Chem. Eng.* **2013**, *1*, 549-553.
- (44) Kubczyk, T. M.; Williams, S. M.; Kean, J. R.; Davies, T. E.; Taylor, S. H.; Graham, A. E. *Green Chem.* **2011**, *13*, 2320-2325.

Chapter 4: Section B

SOLVENT DEPENDENT COPPER IODIDE CLUSTER MOFS AND THEIR UTILITY AS A CATALYST FOR THE ULLMANN COUPLING REACTION



4B.1 Introduction

The rational design and synthesis of cluster-based Metal-Organic Frameworks (MOFs) have been attracted considerable attention due to their intriguing architectures¹⁻⁹ and potential applications in photoluminescence, electric conductivity, magnetism, adsorption, separation, drug delivery and heterogeneous catalysis.¹⁰⁻²¹ The porosity plays a very important role in most of these applications. In certain instances, it has been found that interpenetration or catenation (where two or more separate identical networks self-assemble with each other) within the framework plays a significant role for designing MOFs with tailor made pores. In general, linear and extended linkers will lead to frameworks with large pores and channels. However, such open single frameworks are structurally unstable thus result in framework interpenetration to fill the void space to support its stability. Not surprisingly, interpenetration will decrease the free volume and increase the framework densities, or even diminish the porosity if there is a high degree of interpenetration. On the other hand, interpenetration can also be used to precisely adjust the pore size and surface area to promote more energetically favorable MOF-guest interactions, such as enhance the hydrogen bonding with the adsorption centers, which can improve gas separation or storage abilities and stability of the framework.^{10,22-32}

One of the hallmark properties of the MOFs is their utility in heterogeneous catalysis. In this regard, use of carboxylate based ligands as linkers and polynuclear metal clusters as secondary building units (SBUs) have extensively been explored for various applications.³³⁻³⁵ However, owing versatile coordination modes of the carboxylate group, the design and control of the final products have been complicated in several cases. On the other hand, designing MOFs with nitrogen containing heterocyclic ligands has been pursued for their strong and simple coordination ability to the transition metal ions.³⁶⁻³⁹ Particularly, the coordination complexes of copper (I) halides supported by N-donor functionalized ligands are of great interest due to their luminescence and catalytic properties.⁴⁰⁻⁴² These copper halides (CuI) are well-known to form various clusters such as Cu₂I₂ rhomboid dimer, Cu₄I₄ cubane tetramer, and Cu₆I₆ hexagonal prisms etc., due to their variety of coordination geometries for Cu(I) as well as potential bridging ability for the I⁻ anion.⁵¹⁻⁵⁸ So far, some interesting MOFs based on Cu_nI_n clusters have been synthesized by the reaction of CuI and organic ligands, giving rise to a series of one dimensional (1D) chain, two-dimensional (2D) layer, and three-dimensional (3D) MOF structures.⁵⁹⁻⁶¹ In different solvent systems, these

cluster cores may act as 2-6 connecting nodes which are connected through organic linkers to get interesting, multidimensional coordination network. However, there is no report on there is no report for the five-connected copper iodide cluster core. The construction of MOFs is always affected by many factors such as symmetry of the ligands, the core structure of the precursors and temperature.⁴³⁻⁴⁸ However, the effect of the solvent on the development of cluster-based coordination polymers are less mentioned or explored in the literature.^{49,50} Herein, we report the synthesis of two interesting interpenetrated CuI clusters MOFs **12**, {[TPVS](Cu₂I₂)} and **13**, {[TPVS](Cu₄I₄)} by using the ligand TPVS under different solvent systems. The solvothermal reactions of CuI with TPVS in acetonitrile (ACN) at 90 °C gave a interpenetrated 3D-network **12** consisting of a rhomboid shaped [Cu₂I₂] cluster which initially forms a 2D coordination network that further self-assembles into a 3D porous network **12** through interpenetration. However, the reaction of CuI in a solvent-mixture of acetonitrile (ACN) and tetrahydrofuran (THF) afforded a [Cu₄I₄] based 3D two fold interpenetrated MOFs **13**. In view of numerous research interest for the utility of Cu(I) complexes for the Ullmann C-N cross-coupling reaction, we explored these MOFs as catalysts for these reactions. The Cu(I)-assisted Ullmann C-N cross-coupling reactions have received considerable attention because it is the most valuable and practical method for the N-arylation of amines.⁶²⁻⁶⁵ Even though, Ullmann coupling reactions require harsh reaction conditions such as high reaction temperature, strong base, high boiling polar solvents, large amounts of catalyst, and extended reaction time, these reactions have been extensively used for the synthesis of industrially important intermediates. In a different approach, multinuclear copper clusters have been utilized as efficient catalysts for C-N coupling reactions.⁶⁶⁻⁷³ The Perez group had found that the open-cubane Cu₄I₄ tetramer bearing trispyrazolylmethane shows catalytic properties in the aryl amidation reaction of iodobenzene with 2-pyrrolidinone.^{67,71} The groups of Maheswaran⁶⁶ and wang⁴⁰ found that the Cu₂I₂ cluster bearing N-organic ligands can be used as a procatalyst in C-N cross-coupling reactions. However, all these reactions were found be carried out under drastic reaction conditions. Therefore, it is very important to develop catalyst which facilitates direct C-N cross-coupling reaction in ambient and mild conditions. Interestingly, both these MOFs were shown to be efficient catalysts for Ullmann C-N cross-coupling reaction in acetonitrile at 80 °C which gave the N-arylated products in almost 95% yield within four hours of reaction time.

4B.2 Experimental Section

4B.2.1 General remarks

All manipulations were performed under a dry atmosphere in standard Schlenk-glassware. Tetravinylsilane, 3-bromopyridine, Pd[t-Bu₃P]₂ and CuI were purchased from Aldrich and used as received. Ligand TPVS and TPES were synthesized by obtaining the similar method used in our previous report.⁷⁴ NMR spectra were recorded on a 400 MHz Bruker FT spectrometer (¹H-NMR: 400 MHz, ¹³C{¹H}-NMR: 100 MHz, ²⁹Si-NMR: 80 MHz) at room temperature using SiMe₄ as external standards. FT-IR spectra were taken on a Perkin-Elmer spectrophotometer. The absorption studies were done by a Perkin-Elmer Lambda 45 UV-Visible spectrophotometer. Thermogravimetric analysis (TGA) data was obtained in Perkin-Elmer STA 1000 instrument. The powder X-ray diffraction (PXRD) data were obtained from a Bruker-D8 Advance diffractometer. Gas-adsorption measurements were performed using a BELSORP-max instrument. Elemental analyses were performed on a Vario-EL cube elemental analyser.

4B.2.2 Synthesis

4B.2.2.1 Synthesis of compound [Cu₂(TPVS)]·ACN (12): To a solution of L⁵ (10 mg, 0.25 mmol) in acetonitrile (1 ml), kept in 10 cm long glass tube with 1 mm diameter, was slowly layered a solution of CuI in acetonitrile (10 mg, 0.5 mmol). The layered solutions in the tube were kept at room temperature for 3 days to yield green crystals of **12** (Yield 80%). FT-IR data in powdered sample (cm⁻¹): 3860, 3740, 3642, 3516, 3227, 2901, 2627, 2467, 2186, 1961, 1741, 1607, 1515, 1106, 989, 850, 797. Anal. calc. for C₃₅H₃₈Cl₂CuN₅O_{2.5}Si: C, 58.53; H, 8.10; N, 10.12. Found: C, 58.58; H, 8.15; N, 10.16.

4B.2.2.2 Synthesis of compound [Cu₄(TPVS)₄]·THF (13): To a solution of L⁵ (10 mg, 0.25 mmol) in THF (1 ml), kept in 10 cm long glass tube with 1 mm diameter, was slowly layered a solution of CuI in acetonitrile (5 mg, 0.25 mmol). The layered solutions in the tube were kept at room temperature for 2 days to yield green crystals of **13** (Yield 85%). FT-IR data in powdered sample (cm⁻¹): 3860, 3740, 3642, 3516, 3227, 2901, 2627, 2467, 2186, 1961, 1741, 1607, 1515, 1106, 989, 850, 797. Anal. calc. for C₃₅H₃₈Cl₂CuN₅O_{2.5}Si: C, 58.53; H, 8.10; N, 10.12. Found: C, 58.58; H, 8.15; N, 10.16.

4B.2.3 Crystallography

Reflections were collected on a Bruker Smart Apex Duo diffractometer at 100 K using MoK α radiation ($\lambda = 0.71073 \text{ \AA}$). Structures were refined by full-matrix least-squares against F^2 using all data (SHELX).^{75a} Crystallographic data for all these compounds are listed in (Table 4B.1). All non-hydrogen atoms were refined anisotropically if not stated otherwise. Hydrogen atoms were constrained in geometric positions to their parent atoms. The diffuse solvent molecules in compound **12** and **13** could not be modeled appropriately. Hence, these were treated as diffuse contributions to the overall scattering and were removed by the SQUEEZE/PLATON for a better refinement data.^{75b}

Table 4B.1: Details of crystallographic data collection and structure refinements for **12** and **13**

Compound	12	13
Chemical formula	C ₁₁₂ H ₉₆ Cl ₈ Cu ₄ N ₁₆ O ₂ Si ₄	C ₃₆ H ₆₄ Cl ₄ Cu ₂ N ₈ O ₂ Si ₂
Formula weight	2348.16	1206.12
Temperature	100(2)K	100(2) K
Crystal system	Tetragonal	Tetragonal
Space group	I4/m	I4/m
a (Å); α (°)	14.508(5); 90°	14.104(9); 90°
b (Å); β (°)	14.508(5); 90°	14.104(9); 90°
c (Å); γ (°)	34.921(14); 90°	19.100(12); 90°
V (Å ³); Z	7350(6); 8	3800(6); 2
ρ (calc.) mg m ⁻³	1.061	1.054
μ (Mo K α) mm ⁻¹	0.792	0.768
2 θ_{\max} (°)	48.80	50.054
R(int)	0.10939	0.1265
Completeness to θ	99.9 %	99.9 %
Data / param.	4699/173	1745 / 92
GOF	0.971	1.075
R1 [F > 4 σ (F)]	0.0496	0.0607
wR2 (all data)	0.1627	0.2061
max. peak/hole (e.Å ⁻³)	0.953/-0.505	1.508 /-0.521

4B.2.4 Catalytic properties of **12** and **13**

4B.2.4.1 General catalytic procedure for Ullmann cross-coupling reaction: Imidazole (0.75 mmol), KOH (1.0 mmol) and MOF (**12** or **13**) catalyst (5% wt) were added to a solution of 1-Bromo-4-iodobenzene or 4-Bromonitrobenzene (0.75 mmol) in a dry acetonitrile solvent

(5 ml) under the nitrogen atmosphere in the Schlenk line. The reaction mixture was heated at 80 °C for 2h in an oil bath. The resulting mixture was cooled to room temperature, water (5 ml) was added, and the product was extracted with ethyl acetate. The solvents were evaporated and the obtained crude compound was subsequently purified by column chromatography on silica gel (CH₂Cl₂/petroleum ether = 1: 1) to yield the target product as a white solid (yield, 92 %). ¹H NMR (400 MHz, CDCl₃): δ = 7.91 (s, 2H), 7.33 (m, 6H), 7.20 (t, 2H), 7.17 (dd, 1H), 7.14 (t, 2H), 6.99 (t, 2H), 6.63 (dd, 2H), 5.88 (s, 1H). ¹³C NMR (100 MHz, CDCl₃) δ = 144.1, 136.8, 128.8, 128.3, 127.2, 126.2, 123.7, 122.0, 120.0, 119.3, 111.3, 40.3. MS-EI, m/z, Anal. Calcd: 321.14, Exp: 321.13 (M+H).

4B.3 Results and Discussion

4B.3.1 Synthesis

The ligand L⁵ was synthesized by adopting similar method used in 4A.3.1. Crystals of cluster MOFs **12** and **13** were obtained by the slow diffusion of copper iodide solution in acetonitrile on the solution of ligand L⁵ in acetonitrile (and tetrahydrofuran in case of **13**) at RT through layering method.

4B.3.2 Crystal structure

The molecular structures of both **12** and **13** were solved in Monoclinic P(2)₁/c space group (Figure 4B.1 and 4B.3). The asymmetric unit of **12** consists of two Cu(I) atoms, two iodine ion, one ligand moiety and one guest acetonitrile molecule, while **13** consists of four Cu(I) atoms, four iodine ion, one ligand moiety and one guest tetrahydrofuran molecule. The molecular core of **12** consists of a dimeric Cu₂I₂ cluster in which each I⁻ ion acts as μ₂-bridging unit and Cu(I) ions are located in a tetrahedral coordinate consisting of two I⁻ contacts and two aryls N-donor contact from two different ligand scaffolds of L⁵ (Figure 4B.1a). While each Cu₂I₂ clusters, surrounded by four different tetrahedral ligand segments, act as four connected nodes, the TPVS ligands connected four different dimeric clusters and acted as four connected nodes (Figure 4B.1b). Thus both the ligands and the Cu₂I₂ clusters act as four connected nodes resulting in the formation of a two-dimensional metal-organic framework structure. TOPOS analysis gave a 4-connected uninodal sql/Shubnikov tetragonal plane net represented by the Schläfli symbol {4⁴.6²} for **12** (Figure 4B.1c).⁷⁶⁻⁷⁸ The repeating unit of 2D assembly in **12** consists of 26-membered Cu₄L₂ macrocycles. These 2D polymeric sheets lie perpendicular to each other through the 24 membered macrocycles leading the

formation of an interpenetrated 3D MOFs (Figure 4B.1d and 4B.1e).

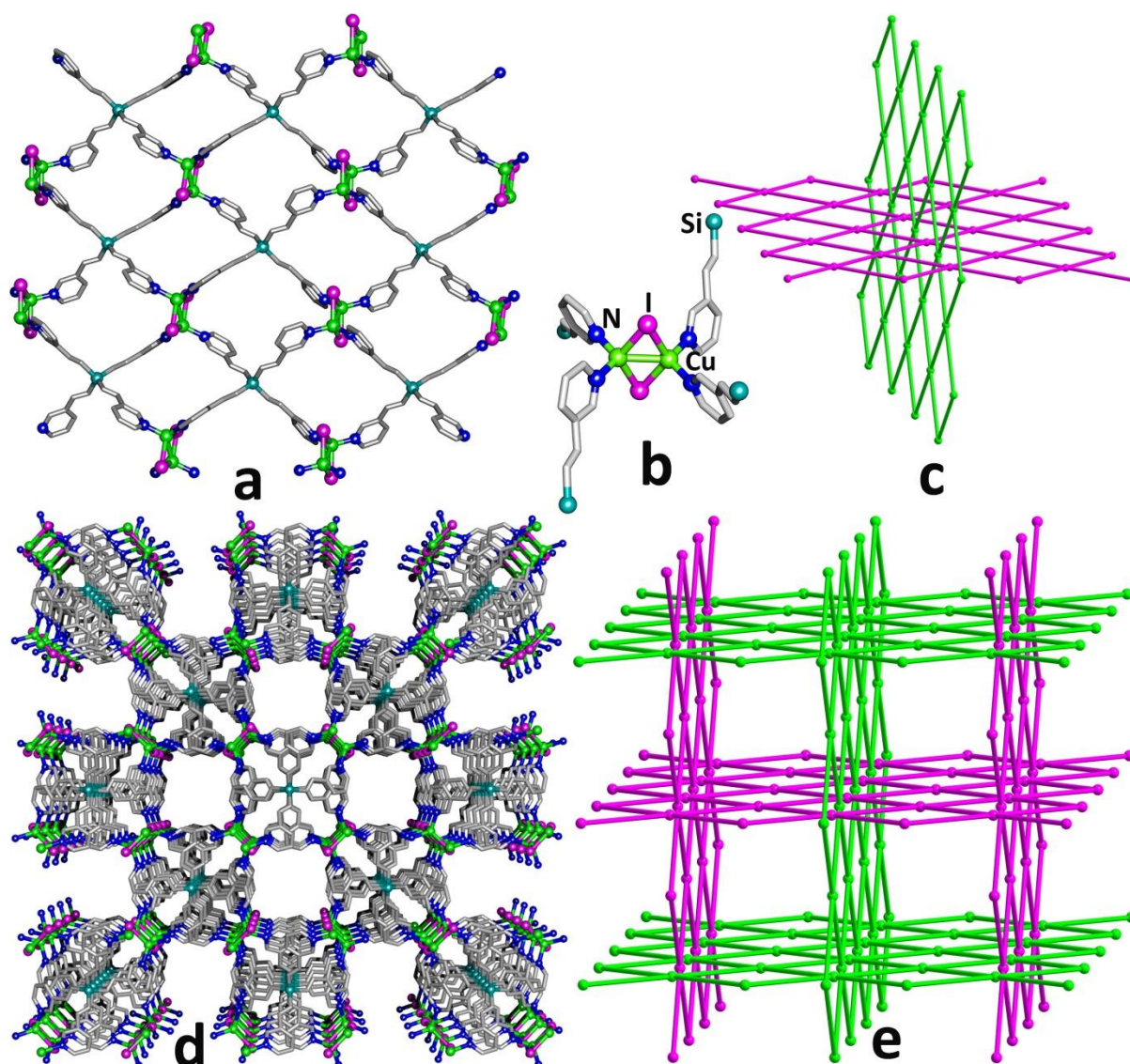


Figure 4B.1: (a) Molecular structure of the 2D-polymeric sheet in **12** (b) shown the arrangement of ligand around the Cu_2I_2 cluster (c) the sql topology of the 2D polymeric sheet lie perpendicular to each other (d) formation of 3D interpenetrated structure and (e) the topological view of 3D interpenetrated MOF **12**

The 3D-packing structure of **12** reveals the presence of 2D-channels and the void volume (excluding the solvent molecules) calculated by Mercury software is 1079 \AA^3 which amounts to 27 % of the unit-cell volume.⁷⁹ TGA shows a weight loss of 13.85 % up to $100 \text{ }^\circ\text{C}$, which is corresponding to the loss of solvent acetonitrile molecules and the desolvated framework is stable up to $230 \text{ }^\circ\text{C}$ (Figure A4B.1, Appendix). The guest molecules of the framework were removed by the evacuating sample at $75 \text{ }^\circ\text{C}$ for 4 h. The PXRD pattern of samples of **12**

reveals that the crystallinity and framework remains the same even after removal of the solvent molecules (Figure A4B.2, Appendix). The gas adsorption studies show that the porous nature of the MOF **12** as it adsorbs selectively CO₂ over the N₂. The CO₂ adsorption at 273 K exhibits type I behaviours with an uptake capacity of 25 cm³g⁻¹ for the MOF **12**.

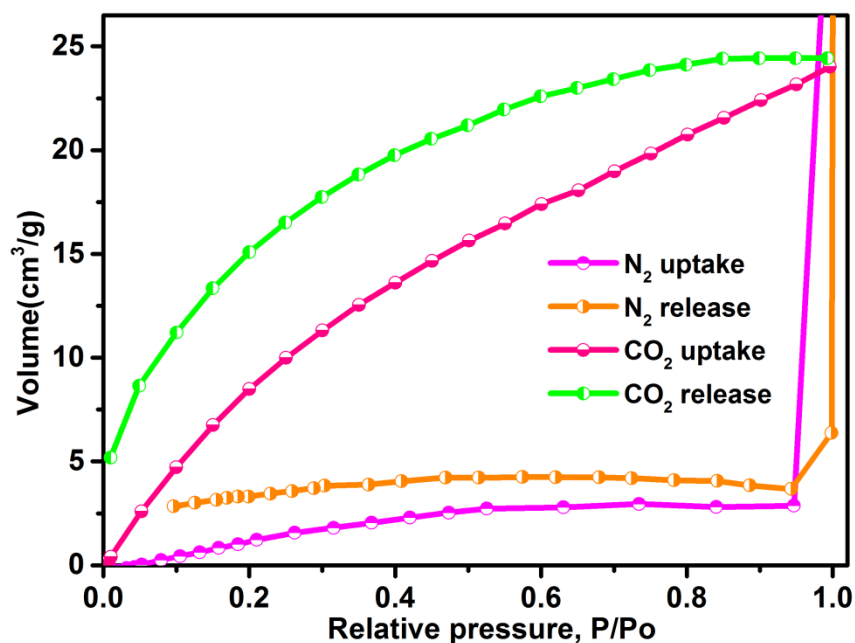


Figure 4B.2: The CO₂ and N₂ adsorption isotherms of **12** at 273 K

The molecular core of **13** consists of the tetrameric cubane like Cu₄I₄ cluster in which each I⁻ ion act as μ₃-bridging unit. The Cu(I) ions are located in a tetrahedral coordination consisting of three I⁻ contacts and one aryl silane N-donor contact. While the Cu₄I₄ cluster, supported by the four tetradentate ligand segments, act as four connected nodes, the tetradentate silane ligand act as four connected nodes and associated with four tetrameric clusters (Figure 4B.3a and 4B.3b). This gives rise to a uninodal four connecting 3D framework with 4²6³8-sra (Sra) topology (Figure 4B.3e).^{76,77} The repeating unit of the 3D structure consists of two distinct 24 and 38 membered Cu₄L₂ and Cu₈L₄ macrocycles, respectively which leads to the small and large cavity 1D channels within the 3D framework (Figure 4B.3c). The large cavities obtained from the 38 membered macrocycles interpenetrate into another identical one, leading to a 2-fold interpenetration 3D network of **13** (Figure 4B.3d). The remaining free voids are filled with guest THF molecules. After removing guest molecule, the unit cell packing diagram in **13** shows that solvent accessible volume of 1815 Å³ (39.8% of the unit cell volume).⁷⁹ TGA profile shows the weight loss of 6 % up to 100 °C, which is corresponding to the loss of solvent THF molecules and the desolvated framework is stable

up to 170 °C (Figure A4B.1, Appendix). The guest molecules were removed by evacuating the sample at 75 °C for 4 h. The PXRD pattern reveals that the framework remains same even after removal of the solvent molecules (Figure A4B.3, Appendix). The gas adsorption studies shows that the non-porous nature of the MOF 13. Thus, in MOF 12 interpenetration helps to obtained porous frameworks while in MOF 13 the large cavity occupied by the interpenetration which leads to the nonporous nature (Figure 4B.4).

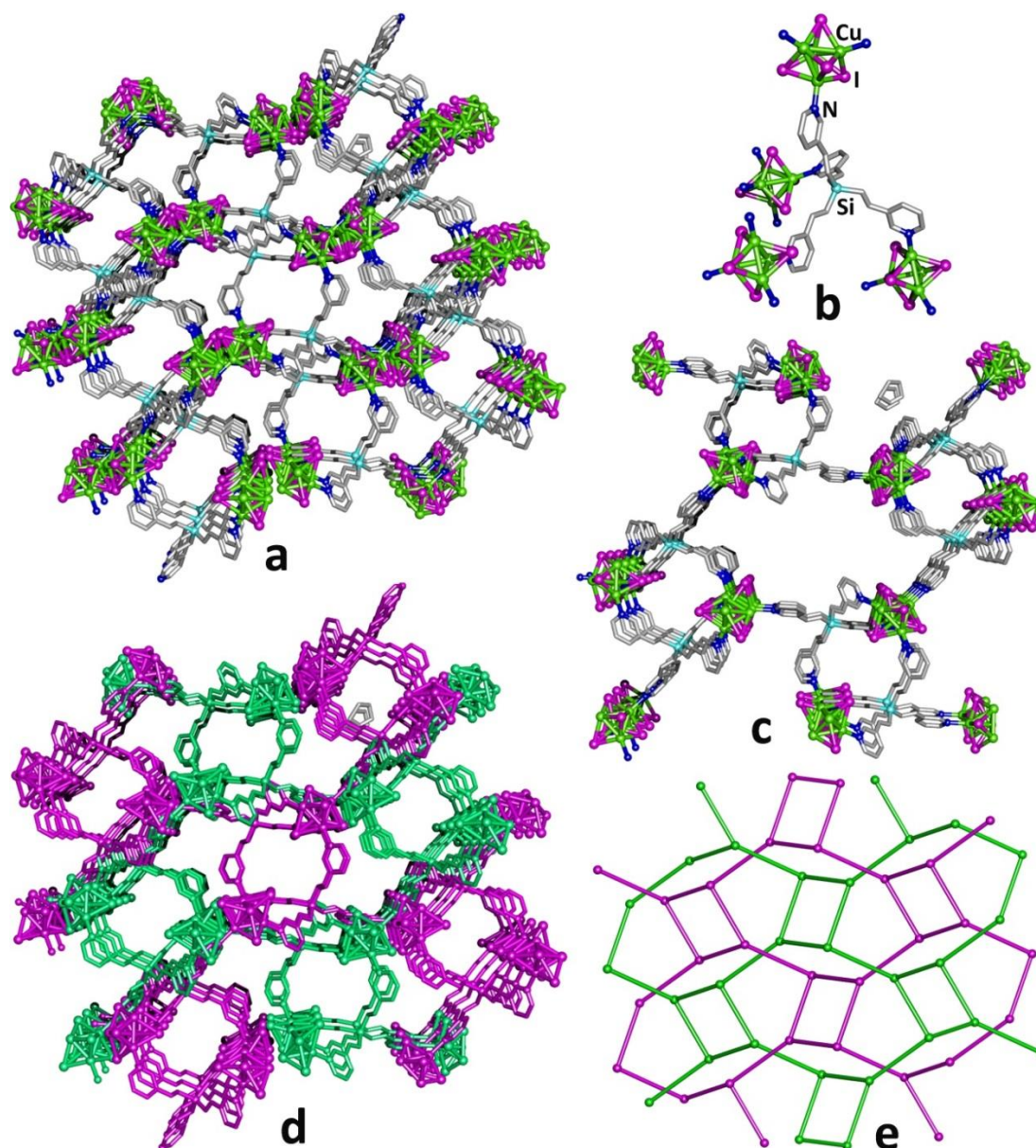


Figure 4B.3: (a) Molecular structure of the 3D MOF in 13 (b) shown the arrangement of Cu_4I_4 cluster around the TPVS (c) the formation of small and large (d) formation of 2-fold interpenetrated 3D MOF and (e) the topological view of 3D two fold interpenetrated MOF

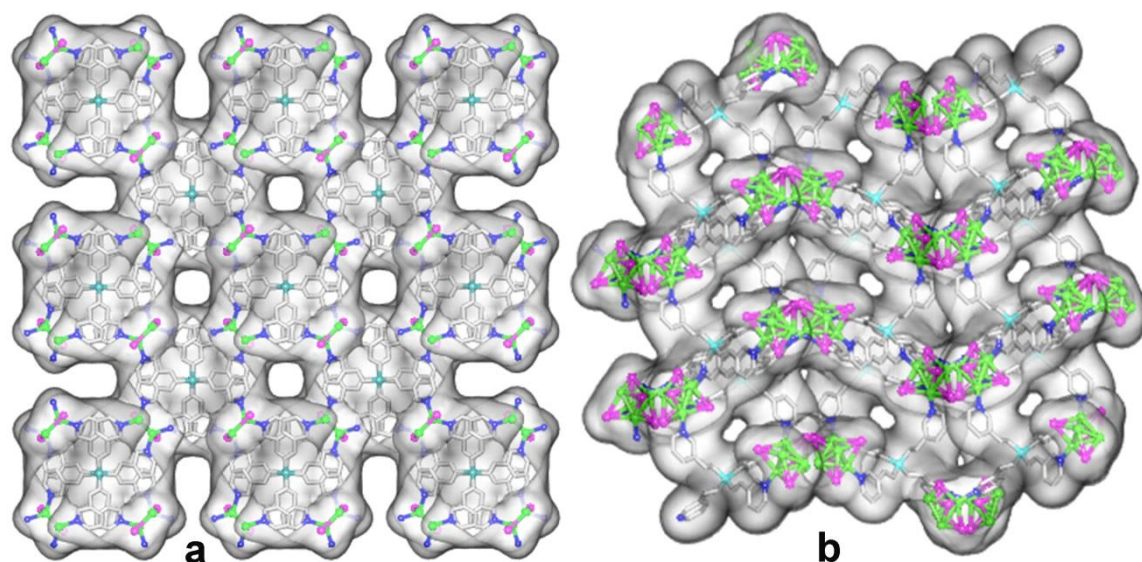
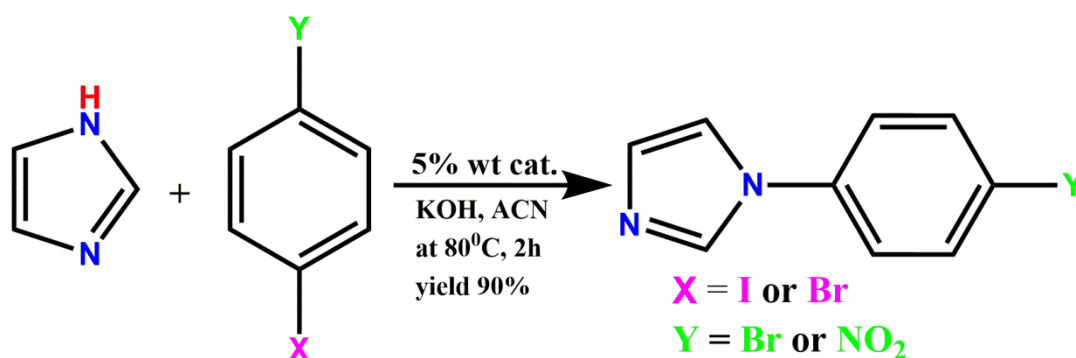


Figure 4B.4: The surface diagram shown (a) interpenetration leads to porous 2D channel MOF 12 and (b) interpenetration leads to the nonporous MOF 13.

4B.3.3 Catalytic studies of 12 and 13

The copper (I) clusters consisting of $\text{Cu}_2\text{X}_2/\text{Cu}_4\text{X}_4$ units have been found to be effective as catalyst precursor in organic reactions, especially in the Ullmann coupling reaction.⁶²⁻⁷³ The Ullmann cross-coupling reaction of 1-Bromo-4-Iodobenzene and 4-bromonitrobenzene with imidazole has been tested with both 12 and 13 MOFs as catalyst and KOH as base at 80 °C in acetonitrile. The experiments were performed with 5 % wt. catalysts which gave the targeted product in a good 90% gas chromatography (GC) yield by utilizing both the catalyst. Further, the effect of bases and solvent on the Ullmann coupling reaction has been investigated by using both the MOFs. Among the organic and inorganic bases examined, KOH is found to be efficient and gives in quantitative yields (Table 4B.2).



Scheme 4B.1: Ullmann cross-coupling reaction catalysed by the MOF 12 and 13

The investigation of a variety of solvents suggests that the use of DMSO and MeCN are the superior to DMF, MeOH and THF. Thus, by using these copper iodide cluster MOFs as catalysts, the corresponding N-arylated products were quantitatively obtained at comparatively mild reaction conditions.

Table 4B.2: Catalytic reaction of MOF 12 and 13 with 1-Bromo-4-Iodobenzene with imidazole at 80 °C for 4h

Entry	Bases	Solvents	Yield (%)
1	KOH	MeCN	90
2	NaOH	MeCN	75
3	K ₂ CO ₃	MeCN	64
4	Et ₃ N	MeCN	5
5	KOH	DMSO	90
6	KOH	DMF	55
7	KOH	MeOH	42
8	KOH	THF	38
9	KOH	H ₂ O	Nil

4B.4 Conclusion

In conclusion, we have demonstrated that the solvent act as a structural direction agent to obtain copper iodide cluster MOFs having Cu₂I₂ and Cu₄I₄ clusters by using rigid tetrahedral silane ligands. The reaction of TPVS ligand with the CuI in acetonitrile solution leads to the 2D polymeric sheet having Cu₂I₂ clusters with the **sql** topology and which on interpenetration from the porous 3D framework. However, the reaction of CuI with the TPVS ligand in the mixture of acetonitrile and THF solvent leads to a two-fold interpenetrated 3D nonporous framework having Cu₄I₄ clusters with two fold **sra** topology. Furthermore, both these cluster MOFs were shown to be efficient catalysts for the Ullmann coupling reaction which gave the corresponding N-arylated products in about 90% yield within 2h of the reaction period.

4B.5 References

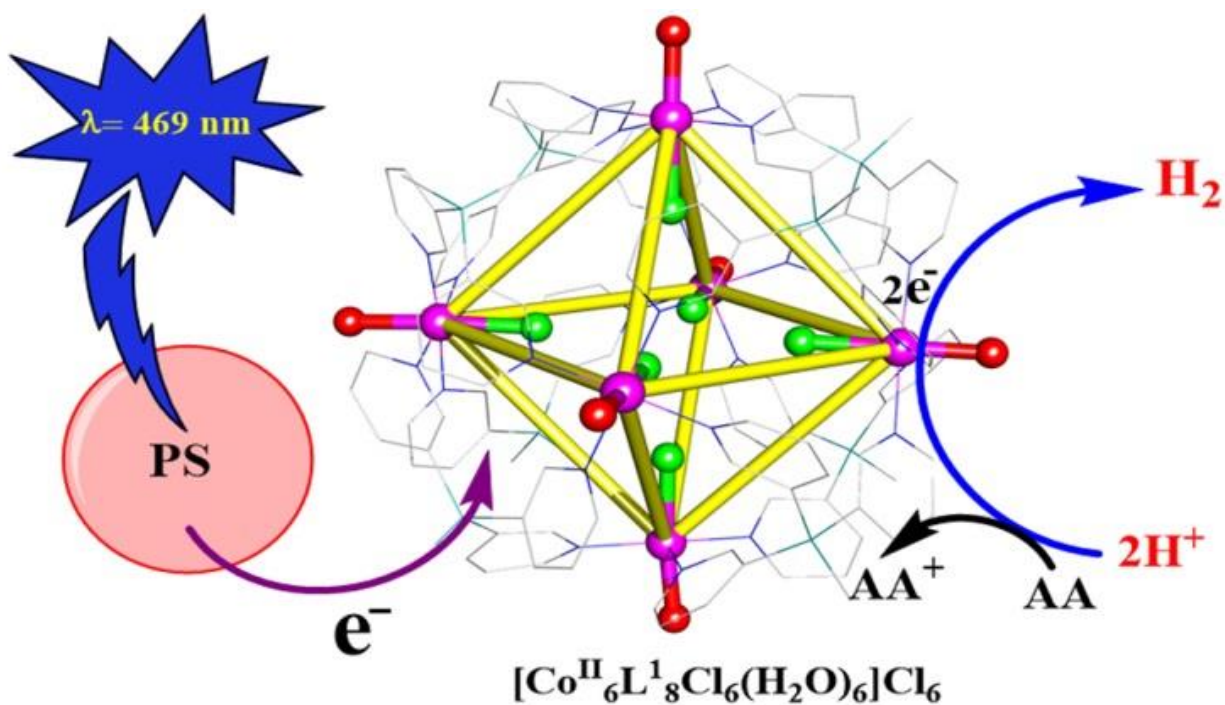
- (1) O’Keeffe, M.; Yaghi, O. M. *Chem. Rev.* **2011**, *112*, 675-702.
- (2) Farha, O. K.; Hupp, J. T. *Acc. Chem. Res.* **2010**, *43*, 1166-1175.
- (3) Kitagawa, S.; Kitaura, R.; Noro, S. I. *Angew. Chem. In. Ed.* **2004**, *43*, 2334-2375.
- (4) Zhou, H.-C.; Long, J. R.; Yaghi, O. M. *Chem. Rev.*, **2012**, *112*, 673-674.
- (5) Tranchemontagne, D. J.; Park, K. S.; Furukawa, H.; Eckert, J.; Knobler, C. B.; Yaghi, O. M. *J. Phys. Chem. C* **2012**, *116*, 13143-13151.
- (6) Zhang, J.-P.; Zhang, Y.-B.; Lin, J.-B.; Chen, X.-M. *Chem. Rev.* **2011**, *112*, 1001-1033.
- (7) Qiu, S.; Zhu, G. *Coord. Chem. Rev.* **2009**, *253*, 2891-2911.
- (8) Férey, G. *Chem. Soc. Rev.* **2008**, *37*, 191-214.
- (9) Jiang, H.-L.; Xu, Q. *Chem. Commun.* **2011**, *47*, 3351-3370.
- (10) Cui, Y.; Yue, Y.; Qian, G.; Chen, B. *Chem. Rev.* **2011**, *112*, 1126-1162.
- (11) Shan, X.-c.; Jiang, F.-l.; Yuan, D.-q.; Zhang, H.-b.; Wu, M.-y.; Chen, L.; Wei, J.; Zhang, S.-q.; Pan, J.; Hong, M.-c. *Chem. Sci.* **2013**, *4*, 1484-1489.
- (12) Liu, Q.-K.; Ma, J.-P.; Dong, Y.-B. *J. Am. Chem. Soc.* **2010**, *132*, 7005-7017.
- (13) Sun, J.-K.; Ji, M.; Chen, C.; Wang, W.-G.; Wang, P.; Chen, R.-P.; Zhang, J. *Chem. Commun.* **2013**, *49*, 1624-1626.
- (14) Li, J.-R.; Kuppler, R. J.; Zhou, H.-C. *Chem. Soc. Rev.* **2009**, *38*, 1477-1504.
- (15) Cram, D. J. *Nature* **1992**, *356*, 29.
- (16) Khan, N. A.; Hasan, Z.; Jhung, S. H. *J. Haz. Mat.* **2013**, *244*, 444-456.
- (17) Kuppler, R. J.; Timmons, D. J.; Fang, Q.-R.; Li, J.-R.; Makal, T. A.; Young, M. D.; Yuan, D.; Zhao, D.; Zhuang, W.; Zhou, H.-C. *Coord. Chem. Rev.* **2009**, *253*, 3042-3066.
- (18) Song, J.; Luo, Z.; Britt, D. K.; Furukawa, H.; Yaghi, O. M.; Hardcastle, K. I.; Hill, C. L. *J. Am. Chem. Soc.* **2011**, *133*, 16839-16846.
- (19) Wu, C.-D.; Hu, A.; Zhang, L.; Lin, W. *J. Am. Chem. Soc.* **2005**, *127*, 8940-8941.
- (20) Chen, B.; Xiang, S.; Qian, G. *Acc. Chem. Res.* **2010**, *43*, 1115-1124.
- (21) Kreno, L. E.; Leong, K.; Farha, O. K.; Allendorf, M.; Van Duyne, R. P.; Hupp, J. T. *Chem. Rev.* **2012**, *112*, 1105-1125.
- (22) Guo, M.; Sun, Z.-M. *J. Mat. Chem.* **2012**, *22*, 15939-15946.
- (23) Reineke, T. M.; Eddaoudi, M.; Moler, D.; O’keeffe, M.; Yaghi, O. *J. Am. Chem. Soc.* **2000**, *122*, 4843-4844.
- (24) Chen, B.; Eddaoudi, M.; Hyde, S.; O’keeffe, M.; Yaghi, O. *Science* **2001**, *291*, 1021-1023.
- (25) Kitaura, R.; Seki, K.; Akiyama, G.; Kitagawa, S. *Angew. Chem. In. Ed.* **2003**, *42*, 428-431.
- (26) Kim, H.; Suh, M. P. *Inorg. Chem.* **2005**, *44*, 810-812.
- (27) Pan, L.; Olson, D. H.; Ciemnomolonski, L. R.; Heddy, R.; Li, J. *Angew. Chem.* **2006**, *118*, 632-635.
- (28) Chen, B.; Liang, C.; Yang, J.; Contreras, D. S.; Clancy, Y. L.; Lobkovsky, E. B.; Yaghi, O. M.; Dai, S. *Angew. Chem.* **2006**, *118*, 1418-1421.
- (29) Maji, T. K.; Matsuda, R.; Kitagawa, S. *Nat. Mater.* **2007**, *6*, 142-148.
- (30) Ryan, P.; Broadbelt, L. J.; Snurr, R. Q. *Chem. Commun.* **2008**, 4132-4134.
- (31) Kishan, M. R.; Tian, J.; Thallapally, P. K.; Fernandez, C. A.; Dalgarno, S. J.; Warren, J. E.; McGrail, B. P.; Atwood, J. L. *Chem. Commun.* **2010**, *46*, 538-540.
- (32) Jiang, H.-L.; Xu, Q. *Chem. Commun.* **2011**, *47*, 3351-3370.
- (33) Li, J.-R.; Sculley, J.; Zhou, H.-C. *Chem. Rev.* **2011**, *112*, 869-932.
- (34) Li, Z.-G.; Wang, G.-H.; Jia, H.-Q.; Hu, N.-H.; Xu, J.-W.; Batten, S. R. *CrystEngComm* **2008**, *10*, 983-985.

- (35) Li, J.-R.; Zhou, H.-C. *Nat. chem.* **2010**, *2*, 893-898.
- (36) Demessence, A.; Long, J. R. *Chem. Eur. J.* **2010**, *16*, 5902-5908.
- (37) Tian, H.; Jia, Q.-X.; Gao, E.-Q.; Wang, Q.-L. *Chem. Commun.* **2010**, *46*, 5349-5351.
- (38) Li, X.; Guo, X.; Weng, X.; Lin, S. *CrystEngComm* **2012**, *14*, 1412-1418.
- (39) Liu, Y.-Y.; Li, J.; Ma, J.-F.; Ma, J.-C.; Yang, J. *CrystEngComm* **2012**, *14*, 169-177.
- (40) Zhao, H.; Li, X.; Wang, J.; Li, L.; Wang, R. *ChemPlusChem* **2013**, *78*, 1491-1502.
- (41) Peng, R.; Li, M.; Li, D. *Coord. Chem. Rev.* **2010**, *254*, 1-18.
- (42) Zhang, J.-P.; Lin, Y.-Y.; Huang, X.-C.; Chen, X.-M. *J. Am. Chem. Soc.* **2005**, *127*, 5495-5506.
- (43) Roland, B. K.; Carter, C.; Zheng, Z. *J. Am. Chem. Soc.* **2002**, *124*, 6234-6235.
- (44) Roland, B. K.; Selby, H. D.; Carducci, M. D.; Zheng, Z. *J. Am. Chem. Soc.* **2002**, *124*, 3222-3223.
- (45) Wang, R. H.; Hong, M. C.; Luo, J. H.; Cao, R.; Weng, J. B. *Eur. J. Inorg. Chem.* **2002**, *2002* (12), 3097-3100.
- (46) Lang, J. P.; Xu, Q. F.; Yuan, R. X.; Abrahams, B. F. *Angew. Chem. Int. Edition* **2004**, *43*, 4741-4745.
- (47) Lang, J.-P.; Xu, Q.-F.; Zhang, W.-H.; Li, H.-X.; Ren, Z.-G.; Chen, J.-X.; Zhang, Y. *Inorg. Chem.* **2006**, *45*, 10487-10496.
- (48) Wang, J.; Zheng, S.-L.; Hu, S.; Zhang, Y.-H.; Tong, M.-L. *Inorg. Chem.* **2007**, *46*, 795-800.
- (49) Zhang, W.-H.; Song, Y.-L.; Zhang, Y.; Lang, J.-P. *Cryst. Growth Des.* **2007**, *8*, 253-258.
- (50) Li, H.-X.; Wu, H.-Z.; Zhang, W.-H.; Ren, Z.-G.; Zhang, Y.; Lang, J.-P. *Chem. Commun.* **2007**, 5052-5054.
- (51) Madhu, V.; Bolligarla, R.; Naik, I. K.; Mekala, R.; Das, S. K. *Eur. J. Inorg. Chem.* **2016**, *2016* (26), 4257-4264.
- (52) Hu, S.; Tong, M.-L. *Dalton Trans.* **2005**, 1165-1167.
- (53) Hu, S.; Zhou, A.-J.; Zhang, Y.-H.; Ding, S.; Tong, M.-L. *Cryst. Growth Des.* **2006**, *6*, 2543-2550.
- (54) Näther, C.; Jeß, I.; Lehnert, N.; Hinz-Hübner, D. *Solid state sciences* **2003**, *5*, 1343-1357.
- (55) Batten, S. R.; Jeffery, J. C.; Ward, M. D. *Inorganica Chim. Acta* **1999**, *292*, 231-237.
- (56) Biradha, K.; Aoyagi, M.; Fujita, M. *J. Am. Chem. Soc.* **2000**, *122*, 2397-2398.
- (57) Blake, A. J.; Brooks, N. R.; Champness, N. R.; Crew, M.; Deveson, A.; Fenske, D.; Gregory, D. H.; Hanton, L. R.; Hubberstey, P.; Schröder, M. *Chem. Commun.* **2001**, 1432-1433.
- (58) Deshmukh, M. S.; Yadav, A.; Pant, R.; Boomishankar, R. *Inorg. Chem.* **2015**, *54*, 1337-1345.
- (59) Hu, S.; Zhang, Z.-M.; Meng, Z.-S.; Lin, Z.-J.; Tong, M.-L. *CrystEngComm* **2010**, *12*, 4378-4385.
- (60) Prajapati, R. K.; Verma, S. *Inorg. Chem.* **2011**, *50*, 3180-3182.
- (61) Yang, X.-J.; Li, H.-X.; Xu, Z.-L.; Li, H.-Y.; Ren, Z.-G.; Lang, J.-P. *CrystEngComm* **2012**, *14*, 1641-1652.
- (62) Monnier, F.; Taillefer, M. *Angew. Chem. Int. Ed.* **2009**, *48*, 6954-6971.
- (63) Chemler, S. R. *Science* **2013**, *341*, 624-626.
- (64) Sambigao, C.; Marsden, S. P.; Blacker, A. J.; McGowan, P. C. *Chem. Soc. Rev.* **2014**, *43*, 3525-3550.
- (65) Brasche, G.; Buchwald, S. L. *Angew. Chem.* **2008**, *120*, 1958-1960.
- (66) Maheswaran, H.; Krishna, G. G.; Prasanth, K. L.; Srinivas, V.; Chaitanya, G. K. *Tetrahedron* **2008**, *64*, 2471-2479.

- (67) Haldon, E.; Alvarez, E.; Nicasio, M. C.; Pérez, P. J. *Organometallics* **2009**, *28*, 3815-3821.
- (68) Li, F.; Hor, T. *Chem.-Eur. J.* **2009**, *15*, 10585-10592.
- (69) Priyadarshini, S.; Joseph, P. A.; Srinivas, P.; Maheswaran, H.; Kantam, M. L.; Bhargava, S. *Tetrahedron Let.* **2011**, *52*, 1615-1618.
- (70) Liu, M.; Reiser, O. *Org. Let.* **2011**, *13*, 1102-1105.
- (71) Haldón, E.; Álvarez, E.; Nicasio, M. C.; Pérez, P. J. *Inorg. Chem.* **2012**, *51*, 8298-8306.
- (72) Ding, H.-Y.; Cheng, H.-J.; Wang, F.; Liu, D.-X.; Li, H.-X.; Fang, Y.-Y.; Zhao, W.; Lang, J.-P. *J. Organomet. Chem.* **2013**, *741*, 1-6.
- (73) Yang, T.; Cui, H.; Zhang, C.; Zhang, L.; Su, C. Y. *ChemCatChem* **2013**, *5*, 3131-3138.
- (74) Deshmukh, M. S.; Vijayakanth, T.; Boomishankar, R. *Inorg. Chem.* **2016**, *55*, 3098-3104.
- (75) (a) Sheldrick, G. M. *Acta Crystallogr.*, **2008**, *A64*, 112-122; (b) Spek, A. L. *Acta Cryst.* **2015**, *C71*, 9-18.
- (76) Blatov, V. A.; Shevchenko, A. P.; Proserpio, D. M. *Cryst. Growth Des.* **2014**, *14*, 3576-3586.
- (77) Blatov, V.; Shevchenko, A.; Serezhkin, V. *J. Appl. Crystallogr.* **2000**, *33*, 1193-1193.
- (78) Blatov, V.; Shevchenko, A.; Serezhkin, V.; Korchagin, D. <http://www.topos.ssu.samara.ru>.
- (79) Macrae, C. F.; Edgington, P. R.; McCabe, P.; Pidcock, E.; Shields, G. P.; Taylor, R.; Towler, M.; Streek, J. v. d. *J. Appl. Crystallogr.* **2006**, *39*, 453-457.

Chapter 5

LIGHT-DRIVEN HYDROGEN EVOLUTION FROM WATER BY A TRIPODAL SILANE BASED $\text{Co}^{\text{II}}_6\text{L}^1_8$ OCTAHEDRAL CAGE



5.1 Introduction

Hydrogen is perceived as a prominent carbon-free fuel to meet the rising demands of the global energy and reduce the emission of greenhouse gases from the consumption of fossil fuels.¹⁻⁴ Sustainable routes to produce hydrogen employs the solar energy to split water into its elements (termed as artificial photosynthesis) by two individual half-reactions of water oxidation and proton reduction.⁵⁻⁹ The reductive part of the water splitting yields hydrogen that can be effectively achieved by a photocatalytic system consisting of a photosensitizer, a proton reduction catalyst (PRC) and a sacrificial reductant.¹⁰⁻¹¹ Over the years, poly-pyridine and cyclometalated complexes of noble and rare-earth metal such as Pt, Rh, Ir, etc. have shown to be efficient catalysts for the proton reduction process.¹²⁻¹⁴ However, due to the low abundance of these expensive metal ions, significant efforts have been made to develop homogeneous and heterogeneous PRCs based on non-noble and earth abundant transition metal ions, especially those of Fe, Ni, Co and Mo.¹⁵⁻²⁰ Amongst these, cobalt complexes of imine and poly-pyridyl ligands have shown promising activity as PRCs.²¹⁻²⁷ While, cobalt imine complexes are excellent electro- and photocatalysts, their activity has been largely confined to the organic medium as these catalysts show poor solubility in water and show signs of degradation by hydrogenation or hydrolysis.²⁸⁻³¹ Inspired by the activity of [Co(bpy)₃]²⁺ as a precatalyst for H₂ evolution, several cobalt-pyridyl complexes of penta- and tetradentate ligands have been developed as efficient PRCs in the aqueous and buffered water medium.³² Interesting examples of pentadentate ligand based on Co complexes have been reported by Alberto,¹⁶ Chang,¹⁹ Long,²³ Zhao and Wang and their co-workers that show excellent efficacy as PRCs.³³ Recently, Lau,²⁵ Thummel²⁶ and their co-workers have developed a series of Co complexes derived from chelating tetradentate ligands in which the pyridyl donor site offers a square planar arrangement for the Co(II) ions. The apical positions in all these Co complexes were taken up by weakly coordinating neutral or anionic donor ligands which were reversibly displaced during the water activation process with the formation of the Co-H intermediate species.³⁴ Alternately, some of these complexes were proposed to facilitate the H₂ evolution by the formation of a dangling protonated pyridyl group during the catalytic cycle.³³ Despite the excellent platforms offered by these penta- and tetradentate ligands as H₂ evolving Co catalysts, still there are challenges involved in the design of such suitable scaffolds. For example, these geometrically tailored ligands require multi-step synthesis and must support the pre-requisite of planar and square pyramidal

coordination to the metal ions. So I looked at a slightly different approach where multinuclear clusters/cages built on Co(II) ions can be stabilized by a self-assembly approach by using simple pyridyl functionalized multi-site ligands. A literature review of such self-assemblies revealed that M_6L_8 type octahedral cages are ubiquitous when C_3 -symmetric tripodal N-donor ligands are employed in the self-assembly reactions.³⁵⁻³⁷ Herein, as a proof of concept, I describe the synthesis and electro- and photocatalytic H_2 evolution activity of a water soluble cobalt cage $[\text{Co}^{\text{II}}_6\text{L}^1_8\text{Cl}_6(\text{H}_2\text{O})_6]\text{Cl}_6$, **14**, derived from a rigid tripodal silane ligand $\text{MeSi}(3\text{-Py})_3$ (L^1) featuring 3-pyridyl functionalities. This cage exhibits an octahedral environment for the six Co(II) atoms with four rigid equatorial N-pyridyl coordination and weakly coordinating aqua and chloride ligands at the apex. Also, the cage **14** is water soluble, due to its high cationic charge (98.8 g/L). The ligand L^1 exhibits a conjugated backbone via the Si atom. Hence, I reasoned that it might facilitate the cage assembly of **14** to accept electrons from the photosensitizer upon light irradiation. The photocatalytic H_2 evolution studies of this cage at pH 4.0 in presence of ascorbic acid (H_2A)/ ascorbate (HA^-) and $[\text{Ru}(\text{bpy})_3]^{2+}$ as a photosensitizer (PS) gave a fairly reasonable turnover number of 43 at 50 μM concentration of **14**.

5.2 Experimental Section

5.2.1 Materials and characterization: All manipulations were performed under a dry atmosphere in standard Schlenk-glassware. The glassware was oven-dried prior to use. Water was deionized with the Millipore Synergy system (18.2 $\text{M}\Omega\cdot\text{cm}$ resistivity) and placed under vacuum and refilled with nitrogen. All other chemical reagents were purchased from commercial vendors and used without further purification. The ligand L^1 was synthesized by using previously reported procedure.³⁸ FT-IR spectra and the UV-Visible spectrum was recorded on a Perkin-Elmer spectrophotometer, DLS analysis was recorded on Malvern Instruments. High Resolution mass spectrometry (HRMS) measurement performed on Bruker, Impact HD ESI-Q TOF mass spectrometer.

5.2.2 Synthesis of cage $[\text{Co}^{\text{II}}_6\text{L}^1_8\text{Cl}_6(\text{H}_2\text{O})_6]\text{Cl}_6$ (14**):** To a solution of L^1 (10 mg, 36 mmol) in MeOH (1 ml) was added 1 ml of methanolic solution of $\text{CoCl}_2\cdot 6\text{H}_2\text{O}$ (6.45 mg, 27 mmol) at room temperature to get a clear pink colored solution which on slow evaporation at room temperature yields blue crystals of **14**. Mass $m/z = 1056.08$ $\{[\text{Co}^{\text{II}}_6\text{L}^1_8\text{Cl}_6(\text{H}_2\text{O})_6]\text{Cl}_3\}^{3+} + (\text{H}_2\text{O}) + \text{K}$, 999.34 $\{[\text{Co}^{\text{II}}_6\text{L}^1_8\text{Cl}_6(\text{H}_2\text{O})_6]\text{Cl}_3\}^{3+}$, 778.97 $\{[\text{Co}^{\text{II}}_6\text{L}^1_8\text{Cl}_6(\text{H}_2\text{O})_6]\text{Cl}_2\}^{4+} + \text{K}$, and 520.39 $[\text{Co}^{\text{II}}_6\text{L}^1_8\text{Cl}_6(\text{H}_2\text{O})_6]^{6+} + \text{K}$. FT-IR data in powdered

sample (cm⁻¹): 2956, 2924, 1605, 1581, 1482, 1432, 1262, 1193, 1135, 1062, 799, 700, 655. Anal. Calcd for C₁₃₁H₁₃₄Cl₁₂Co₆N₂₄O₄Si₈: C, 50.55; H, 4.34; N, 10.80. Found: C, 50.57; H, 4.32; N, 10.83 %.

5.2.3 Crystallography: Reflections were collected on a Bruker Smart Apex Duo diffractometer at 100 K using MoK α radiation ($\lambda = 0.71073 \text{ \AA}$). Structures were refined by full-matrix least-squares against F² using all data (SHELX).^{38a} Crystallographic data for all these compounds are listed in (Table 5.1 and Appendix, A5.1). All non-hydrogen atoms were refined anisotropically if not stated otherwise. Hydrogen atoms were constrained in geometric positions to their parent atoms. The diffuse solvent molecules in cage **14** could not be modeled appropriately. Hence, these were treated as diffuse contributions to the overall scattering and removed by the SQUEEZE/PLATON for a better refinement data.^{38b}

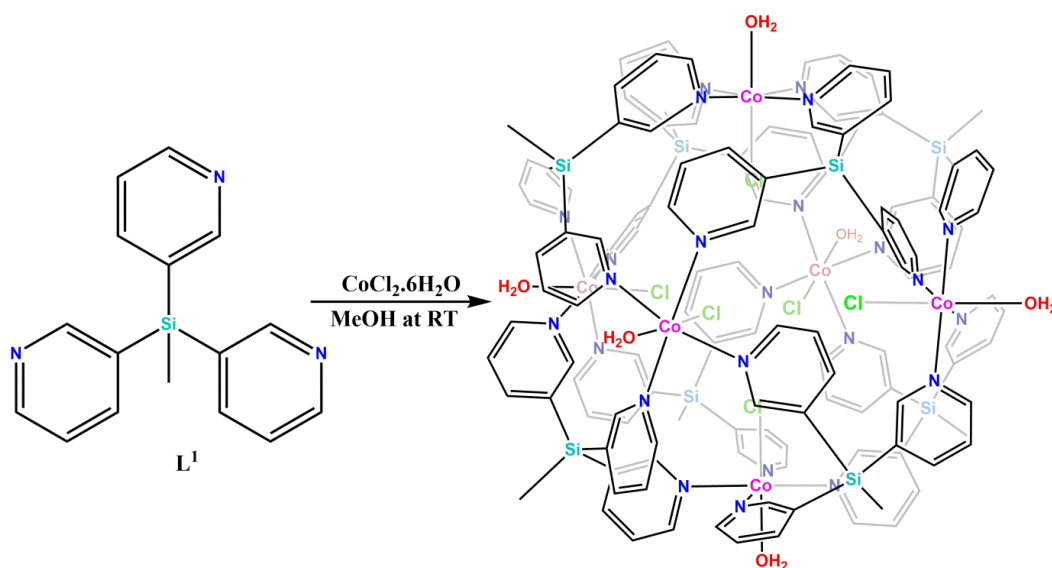
Table 5.1: Details of crystallographic data collection and structure refinements for cage

Compound	14
Chemical formula	C ₁₂₈ H ₁₃₄ Cl ₁₂ N ₂₄ O ₆ Si ₈ Co ₆
Formula weight	3106.21
Temperature	100(2)K
Crystal system	Orthorhombic
Space group	Pbcn
a (Å); α (°)	21.048(5); 90°.
b (Å); β (°)	29.141(7); 90°.
c (Å); γ (°)	32.738(8); 90°.
V (Å ³); Z	20080(8); 4
ρ (calc.) mg m ⁻³	1.023
μ (Mo K α) mm ⁻¹	0.735
2 θ _{max} (°)	50.052
R(int)	0.2118
Completeness to θ	99.9 %
Data / param.	17730/863
GOF	1.058
R1 [F > 4 σ (F)]	0.0768
wR2 (all data)	0.2642
max. peak/hole (e.Å ⁻³)	1.105/-1.171

5.2.4 General procedure for light driven hydrogen evolution: The proton reduction studies were performed in a 33 mL round bottom flask capped with a septum and equipped with a stir bar. The flask that contained **14**, 0.5 mM Ru(bpy)₃²⁺ and 0.3 M ascorbic acid as electron donor in pH 4 ascorbate buffer solution (5 mL) was seated in a thermally control water bath

(25 °C) was wrapped with blue LED strips ($\lambda = 469 \text{ nm}$) and connected to a port of a pressure transducer (PXM409-002BAUSBH). The catalyst concentration was varied from 50 to 250 μM . The evolved hydrogen gas was monitored by recording the increase in headspace pressure at every 10 seconds for 2-3 hours. The obtained pressure measurements were converted into a number of moles, using the equation, $PV = nRT$. The generated hydrogen gas was identified by gas chromatography (GC) using a 5 Å molecular sieve column (8 ft \times 1/8 in) with argon as the carrier gas and TCD detector. The reaction solution and headspace were purged by nitrogen gas to allow accurate measurement of the amount of H_2 produced during the experiment. This experiment was performed in triplicate. The thermodynamic stability and kinetic stability of the **14** was measured in terms of turnover number (TON) = [generated H_2] / [catalyst] in moles and turnover frequency (TOF) = TON/unit time respectively.

5.2.5 Electrochemical studies: Electrochemical measurements were carried out with a CH-electrochemical analyzer model 1100A using glassy carbon disk electrode (diameter 3 mm) as the working electrode and platinum wire as the counter-electrode and SCE (Saturated Calomel Electrode) as a reference electrode in 0.1 M (n-Bu₄N)PF₆ and KNO₃ as supporting electrolyte. The acetonitrile solvent and B. R. Buffer (Britton Robinson Buffer) were used as non-aqueous and aqueous solution respectively for electrochemical studies. The bulk electrolysis was performed in 1.0 M aqueous phosphate buffer (pH 7) by using SCE as the working electrode.



Scheme 5.1: Scheme for the preparation of the cationic cage assembly of 14

5.3 Result and Discussion

5.3.1 Syntheses

The silane ligand L^1 was prepared by our earlier reported procedure in a single step.³⁹ The cage molecule of **14** was obtained by the slow addition of methanolic solution of cobalt (II) chloride to a stirred solution of L^1 in methanol at room temperature (Scheme 5.1). The blue-colored single crystals suitable for X-ray crystallographic analysis were obtained by slow evaporation. The ESI mass spectrum of **14** in water exhibits several peaks centered at $m/z = 1056.08$ for the $\{[\text{Co}^{\text{II}}\text{L}^1_8\text{Cl}_6(\text{H}_2\text{O})_6]\text{Cl}_3\}^{3+} + (\text{H}_2\text{O}) + \text{K}$, 999.34 for the $\{[\text{Co}^{\text{II}}\text{L}^1_8\text{Cl}_6(\text{H}_2\text{O})_6]\text{Cl}_3\}^{3+}$, 778.97 for the $\{[\text{Co}^{\text{II}}\text{L}^1_8\text{Cl}_6(\text{H}_2\text{O})_6]\text{Cl}_2\}^{4+} + \text{K}$, and 520.39 for the $[\text{Co}^{\text{II}}\text{L}^1_8\text{Cl}_6(\text{H}_2\text{O})_6]^{6+} + \text{K}$. All these peaks indicate that the cage remains intact in the solution (Figure 5.1). The isotope patterns for the cage **14** have been calculated which matches well with the experimental values (Appendix, A5.1).

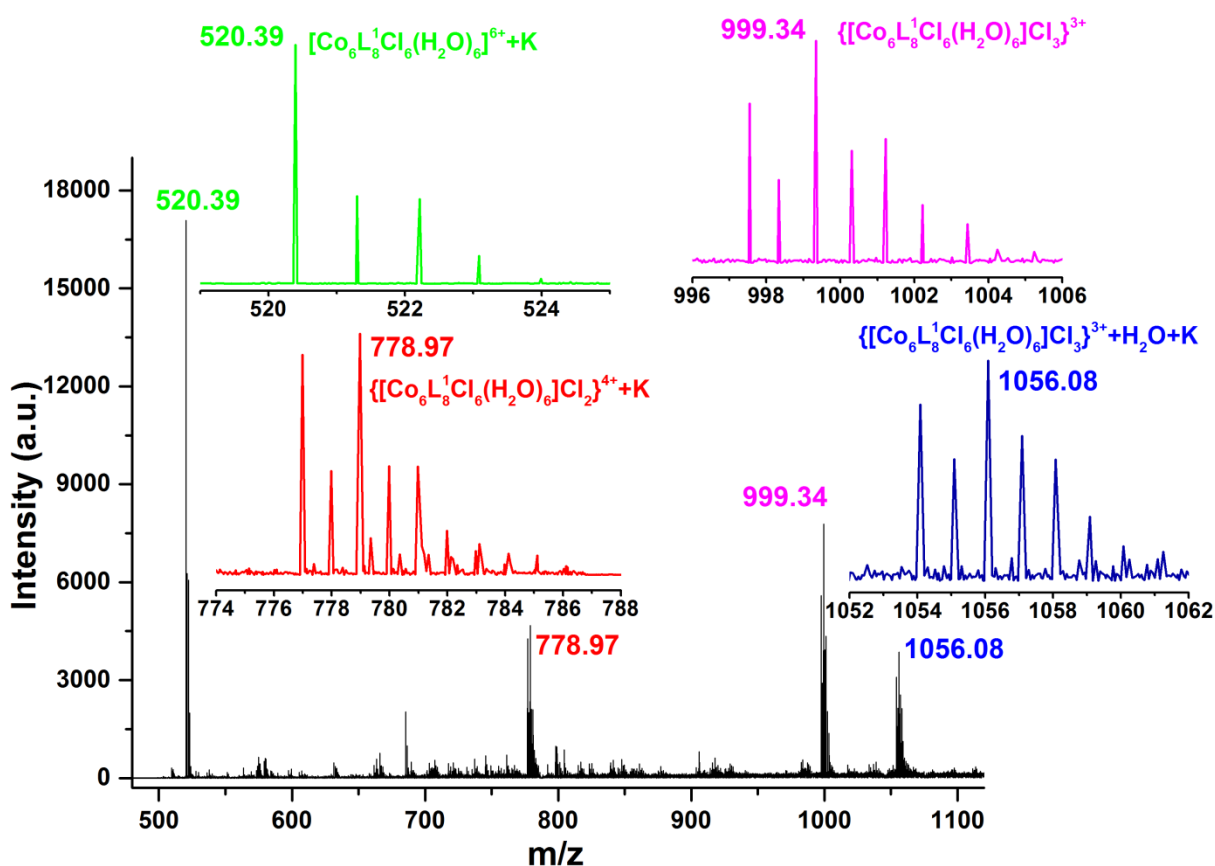


Figure 5.1: ESI mass spectra of cage **14** in water

5.3.2 Crystal structures

The molecular structure of the cage assembly was solved in the orthorhombic space group $Pbcn$ as its solvate adduct of formula $\mathbf{14} \cdot 3\text{MeOH} \cdot \text{H}_2\text{O}$ (Figure 5.2 and Appendix, A5.2 and A5.3). The structural analysis reveals that the Co_6L_8^1 core has an octahedral geometry in

which the six Co(II) atoms are located at the corners and eight equivalent silane ligands act as three connected linkers. Each Co(II) atom lies in an octahedral coordination sphere, where the equatorial square plane is occupied by four $\text{N}_{\text{pyridyl}}$ atoms from four different L^1 segments, while the axial positions are occupied by one water molecule outside and one chloride ion inside the cage. The Co-N distances range from 2.141(0) to 2.303(0) Å, and the Co-Cl distance range from 2.333(1) to 2.368(1) Å. The average distance between axially located Co centers is 11.32 Å, and that between equatorial Co centers is 8.06 Å. The average distance between the opposite Si atoms situated at the terminus of the 3-fold axis is 13.889 Å. There are three crystallographically imposed 4-fold axes passing through two opposite Co(II) centers and four 3-fold axes passing through the opposite pairs of ligand Si-Me groups. The cage adopts a local 432 symmetry (chiral, O) due to the absence of any plane(s) of symmetry. Furthermore, the rigid topology of the ligand (and that of the cage) arises from the absence of any spacers between the Si atom and the pyridyl rings. As a result the cage is very dense resembling a small nano-cluster of metal atoms and has no internal cavity to accommodate guest molecules. However, this arrangement makes this cage very stable in an aqueous environment as observed by its mass spectrum

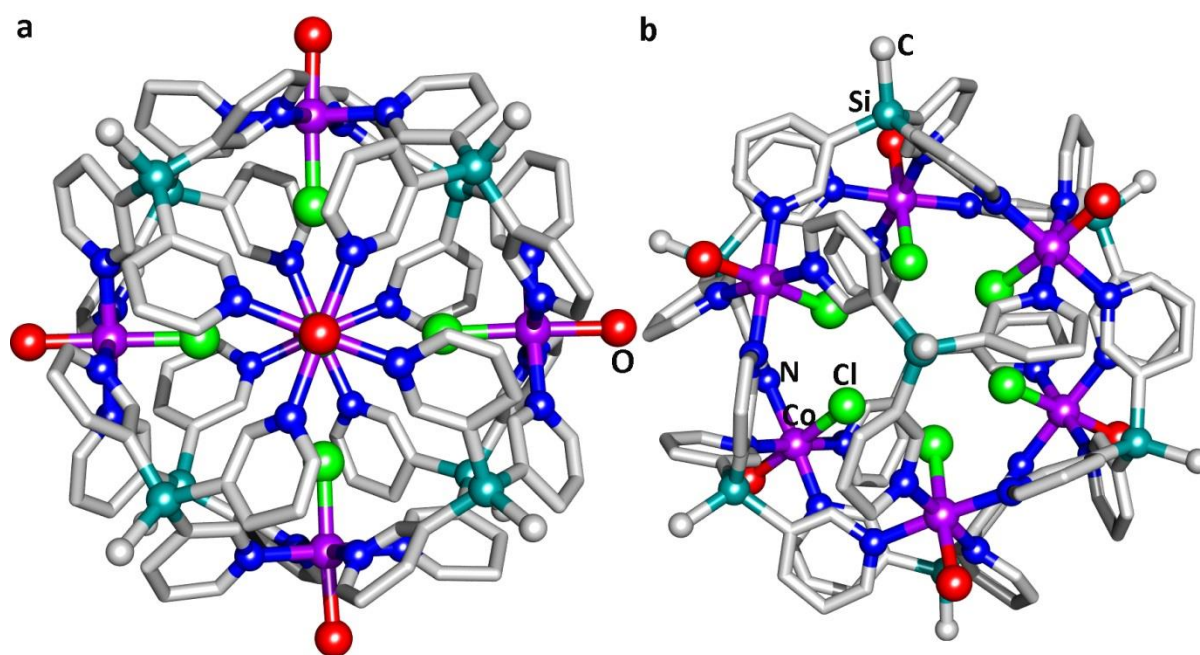
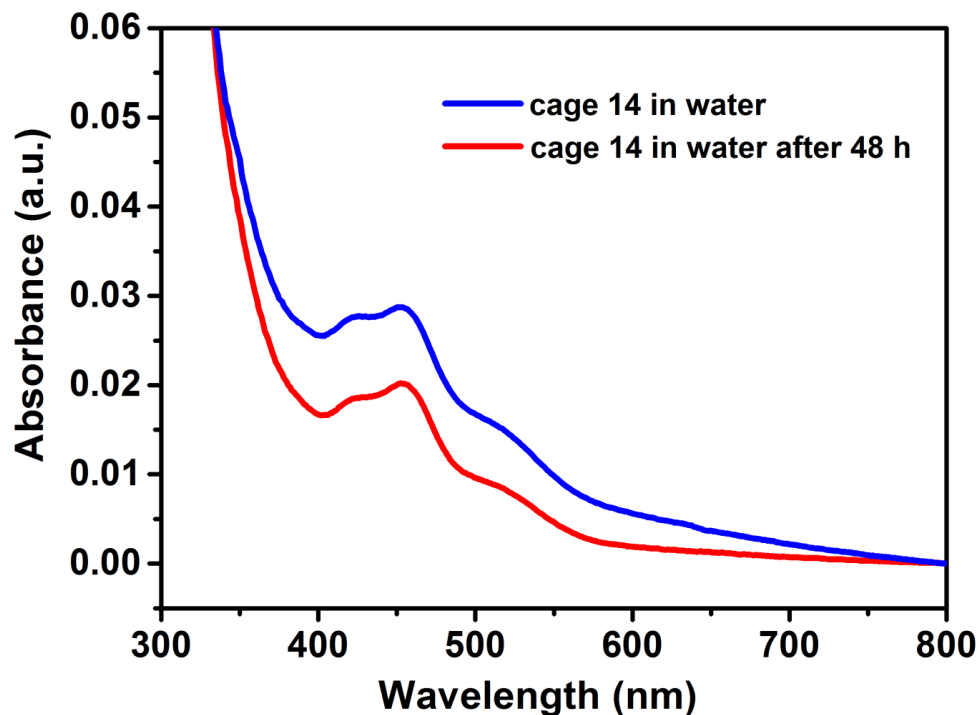


Figure 5.2: Crystal structure of **14** viewed along (a) the 4-fold axis and (b) the 3-fold axis

The UV-vis spectra of **14** in water exhibit three absorption maxima at 421, 452 and 518 nm which are attributed to the ${}^4\text{T}_{1g} \rightarrow {}^4\text{T}_{1g}(\text{P})$, ${}^4\text{T}_{1g} \rightarrow {}^4\text{A}_{2g}$ and ${}^4\text{T}_{1g} \rightarrow {}^4\text{T}_{2g}$ d-d transition, respectively, for the octahedral Co(II) complexes^{40,41} Further these peaks did not change even

after 48 h (Figure 5.3) albeit with a decrease in the intensity of peaks. This might be due to the slow degradation of the cage in low quantities. Also, measurement of the UV-Visible spectra at different pH conditions did not change the aqueous phase absorption profile indicating the thermodynamic stability of **14** in low pH (Appendix, A5.4).



*Figure 5.3: UV visible spectra of **14** in water before and after the 24 h*

5.3.3 Electrochemical behavior

The cyclic voltammogram (CV) of **14** was performed in aqueous solution. It exhibits one quasi-reversible couple at $E_{1/2} = 0.75$ V for the $\text{Co}^{\text{III}}/\text{Co}^{\text{II}}$ process and one irreversible event at -0.83 V for the $\text{Co}^{\text{II}}/\text{Co}^{\text{I}}$ (all potentials vs SCE) (Figure 5.4). Sweeping further towards the cathode reveals one irreversible electron waves at -1.5 V assigned to the ligand-centered event. This peak compares well with that of the free ligand L^1 (with a slight positive shift) which shows four redox events in acetonitrile (-0.95 , -1.33 , -1.83 , and -2.01 V) (Appendix A5.5). The redox events for $\text{Co}^{\text{II}}/\text{Co}^{\text{I}}$ appear at -0.83 V which is more positive than that of the ligand event at -0.95 V. Thus, the observed irreversible redox event at -0.83 V is clearly attributed to the $\text{Co}^{\text{II}}/\text{Co}^{\text{I}}$ process.⁴² Further, I have calculated the number of electrons involved in the redox events observed in the aqueous system by Coulometry using the formula $Q = nFm$ (Q = charge built, n = number of electron, F = faraday's constant and m = moles of the materials).⁴³ These results show that each metal centered event is approximately an one electron process (Appendix, A5.6 and A5.7).

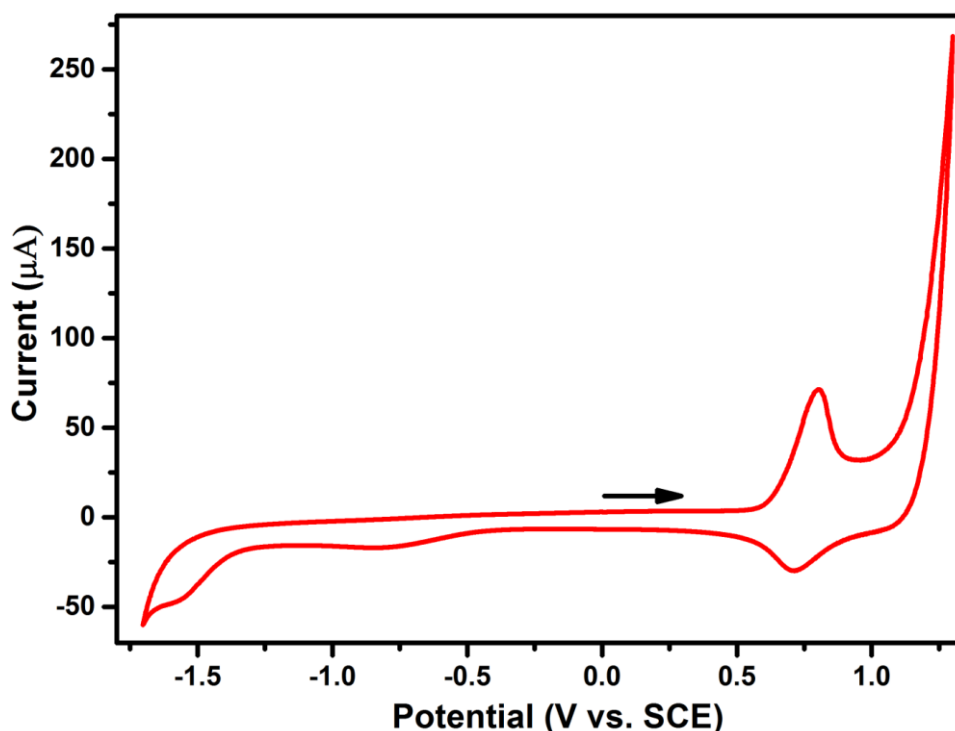


Figure 5.4: CV of 1 mM **14** in water at a scan rate of 100 mV/s at 25 °C. Supporting electrolyte: KNO_3 (0.1 M); SCE as reference electrode; glassy carbon: working electrode; Pt wire: auxiliary electrode.

We further explored the electrochemical behavior of **14** in buffered aqueous solution between pH 2 to 7, the range normally associated with the catalytic proton reduction. In pH 4.0 buffered solution, the $\text{Co}^{\text{II}}/\text{Co}^{\text{I}}$ redox process for **14** was observed at $E_{1/2} = -0.62$ V (Appendix, A5.8). The pH dependence of the redox potentials for **14** in the range 2 to 6.5 (aqueous Britton Robinson buffer solution) have been determined by using DPV measurements. The Pourbaix diagram indicates the changes in the $\text{Co}^{\text{II}}/\text{Co}^{\text{I}}$ redox couples with increasing pH. Initially it shows pH independent from 1.5 to 2.8 further, it exhibits a sharp linear dependence from pH 2.8 to 5.6 with the slope approximately equal to -59 mV/pH and finally it shows independence behavior from pH 5.6 to 7.5. However, the $\text{Co}^{\text{III}}/\text{Co}^{\text{II}}$ redox couple was found to be independent with the pH (Appendix, A5.9). This indicates the proton coupled electron transfer process (PCET) involved in the complex that could play a vital pathway for the proton reduction reaction. The cathodic scans performed on **14** at different pH indicate that the onset of the catalytic current is influenced by the variation in the pH and shows a linear decline in the corresponding redox potentials (Figure 5.5). For instance, for a fixed $40 \mu\text{A}$ catalytic current ($j = 0.6 \text{ mA}/\text{cm}^2$) the applied potential drops linearly with increasing pH and indicates the involvement of proton in the initial stages of the electrochemical catalysis by **14**

(Figure 5.5, inset). Based on the electrochemical characteristics we propose a probable mechanistic scheme for hydrogen evolution by **14** (Appendix, A5.10).⁴⁴

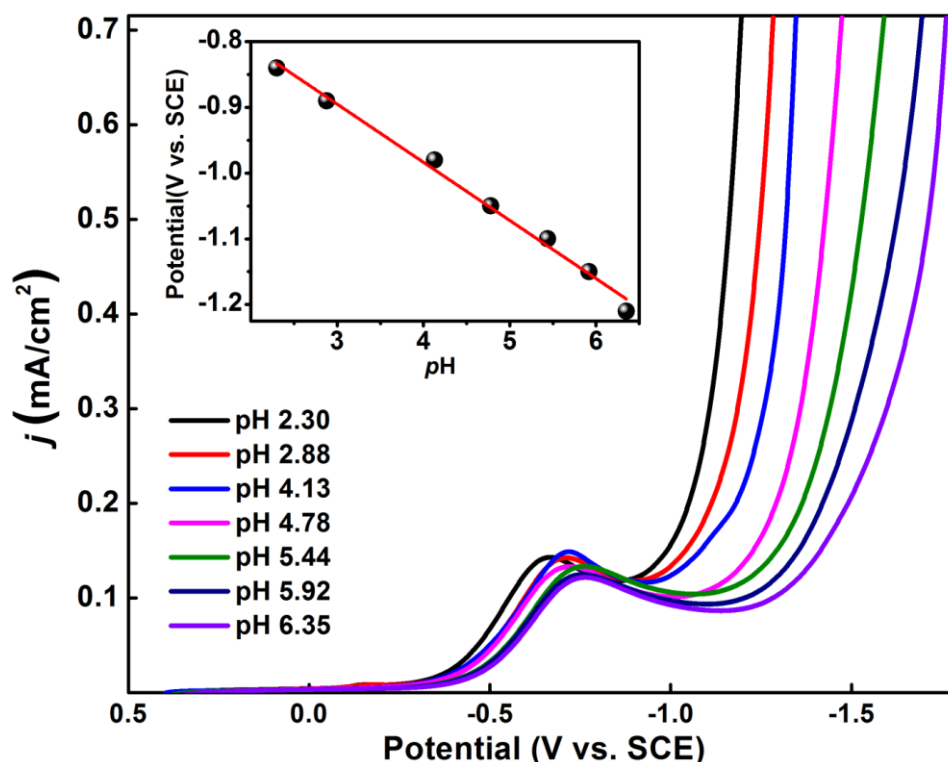


Figure 5.5: Cathodic scan rate of **14** in 0.1 M buffered solution at various pH values. Inset: Dependence of the catalytic potential of a catalytic current of 50 μA on the solution pH.

5.3.4 Electro-catalytic hydrogen Evolution

Furthermore, the electrocatalytic studies of **14** were carried out in its 1.0 M aqueous phosphate buffer solution (pH 7). For this experiment, bulk electrolysis of **14** (0.5 μM) was performed by using a glassy carbon disk as the working electrode in the potential range of -1.0 to -1.5 V. The charge build on the system was monitored as a function of time during the measurements. For example, when the applied potential was -1.4 V versus SCE, the maximum charge built was found to be 48 mC during the two minutes of electrolysis which accompanied with the evolution of gases (Figures 5.6 and Appendix, A5.11). The control experiments under the same potential (-1.4 V) with a catalyst-free solution gave a charge of only 3 mC (Appendix, A5.11). This clearly indicates that **14** serves as a hydrogen evolution catalyst. The total charge obtained in the bulk electrolysis was found to increase significantly upon progressively increasing the negative potentials from -1.0 to -1.5 V. The overpotential values reached in each of the electrocatalytic cycles were calculated by using the method described by Evans and co-workers.⁴⁵ The maximum TOF for the electrocatalytic hydrogen

evolution by **14** is 16 h^{-1} (Appendix, A5.13 and Equation A5.1). The stability of cage **14** was confirmed by recording ESI mass before and after the bulk electrolysis which shows no apparent change in the peak patterns (Appendix, A5.14)

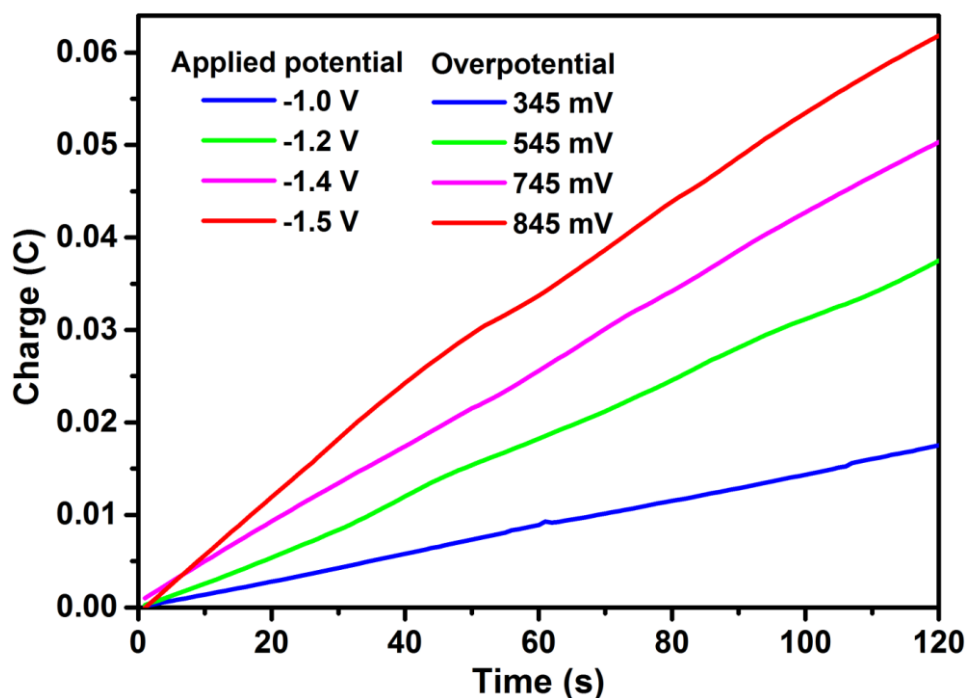


Figure 5.6: Charge build-up over time by the bulk electrolysis of $0.5 \mu\text{M}$ **14** in 1.0 M aqueous phosphate buffer (pH 7.0). All the data reported have been deducted from the blank.

5.3.5 Photocatalytic activity

These photophysical and electrochemical analysis evidence that **14** can be a molecular catalyst which can drive the proton reduction in water. Thus, we set out to probe the suitability of **14** as PRC in visible light driven H_2 evolution from water by employing $[\text{Ru}(\text{bpy})_3]\text{Cl}_2$ as a photosensitizer (PS) and ascorbic acid (AA) as a sacrificial electron donor (SED) in aqueous solution. It has earlier been demonstrated that quenching of photo excited $[\text{Ru}(\text{bpy})_3]^{2+*}$ by ascorbic acid, yields $[\text{Ru}(\text{bpy})_3]^+$ which drives the PRC to liberate hydrogen from water.^{10,32} The photocatalytic reaction was monitored in a 33 mL round-bottom flask fitted with the pressure transducer in the presence of an LED light strip ($\lambda_{\text{max}} = 469 \text{ nm}$) as a light source which is wrapped around a temperature controlled water jacketed beaker. The pressure developed in the flask due to the evolution of hydrogen was continuously measured by the pressure transducer for a period up to 2 hours. The identity of evolved hydrogen was confirmed by the GC equipped with a thermal conductivity detector (TCD). The liberated hydrogen vs. time profile at catalyst concentrations ranging from 50 to 250 μM are shown in

Figure 5.7. The turnover number (TON) after 2 h irradiation of the reaction mixture containing $50 \mu\text{M}$ of **14** was found to be 43. If **14** is replaced by $\text{CoCl}_2 \cdot 6\text{H}_2\text{O}$, negligible H_2 evolution was observed upon irradiation even at a relatively higher concentration of 1 mM . Similarly, a much lower amount of H_2 evolution was observed when $[\text{Ru}(\text{bpy})_3]\text{Cl}_2$ (0.5 mM) alone was employed in absence of the catalyst **14**. These control experiments rule out any contribution from the simple hydrated $\text{Co}(\text{II})$ cation (formed via leaching of **14**) or $[\text{Ru}(\text{bpy})_3]\text{Cl}_2$ itself as a catalyst for the light-driven H_2 evolution. Further, the absence of cobalt oxide nanoparticles formed during the catalysis was confirmed by DLS analysis (Appendix, A5.15). A plot of the initial rate of hydrogen generation vs. catalyst concentration indicates the pseudo-first order origin of the reaction kinetics. The rate constant derived from this plot is found to be 20.50 h^{-1} and is consistent with the obtained turnover number (TON) at the measured concentration range (Figure 5.7).

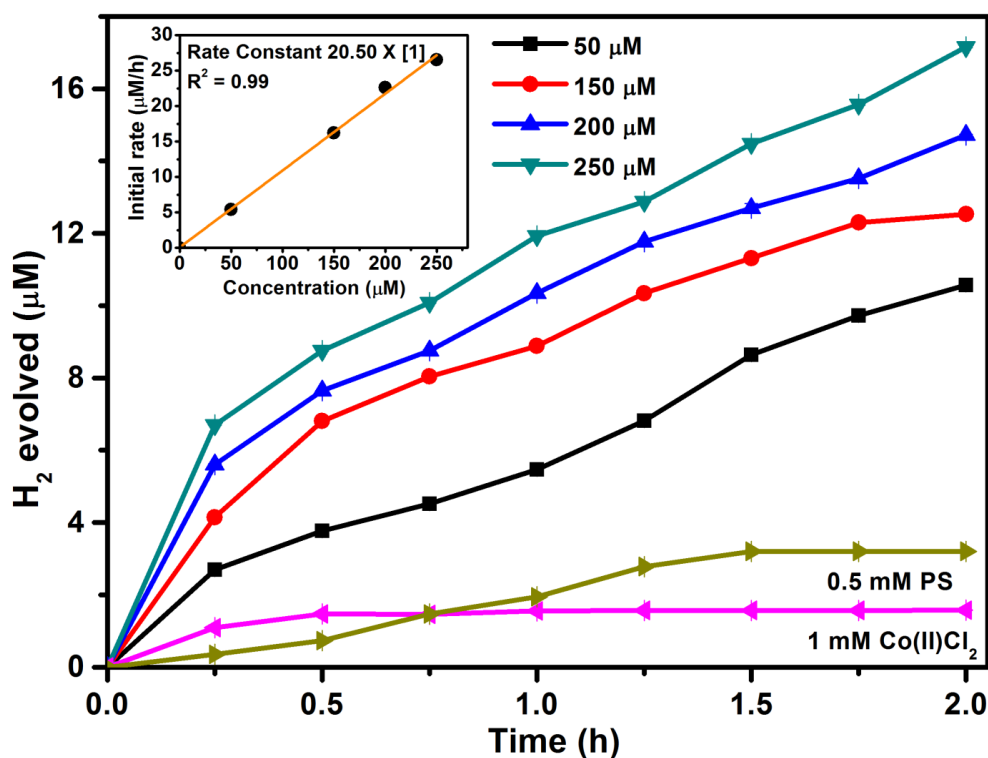


Figure 5.7: The kinetic plots of light-driven H_2 evolution by employing **15** at $50 \mu\text{M}$, $150 \mu\text{M}$, $200 \mu\text{M}$, and $250 \mu\text{M}$ in the presence of 0.3 M ascorbic acid solution ($\text{pH} = 4$) and 0.5 mM $[\text{Ru}(\text{bpy})_3]\text{Cl}_2$ as photosensitizer (PS). Control experiments with 1 mM CoCl_2 and 0.5 mM PS have also been plotted. Inset: the Initial rate of H_2 evolution.

In order to understand the cause of early saturation of the catalytic activity, we performed control experiments. Thus, one of the three components (ascorbic acid, $[\text{Ru}(\text{bpy})_3]^{2+}$ as PS or

14) of the catalytic system was added (separately or a combination of two) to the reaction flask after cessation of the H₂ evolution to see if the H₂ evolution could be resumed. However, the addition of any one of the three components, in the same amount as used in the photocatalytic reaction, resulted in no significant amount of H₂ formation, suggesting that decomposition of at least two of the three species occurred during the photocatalytic H₂ evolution. A combined addition of **14** and the [Ru(bpy)₃]²⁺ as a photosensitizer resumed substantial H₂ evolution. However, no significant amount of H₂ was produced when ascorbic acid and **14** were added, suggesting the decomposition of [Ru(bpy)₃]²⁺ under these reaction conditions.⁴⁶ This may be due to the presence of trace amounts of air in the reaction flask that may lead to the decomposition of the catalytic system.⁴⁷⁻⁴⁹ The evolution of H₂ in the presence of bulk air was negligible suggesting that O₂ inhibits the evolution of H₂ (Appendix, A5.16).

5.4 Conclusion

In conclusion, I show here for the first time that a self-assembled metal-organic cage based on Co(II) ions can be employed as both electro- and photocatalyst for H₂ evolution. The cage assembly of **14** can be synthesized in a one-step reaction and contains six Co(II) ions in octahedral coordination in which the apical positions are occupied with labile ligands. The photophysical and electrochemical investigations show that the cage can behave as a molecular catalyst. Also, the pH dependence of the potentials and catalytic currents of **14** indicates the apparent involvement of the proton-coupled electron transfer process in the hydrogen evolution. Electrocatalytic hydrogen evolution experiments with **14** gave a turnover frequency of 16 h⁻¹. Further, it has been shown to act as an efficient photocatalyst for the light-driven the evolution of H₂ from water in presence of Ru(bpy)₃²⁺ as PS and ascorbic acid as SED. The obtained turnover number of 43 by applying 50 μM of **14** as a catalyst gave a pseudo-first order rate constant value of 20.50 h⁻¹. These results promise the utility of a self-assembly approach for designing suitable catalysts for water splitting reactions. Current efforts are aimed at boosting the efficiency of such self-assembled cages by coupling them with suitable electron-injecting semiconductors.

5.5 References

- (1) Turner, J. A. *Science*, **2004**, *305*, 972-974.
- (2) Lewis, N. S.; Nocera, D. G. *Proc. Natl. Acad. Sci. U.S.A.*, **2006**, *103*, 15729-15735.
- (3) Esswein, A. J.; Nocera, D. G. *Chem. Rev.* **2007**, *107*, 4022-4047.
- (4) Cook, T. R.; Dogutan, D. K.; Reece, S. Y.; Surendranath, Y.; Teets, T. S.; Nocera, D. G. *Chem. Rev.* **2010**, *110*, 6474-6502.
- (5) Walter, M. G.; Warren, E. L.; McKone, J. R.; Boettcher, S. W.; Mi, Q.; Santori, E. A.; Lewis, N. S. *Chem. Rev.* **2010**, *110*, 6446-6473.
- (6) Karkas, M. D.; Verho, O.; Johnston, E. V.; Åkermark, B. R. *Chem. Rev.* **2014**, *114*, 11863-12001.
- (7) Swierk, J. R.; Mallouk, T. E. *Chem. Soc. Rev.* **2013**, *42*, 2357-2387.
- (8) Nocera, D. G. *Acc. Chem. Res.* **2012**, *45*, 767-776.
- (9) Tran, P. D.; Artero, V.; Fontecave, M. *Energy Environ. Sci.* **2010**, *3*, 727-747.
- (10) Creutz, C.; Sutin, N. *Coord. Chem. Rev.* **1985**, *64*, 321-341.
- (11) Alstrum-Acevedo, J. H.; Brennaman, M. K.; Meyer, T. J. *Inorg. Chem.* **2005**, *44*, 6802-6827.
- (12) Du, P.; Schneider, J.; Jarosz, P.; Zhang, J.; Brennessel, W. W.; Eisenberg, R. *J. Phys. Chem. B.* **2007**, *111*, 6887-6894.
- (13) Cline, E. D.; Adamson, S. E.; Bernhard, S. *Inorg. Chem.* **2008**, *47*, 10378-10388.
- (14) Curtin, P. N.; Tinker, L. L.; Burgess, C. M.; Cline, E. D.; Bernhard, S. *Inorg. Chem.* **2009**, *48*, 10498-10506.
- (15) Du, P.; Eisenberg, R. *Energy Environ. Sci.* **2012**, *5*, 6012-6021.
- (16) Bachmann, C.; Guttentag, M.; Spingler, B.; Alberto, R. *Inorg. Chem.* **2013**, *52*, 6055-6061.
- (17) Eckenhoff, W. T.; Brennessel, W. W.; Eisenberg, R. *Inorg. Chem.* **2014**, *53*, 9860-9869.
- (18) Han, Z.; Shen, L.; Brennessel, W. W.; Holland, P. L.; Eisenberg, R. *J. Am. Chem. Soc.* **2013**, *135*, 14659-14669.
- (19) Thoi, V. S.; Sun, Y.; Long, J. R.; Chang, C. J. *Chem. Soc. Rev.* **2013**, *42*, 2388-2400.
- (20) DuBois, D. L. *Inorg. Chem.* **2014**, *53*, 3935-3960.
- (21) Artero, V.; Chavarot-Kerlidou, M.; Fontecave, M. *Angew. Chem., Int. Ed.* **2011**, *50*, 7238-7266.
- (22) Singh, W. M.; Baine, T.; Kudo, S.; Tian, S.; Ma, X. A. N.; Zhou, H.; DeYonker, N. J.; Pham, T. C.; Bollinger, J. C.; Baker, D. L. *Angew. Chem., Int. Ed.* **2012**, *51*, 5941-5944.
- (23) Khnayzer, R.; Thoi, V.; Nippe, M.; King, A.; Jurss, J.; El Roz, K.; Long, J.; Chang, C.; Castellano, F. *Energy Environ. Sci.* **2014**, *7*, 1477-1488.
- (24) Call, A.; Codolà, Z.; Acuña-Parés, F.; Lloret-Fillol, J. *Chem. Eur. J.* **2014**, *20*, 6171-6183.
- (25) Leung, C.-F.; Ng, S.-M.; Ko, C.-C.; Man, W.-L.; Wu, J.; Chen, L.; Lau, T.-C. *Energy Environ. Sci.* **2012**, *5*, 7903-7907.
- (26) Tong, L.; Zong, R.; Thummel, R. P. *J. Am. Chem. Soc.* **2014**, *136*, 4881-4884.
- (27) Du, P.; Schneider, J.; Luo, G.; Brennessel, W. W.; Eisenberg, R. *Inorg. Chem.* **2009**, *48*, 4952-4962.

- (28) Losse, S.; Vos, J. G.; Rau, S. *Coord. Chem. Rev.* **2010**, *254*, 2492-2504.
- (29) Hawecker, J.; Lehn, J. M.; Ziessel, R. *New J. Chem.* **1983**, *7*, 271–277
- (30) Jacques, P.-A.; Artero, V.; Pécaut, J.; Fontecave, M. *Proc. Natl. Acad. Sci. U.S.A.* **2009**, *106*, 20627-20632
- (31) McCrory, C. C.; Uyeda, C.; Peters, J. C. *J. Am. Chem. Soc.* **2012**, *134*, 3164-3170.
- (32) Creutz, C.; Sutin, N. *Coord. Chem. Rev.* **1985**, *64*, 321–341
- (33) Xie, J.; Zhou, Q.; Li, C.; Wang, W.; Hou, Y.; Zhang, B.; Wang, X. *Chem. Comm.* **2014**, *50*, 6520-6522.
- (34) Tong, L.; Kopecky, A.; Zong, R.; Gagnon, K. J.; Ahlquist, M. S.; Thummel, R. P. *Inorg. Chem.* **2015**, *54*, 7873-7884.
- (35) Li, X.-J.; Jiang, F.-L.; Wu, M.-Y.; Zhang, S.-Q.; Zhou, Y.-F.; Hong, M.-C. *Inorg. Chem.* **2012**, *51*, 4116-4122.
- (36) Yoneya, M.; Yamaguchi, T.; Sato, S.; Fujita, M. *J. Am. Chem. Soc.* **2012**, *134*, 14401-14407.
- (37) Moon, D.; Kang, S.; Park, J.; Lee, K.; John, R. P.; Won, H.; Seong, G. H.; Kim, Y. S.; Kim, G. H.; Rhee, H. *J. Am. Chem. Soc.* **2006**, *128*, 3530-3531.
- (38) (a) G. M. Sheldrick. *Acta Crystallogr.* **2007**, *64*, 112-122; (b) Spek, A. L. *Acta Cryst.* **2015**, *C71*, 9-18.
- (39) Deshmukh, M. S.; Yadav, A.; Pant, R. *Inorg. Chem.* **2015**, *54*, 1337-1345.
- (40) Aizawa, S.-i.; Funahashi, S. *Inorg. Chem.*, **2002**, *41*, 4555-4549.
- (41) Pandey, S.; Das, P. P.; Singh, A. K.; Mukherjee, R. *Dalton Trans.*, **2011**, *40*, 10758–10768.
- (42) Silva, T. F. S.; Martins, L. M. D. R. S.; Guedes da Silva, M. F. C.; Fernandes, A. R.; Silva, A.; Borralho, P. M.; Santos, S.; Rodrigues, C. M. P.; Pombeiro, A. J. L. *Dalton Trans.* **2012**, *41*, 12888– 12897.
- (43) Feldman, B.J.; Gheller, S. F.; Bailey, G. F.; Newton, W. E.; Schultz, F. A. *Anal. Biochem.* **1990**, *185*, 170-175.
- (44) Kochubey, D.; Kaichev, V.; Saraev, A.; Tomy, S.; Belov, A.; Y. *J. Phys. Chem. C*, **2013**, *117*, 2753–2759
- (45) Felton, G. A. N.; Glass, R. S.; Lichtenberger, D. L.; Evans, D. H. *Inorg. Chem.* **2006**, *45*, 9181–9184.
- (46) Khnayzer, R. S.; Thoi, V. S.; Nippe, M.; King, A. E.; Jurss, J. W.; El Roz, K. A.; Long, J. R.; Chang, C. J.; Castellano, F. N. *Energy Environ. Sci.*, **2014**, *7*, 1477-1488.
- (47) Biswajit, M.; Dey, A. *Chem. Commun.*, **2017**, *53*, 7707-7715
- (48) Dey, S.; Rana, A.; Crouthers, D.; Mondal, B.; Das, P. K.; Darensbourg, M. Y.; Dey, A. *J. Am. Chem. Soc.*, **2014**, *136*, 8847–8850.
- (49) Swanson, K. D.; Ratzloff, M. W.; Mulder, D. W.; Artz, J. H.; Ghose, S.; Hoffman, A.; White, S.; Zadovnyy, O. A.; Broderick, J. B.; Bothner, B.; King P. W.; Peters, J. W. [FeFe]-*J. Am. Chem. Soc.*, **2015**, *137*, 1809–1816.

Chapter 6

THESIS CONCLUSION AND FUTURE PERSPECTIVES

In summary, this thesis presents a systematic design and synthesis of silicon centered ligands for the assembly of cages, clusters and coordination polymers. As mentioned in the introduction chapter, use of silicon centric ligands for the construction of coordination assemblies is an interesting approach as it largely simplifies the synthetic procedures required for the preparation of multi-site coordinating ligands. Thus, we have synthesized a series of N-donor functionalized silane ligands and utilized them to obtain multi-dimensional coordination polymers and utilized them for various applications in the areas of tunable luminescence, catalysis, and chemical adsorption. In addition, this thesis presents first time the synthesis of pyridine functionalized cyclotetrasiloxane ligands and the separation of the three stereoisomers out of four and their stereochemistry were established with the help of NMR and crystal structure analysis. Also, it reports for the first time on the metal complexes based on the cyclic tetrasiloxane backbone. Owing to the interest in the N-donor supported Cu_xI_x type of clusters and their rich photophysical properties, two iso-structural MOF materials featuring Cu_6I_6 clusters have been synthesized from tridentate arylsilane ligands of the type $MeSi(3-Py)_3$ (3-Py = 3-pyridyl, L^1) and $MeSi(3-Qy)_3$ (3-Qy = 3-quinolyl, L^2), respectively. These MOFs have shown a very interesting thermochromic and mechanochromic luminescence umpolung behaviour (chapter 2). Next, We have synthesized new cyclotetrasiloxane scaffolds containing peripherally functionalized 3-pyridyl moieties, $[MeSiO(CH=CH3-Py)]_4$ (L^3) by using Heck Coupling reaction and $[MeSiO(CH_2CH_23-Py)]_4$ (L^4), by reducing the double bonds present in (L^3) in the presence of Pd(0)/C as a catalyst and triethylsilane as reducing agent. Furthermore, we have studied their stereochemistry with the proton and silicon NMR as well as their complexation with certain d^{10} metal ions (chapter 3). We have also synthesized rigid and flexible tetrahedral tetra-pyridyl silane ligands by using Heck coupling reaction and utilized them to obtain charge-separated Cu(II) containing 3D MOFs having unique linear $Cu^{II}_4Cl_3(H_2O)_2$ and $Cu^{II}_4Cl_3(H_2O)_2$ clusters. These MOFs were shown to exhibit a reversible iodine uptake in both solid and solution state and act as Lewis acidic heterogeneous catalysts for Friedel-Crafts alkylation reactions under solvent-free conditions (chapter 4A). By using the same rigid silane ligand, two solvent dependent copper iodide cluster MOFs having Cu_2I_2 and Cu_4I_4 as nodes have been synthesized and utilize them as catalysts for Ullmann coupling reaction (chapter 4B). Finally, we have synthesized a self-assembled octahedral cobalt (II) cage as a homogeneous catalyst for

both electro- and photocatalytic hydrogen evolution from the water (chapter 5). Taking inspiration from all the results of this thesis which mainly focus on the 3-pyridyl moieties as metal binding sites, it will be interesting to look for ligand scaffolds based on 2- and 4-pyridyl moieties as well as to check the coordination chemistry of metal binding moieties such as O, P, S by using Heck or silylative reaction and studies. In addition to the ligands based on simple silane and siloxane backbone, it is worthwhile to extend this approach to functionalized higher silicon precursors such as POSS and Hexa-vinyl-disiloxanes. Nevertheless, the results demonstrated in this thesis provides some useful input in developing rational approaches and design strategies for the synthesis of silicon based ligands for coordination chemistry.

References:

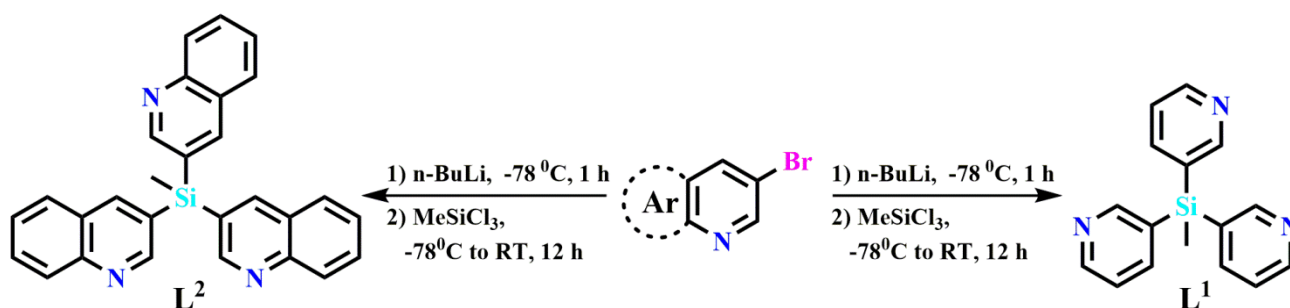
- 1) Jung, O.-S.; Kim, Y. J.; Kim, K. M.; Lee, Y.-A. *J. Am. Chem. Soc.* **2002**, *124*, 7906-7907.
- 2) Davies, R.; Less, R.; Lickiss, P.; Robertson, K.; White, A. *Inorg. Chem.* **2008**, *47*, 9958-9964.
- 3) Goodgame, D. M.; Lickiss, P. D.; Rooke, S. J.; White, A. J.; Williams, D. J. *Inorganica Chim. Acta* **2001**, *324*, 218-231.
- 4) Timokhin, I.; White, A.; Lickiss, P.; Pettinari, C.; Davies, R. *CrystEngComm* **2014**, *16*, 8094-8097.
- 5) Marciniak, B.; Walczuk-Guściora, E.; Pietraszuk, C. *Organometallics* **2001**, *20*, 3423-3428.
- 6) Cordes, D. B.; Lickiss, P. D.; Rataboul, F. *Chem. Rev* **2010**, *110*, 2081-2173.
- 7) Delmas, L. C.; Horton, P. N.; White, A. J.; Coles, S. J.; Lickiss, P. D.; Davies, R. P. *Chem. Commun.* **2017**, *53*, 12524-12527.
- 8) Deshmukh, M. S.; Yadav, A.; Pant, R.; Boomishankar, R. *Inorg. Chem.* **2015**, *50*, 1337-1345.
- 9) Deshmukh, M. S.; Vijayakanth, T.; Boomishankar, R. *Inorg. Chem.* **2016**, *51*, 3098-3104.
- 10) Deshmukh, M. S.; Chaudhary, A.; Zolotarey, P. N.; Boomishankar, R. *Inorg. Chem.* **2017**, *56*, 11762-11767.
- 11) Deshmukh, M. S.; Mane, V. S.; Kumbhar, A. S.; Boomishankar, R. *Inorg. Chem.* **2017**, *56*, 13286-13292.

APPENDIX

Table A2.1: Selected bond-lengths (Å) and angles (°) for **L¹**, **1**, **2**, **3** and **4**.

Compound	Bond length		Bond angle	
L¹	Si(1)-C(1)	1.863(5)	C(1)-Si(1)-C(11)	110.45(9)
	Si(1)-C(11)	1.874(3)	C(1)-Si(1)-C(11)#1	110.45(9)
	Si(1)-C(11)#1	1.874(3)	C(11)-Si(1)-C(11)#1	108.47(10)
	C(12)-N(13)	1.372(5)	C(16)-C(11)-Si(1)	120.1(2)
	N(13)-C(14)	1.397(5)	C(12)-C(11)-Si(1)	124.1(2)
1 at 100 K	I(1)-Cu(1)	2.5978(5)	Cu(1)-I(1)-Cu(1)#1	62.031(10)
	I(1)-Cu(1)#1	2.6676(5)	Cu(1)-I(1)-Cu(1)#2	95.872(14)
	I(1)-Cu(1)#2	2.6814(5)	N(13)-Cu(1)-I(1)	109.10(5)
	Cu(1)-N(13)	2.0629(19)	N(13)-Cu(1)-I(1)#3	97.61(5)
	Cu(1)-I(1)#3	2.6677(5)	I(1)-Cu(1)-I(1)#3	119.434(12)
	Cu(1)-I(1)#4	2.6815(5)	I(1)-Cu(1)-I(1)#4	107.915(14)
	Cu(1)-Cu(1)#1	2.7138(5)	I(1)#3-Cu(1)-I(1)#4	116.437(12)
	Cu(1)-Cu(1)#3	2.7138(5)	N(13)-Cu(1)-Cu(1)#1	124.56(5)
	Si(1)-C(1)	1.861(4)	I(1)-Cu(1)-Cu(1)#1	60.249(13)
	Si(1)-C(11)#5	1.878(2)	I(1)#4-Cu(1)-Cu(1)#1	130.806(8)
	Si(1)-C(11)#6	1.878(2)	N(13)-Cu(1)-Cu(1)#3	118.44(5)
	Si(1)-C(11)	1.878(2)	I(1)#4-Cu(1)-Cu(1)#3	59.263(13)
1 at 296K	I(1)-Cu(1)#1	2.587(2)	Cu(1)#1-I(1)-Cu(1)#2	63.06(4)
	I(1)-Cu(1)#2	2.661(3)	Cu(1)#1-I(1)-Cu(1)	97.33(5)
	I(1)-Cu(1)	2.696(2)	Cu(1)#2-I(1)-Cu(1)	61.65(4)
	Cu(1)-N(13)	2.064(6)	I(1)#3-Cu(1)-I(1)#4	119.15(5)
	Cu(1)-I(1)#3	2.587(2)	N(13)-Cu(1)-I(1)	104.51(17)
	Cu(1)-I(1)#4	2.660(3)	N(13)-Cu(1)-Cu(1)#2	118.00(16)
	Cu(1)-Cu(1)#2	2.745(2)	I(1)#3-Cu(1)-Cu(1)#2	131.93(3)
	Cu(1)-Cu(1)#4	2.745(2)	N(13)-Cu(1)-Cu(1)#4	125.56(18)
			I(1)#3-Cu(1)-Cu(1)#4	59.77(7)
		Cu(1)#2-Cu(1)-Cu(1)#4	92.55(8)	
2	I(1)-Cu(1)#1	2.5828(6)	Cu(1)#1-I(1)-Cu(1)#2	72.681(13)
	I(1)-Cu(1)#2	2.6759(6)	Cu(1)#1-I(1)-Cu(1)	111.365(18)
	I(1)-Cu(1)	2.7359(6)	Cu(1)#2-I(1)-Cu(1)	70.329(13)
	Cu(1)-N(13)	2.059(2)	N(13)-Cu(1)-I(1)#3	126.89(8)
	Cu(1)-I(1)#3	2.5829(5)	N(13)-Cu(1)-I(1)#4	104.72(8)
	Cu(1)-I(1)#4	2.6759(6)	I(1)#3-Cu(1)-I(1)#4	110.752(16)
			N(13)-Cu(1)-I(1)	97.47(7)

2 at 296 K	I(1)-Cu(1)	2.5803(7)	Cu(1)-I(1)-Cu(1)#1	73.443(18)
	I(1)-Cu(1)#1	2.6831(8)	Cu(1)-I(1)-Cu(1)#2	112.00(2)
	I(1)-Cu(1)#2	2.7565(7)	Cu(1)#1-I(1)-Cu(1)#2	70.711(17)
	Cu(1)-N(13)	2.063(3)	N(13)-Cu(1)-I(1)	126.78(9)
	Cu(1)-I(1)#3	2.6832(8)	N(13)-Cu(1)-I(1)#3	105.44(9)
	Cu(1)-I(1)#4	2.7566(7)	I(1)-Cu(1)-I(1)#3	110.48(2)
			N(13)-Cu(1)-I(1)#4	97.42(9)
3	I(1)-Cu(1)#1	2.6292(15)	Cu(1)#1-I(1)-Cu(1)	63.05(4)
	I(1)-Cu(1)	2.6378(14)	N(33)#2-Cu(1)-N(13)	103.8(3)
	Cu(1)-N(33)#2	2.111(6)	N(33)#2-Cu(1)-I(1)#1	108.8(2)
	Cu(1)-N(13)	2.116(8)	N(13)-Cu(1)-I(1)#1	105.0(2)
	Cu(1)-I(1)#1	2.6292(15)	N(33)#2-Cu(1)-I(1)	109.4(2)
	Cu(1)-Cu(1)#1	2.7541(18)	N(13)-Cu(1)-I(1)	112.0(2)
			I(1)#1-Cu(1)-I(1)	116.95(4)
4	I(1)-Cu(1)	2.6025(5)	N(33)-Cu(1)-N(23)#1	118.78(10)
	Cu(1)-N(33)	2.042(2)	N(33)-Cu(1)-N(13)#2	103.58(10)
	Cu(1)-N(23)#1	2.100(3)	N(23)#1-Cu(1)-N(13)#2	98.68(10)
	Cu(1)-N(13)#2	2.141(2)	N(33)-Cu(1)-I(1)	118.44(7)
	Si(1)-C(1)	1.866(3)	N(23)#1-Cu(1)-I(1)	102.16(7)
	Si(1)-C(31)	1.871(3)	N(13)#2-Cu(1)-I(1)	113.84(7)
	Si(1)-C(21)	1.878(3)	C(1)-Si(1)-C(31)	110.80(15)
	Si(1)-C(11)	1.881(3)	C(1)-Si(1)-C(21)	110.83(14)

Figure A2.1: synthetic scheme of L¹ and L².

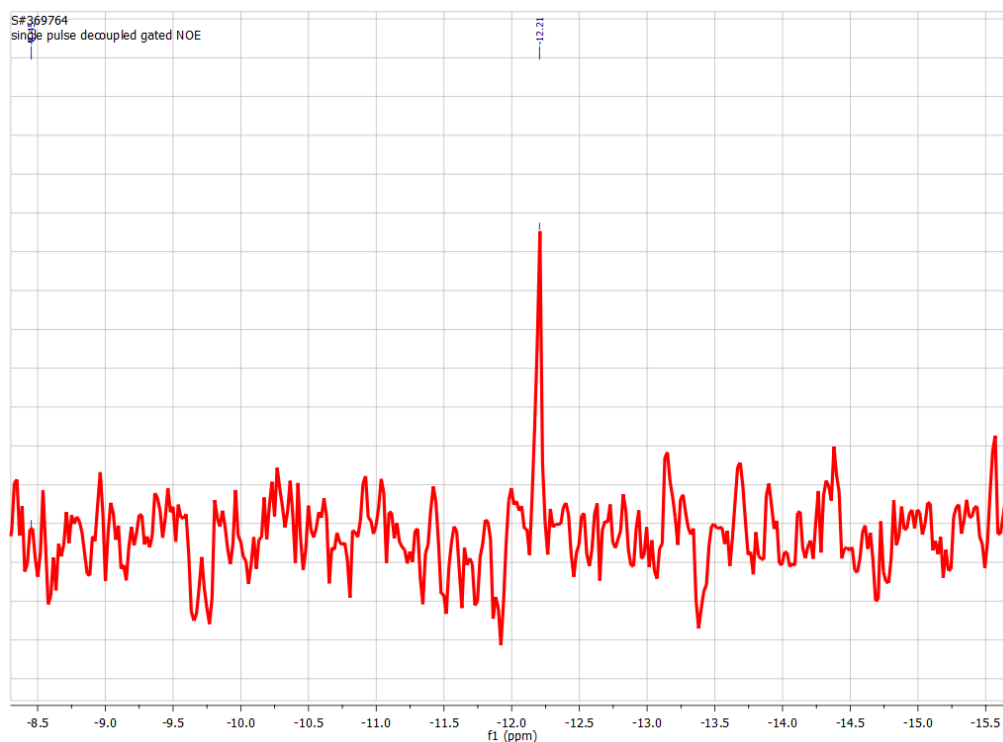


Figure A2.2: ²⁹Si NMR for ligand L¹.

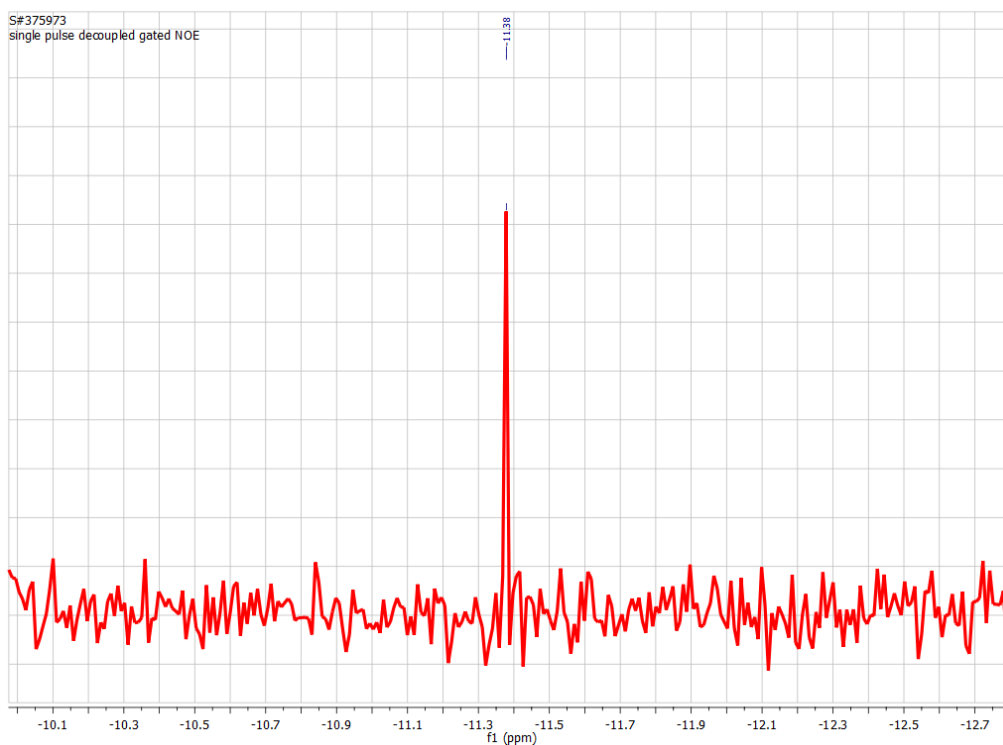


Figure A2.3: ²⁹Si NMR for ligand L².

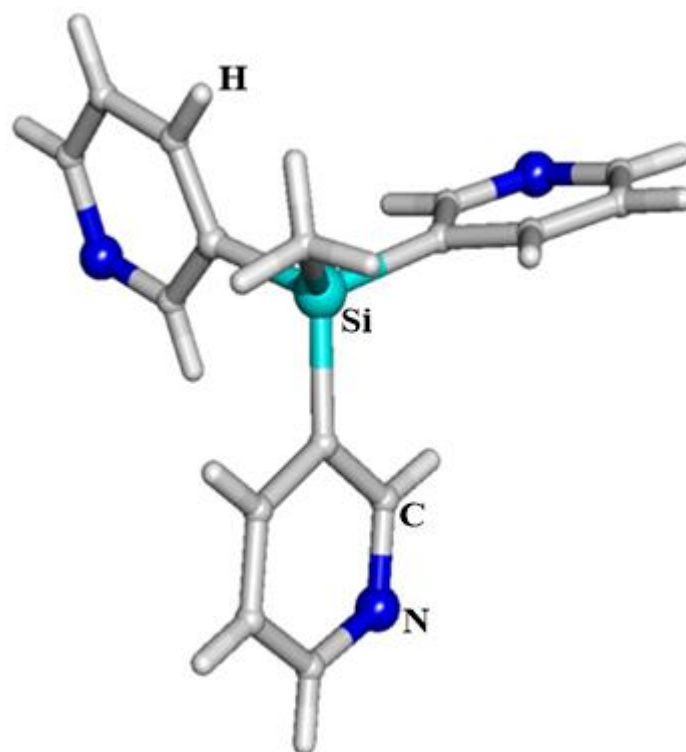


Figure A2.4: Crystal structure of L^1 .

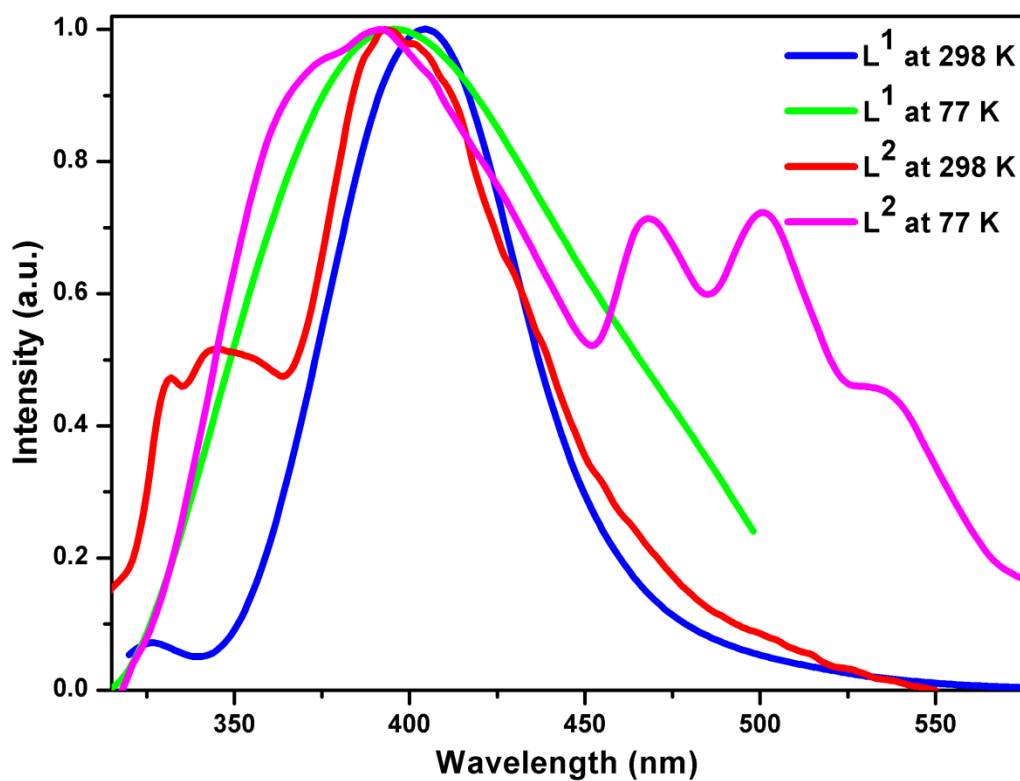


Figure A2.5: emission spectra of ligand L^1 and L^2 at 298 K (a) in blue for L^1 (b) in red for L^2 and at 77 K (c) in green for L^1 (d) in magenta for L^2 ($\lambda_{\text{exi}}=300$ nm).

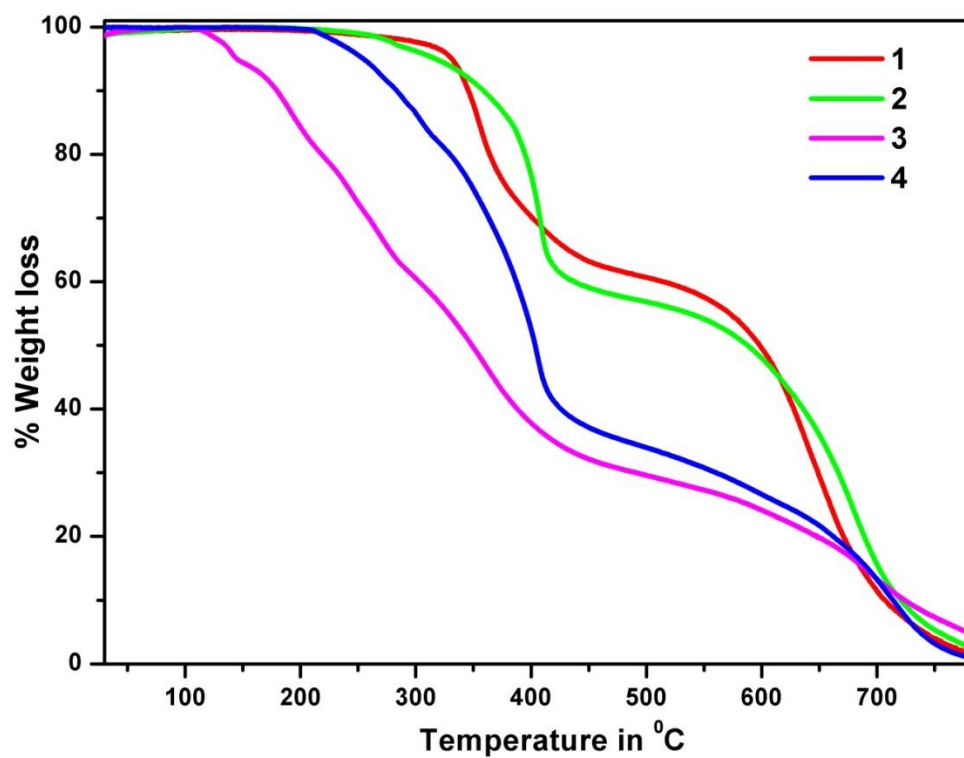


Figure A2.6: Thermogravimetric measurements of 1, 2, 3 and 4.

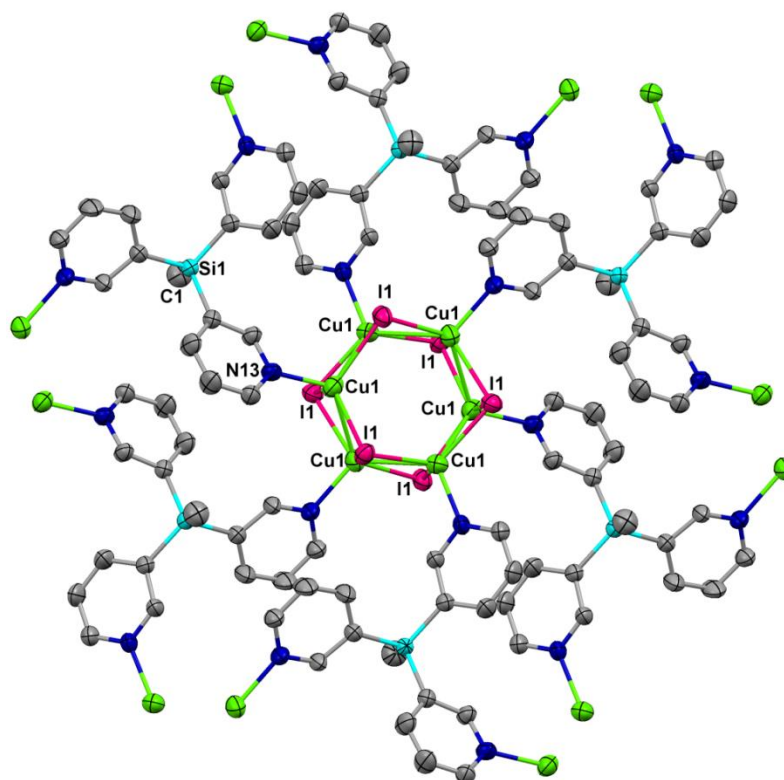


Figure A2.7: Ortep plot at 50% ellipsoid probabilities for 1 at 298 K

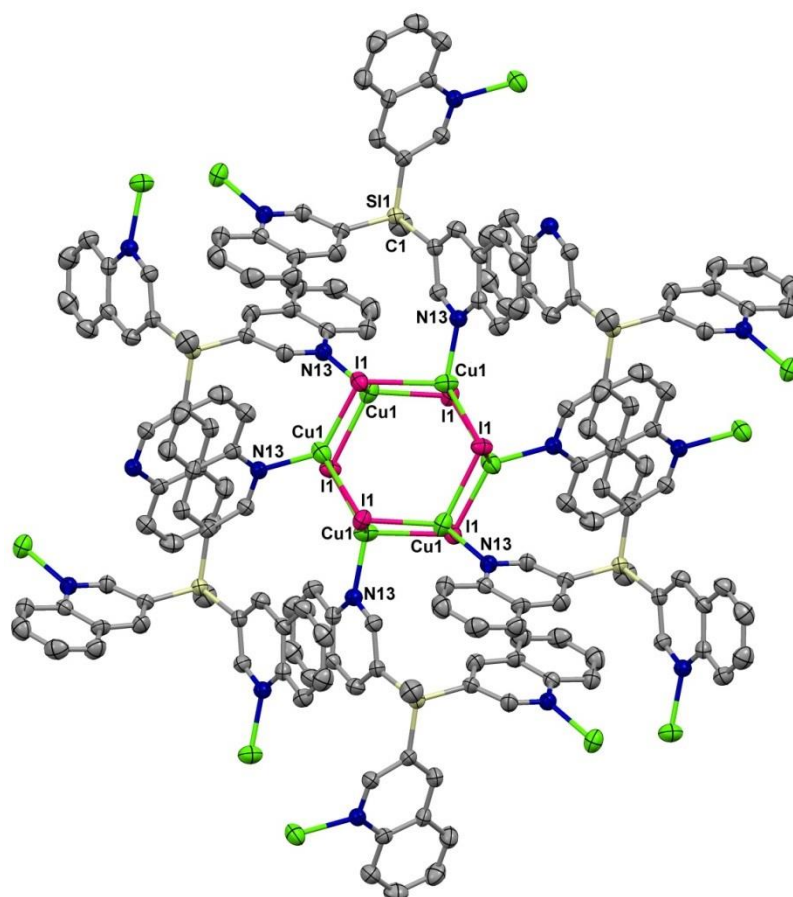


Figure A2.8: Ortep plot at 50% ellipsoid probabilities for **2** at 298 K

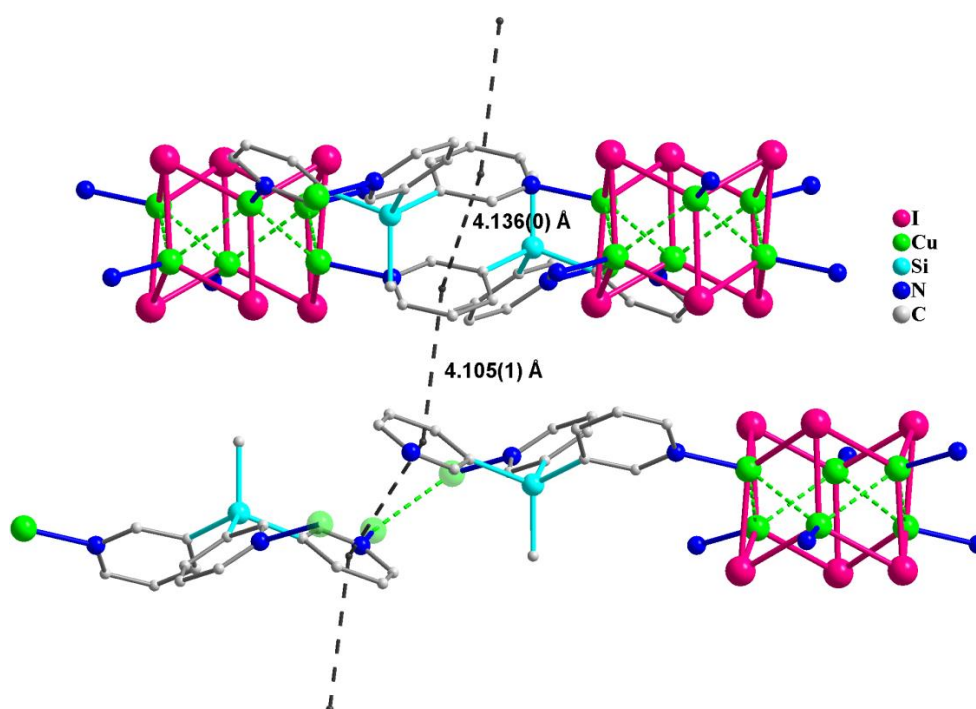


Figure A2.9: Inter- and intra-sheet π ... π interactions between the 3-Py moieties in **1**.

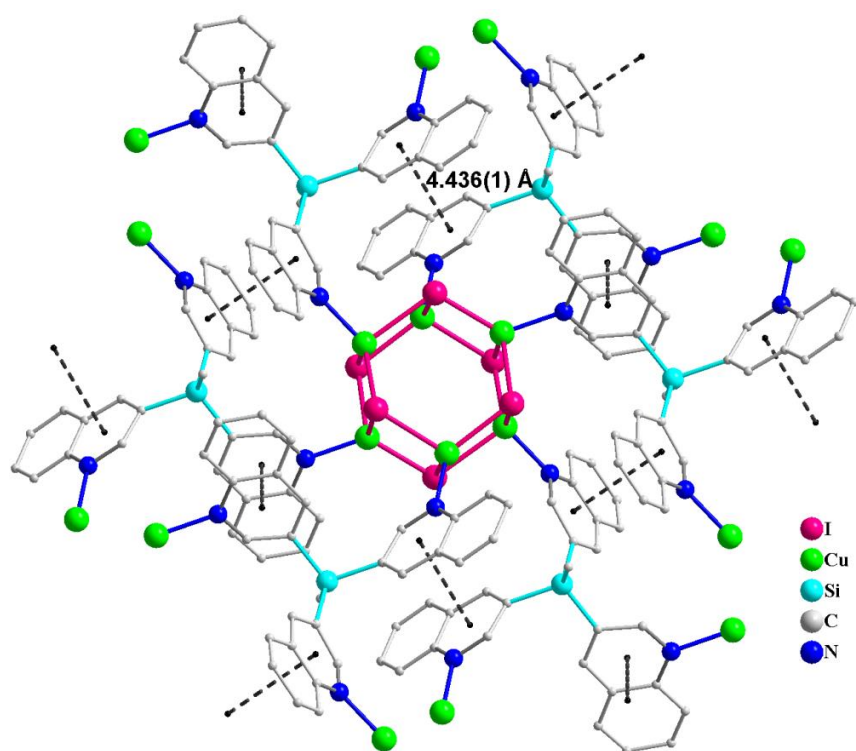


Figure A2.10: Intra-sheet $\pi\cdots\pi$ interactions between the 3-Qy moieties in **2**.

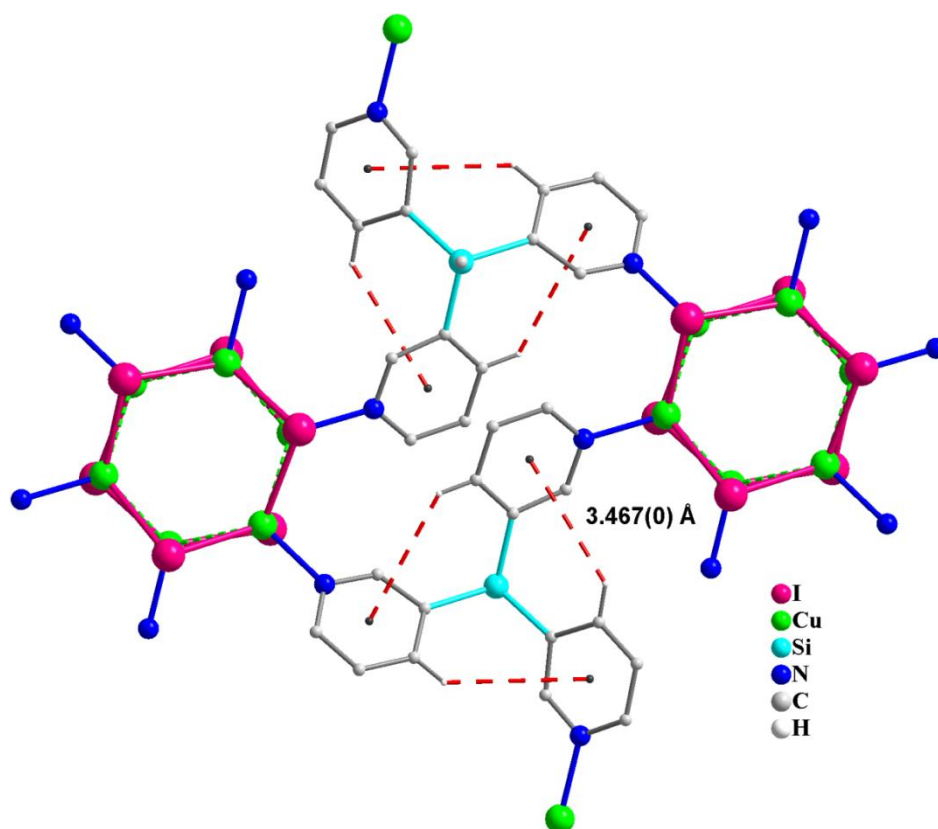


Figure A2.11: inra-sheet C-H $\cdots\pi$ interactions in **1**.

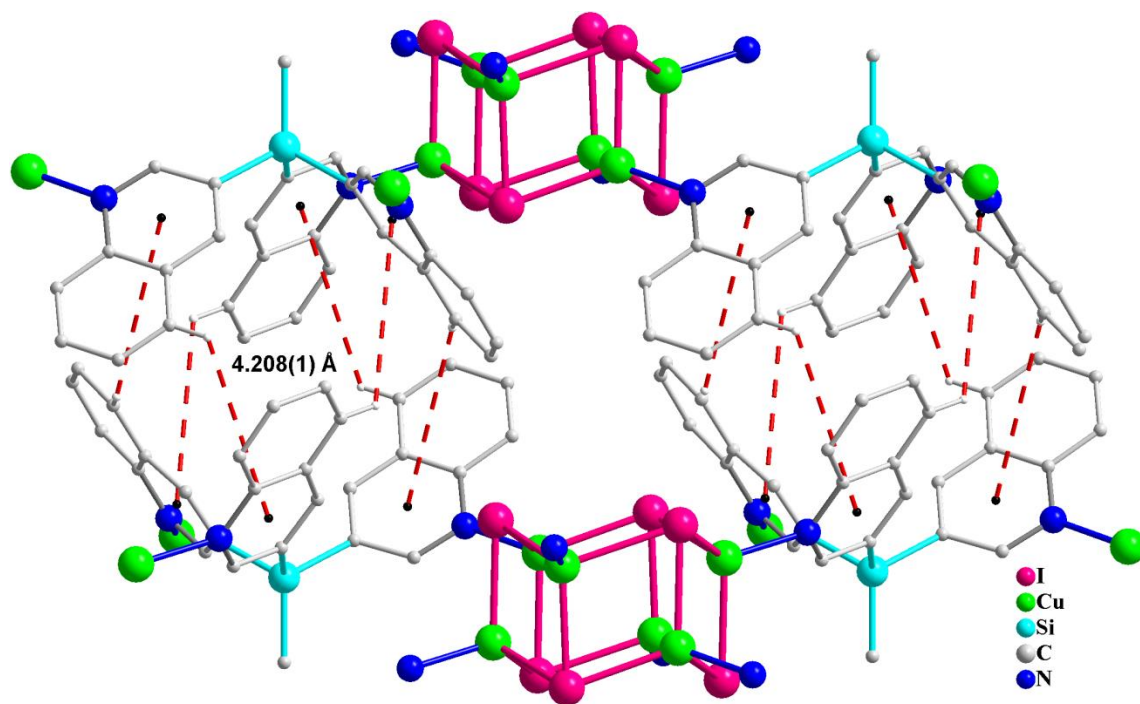


Figure A2.12: weak inter-sheet C-H... π interactions in **2**.

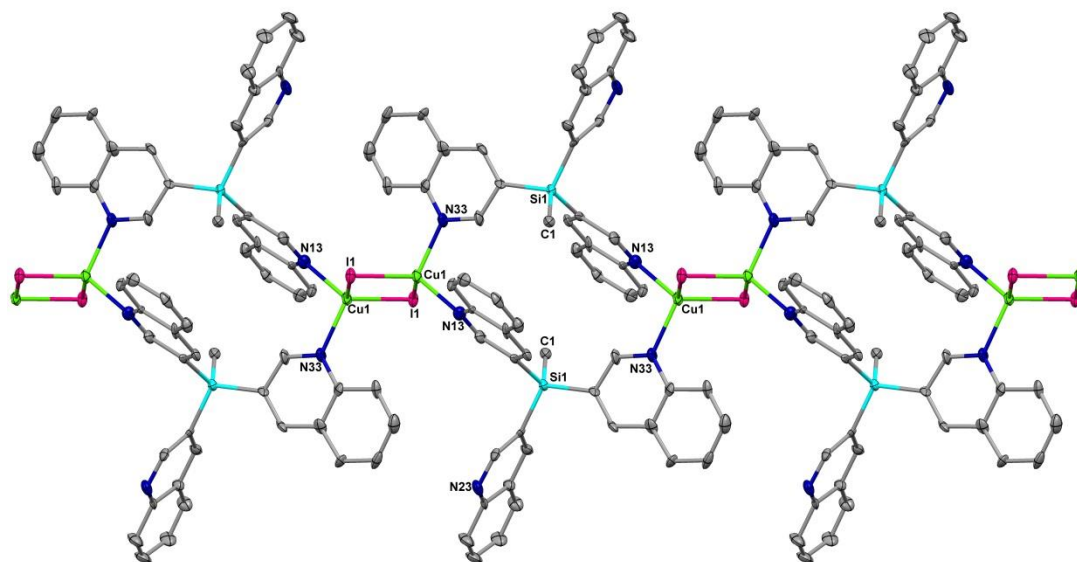


Figure A2.13 : Ortep plot at 50% ellipsoid probabilities for **3**. The coordination environment around the Cu(I) ion consists of two μ_2 -bridging Γ ion and two 3-Qy N-donor contacts. The repeating unit of the 1D-chain consists of a 16-membered Cu_2L_2 macrocycle which are formally bridged by the two Γ ions at the Cu(I) centers.

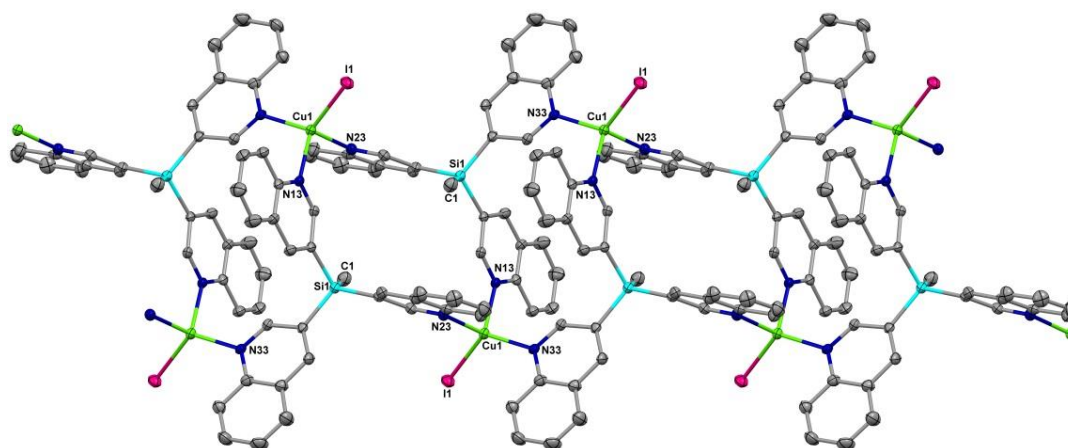


Figure A2.14: Ortep plot at 50% ellipsoid probabilities for **4**. The repeat unit of the 1D-polymer is a 16-membered Cu_2L_2 macrocycle which are connected to each other at Cu or Si atoms located at the corners. Unlike **3** where the adjacent macrocycles, connected by iodide ions, are aligned parallel to each other, the fused macrocycles in **4** are arranged nearly perpendicular with respect to each other. Owing to the densely packed nature of **4** no appreciable solvent accessible void space could be found in its crystal packing.

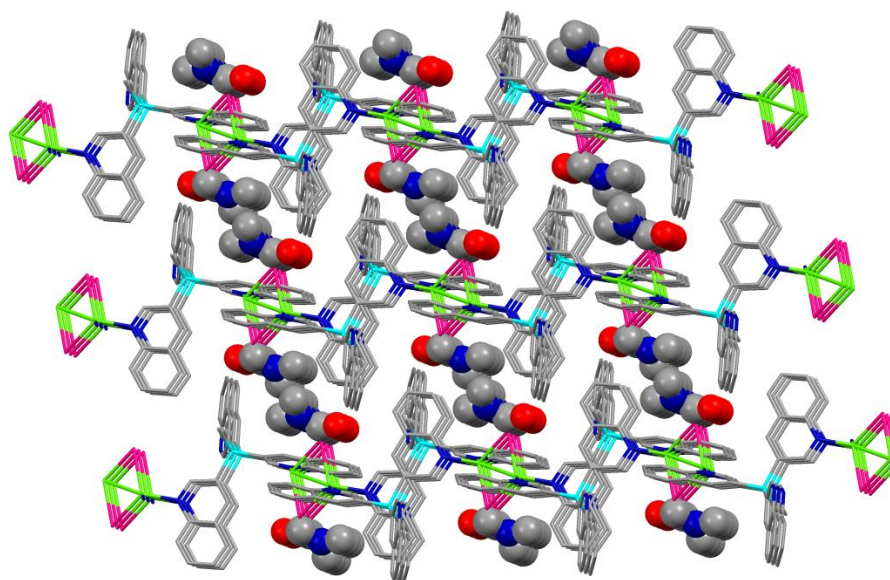


Figure A2.15: The packing diagram of the **3** shows the presence of a channel structure which consists of the solvated molecules of DMF.

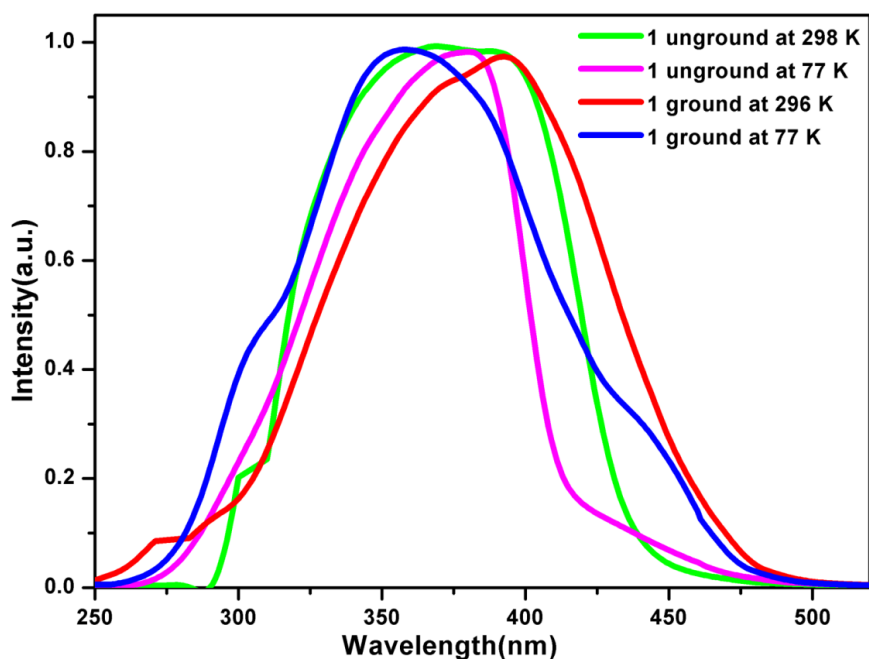


Figure A2.16: Solid state excitation spectrum for **1** in unground and ground state at 298 K and 77 K.

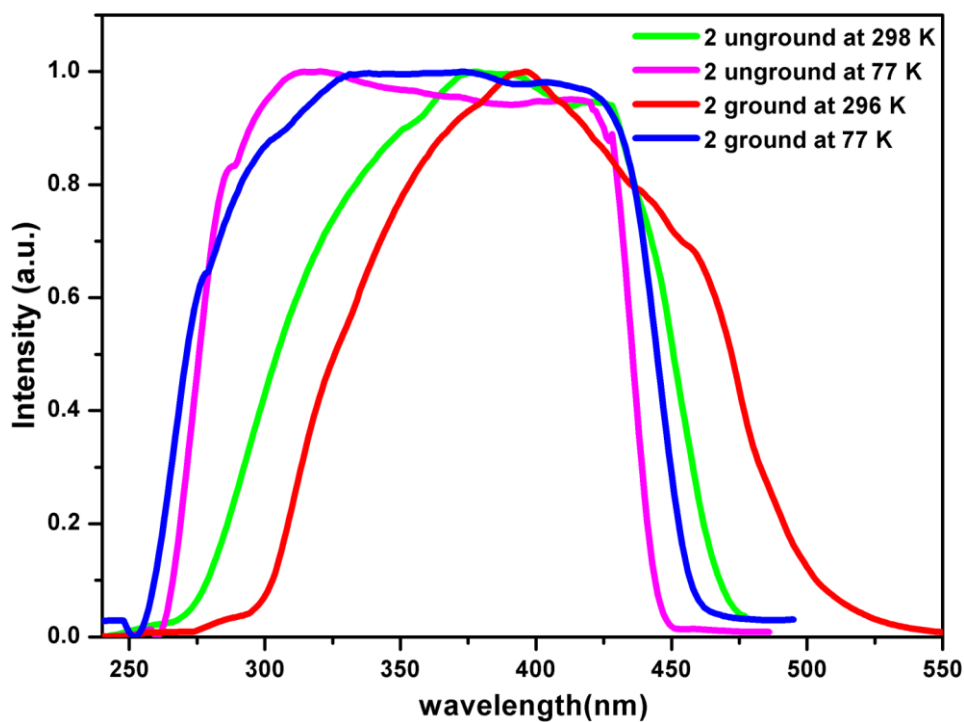


Figure A2.17: Solid state excitation spectra for **2** in unground and ground state at 298 K and 77 K.

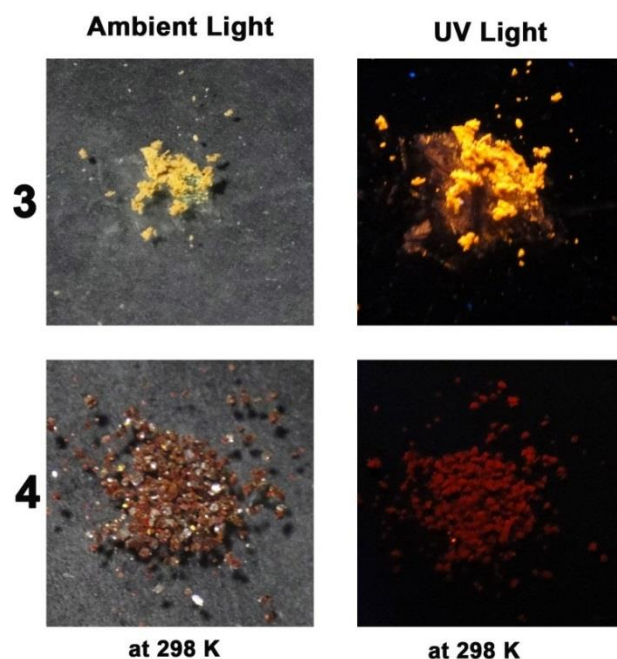


Figure A2.18: Solid State emission colors of various samples of **3** and **4** under ambient light and UV-lamp (irradiated at 365 nm)

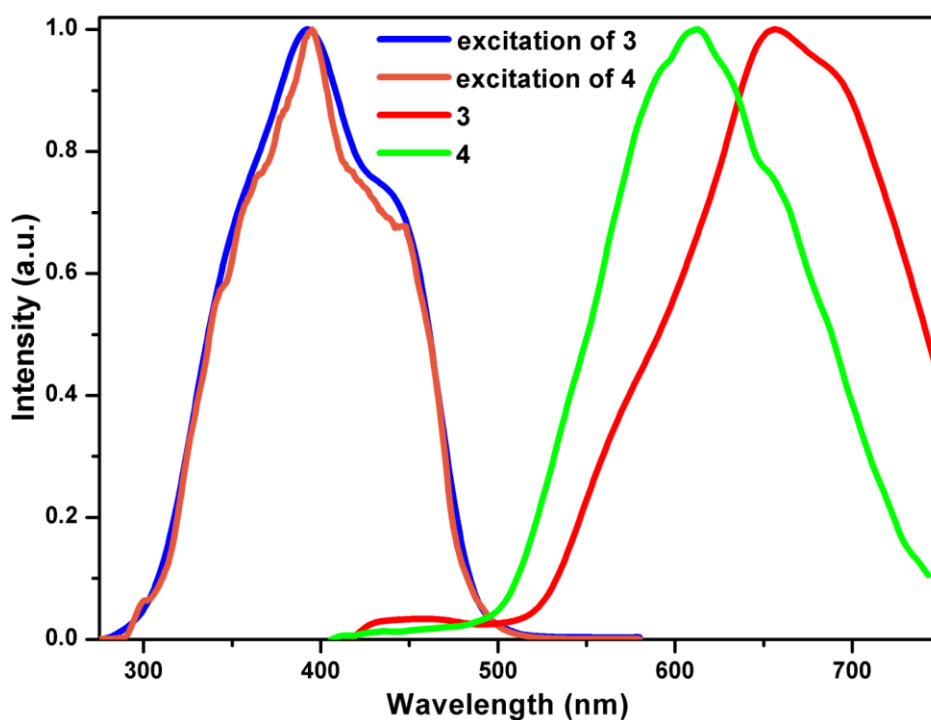


Figure A2.19: emission spectra for compounds **3** and **4** at 298 K (a) in blue and orange excitation spectra (b) in red emission spectra for compound **3** and (c) in green emission spectra for compound **4**

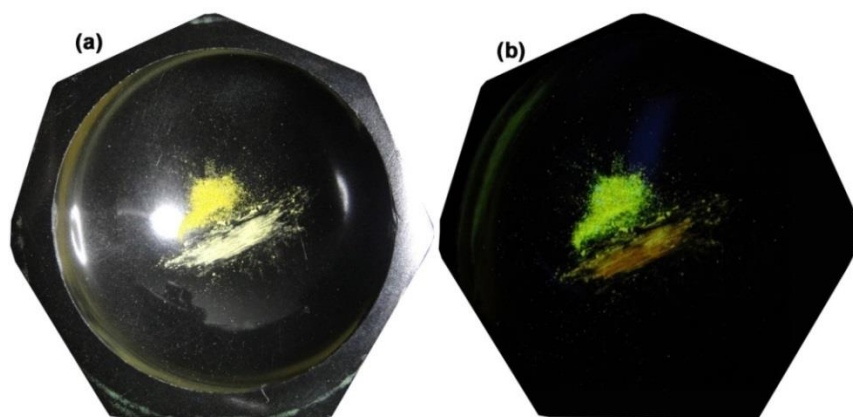


Figure A2.20: Photos of the ground (right) and intact (left) crystalline powder of **2** (a) under ambient light and (b) under UV irradiation at 365 nm (UV lamp) at room temperature.

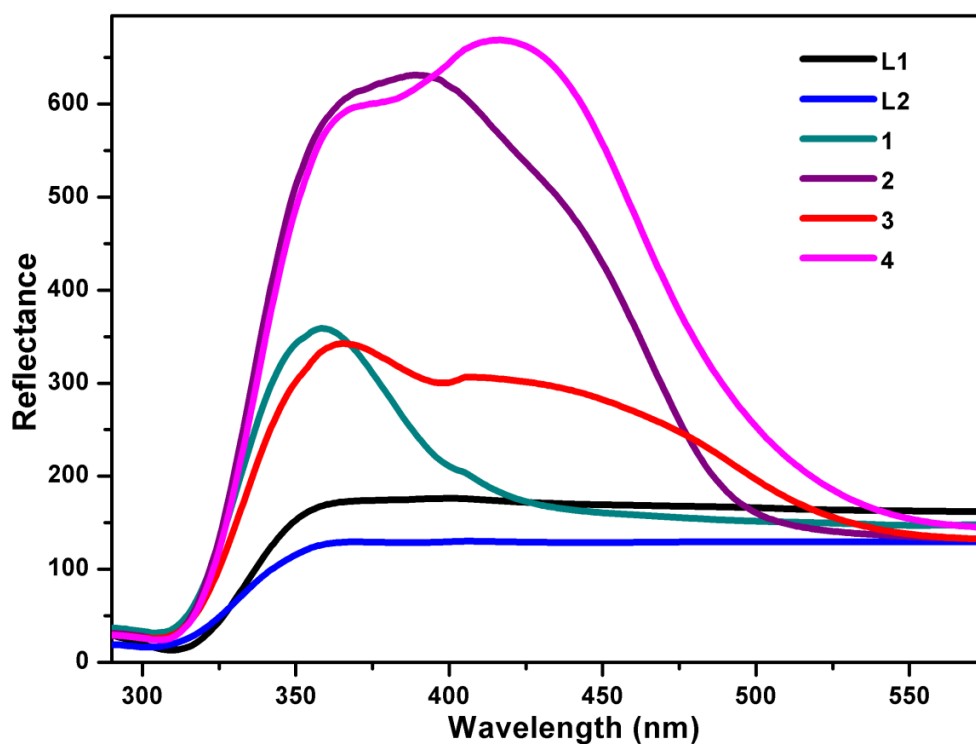


Figure A2.21: Solid state UV-visible spectrum for L¹, L², 1, 2, 3 and 4.

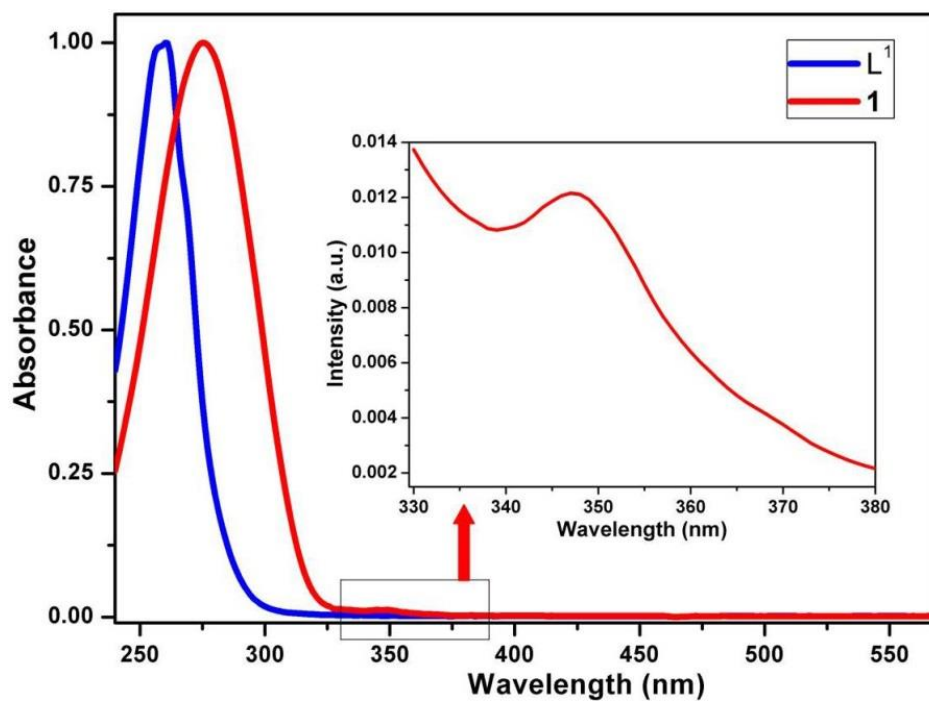


Figure A2.22: UV-visible spectrum of 1 in DCM suspension.

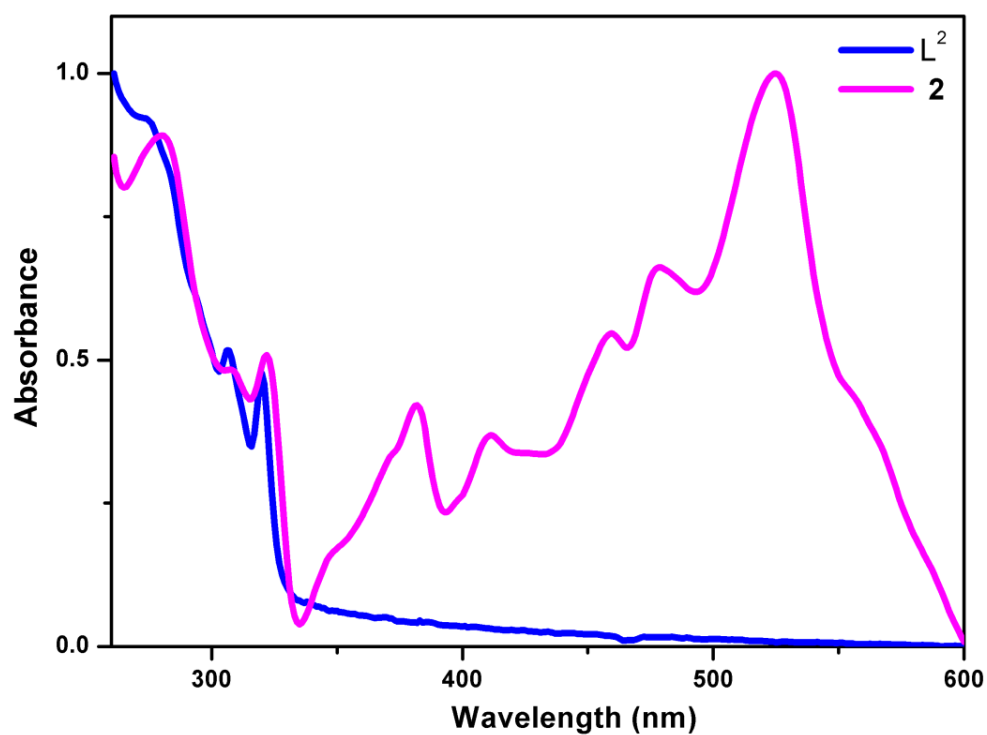


Figure A2.23: UV-visible spectrum of 2 in DCM suspension.

Table A2.2: Comparison of unit-Cell parameters for **1** and **2** in ground and unground states.

Compound	Unground (derived from single-crystal data)	Ground (derived from PXRD data)
1 (298 K) Space group: R-3c	a= 13.291(11) Å; $\alpha= 90^\circ$ b= 13.291(11) Å; $\beta= 90^\circ$ c= 41.790(4) Å; $\gamma= 120^\circ$ Volume = 6394.03 Å ³	a= 13.812 (2) Å; $\alpha= 90^\circ$ b= 13.812 (4) Å; $\beta= 90^\circ$ c= 43.627 (6) Å; $\gamma= 120^\circ$ Volume = 7207.58 Å ³
2 (298 K) Space group: R-3	a= 13.076(2) Å; $\alpha= 90^\circ$ b= 13.076(2) Å; $\beta= 90^\circ$ c= 30.416(5) Å; $\gamma= 120^\circ$ Volume = 4503.75 Å ³	a= 13.915(3) Å; $\alpha= 90^\circ$ b= 13.915(3) Å; $\beta= 90^\circ$ c= 30.697(7) Å; $\gamma= 120^\circ$ Volume = 5147.76 Å ³

Table A2.3: TDDFT computed transition wavelengths (λ), oscillator strengths (f), and major orbital contributions (%) for selected Singlet-Singlet Transitions in **1a**. (H and L denotes HOMO and LUMO)

λ (nm)	f	Orbitals involved (%)
395.30	0.0017	H-4->LUMO (16%), H-2->L+1 (44%)
393.44	0.0028	H-4->L+3 (12%), H-1->L+2 (33%)
392.20	0.0025	H-5->L+5 (20%), H-2->L+4 (10%), H-1->L+2 (11%), H-1->L+4 (12%)
388.29	0.004	H-2->L+2 (21%), H-1->L+4 (10%), HOMO->L+3 (52%)
387.01	0.0053	H-2->L+4 (25%), HOMO->L+5 (53%)
378.35	0.0059	H-3->L+1 (67%), H-2->L+1 (10%)
376.63	0.005	H-3->L+2 (69%)
375.17	0.0019	H-3->L+4 (69%)
352.62	0.0041	H-4->L+6 (21%), H-2->L+7 (41%)
351.71	0.015	H-5->LUMO (20%), H-4->L+8 (11%), H-1->L+7 (11%), H-1->L+10 (12%)
351.13	0.0012	H-5->LUMO (12%), H-1->L+7 (24%), HOMO->L+6 (31%)
350.52	0.0177	H-4->L+3 (12%), H-1->L+10 (23%), HOMO->L+6 (10%)
350.13	0.0139	H-5->L+3 (22%), H-4->LUMO (10%), HOMO->L+6 (13%)
349.66	0.0012	H-5->L+9 (15%), H-2->L+10 (21%), H-1->L+11 (10%)
348.90	0.0047	H-7->LUMO (10%), H-5->L+3 (24%), H-4->L+5 (36%)
348.87	0.001	H-7->LUMO (27%), H-6->LUMO (19%), H-4->L+5 (17%)
348.44	0.0174	H-1->L+11 (12%), HOMO->L+8 (47%)
347.74	0.0128	H-2->L+11 (12%), HOMO->L+9 (43%)

347.66	0.0098	H-7->LUMO (18%), H-6->LUMO (23%), HOMO->L+9 (12%)
--------	--------	--

Table A2.4. TDDFT computed transition wavelengths (λ), oscillator strengths (f), and major orbital contributions (%) for selected Singlet-Singlet Transitions of **2a**. (H and L denote HOMO and LUMO).

λ (nm)	f	Orbitals involved (%)
498.00	0.0029	H-1->L+1 (11%), HOMO->L+1 (65%)
492.32	0.0019	H-1->LUMO (38%), HOMO->LUMO (32%)
490.24	0.0019	H-4->L+3 (23%), HOMO->L+3 (65%)
488.98	0.0013	H-4->L+5 (16%), HOMO->L+5 (68%)
484.85	0.0035	H-3->LUMO (15%), H-2->LUMO (10%), H-1->LUMO (35%), HOMO->LUMO (27%)
479.31	0.0024	H-1->L+2 (63%)
478.51	0.0014	H-2->L+4 (19%), H-1->L+4 (44%), HOMO->L+4 (20%)
474.74	0.0023	H-3->L+3 (12%), H-2->L+3 (19%), H-1->L+3 (57%)
471.16	0.0051	H-6->L+1 (10%), H-5->L+1 (12%), H-3->L+1 (22%), H-2->L+1 (47%)
465.66	0.0065	H-5->L+4 (11%), H-4->L+4 (11%), H-2->L+4 (55%)
435.42	0.0065	H-5->L+4 (16%), H-4->L+4 (32%), H-1->L+4 (21%)
434.40	0.0031	H-5->L+2 (12%), H-4->L+2 (66%)
432.73	0.003	H-6->L+1 (18%), H-5->L+1 (57%)
427.69	0.0049	H-5->L+4 (15%), H-5->L+5 (55%), H-4->L+4 (11%)
427.35	0.005	H-6->L+4 (15%), H-5->L+4 (21%), H-5->L+5 (28%), H-4->L+4 (25%)
426.05	0.0038	H-5->L+3 (70%)
425.47	0.0016	H-6->L+2 (53%), H-5->L+2 (16%)

Table A2.5: Optimized Geometrical parameters for the Optimized DFT Structures of **1a** in the S_0 , T_1 , and T_2 states, Compared to the X-ray Structural Data

Parameters	Experimental	S_0	T_2
Cu—Cu Å	2.745(1)	2.939-2.978 (2.958)	2.919-3.609 (3.133)
Cu-I Å	2.587(2)- 2.696(1) (2.648)	2.754-2.826 (2.791)	2.715-2.847 (2.788)
Cu-N Å	2.0639(2)	2.125-2.126 (2.125)	1.916-2.116 (2.074)
I—I Å	4.525(1)	4.239-4.723 (4.631)	4.251-4.756 (4.596)

Table A2.6: Optimized Geometrical parameters for the Optimized DFT Structures of **2a** in the S_0 , and T_2 states, Compared to the X-ray Structural Data

Parameters	Experimental	S_0	T_2
Cu—Cu Å	3.148(0)	3.132-3.304 (3.248)	3.008-3.766 (3.390)
Cu—I Å	2.58(1)-2.757(0) (2.673)	2.740-2.875 (2.961)	2.725-2.881 (2.797)
Cu-N Å Å	2.062(1)	2.127-2.137 (2.133)	1.970-2.110 (2.080)
I—I Å	4.325(0)	4.502-4.608 (4.547)	4.095-4.686 (4.409)

Table A3.1: Selected bond-lengths (Å) and angles (°) for 5, 6, 7, 8 and 9.

Compound	Bond length		Bond angle	
5	Si(1)-O(1)	1.640(13)	O(1)-Si(1)-O(2)	106.4(6)
	Si(1)-O(2)	1.656(12)	C(16)-N(15)-Zn(1)	120.4(12)
	N(15)-Zn(1)	2.021(12)	C(14)-N(15)-Zn(1)	122.5(12)
	Si(2)-O(1)	1.607(13)	O(1)-Si(2)-O(2)#1	109.2(6)
	Si(2)-O(2)#1	1.630(13)	Si(2)-O(1)-Si(1)	146.5(7)
	N(25)-Zn(1)#2	2.061(13)	Si(2)#1-O(2)-Si(1)	143.4(10)
	Si(2')-O(1)	1.58(3)	N(15)-Zn(1)-N(25)#3	99.2(5)
	Si(1')-O(1)	1.67(3)	N(15)-Zn(1)-I(2)	126.1(8)
	Si(1')-O(2)	1.84(3)	N(15)-Zn(1)-I(1'')	109.6(5)
	O(2)-Si(2)#1	1.630(13)	N(15)-Zn(1)-I(1')	107.5(5)
	Zn(1)-N(25)#3	2.060(13)	N(15)-Zn(1)-I(2')	105.4(6)
	Zn(1)-I(2)	2.324(10)	N(25)#3-Zn(1)-I(2')	109.2(6)
	Zn(1)-I(1'')	2.403(14)	I(1')-Zn(1)-I(2')	123.6(8)
	Zn(1)-I(2')	2.62(2)	N(15)-Zn(1)-I(2'')	104.3(6)
	Zn(1)-I(1)	2.89(2)	N(25)#3-Zn(1)-I(2'')	106.8(5)
			I(1'')-Zn(1)-I(2'')	123.5(3)
			N(15)-Zn(1)-I(1)	107.0(6)
		N(25)#3-Zn(1)-I(1)	100.2(7)	
		I(2)-Zn(1)-I(1)	116.0(5)	
6	Ag(1)-N(15)	1.914(19)	N(15)-Ag(1)-N(35)#1	166.1(8)
	Ag(1)-Ag(1)#1	3.112(6)	N(15)-Ag(1)-Ag(1)#1	92.6(6)
	Ag(1')-N(15)	2.397(19)	N(35)#1-Ag(1')-N(15)	156.3(8)
	Ag(1')-Ag(1')#1	3.362(7)	N(45)#2-Ag(2)-N(25)	171.7(5)
	Ag(2)-N(25)	2.121(15)	C(16)-N(15)-Ag(1)	121.1(17)
	Si(1)-O(4)	1.615(12)	C(14)-N(15)-Ag(1)	123.5(15)
	Si(1)-O(1)	1.622(13)	C(24)-N(25)-Ag(2)	120.1(12)
	Si(1)-C(1)	1.81(2)	C(26)-N(25)-Ag(2)	123.4(13)
	Si(2)-O(2)	1.578(12)	C(36)-N(35)-Ag(1')#1	119.7(17)
	Si(2)-O(1)	1.609(12)	C(34)-N(35)-Ag(1')#1	128.6(15)
	Si(2)-C(21)	1.858(15)	C(36)-N(35)-Ag(1)#1	138.1(17)
	Si(3)-O(3)	1.580(14)	C(34)-N(35)-Ag(1)#1	110.2(14)
	Si(3)-C(3)	1.84(2)	C(46)-N(45)-Ag(2)#2	121.1(11)
	Si(4)-O(4)	1.627(14)	C(44)-N(45)-Ag(2)#2	121.4(11)

7	Cu(1)-N(15)	2.08(2)	N(15)-Cu(1)-Cu(2)#1	136.3(8)
	Cu(1)-Cu(1)#1	2.673(11)	Cu(1)#1-Cu(1)-Cu(2)#1	61.5(2)
	Cu(1)-I(1)	2.703(7)	N(15)-Cu(1)-I(1)	110.5(8)
	Cu(1)-Cu(2)	2.736(8)	Cu(1)#1-Cu(1)-I(1)	63.5(2)
	Cu(1)-I(1)#1	2.831(9)	I(1)-Cu(1)-Cu(2)	61.3(2)
	Cu(2)-Cu(1)#1	2.682(9)	N(15)-Cu(1)-I(2)	105.5(8)
	Cu(2)-Cu(2)#1	2.690(12)	Cu(1)#1-Cu(1)-I(2)	110.43(12)
	Cu(2)-I(2)	2.726(7)	I(1)-Cu(1)-I(2)	109.7(2)
	Cu(2)-I(1)	2.772(8)	Cu(1)#1-Cu(1)-I(1)#1	58.7(3)
	I(1)-Cu(1)#1	2.831(9)	Cu(2)#1-Cu(1)-I(1)#1	60.3(2)
	I(2)-Cu(2)#1	2.771(8)	I(1)-Cu(1)-I(1)#1	115.1(2)
	Si(1)-O(4)	1.58(6)	Cu(2)-Cu(1)-I(1)#1	107.6(2)
			I(2)-Cu(1)-I(1)#1	115.9(2)
			N(25)#2-Cu(2)-I(2)	111(6)
		Cu(2)#1-Cu(2)-I(2)	61.5(2)	
8	Cd(01)-N(013)	231(2)	N(013)-Cd(01)-N(21)#1	87.4(10)
	Cd(01)-N(21)#1	233(3)	N(013)-Cd(01)-N(01D)#2	176.2(9)
	Cd(01)-O(00E)	248(2)	N(21)#1-Cd(01)-O(00E)	84.5(10)
	Cd(01)-O(01C)	249(3)	N(01D)#2-Cd(01)-O(00E)	88.5(8)
	Cd(02)-N(01A)	242(3)	O(00E)-Cd(01)-O(01C)	153.7(10)
	Cd(02)-O(00S)	244(2)	N(20)-Cd(02)-N(3)#3	90.1(11)
	Si(03)-O(00I)	162(3)	N(20)-Cd(02)-O(00S)	89.1(10)
	Si(03)-C(021)	187(4)	N(3)#3-Cd(02)-O(00S)	74.3(9)
	Si(04)-O(00C)	164(3)	N(00Y)#4-Cd(02)-O(00S)	96.2(10)
	N(20)-C(30)	131(4)	N(01A)-Cd(02)-O(00S)	123.8(10)
	N(21)-C(035)	134(4)	N(20)-Cd(02)-O(00O)	89.9(11)
			N(3)#3-Cd(02)-O(00O)	74.3(8)

9	Cd(1)-O(5B)	228.1(8)	O(5B)-Cd(1)-N(15)	87.5(4)
	Cd(1)-N(15)	229.5(14)	N(15)-Cd(1)-N(35)#1	176.0(4)
	Cd(1)-C(15B)	273.0(12)	O(5B)-Cd(1)-O(2B)	141.1(3)
	Cd(2)-O(8B)	225.0(9)	N(15)-Cd(1)-O(2B)	89.1(4)
	Cd(2)-O(7B)	258.0(9)	O(1B)#1-Cd(1)-O(6B)	142.0(3)
	Cd(2)-C(28B)	272.9(12)	O(5B)-Cd(1)-C(15B)	27.4(4)
	Si(1)-O(1)	160.1(14)	N(15)-Cd(1)-C(15B)	84.3(4)
	Si(1)-C(1)	178(2)	O(2B)-Cd(1)-C(15B)	113.7(4)
	Si(2)-O(2)	158.7(12)	O(8B)-Cd(2)-N(25)	91.5(4)
	Si(2)-C(21)	180(2)	N(25)-Cd(2)-C(14B)#3	91.9(4)
	Si(3)-O(3)	162.9(12)	O(4B)#3-Cd(2)-C(14B)#3	27.7(3)
	C(11)-C(12)	148(3)	O(1)-Si(1)-O(4)	106.7(7)
			O(1)-Si(1)-C(1)	109.9(10)
			O(4)-Si(1)-C(1)	105.0(9)
		O(2)-Si(2)-O(1)	106.4(7)	
		O(2)-Si(2)-C(21)	115.3(9)	
		O(1)-Si(2)-C(2)	105.3(9)	
		C(21)-Si(2)-C(2)	114.5(11)	

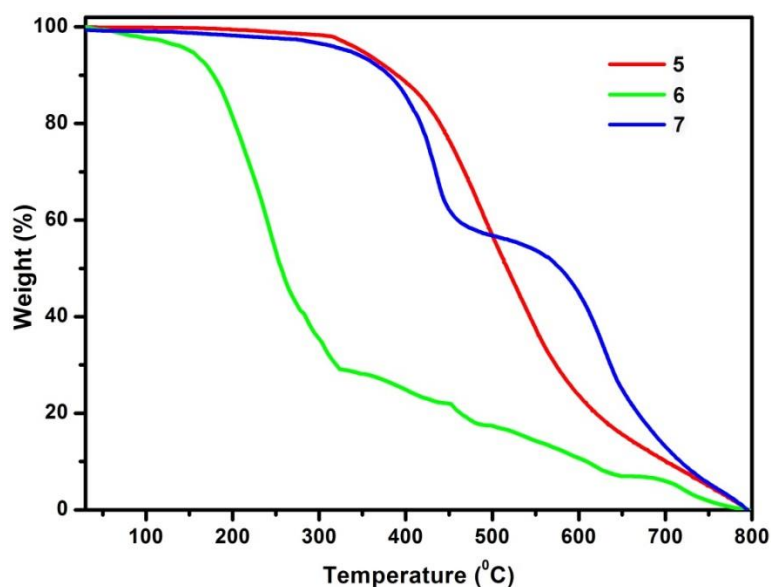
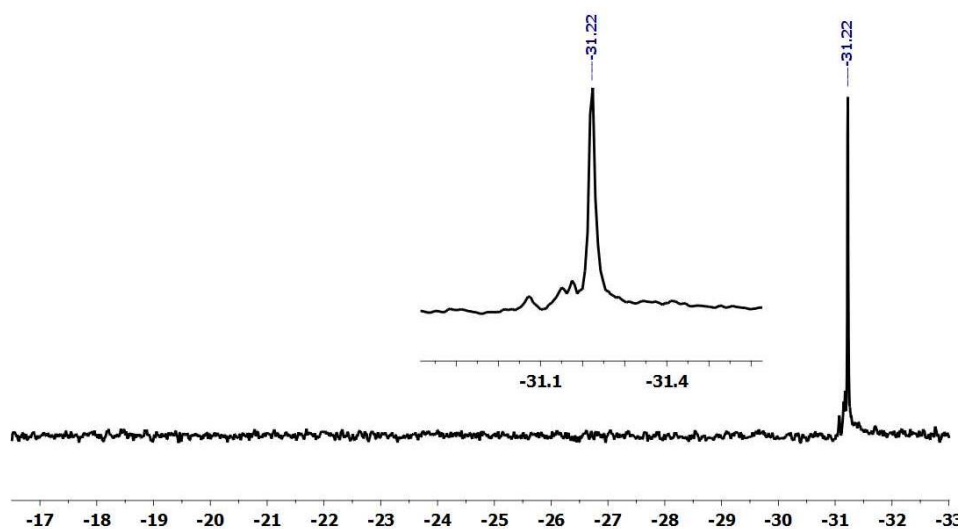
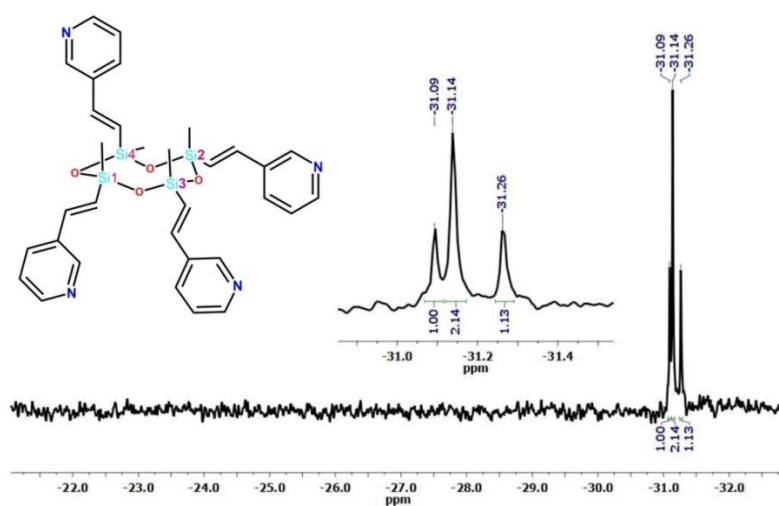
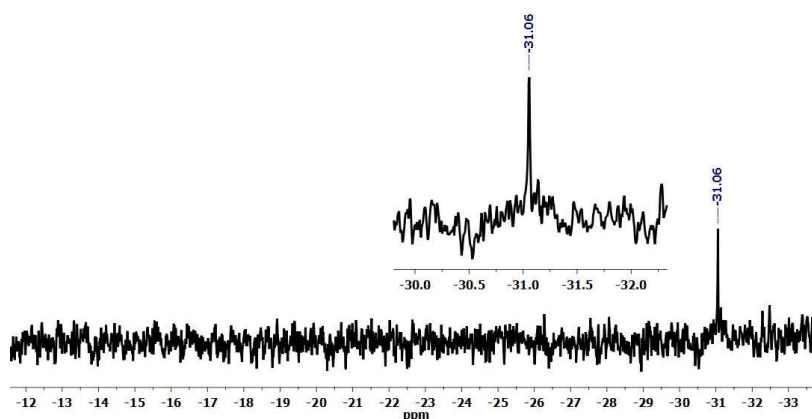


Figure A3.1. TGA profiles of **5**, **6** and **7**; (a) compound **5** and **7** are stable up to 350 °C (b) compound **6** showing loss of 5% weight up to 110 °C

Figure A3.2: ^{29}Si NMR for ligand $\text{L}^{3\text{A}}$ Figure A3.3: ^{29}Si NMR for ligand $\text{L}^{3\text{B}}$ Figure A3.4: ^{29}Si NMR for ligand $\text{L}^{3\text{C}}$

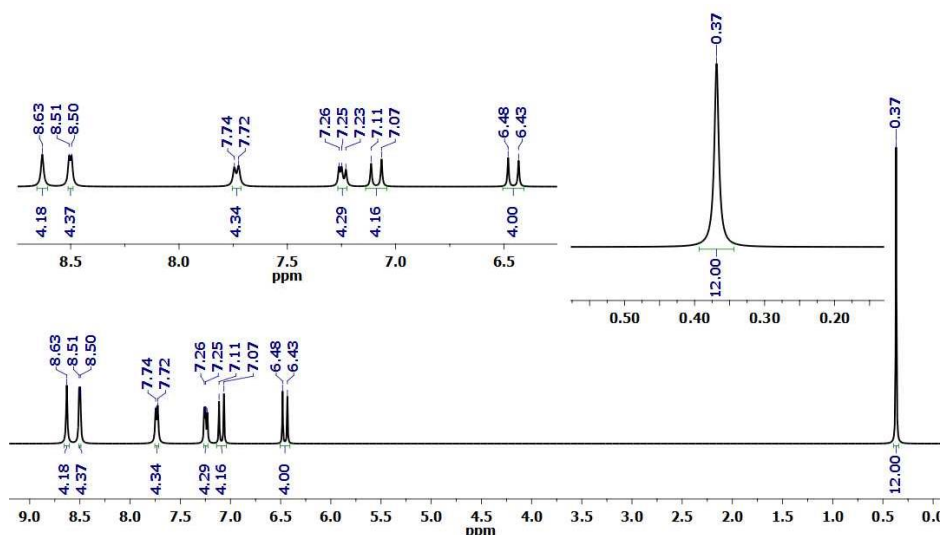


Figure A3.5: ^1H NMR for ligand $\text{L}^{3\text{A}}$ in that shown the expansion of methyl, vinylic and pyridyl region. The methyl proton gives singlet at 0.37 ppm while the signals due to all the four vinyl moieties and pyridyl groups were also found to be equivalent. The vinyl groups gave two doublets at 6.46 and 7.09 ppm; the pyridyl groups gave one doublet of doublet, two doublets and one singlet centred at 7.24, 7.73, 8.53 and 8.63 ppm respectively.

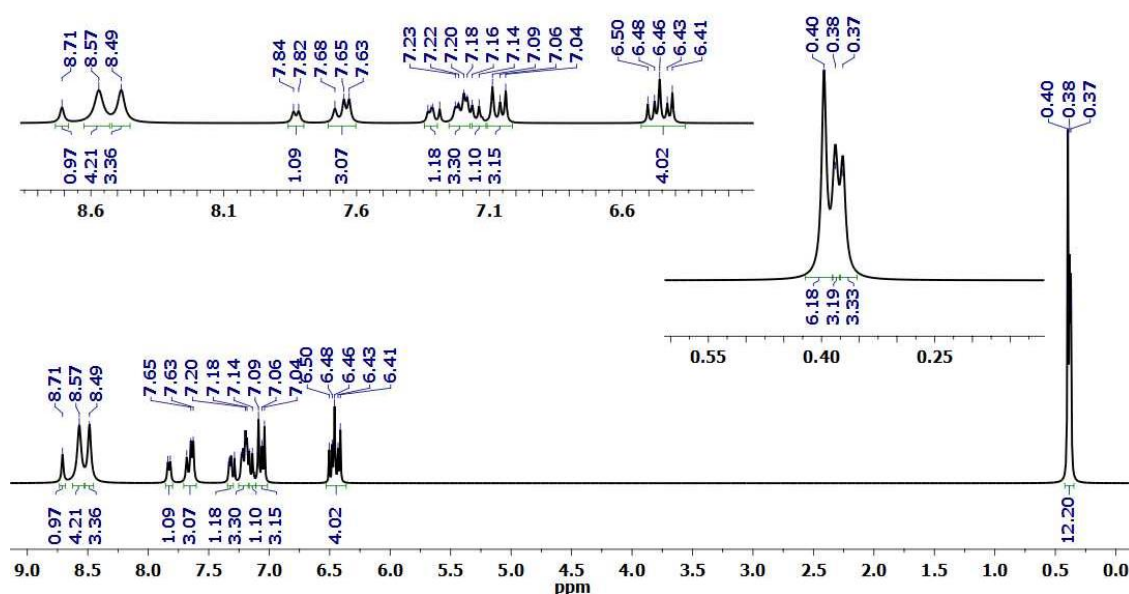


Figure A3.6: ^1H NMR for ligand $\text{L}^{3\text{B}}$ in that shown the expansion of Methyl, vinylic and pyridyl region. The methyl proton gave three singlet in the 3:1:1 ratio at 0.40, 0.38 and 0.37 respectively. The Vinyl protons in $\text{L}^{1\text{B}}$ gave a set of two doublets in the 1:3 ratios at 6.46 and 7.09. Similarly, the pyridyl groups, owing to their two unique conformations, display two sets of four chemical shift values in 3:1 ratio in the range between 7.21-8.72 ppm

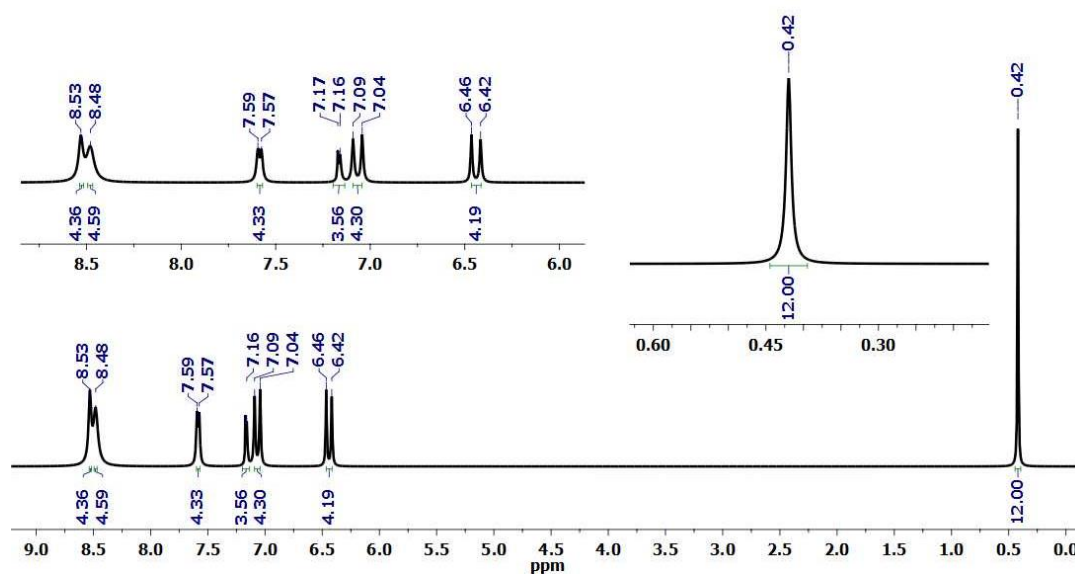


Figure A3.7: ^1H NMR for ligand $\text{L}^{3\text{C}}$ in that shown the expansion of methyl, vinylic and pyridyl region. The methyl groups gave a single resonance at 0.42 ppm. As the $\text{L}^{1\text{A}}$ similar trend has been observed for both vinyl and pyridyl protons as well

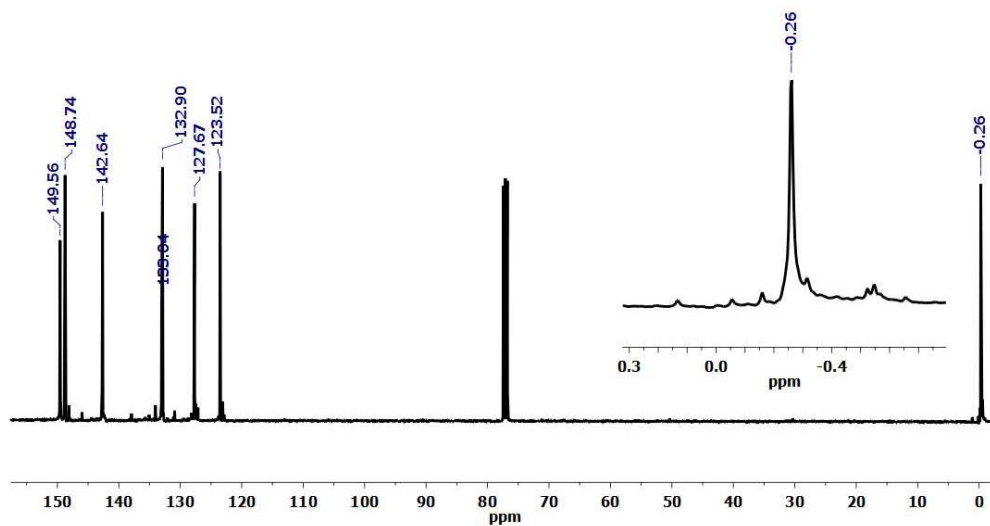
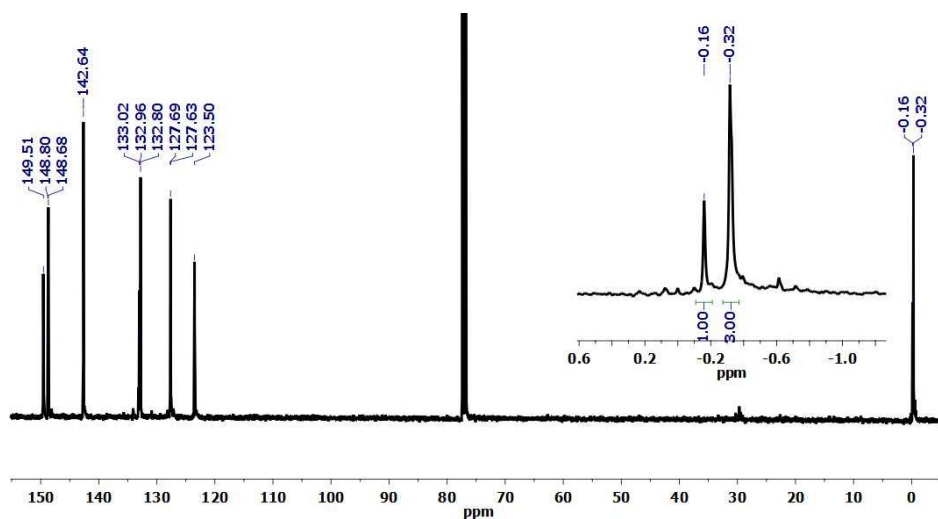
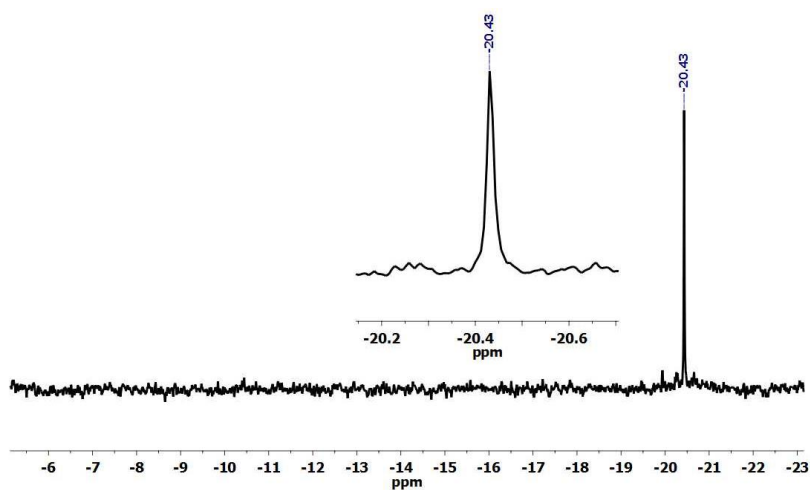
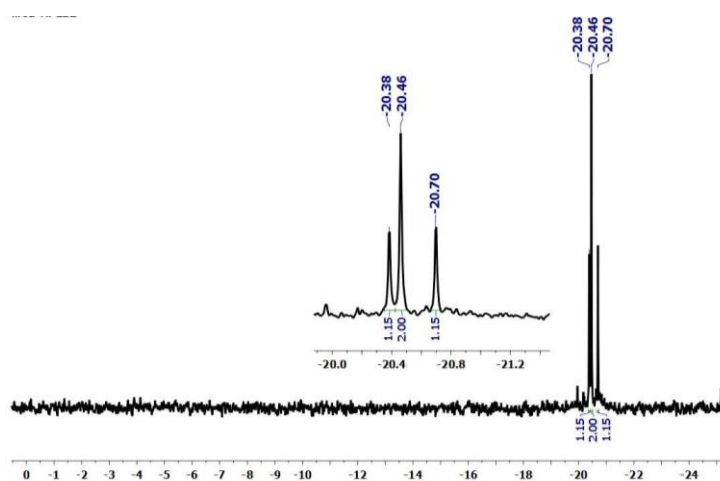


Figure A3.8: ^{13}C NMR for ligand $\text{L}^{1\text{A}}$

Figure A3.9: ^{13}C NMR for ligand $\text{L}^{3\text{B}}$.Figure A3.10. ^{29}Si NMR for ligand $\text{L}^{2\text{A}}$.Figure A3.11: ^{29}Si NMR for ligand $\text{L}^{4\text{B}}$

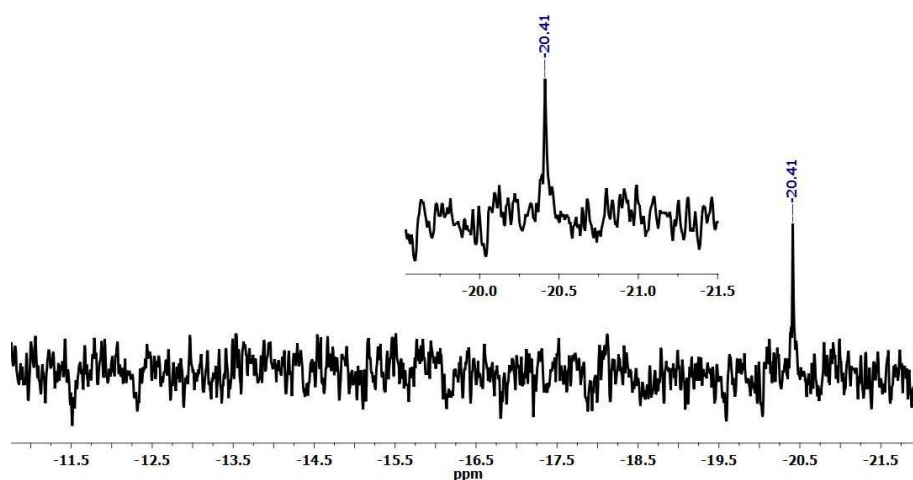


Figure A3.12: ^{29}Si NMR for ligand $\text{L}^{4\text{C}}$.

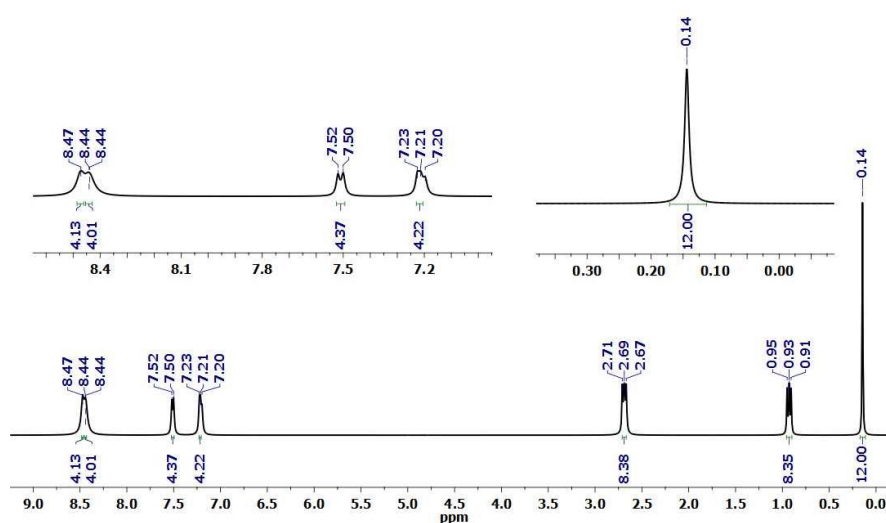


Figure A3.13: ^1H NMR for ligand $\text{L}^{4\text{A}}$ in that shown the expansion of the Methyl, ethyl and pyridyl. The methyl protons attached to the Si-atoms gave a single resonance at 0.14. The signals due to ethyl moieties give the triplet and the pyridyl groups were also found to be equivalent.

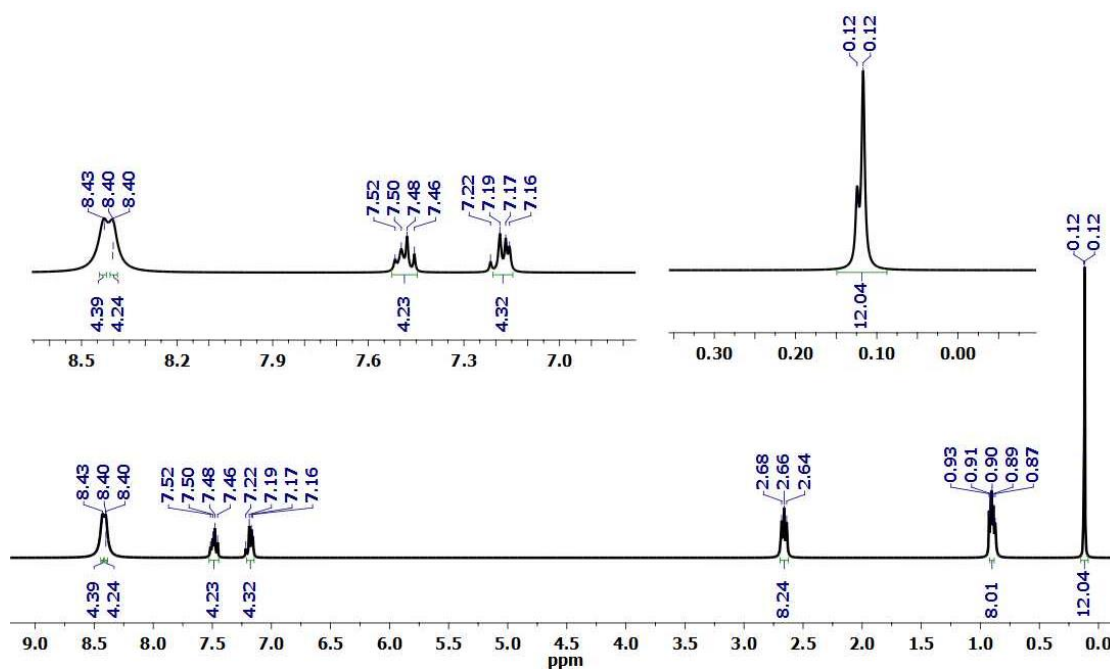


Figure A3.14: ^1H NMR for ligand $\text{L}^{4\text{B}}$ in that shown the expansion of the Methyl, ethyl and pyridyl. The methyl protons attached to the Si-atoms gave two overlapping peaks at 0.12 ppm. The signals due to ethyl proton near to silicon atom gives the multiple at 0.9 ppm while the second ethyl proton gives triplet at 2.66 ppm and the pyridyl groups were also found to be equivalent.

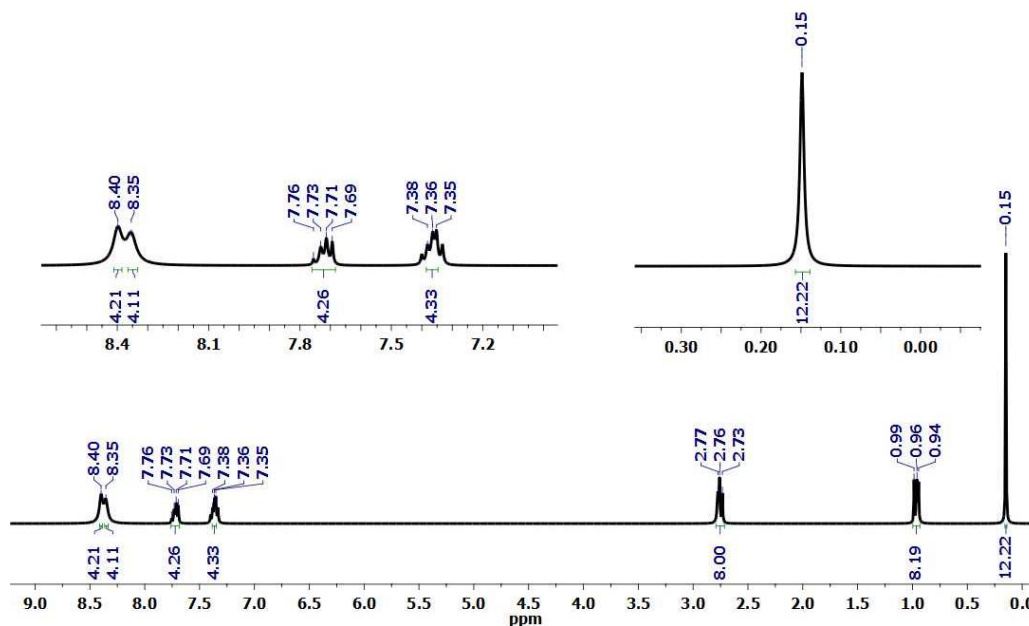


Figure A3.15: ^1H NMR for ligand $\text{L}^{4\text{C}}$ in that shown the expansion of the Methyl, ethyl and pyridyl. The methyl protons attached to the Si-atoms gave a single resonance at 0.15. The signals due to ethyl moieties give the triplet and the pyridyl groups were also found to be equivalent.

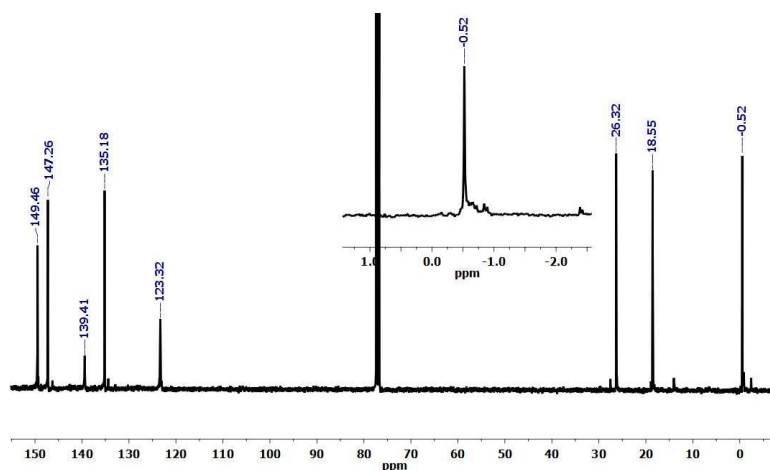


Figure A3.16: ^{13}C NMR for ligand $\text{L}^{4\text{A}}$.

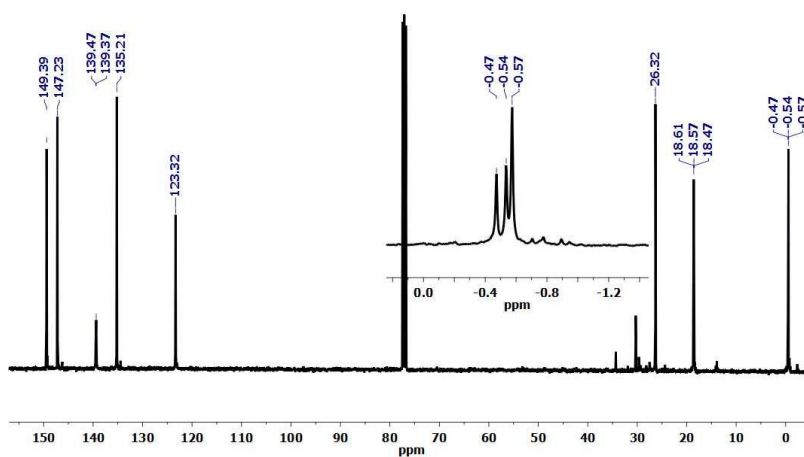


Figure A3.17: ^{13}C NMR for ligand $\text{L}^{4\text{B}}$.

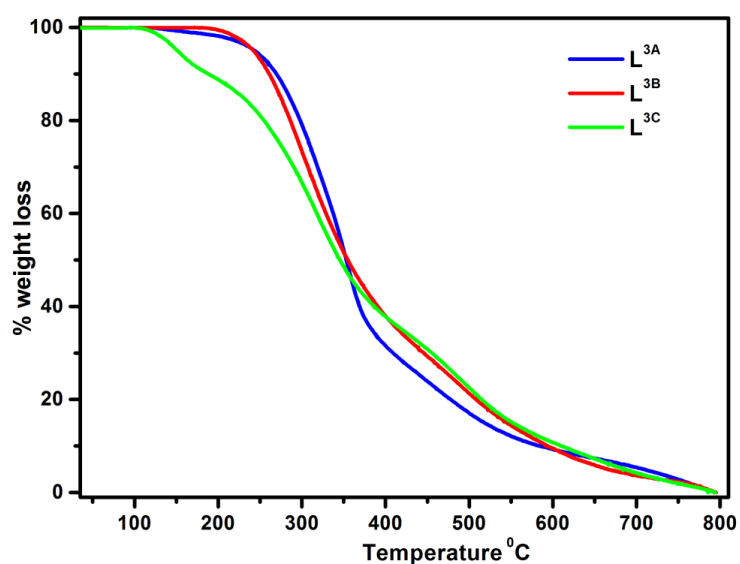


Figure A3.18: TGA profiles of L^3 ; (a) ligand $\text{L}^{3\text{A}}$ is stable up to 190 $^{\circ}\text{C}$ (b) Ligand $\text{L}^{3\text{B}}$ is stable up to 180 $^{\circ}\text{C}$ and (c) ligand $\text{L}^{3\text{C}}$ is stable up to 120 $^{\circ}\text{C}$

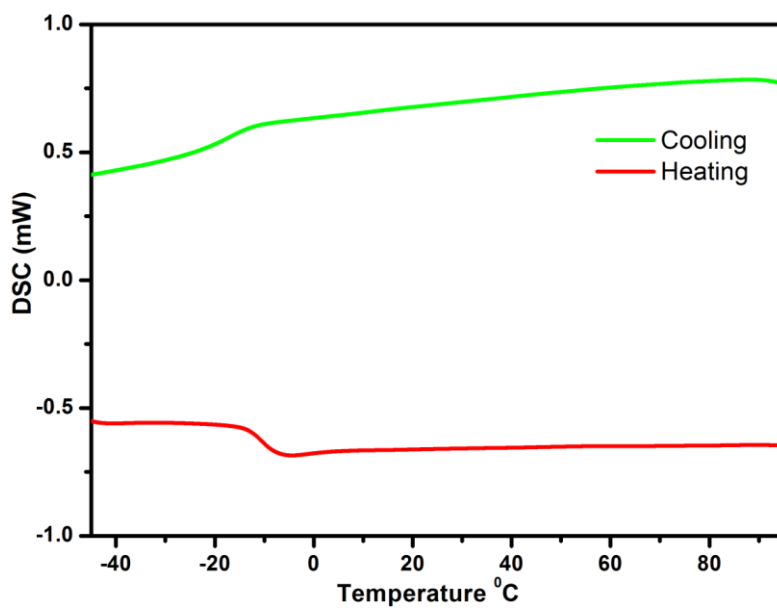


Figure A3.19. DSC profile of L^{3A}

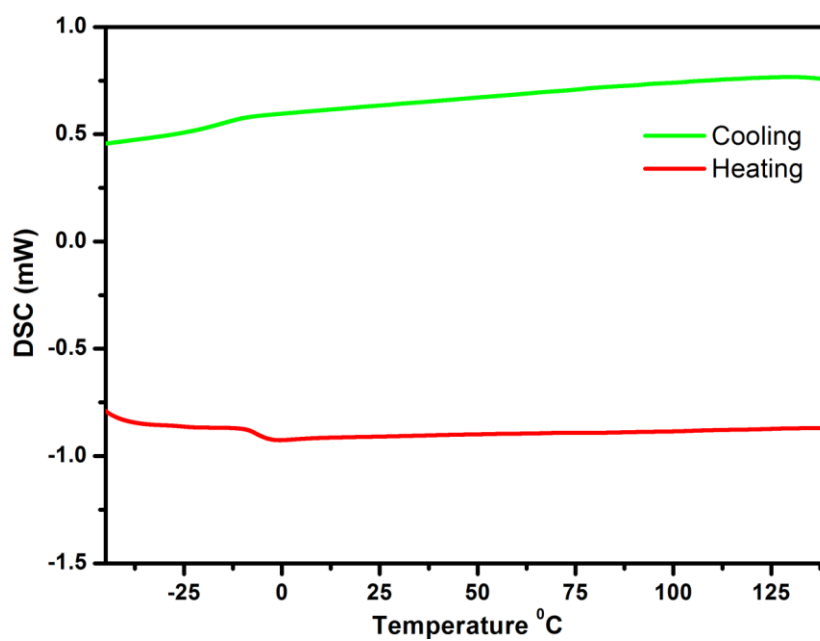


Figure A3.20: DSC profile of L^{3B}

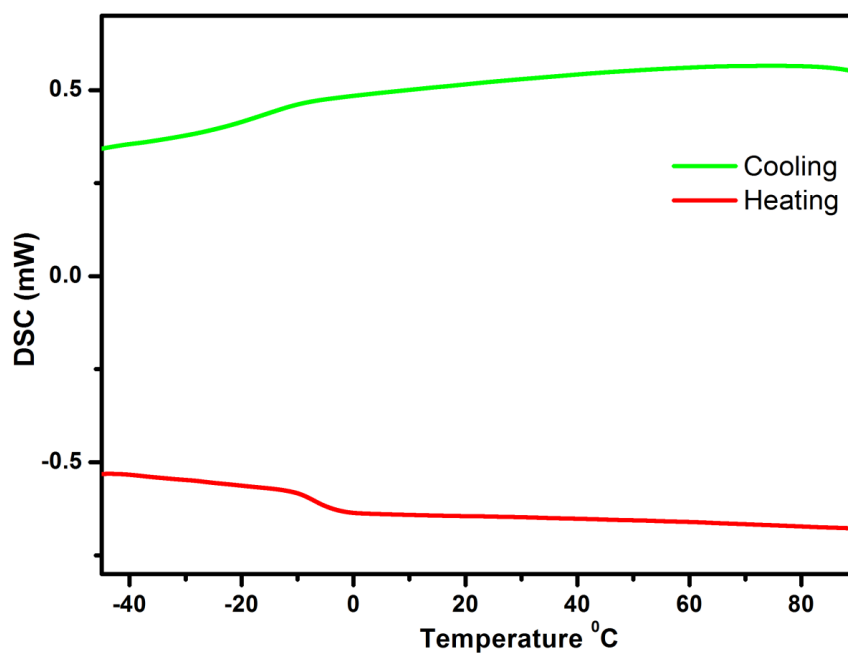


Figure A3.21: DSC profile of L^{3C}

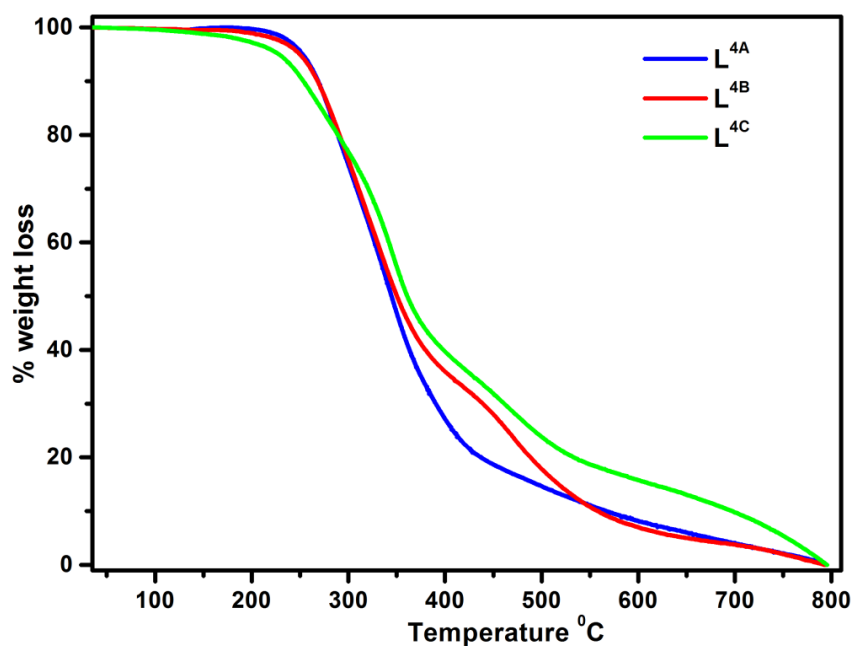
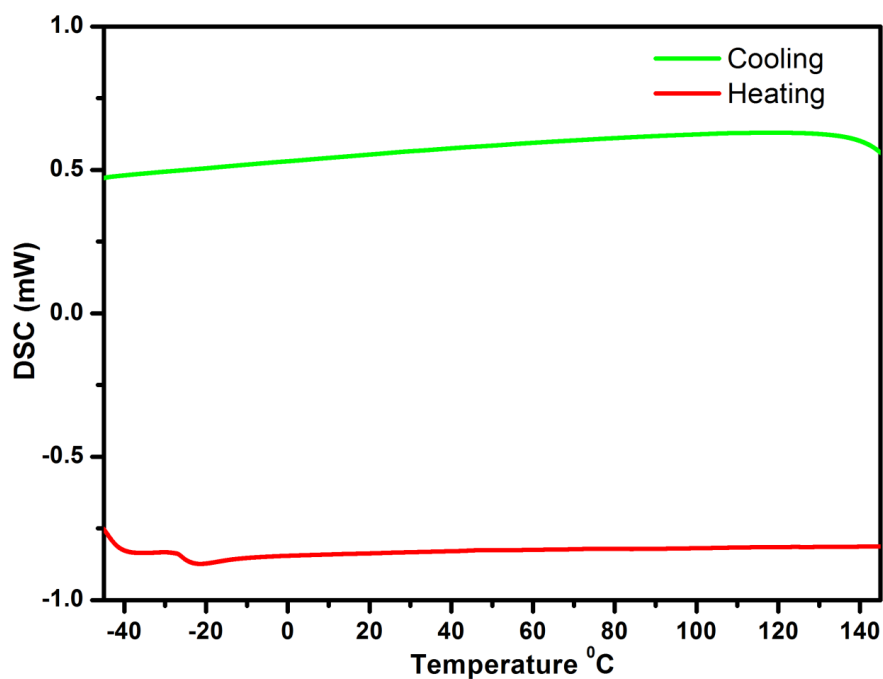
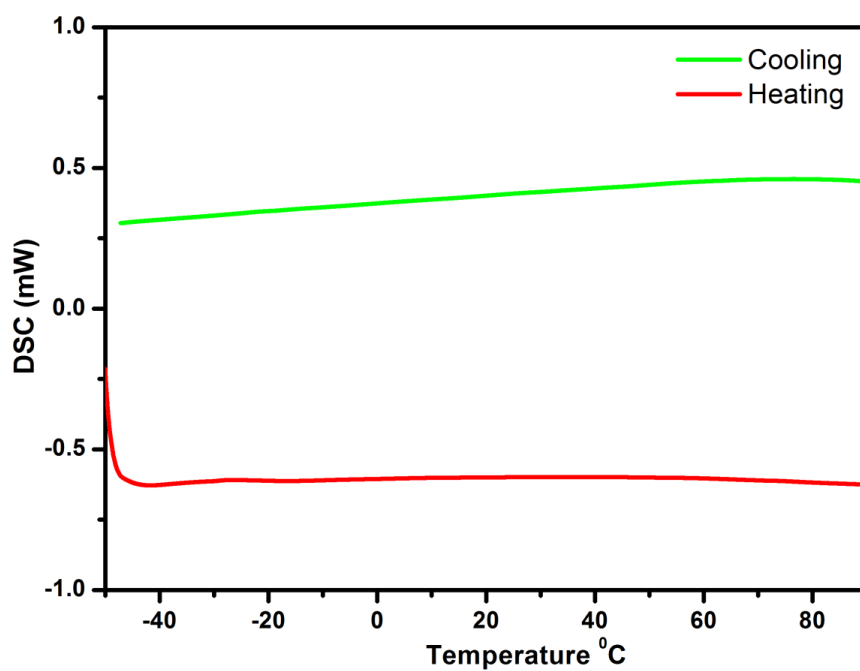


Figure A3.22. TGA profiles of L⁴; (a) ligand L^{4A} is stable up to 190 °C (b) Ligand L^{4B} is stable up to 180 °C and (c) ligand L^{4C} is stable up to 150 °C

Figure A3.23: DSC profile of L^{4A}Figure A3.24: DSC profile of L^{4B}

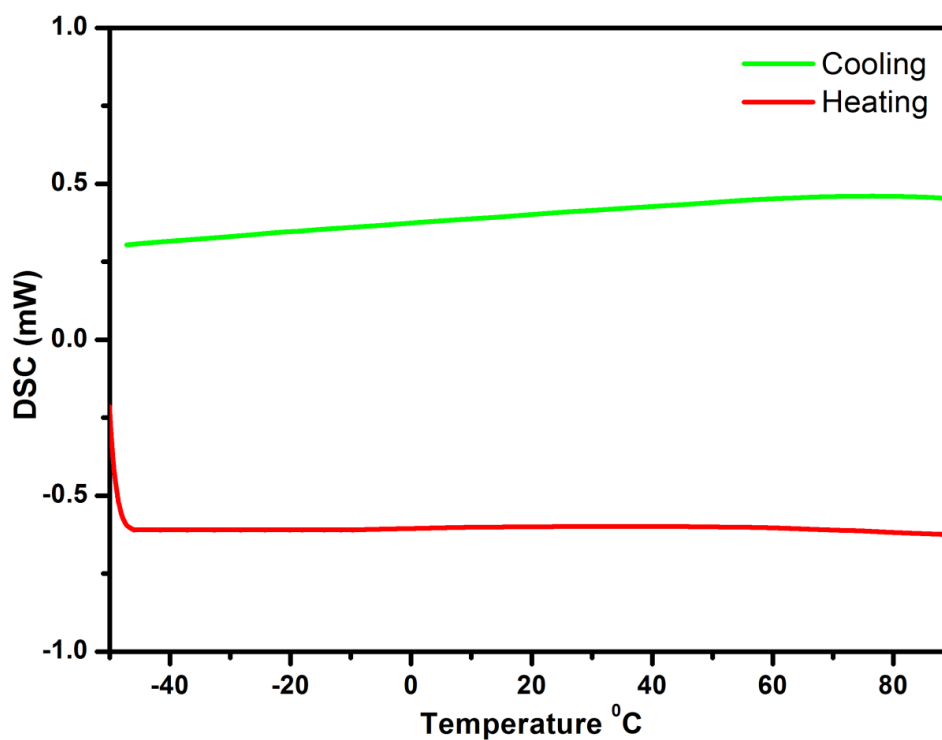
Figure A3.25: DSC profile of L^{4C}

Table A3.2: TGA and DSC data for tetrasiloxane ligands

ligand	Decomposition temp. (°C)	DSC ^a	
		Melting Temp. (°C)	Crystlization Temp. (°C)
L ^{1A}	190	-7	-13
L ^{1B}	180	-3	-9
L ^{1C}	130	-4	-10
L ^{2A}	190	-22	-
L ^{2B}	180	-40	-
L ^{2C}	150	-	-

^aFor L^{4C} the melting temperature is expected to be observed below -50 °C based on the values observed for L^{4A} and L^{4B}. However, owing to the instrumental limitation we were unable to record the melting/crystallization temperature for L^{4C}.

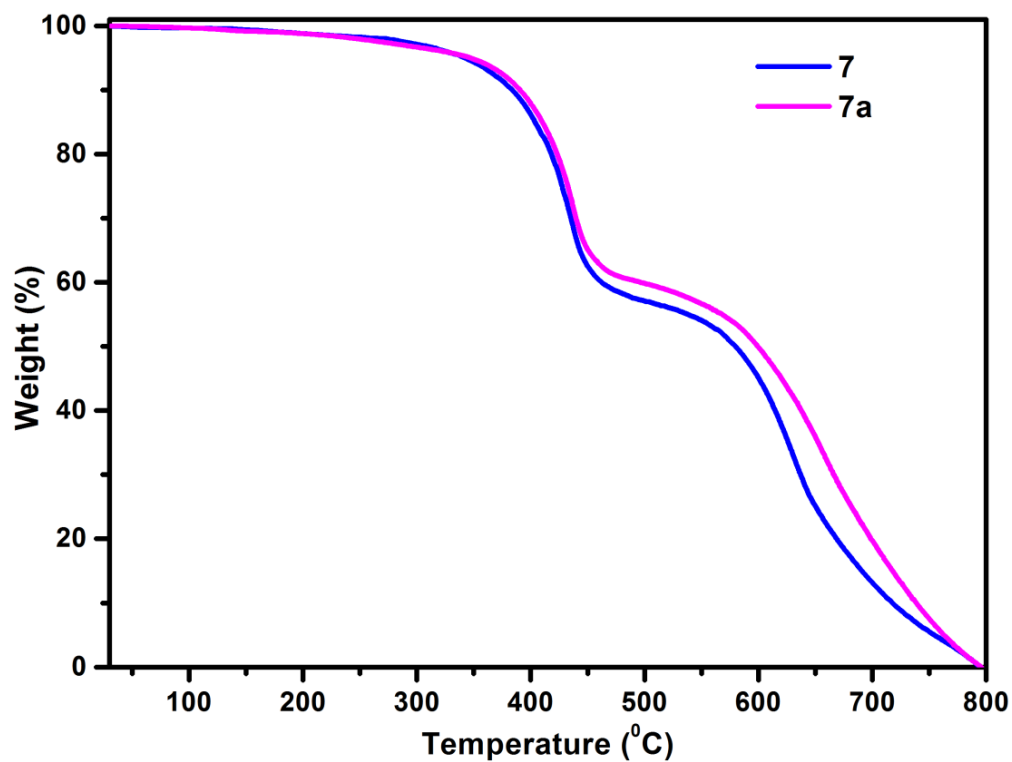
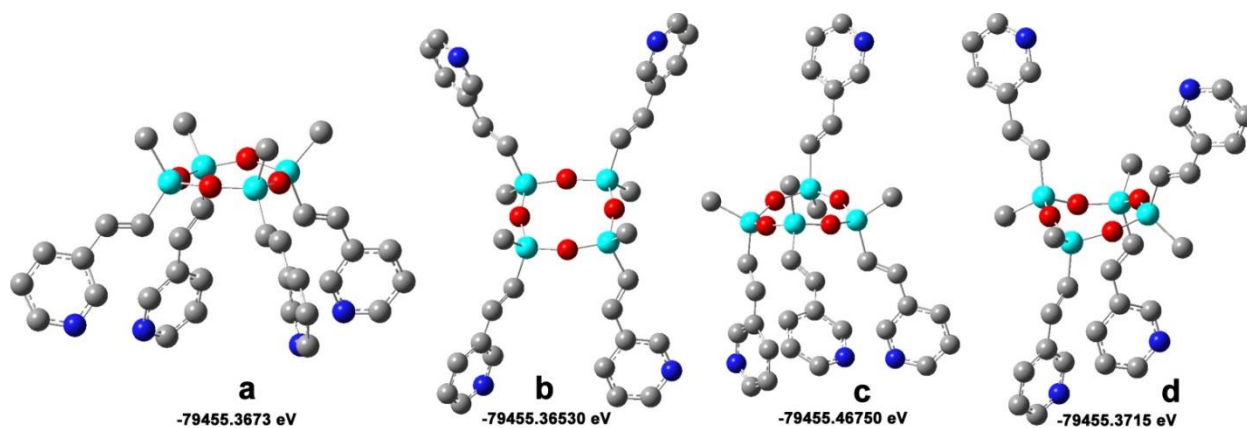


Figure A3.26: TGA profiles of 7 and 7a

Figure A3.27. optimized geometrys of cyclotetrasiloxane ligand L^{3a} shown the similar energy.

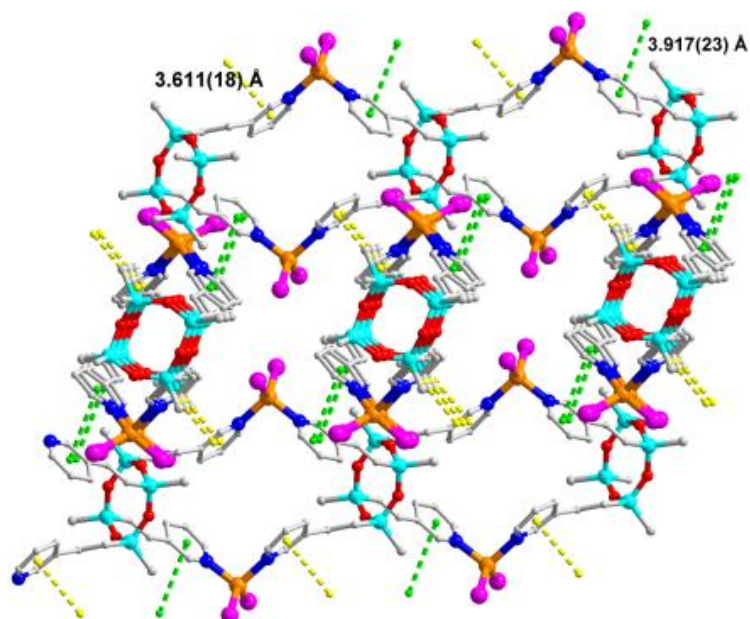


Figure A3.28: View of the π - π interactions in **5**. The 1D-chains of the adjacent layers are aligned perpendicular to each other and linked via two distinct π - π interactions (3.610 Å and 3.917 Å) of the pyridyl groups.

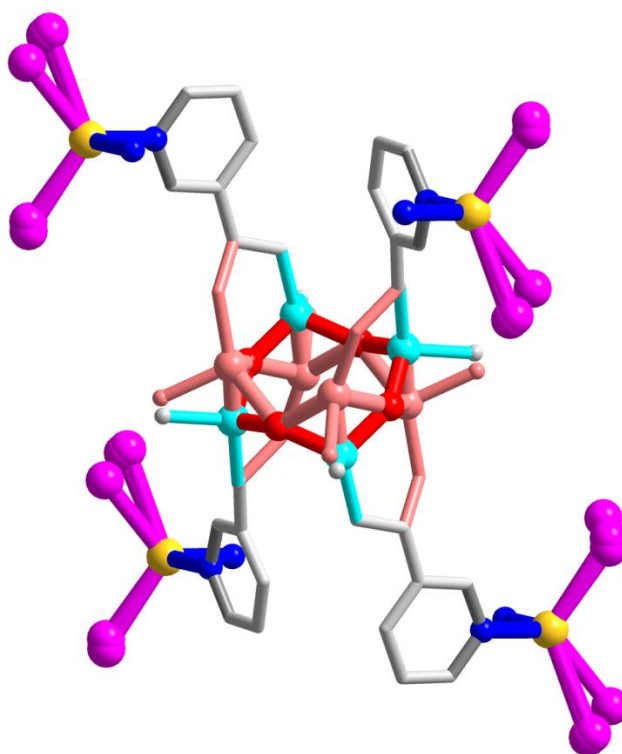
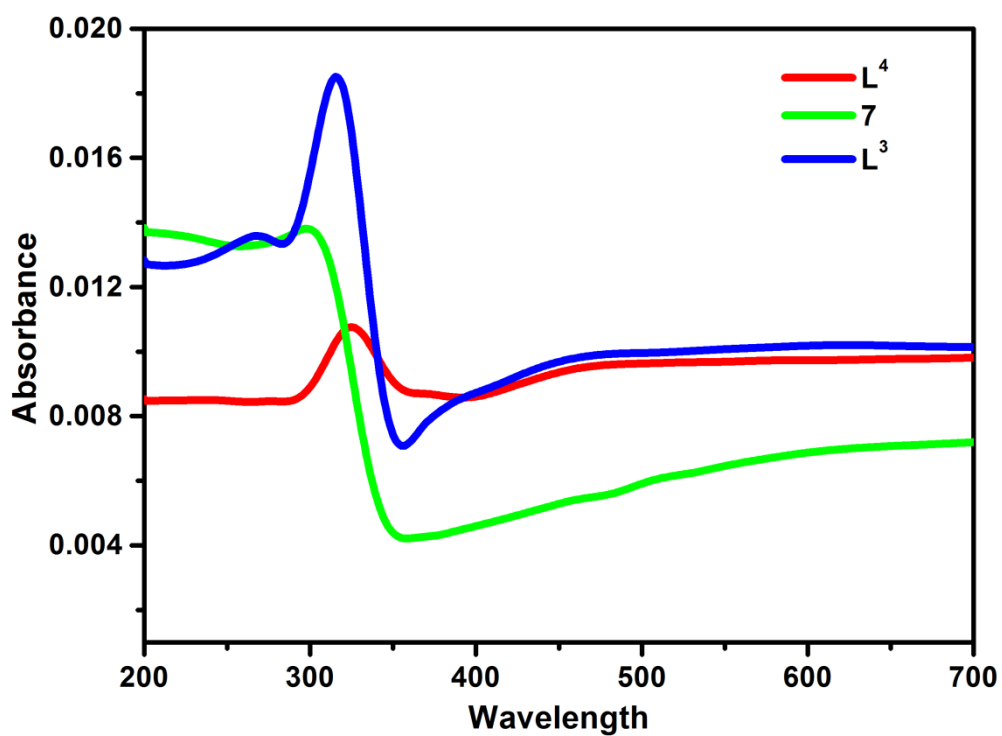


Figure A3.29: View of disordered nature of the tetrakisoxane and the vinylic C-atoms

Table A3.3: Photoluminescence data of compounds used in this study

Complex	Temp./K	$\lambda_{\text{ex}}/\text{nm}$	$\lambda_{\text{em}}/\text{nm}$	τ_{em}
7	298	395	595	1.6 ns
	77	301	475	1.1 μs
			162 μs	
L^3	298	315	406	0.8 ns
	77	315	405	4.9 ns 0.8 ns
L^4	298	325	427	3.4 ns
	77	325	425	1.8 ns 0.2 μs

Figure A3.30: Solid state UV-visible spectrum for L^3 , L^4 and 7

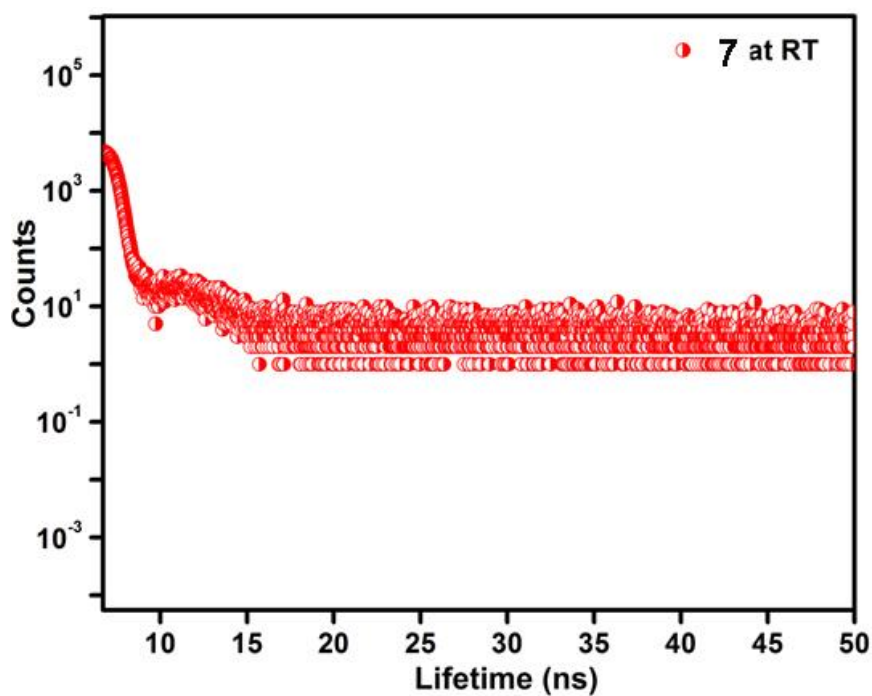


Figure A3.31: Solid-state phosphorescence decay profiles of 7 at 298 K.

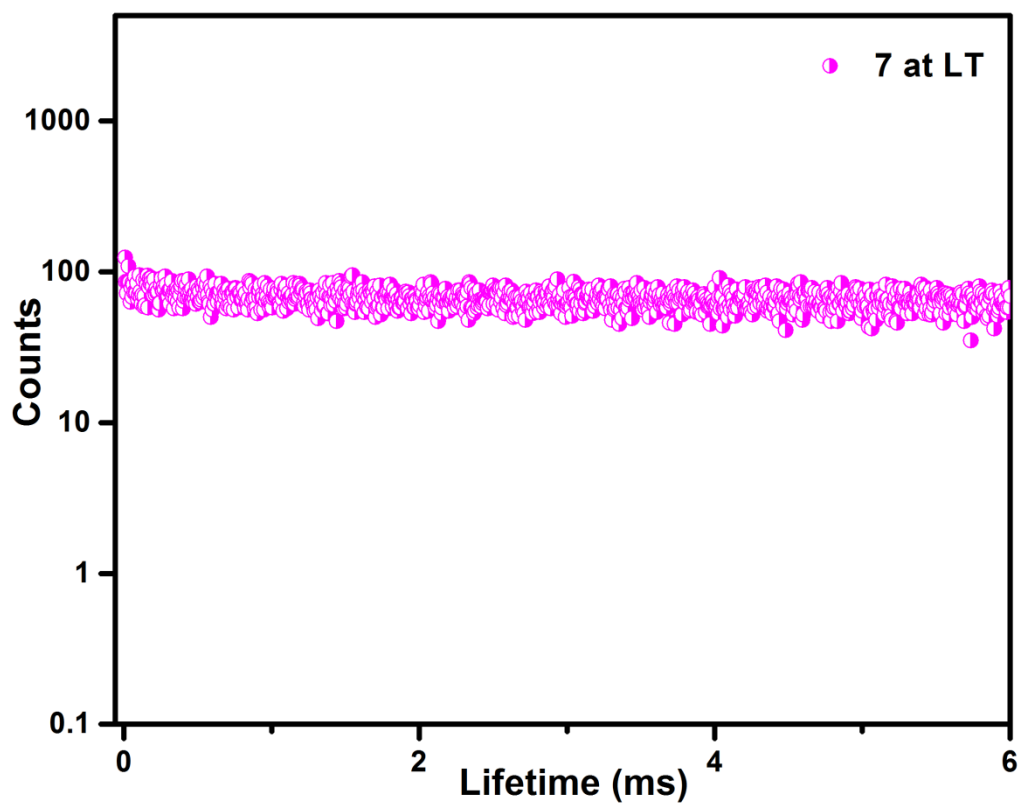


Figure A3.32: Solid-state phosphorescence decay profiles of 7 at 77 K.

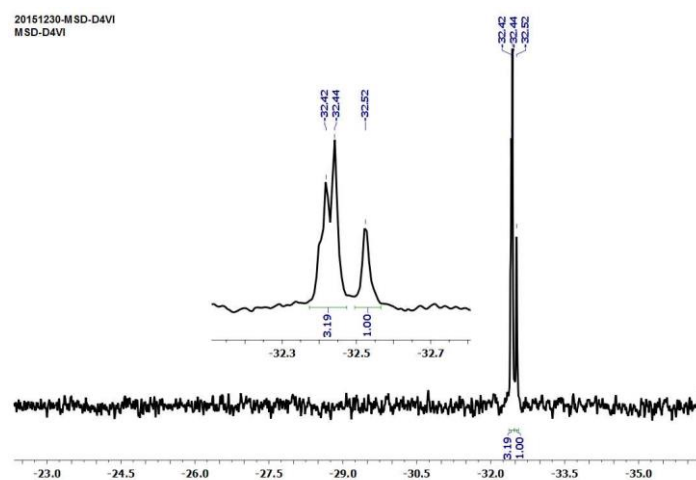


Figure A3.33: ^{29}Si NMR of commercial (95 % pure) 2,4,6,8-Tetravinyl-2,4,6,8-tetramethylcyclotetrasiloxane (D_4^{vi}) showing a *cis-cis-trans* type peak pattern. A small hump near 33.42 ppm is indicative of a minor impurity.

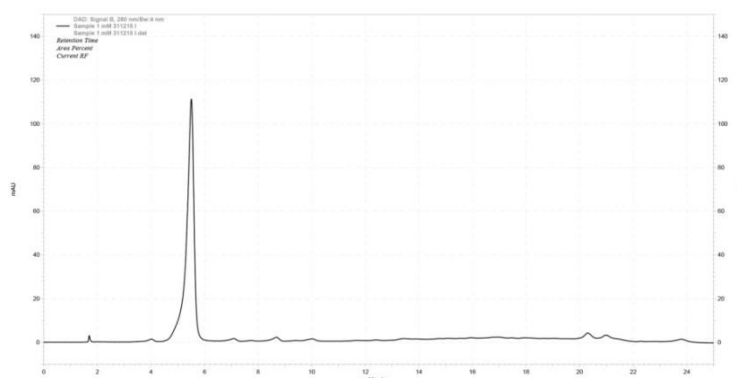


Figure A3.34: HPLC plot of commercial (95 % pure) 2,4,6,8-Tetravinyl-2,4,6,8-tetramethylcyclotetrasiloxane (D_4^{vi}) in 1mmol solution in acetonitrile showing the presence of one major isomer (most likely *cis-cis-trans*)

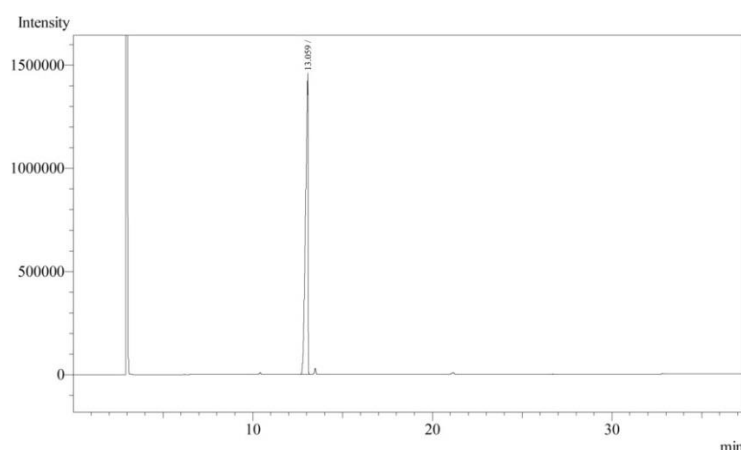


Figure A3.35: GC plot of commercial (95 % pure) 2,4,6,8-Tetravinyl-2,4,6,8-tetramethylcyclotetrasiloxane (D_4^{vi}) showing one major isomer (most likely *cis-cis-trans*)

Table A4A.1: Selected bond-lengths (Å) and angles (°) for TPVS, **10** and **11**.

Compound	Bond length		Bond angle	
TPVS	Si(1)-C(1)	1.864(3)	C(1)-Si(1)-C(1)#1	111.88(10)
	Si(1)-C(1)#1	1.864(3)	C(1)-Si(1)-C(1)#2	104.76(19)
	Si(1)-C(1)#2	1.864(3)	C(1)#1-Si(1)-C(1)#2	111.88(10)
	Si(1)-C(1)#3	1.864(3)	C(1)-Si(1)-C(1)#3	111.88(10)
	C(1)-C(2)	1.337(4)	C(1)#1-Si(1)-C(1)#3	104.76(19)
	C(4)-N(5)	1.343(5)	C(1)#2-Si(1)-C(1)#3	111.88(10)
	C(4)-C(3)	1.395(5)	C(2)-C(1)-Si(1)	125.4(2)
	C(3)-C(8)	1.399(5)	C(8)-C(3)-C(2)	122.5(3)
	C(6)-N(5)	1.342(5)	C(6)-N(5)-C(4)	116.8(3A)
10	Cu(1)-N(15)#1	2.029(2)	N(15)#1-Cu(1)-N(15)#2	173.53(13)
	Cu(1)-N(15)	2.029(2)	N(15)#1-Cu(1)-N(15)#3	89.818(8)
	Cu(1)-Cl(1)	2.5527(17)	N(15)#3-Cu(1)-N(15)	173.54(13)
	Cu(2)-N(25)#4	2.032(2)	N(15)#1-Cu(1)-Cl(1)	93.23(7)
	Cu(2)-Cl(2)	2.5462(12)	N(25)#4-Cu(2)-N(25)#5	89.816(8)
	Si(1)-C(21)	1.849(3)	N(25)#5-Cu(2)-N(25)#6	173.50(13)
	Si(1)-C(11)#8	1.857(3)	N(25)#4-Cu(2)-N(25)	173.50(13)
	C(11)-C(12)	1.337(4)	N(25)#5-Cu(2)-N(25)	89.815(8)
	N(15)-C(16)	1.341(4)	N(25)#4-Cu(2)-Cl(2)	93.25(7)
	C(16)-C(17)	1.384(4)	C(21)-Si(1)-C(21)#8	108.18(18)
	N(25)-C(26)	1.339(4)	C(21)-Si(1)-C(11)#8	111.13(12)
	C(26)-C(27)	1.381(4)	C(21)#8-Si(1)-C(11)#8	110.64(12)
	C(27)-C(28)	1.383(5)	C(11)#8-Si(1)-C(11)	105.14(18)
			C(12)-C(11)-Si(1)	123.1(2)
11	Cu(1)-N(5)	2.021(4)	N(5)-Cu(1)-N(5)#1	178.0(2)
	Cu(1)-N(5)#1	2.021(4)	N(5)-Cu(1)-N(5)#2	89.984(4)
	Cu(1)-Cl(1)	2.707(2)	N(5)#2-Cu(1)-N(5)#3	178.0(2)
	Si(1)-C(1)	1.868(4)	N(5)-Cu(1)-Cl(1)	91.01(10)
	C(1)-C(2)	1.542(6)	Cu(1)-Cl(1)-Cu(1)#4	180.0
	C(2)-C(3)	1.491(6)	C(1)-Si(1)-C(1)#5	110.04(14)
	C(3)-C(4)	1.379(6)	C(1)#5-Si(1)-C(1)#6	108.3(3)
	C(3)-C(8)	1.381(6)	C(1)#5-Si(1)-C(1)#7	110.04(14)
	C(4)-N(5)	1.343(5)	C(1)#6-Si(1)-C(1)#7	110.04(14)
			C(2)-C(1)-Si(1)	113.6(3)
			C(4)-N(5)-Cu(1)	120.4(3)
			C(6)-N(5)-Cu(1)	121.6(3)
			N(5)-C(6)-C(7)	122.2(4)

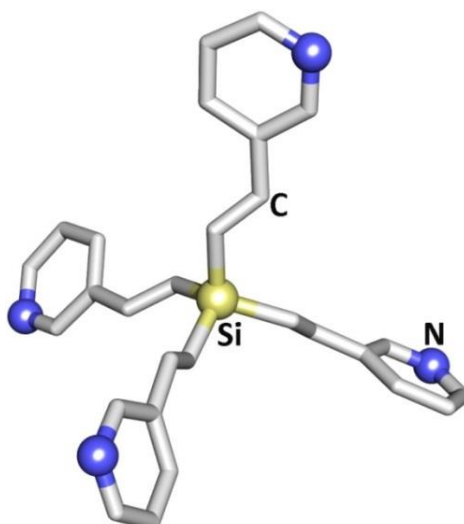


Figure A4A.1: Crystal structure of TPVS ligand

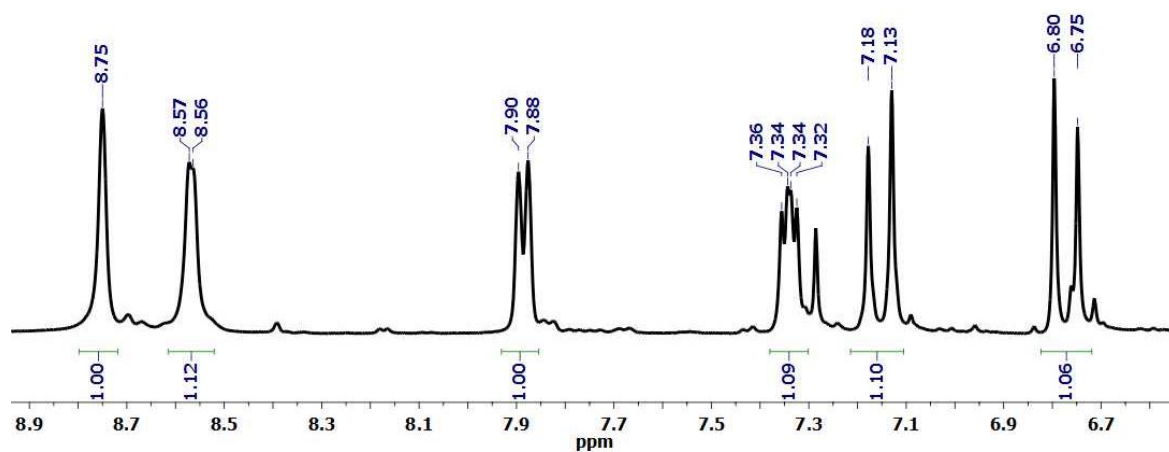


Figure A4A.2: Proton NMR of TPVS ligand

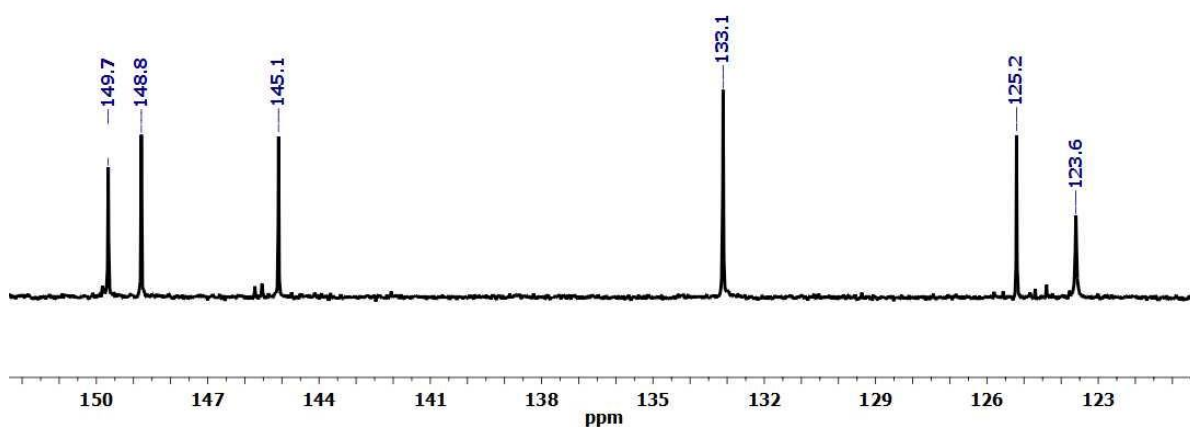


Figure A4A.3: Carbon NMR of TPVS ligand

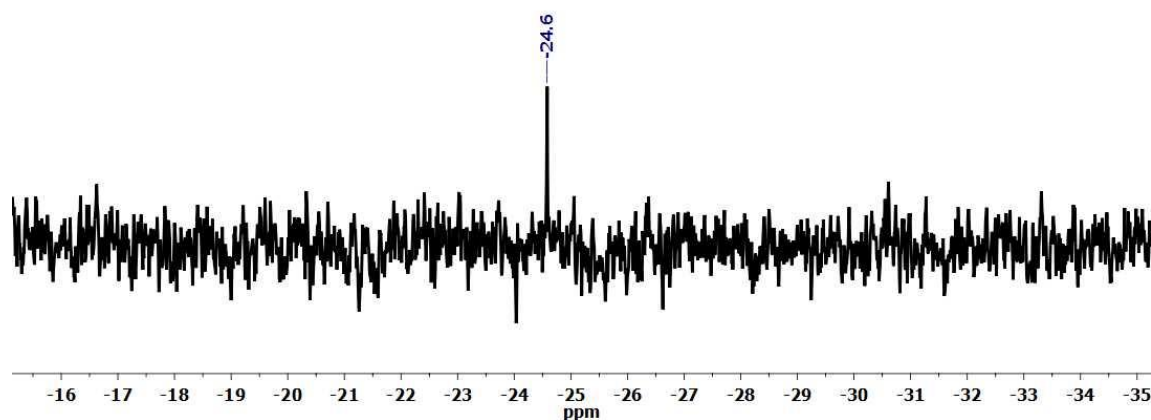


Figure A4A.4: Silicon NMR of TPVS ligand

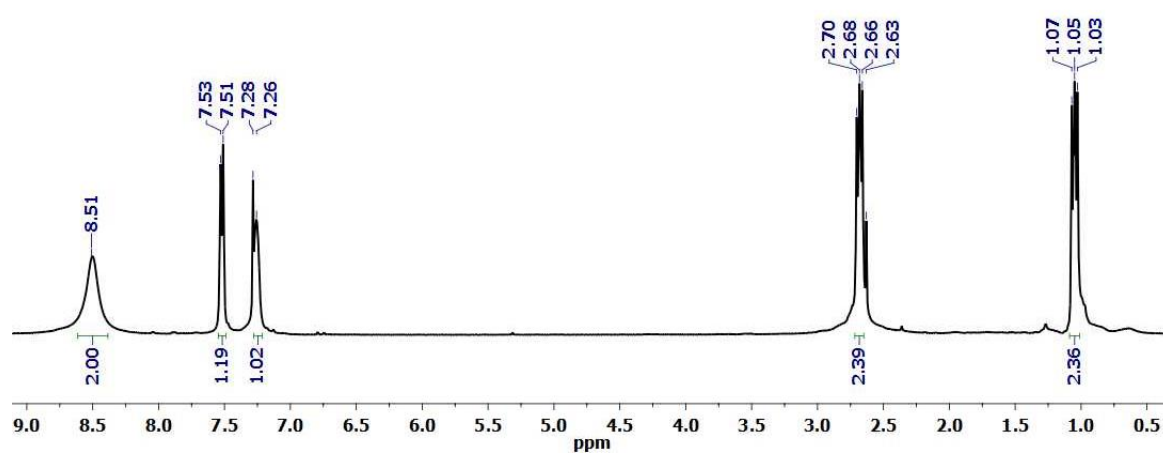


Figure A4A.5: Proton NMR of TPES ligand

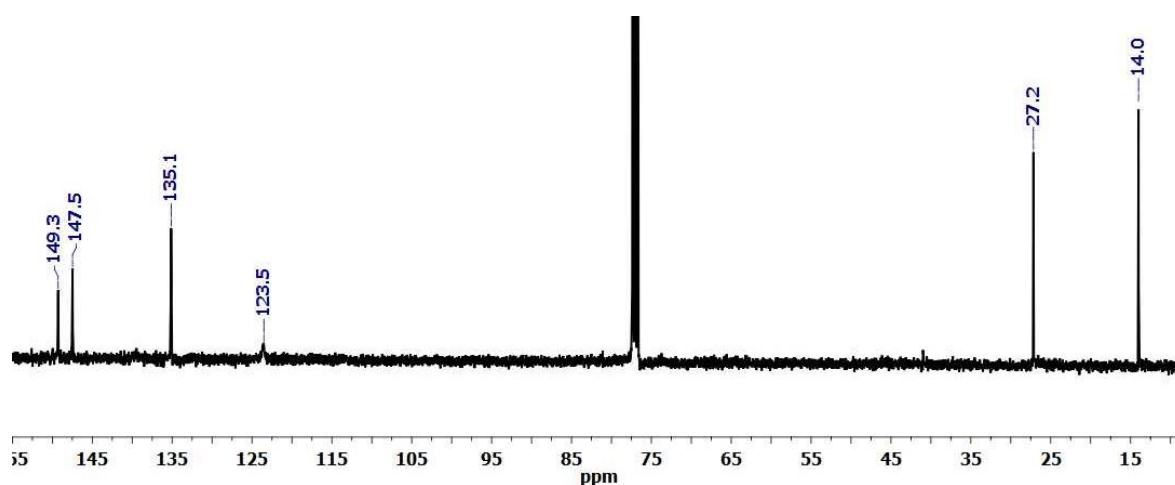


Figure A4A.6: Carbon NMR of TPES ligand

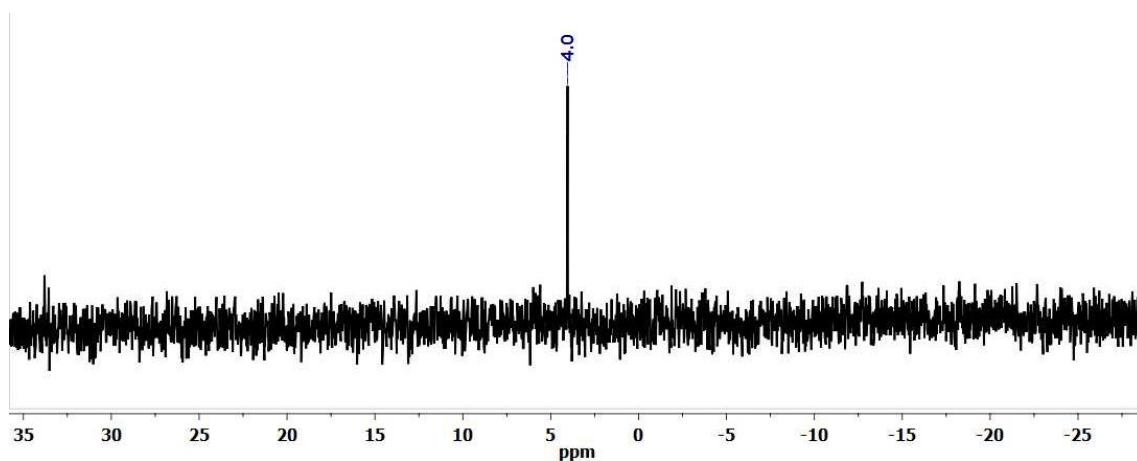


Figure A4A.7: Silicon NMR of TPES ligand

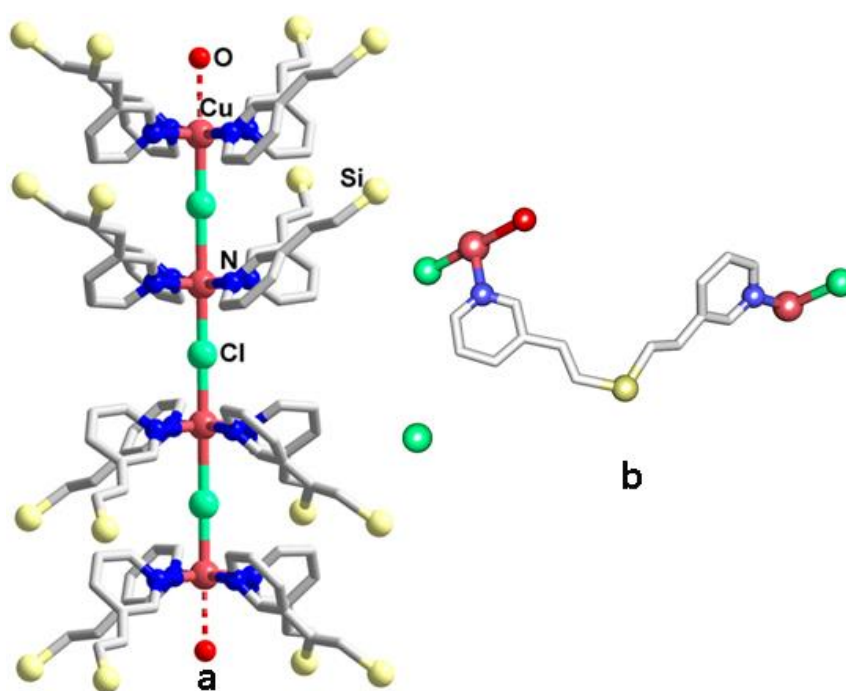


Figure A4A.8: (a) Crystal structure of **10** showing the arrangement of ligands around the linear $\text{Cu}_4\text{Cl}_3(\text{H}_2\text{O})_2$ cluster. (b) View of the asymmetric units consisting of half of the ligand moieties, three chloride ions out of which two are μ_2 -bridged and one is free, and one aqua ligand. Hydrogen atoms and disorder solvent molecules are omitted for clarity.

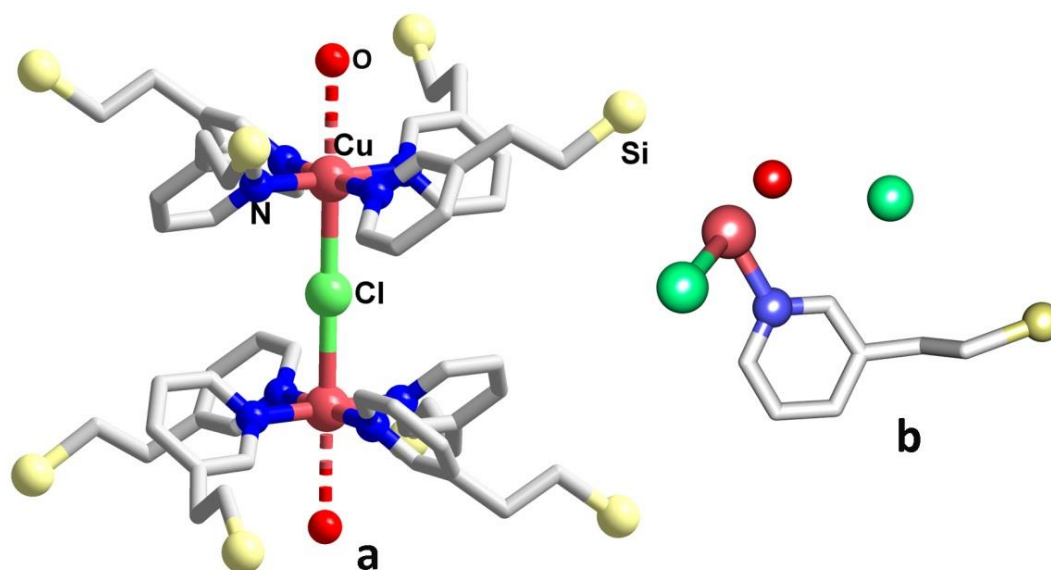


Figure A4A.9: (a) Crystal structure of **11** showing the arrangement of ligands around the linear Cu₂Cl (H₂O)₂ cluster; (b) view of the asymmetric units showing one fourth of the ligand moieties, two chloride ions (one is μ₂-bridged and one is free) and one aqua ligand. Hydrogen and disorder solvent molecules are omitted for clarity.

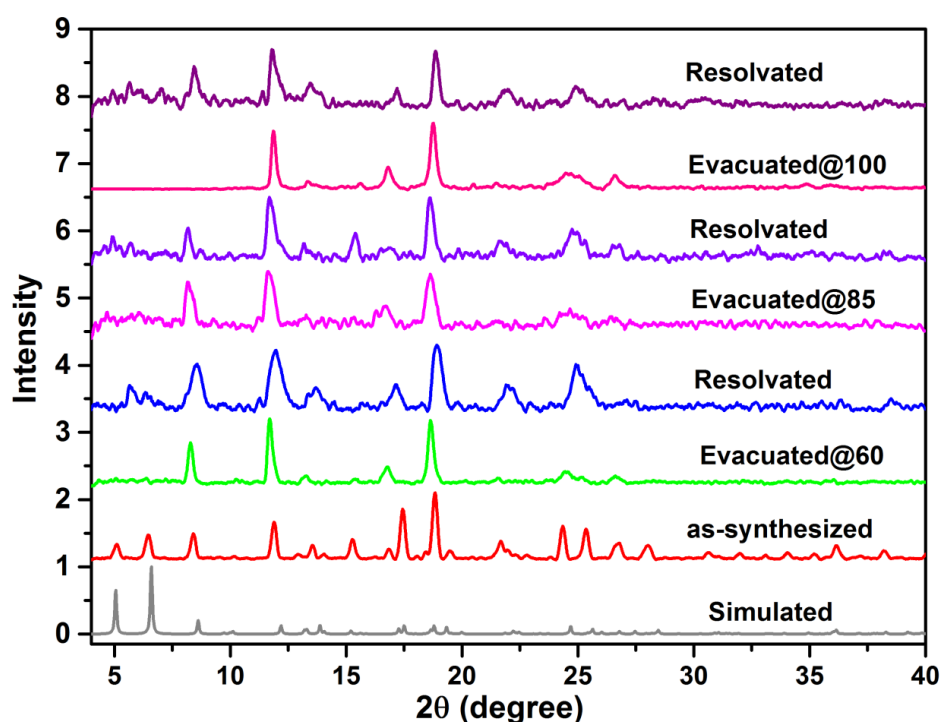


Figure A4A.10: PXRD patterns of **10** at various states: as-synthesised, activated at different temperatures and re-solvated.

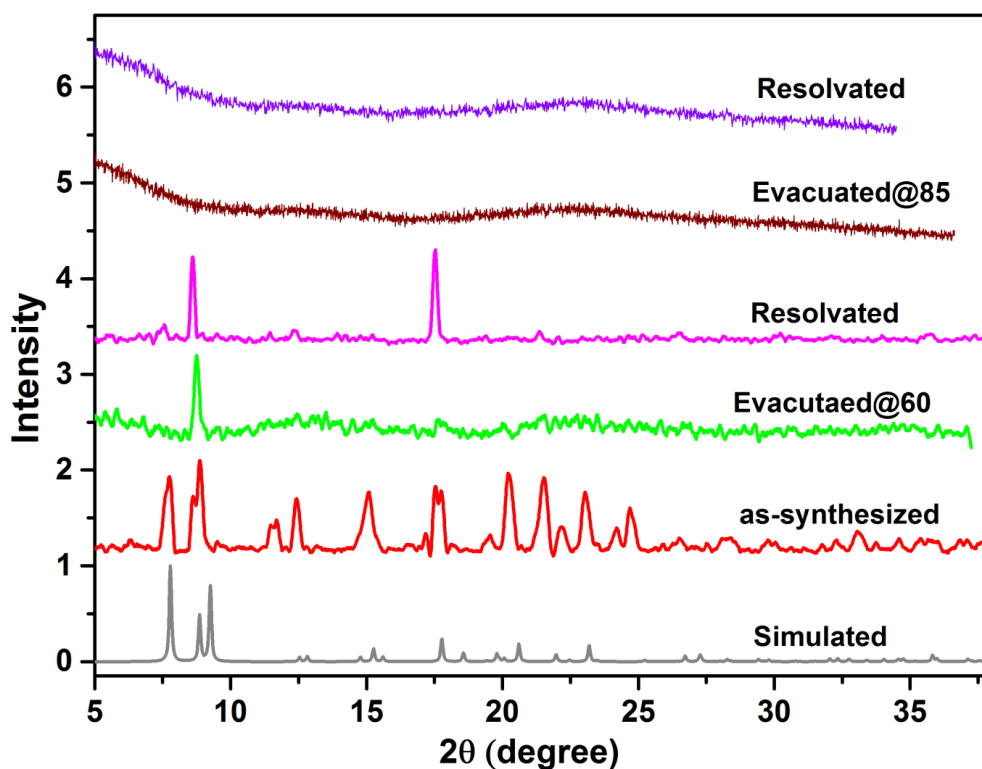


Figure A4A.11: The PXRD patterns of **11** at various states: as-synthesised, activated at different temperature and re-solvated

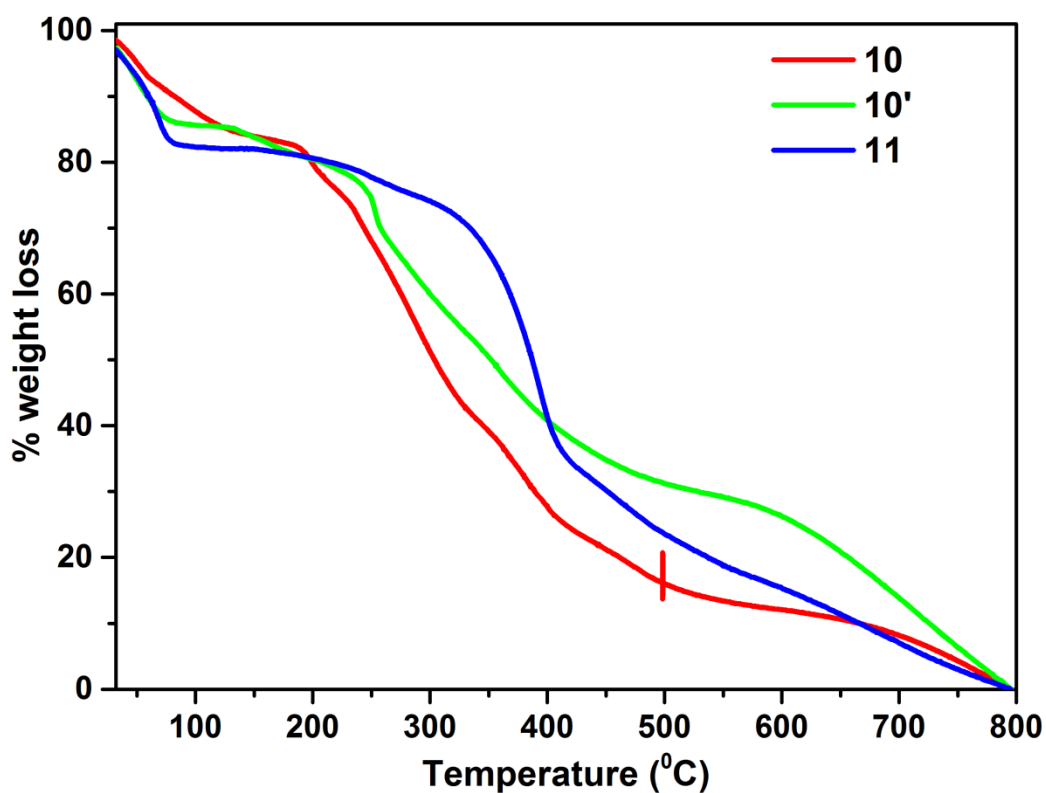


Figure A4A.12: TGA profiles of **10** and **11** in case of **10** showed the exchange of high boiling point solvent DMF with MeOH.

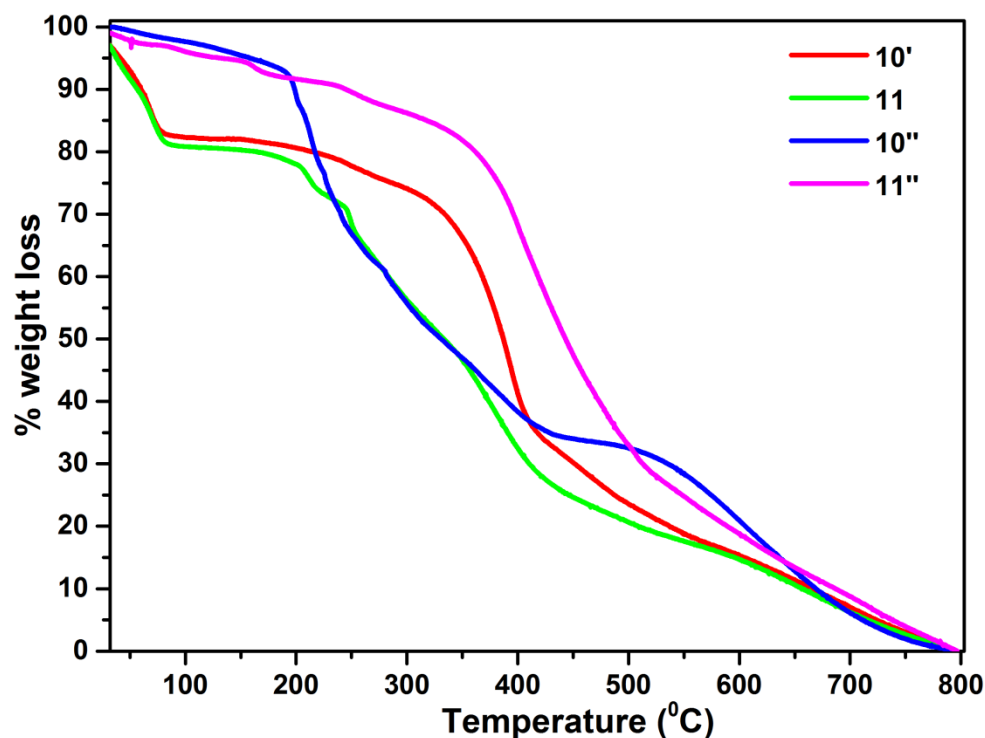


Figure A4A.13: TGA profiles of **10** and **11** in the pristine, solvent exchanged and in the evacuated forms showing the complete remove of solvent after activation

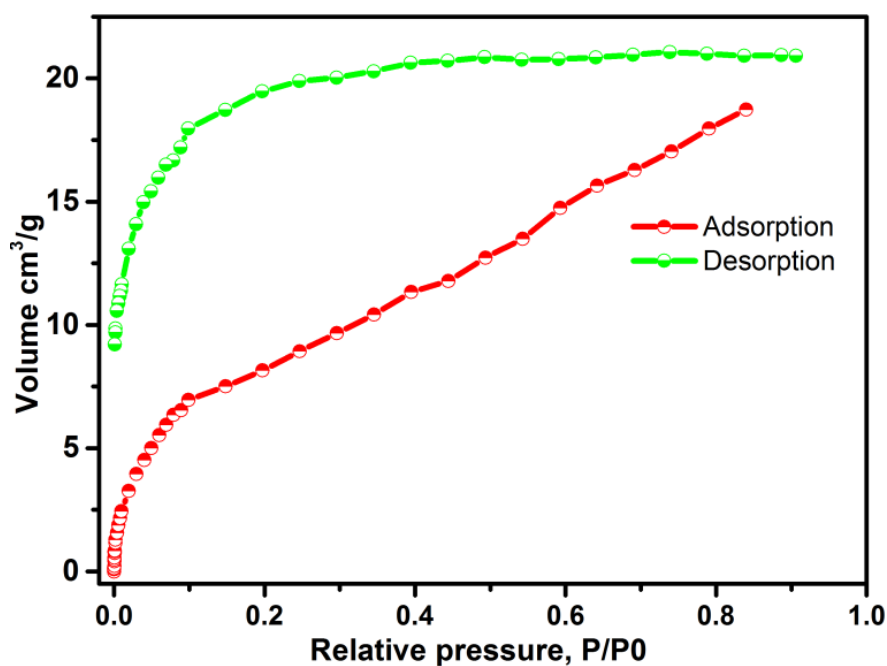


Figure A4A.14: CO₂ adsorption and desorption of **10''** at 195K; Gas adsorption (N₂ and CO₂) measurements on **1''** showed very small uptake characteristics, despite the framework exhibiting a large void space. This could presumably be due to the crystallization of free chloride ions in its pore which makes the framework polar.

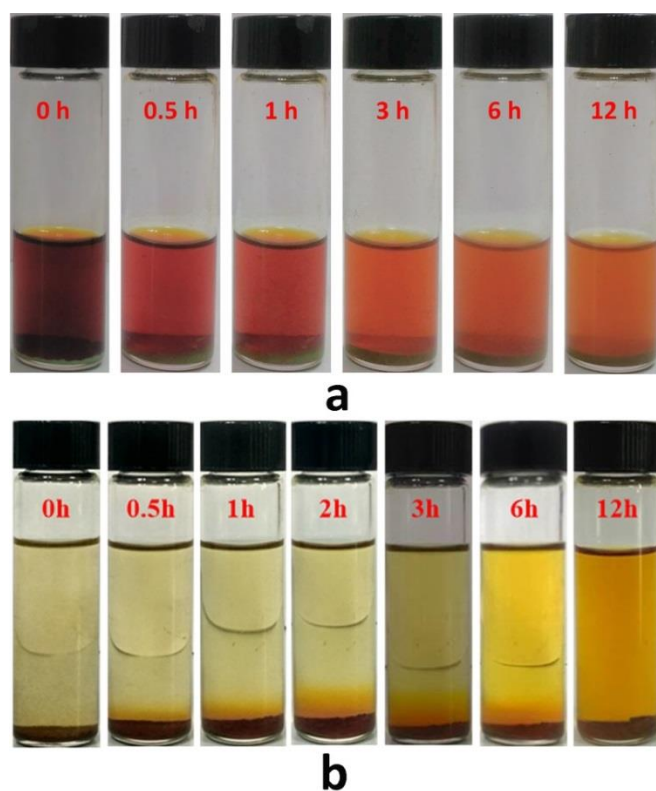


Figure A4A.15: Photographic displays of (a) uptake of iodine by 50 mg of $10''$ from 0.03M ethanol (3 ml) solution (b) Release of iodine from 10 mg of $I_2 \subset 10''$ in 5 ml of ethanol over a period of time.

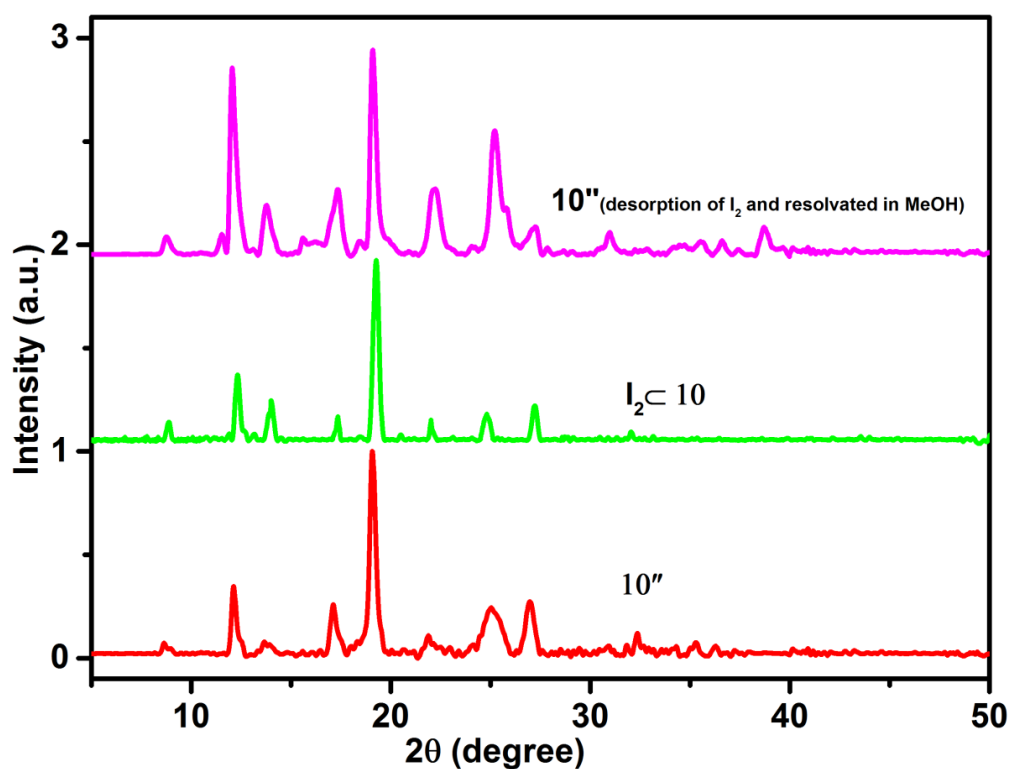


Figure A4A.16: PXRD pattern of $10''$ before and after iodine adsorption then after resolved in methanol.

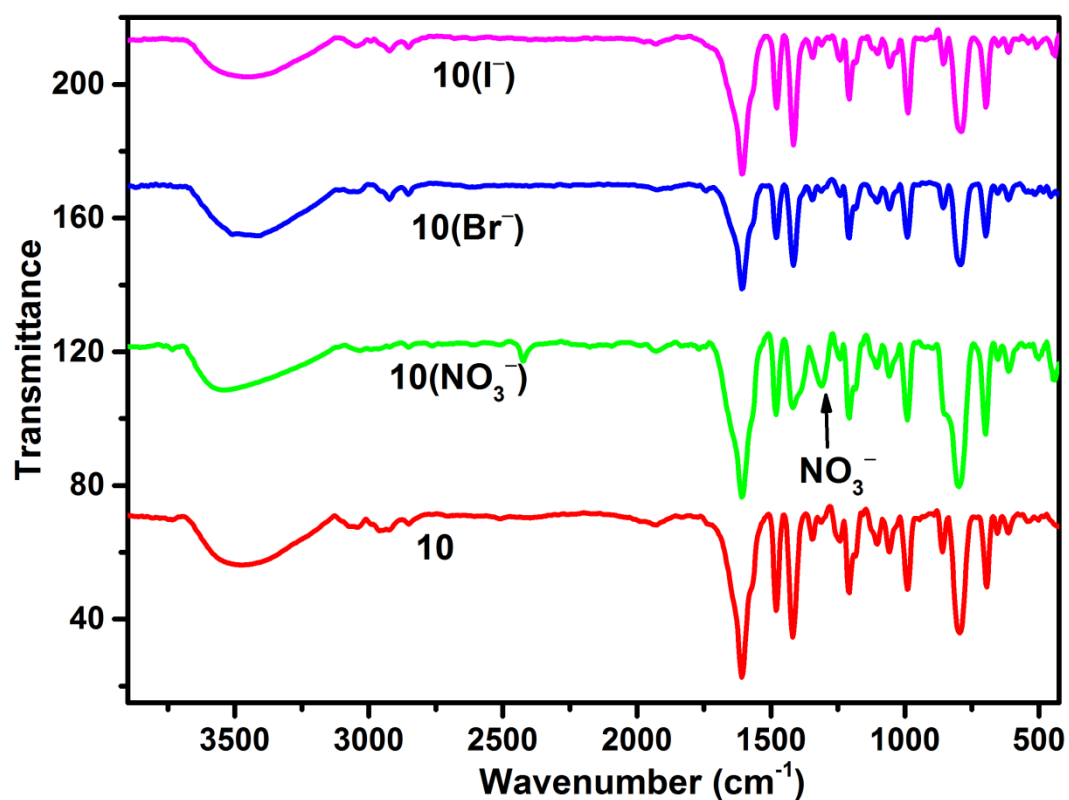


Figure A4A.17: Comparison IR spectra with anion-exchange samples

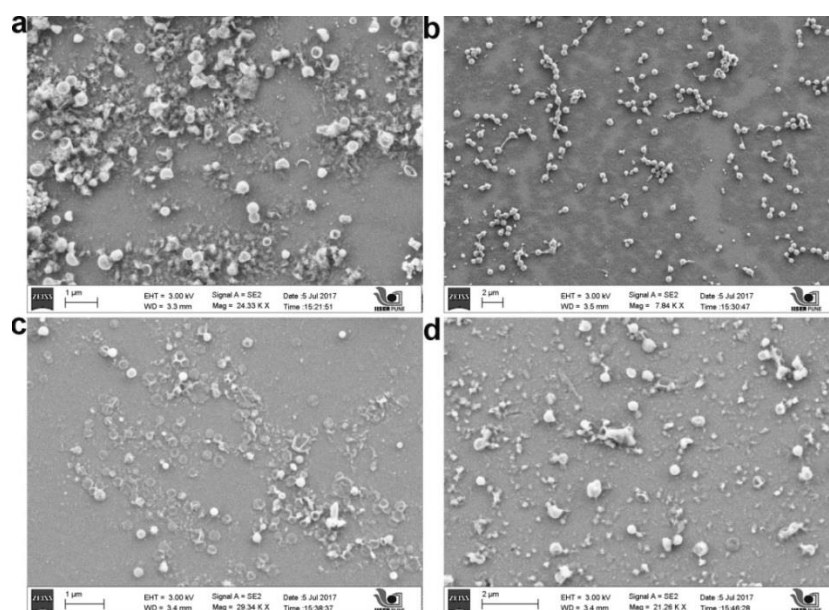


Figure A4A.18: SEM images of (a) **10** and anion-exchanged samples of **10** with (b) nitrate (c) bromide and (d) iodide ions. The SEM samples were prepared by dropcasting the methanol suspensions of the samples on silica wafer.

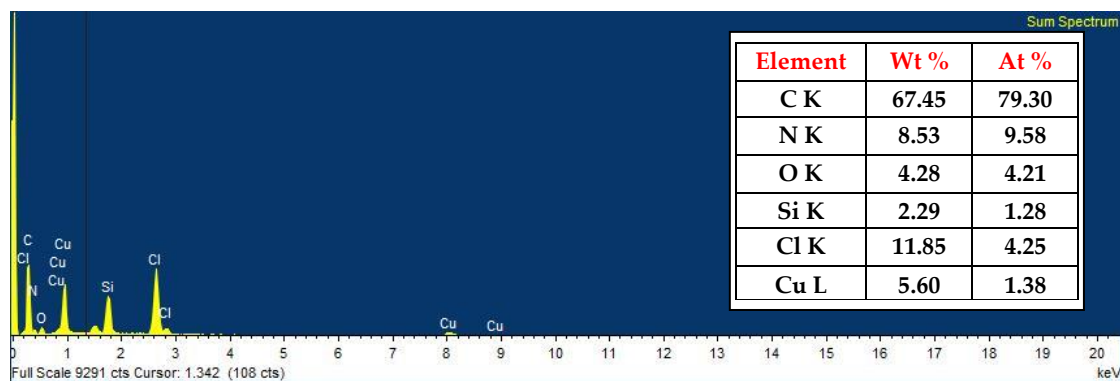


Figure A4A.19: EDX of compound 10

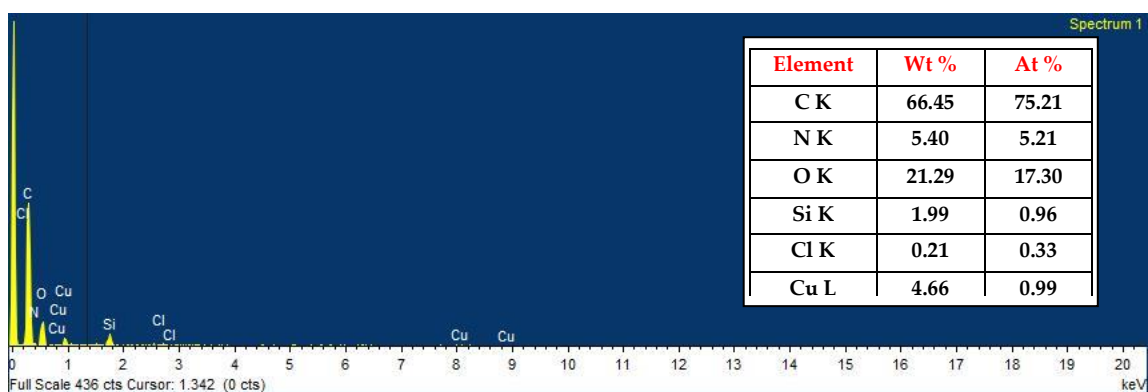


Figure A4A.20: EDX of nitrate exchanged sample of 10

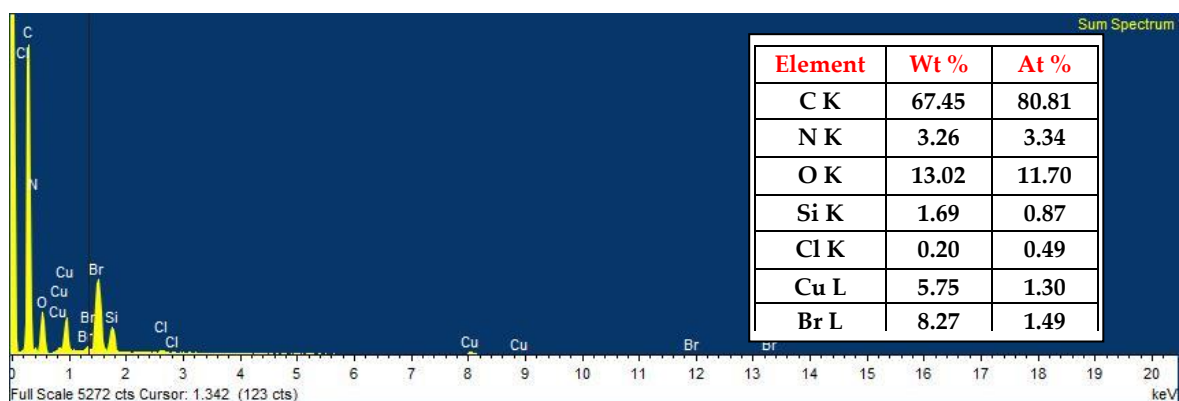


Figure A4A.21: EDX of bromide exchanged sample of 10

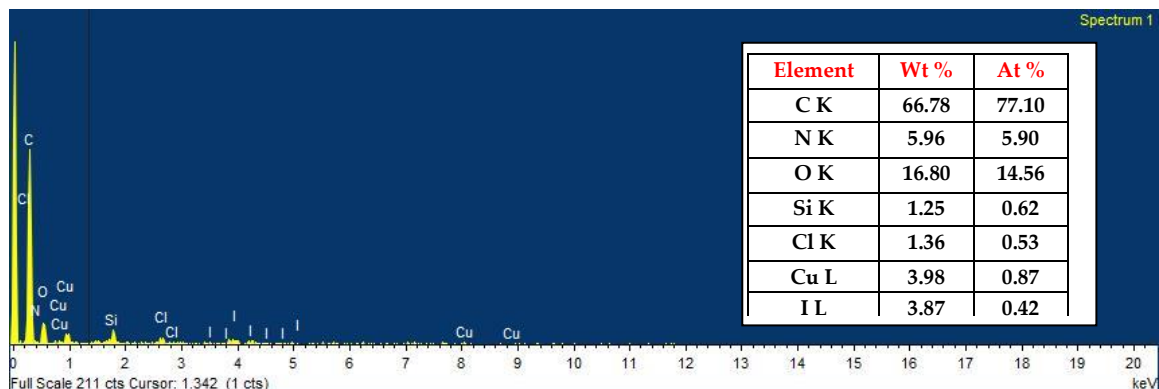


Figure A4A.23: EDX of iodine exchanged sample of 10

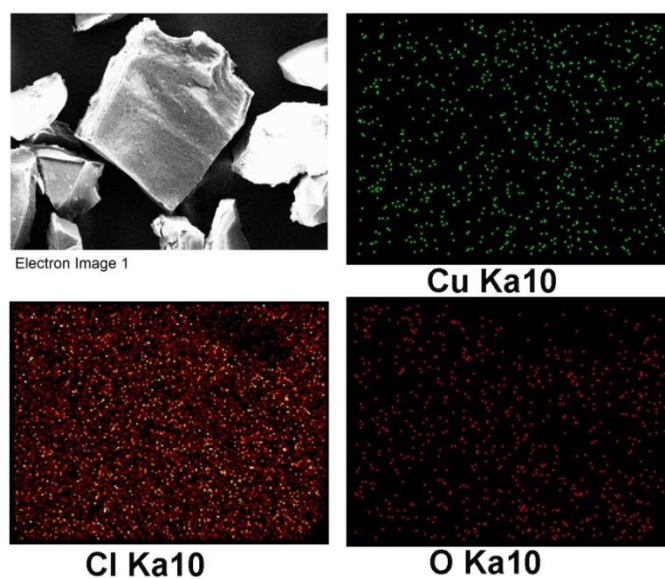


Figure A4A.23: SEM image and Elemental mapping of the MOF 10 crystals

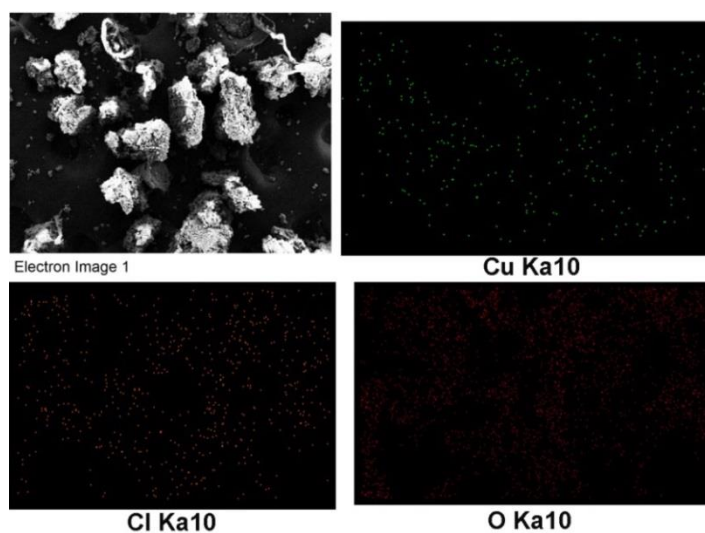


Figure A4A.24: SEM image and Elemental mapping of nitrate exchanged crystals of 10

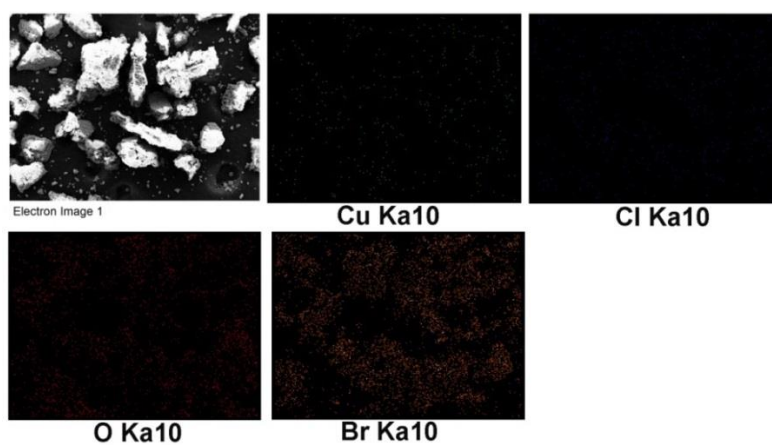


Figure A4A.25: SEM image and Elemental mapping of bromide exchanged crystals of 10

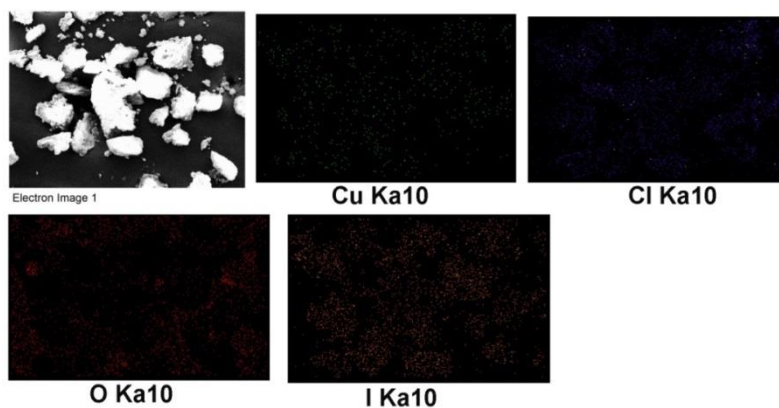


Figure A4A.26: SEM image and Elemental mapping of iodide exchanged crystals of **10**

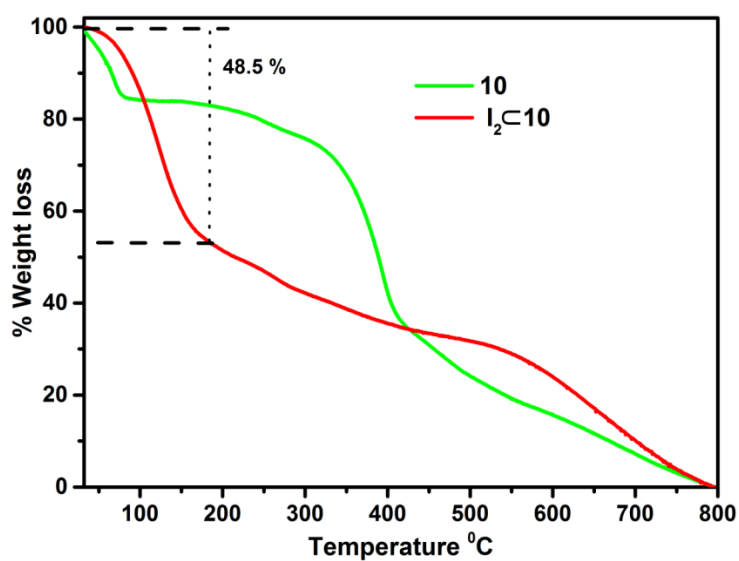


Figure A4A.27: TGA Profile of **10** and I_2C10

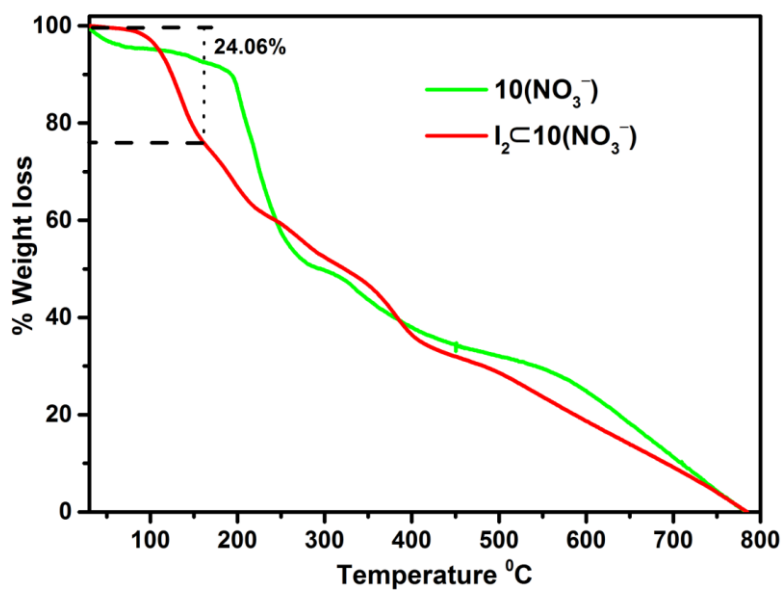


Figure A4A.28: TGA profile of nitrate exchanged samples of **10(NO₃⁻)** and $I_2C10(NO_3^-)$

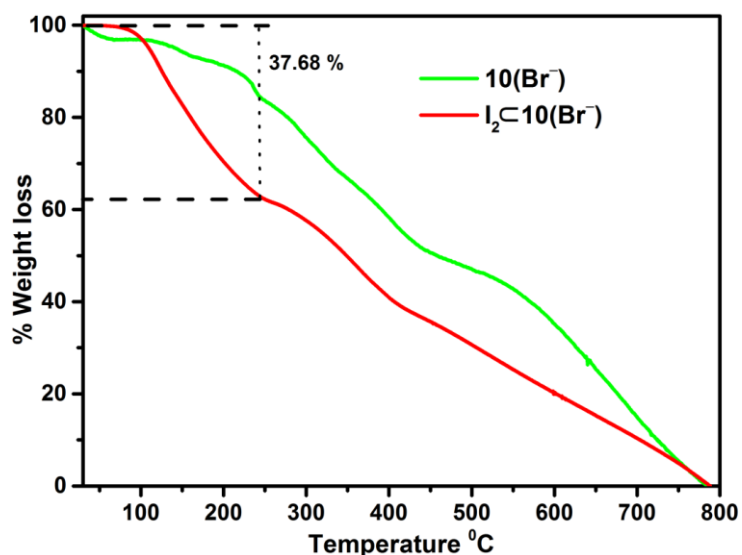


Figure A4A.29: TGA profile of bromide exchange samples of $10(\text{Br}^-)$ and $\text{I}_2\text{C}10(\text{Br}^-)$

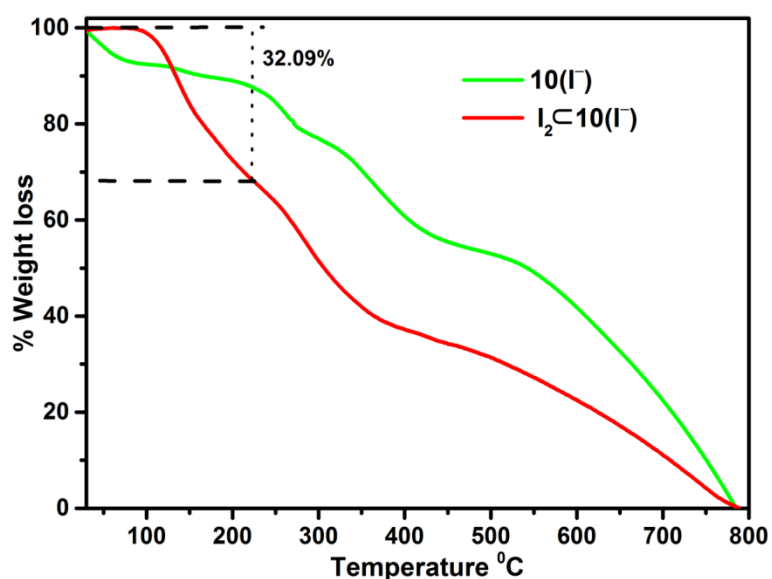


Figure A4A.30: TGA profile of iodide exchanged samples of $10(\text{I}^-)$ and $\text{I}_2\text{C}10(\text{I}^-)$

Table A4A.2: shown the catalytic reaction of indole with various aldehydes.

Entry	Aldehyde	% Yields of the product	
		1''	2
1	R = H	92	85
2	R = Br	83	62
3	R = NO ₂	65	50
4	R = CH ₃	75	55

Characterization of Substituted Bis(indolyl)methanes:

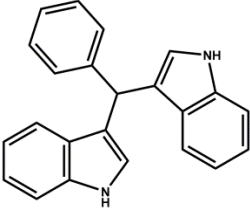
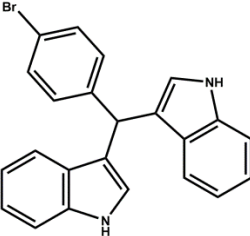
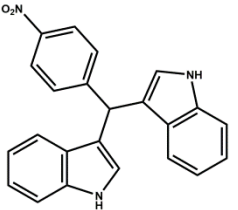
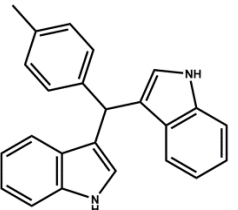
Compound	Characterization data
	$^1\text{H NMR}$ (400 MHz, CDCl_3): $\delta = 7.91(\text{s}, 2\text{H}), 7.33(\text{m}, 6\text{H}), 7.20(\text{t}, 2\text{H}), 7.17(\text{dd}, 1\text{H}), 7.14(\text{t}, 2\text{H}), 6.99(\text{t}, 2\text{H}), 6.63(\text{dd}, 2\text{H}), 5.88(\text{s}, 1\text{H})$. $^{13}\text{C NMR}$ (100 MHz, CDCl_3) $\delta = 144.1, 136.8, 128.8, 128.3, 127.2, 126.2, 123.7, 122.0, 120.0, 119.3, 111.3, 40.3$. MS-EI, m/z, Anal. Calcd: 321.14, Exp: 321.13 (M+H).
	$^1\text{H NMR}$ (400 MHz, CDCl_3): $\delta = 7.96(\text{s}, 2\text{H}), 7.41-7.43(\text{dt}, 2\text{H}), 7.38-7.40(\text{d}, 3\text{H}), 7.19-7.25(\text{m}, 4\text{H}), 7.02-7.06(\text{t}, 2\text{H}), 6.68(\text{d}, 2\text{H}), 5.87(\text{s}, 1\text{H})$. $^{13}\text{C NMR}$ (100 MHz, CDCl_3): $\delta = 145.0, 137.0, 131.3, 131.0, 126.8, 124.0, 121.2, 119.2, 118.7, 117.9, 112.0, 60.1$. MS-EI, m/z, Anal. Calcd: 401.05, Exp: 401.05 (M+H).
	$^1\text{H NMR}$ (400 MHz, CDCl_3) $\delta = 8.15-8.17(\text{d}, 2\text{H}), 8.05(\text{s}, 2\text{H}), 7.52-7.54(\text{d}, 2\text{H}), 7.40-7.42(\text{d}, 2\text{H}), 7.35-7.37(\text{d}, 2\text{H}), 7.21-7.24(\text{t}, 2\text{H}), 7.03-7.07(\text{t}, 2\text{H}), 7.72(\text{d}, 2\text{H}), 6.02(\text{s}, 1\text{H})$. $^{13}\text{C NMR}$ (100 MHz, CDCl_3): $\delta = 153.6, 146.3, 137.1, 129.9, 126.7, 124.4, 123.9, 121.6, 119.4, 118.9, 117.2, 112.1, 40.0$. MS-EI, m/z, Anal. Calcd: 368.14, Exp: 368.15 (M+H).
	$^1\text{H NMR}$ (400 MHz, CDCl_3) $\delta = 7.94(\text{s}, 2\text{H}), 7.41-7.43(\text{d}, 2\text{H}), 7.37-7.38(\text{d}, 2\text{H}), 7.25-7.27(\text{d}, 2\text{H}), 7.16-7.20(\text{td}, 3\text{H}), 7.10-7.12(\text{d}, 1\text{H}), 7.0-7.04(\text{td}, 1\text{H}), 6.70(\text{dd}, 2\text{H}), 5.88(\text{s}, 2\text{H}), 2.34(\text{s}, 3\text{H})$. $^{13}\text{C NMR}$ (100 MHz, CDCl_3) $\delta = 141.2, 136.7, 135.6, 129.1, 128.7, 127.2, 123.7, 122.0, 120.1, 120.0, 119.3, 111.2, 39.9, 21.2$. MS-EI, m/z, Anal. Calcd: 337.17, Exp: 337.13 (M+H).

Table A4A.3: Catalytic reaction of **10** and **11** with benzaldehyde (R = H) reused up to five cycles with % of yields.

cycle	Catalyst 10	Catalyst 11	$\text{CuCl}_2 \cdot 2\text{H}_2\text{O}$
1 st	92 %	85 %	15%
2 nd	90%	80%	
3 rd	90%	80%	
4 th	88%	75%	
5 th	85%	70%	

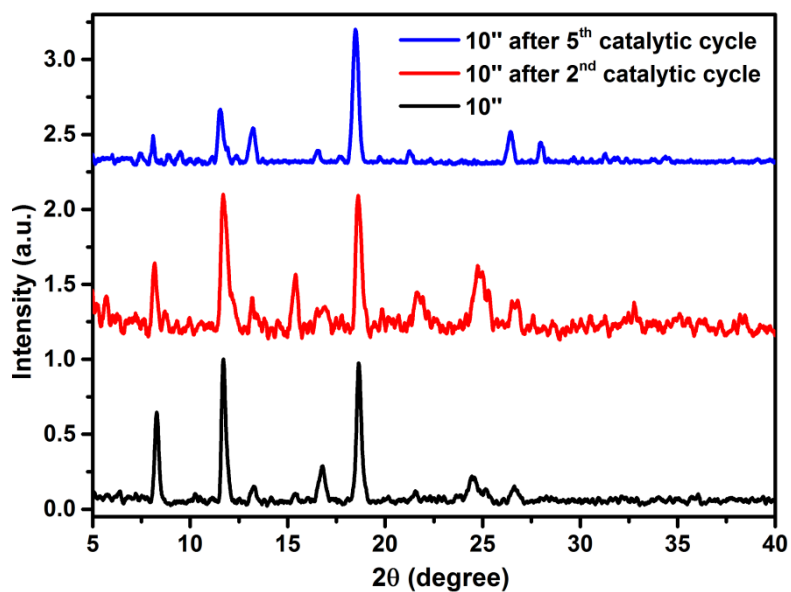


Figure A4A.31: PXRD pattern of 10'' before the catalytic cycle and after the 2nd and 5th catalytic cycle

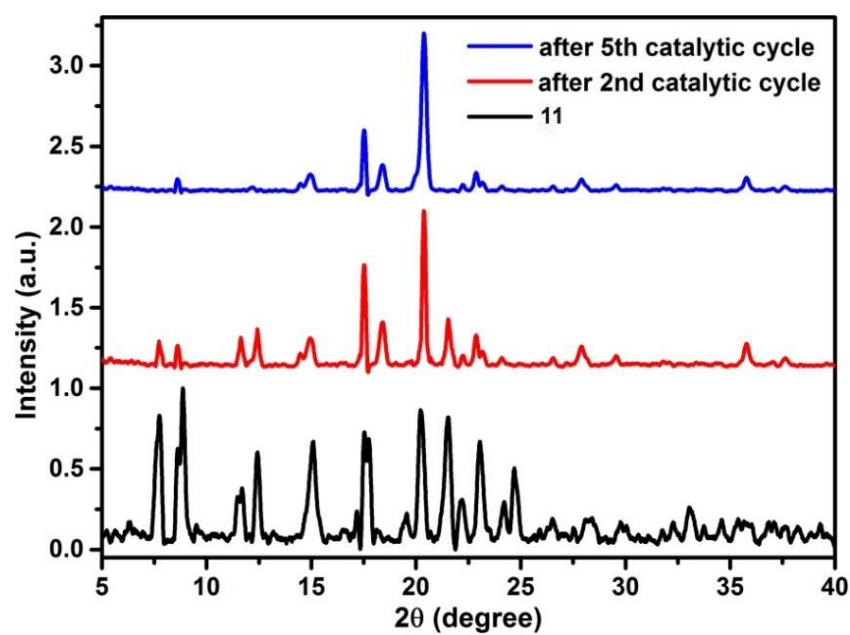


Figure A4A.32: PXRD pattern of 11 before the catalytic cycle and after the 2nd and 5th catalytic cycle

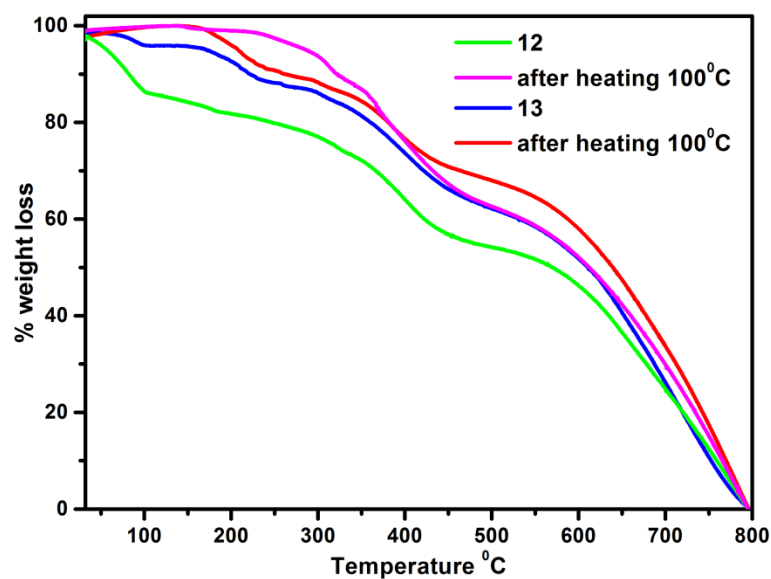


Figure A4B.1: TGA profiles of **12** and **13** in the pristine and in the evacuated forms showing the complete remove of solvent after activation

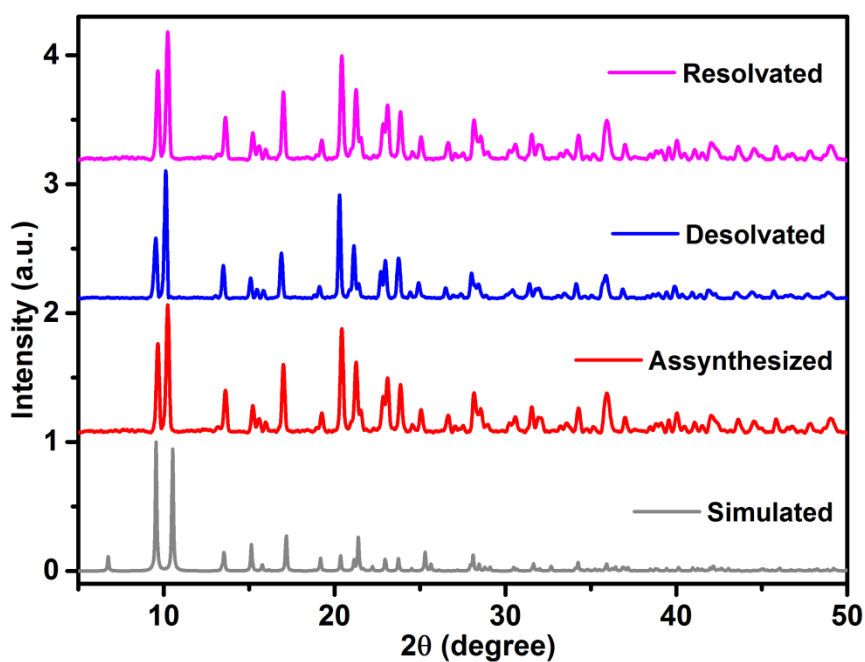


Figure A4B.2: PXRD patterns of **12** at various states: as-synthesised, activated at 80 °C and re-solvated

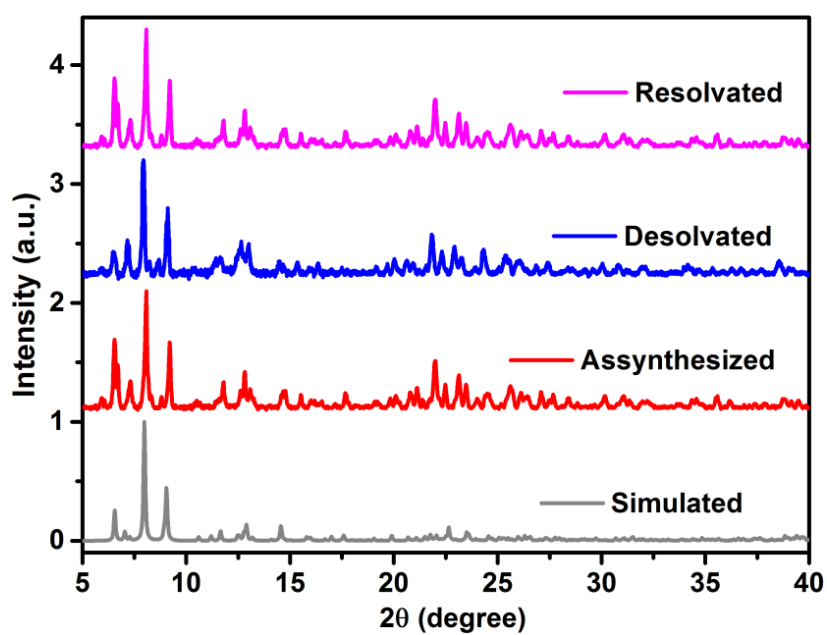


Figure A4B.3: PXRD patterns of **13** at various states: as-synthesised, activated at 80 °C and re-solvated

Table A5.1: Selected bond-lengths (Å) and angles (°) for **14**.

Compound	Bond length		Bond angle	
14	Co(1)-O(1)	2.116(5)	O(1)-Co(1)-N(113)	87.4(2)
	Co(1)-N(113)	2.126(6)	N(113)-Co(1)-N(313)	175.1(2)
	Co(1)-N(313)	2.141(6)	O(1)-Co(1)-N(213)	89.0(2)
	Co(1)-N(213)	2.173(6)	O(1)-Co(1)-N(433)#1	90.0(2)
	Co(1)-N(433)#1	2.177(6)	N(113)-Co(1)-N(433)#1	89.8(2)
	Co(1)-Cl(1)	2.351(3)	N(313)-Co(1)-N(433)#1	91.2(2)
	Co(2)-O(2)	2.143(7)	N(213)-Co(1)-N(433)#1	178.5(2)
	Co(2)-N(123)	2.170(6)	N(113)-Co(1)-Cl(1)	92.59(18)
	Co(2)-N(123)#1	2.170(6)	N(313)-Co(1)-Cl(1)	92.18(17)
	Co(2)-N(223)#1	2.177(6)	N(213)-Co(1)-Cl(1)	90.32(16)
	Co(2)-N(223)	2.178(6)	N(433)#1-Co(1)-Cl(1)	90.69(16)
	Co(2)-Cl(2)	2.340(4)	O(2)-Co(2)-N(123)	87.91(15)
	Co(3)-O(3)	2.128(5)	N(123)-Co(2)-N(123)#1	175.8(3)
	Co(3)-N(233)	2.154(6)	O(2)-Co(2)-N(223)#1	90.71(15)
	Co(3)-N(413)	2.160(6)	N(123)#1-Co(2)-N(223)#1	89.6(2)
	Co(3)-N(333)	2.190(6)	O(2)-Co(2)-N(223)	90.71(15)
	Co(3)-N(133)#1	2.195(6)	N(123)-Co(2)-N(223)	89.6(2)
	Co(3)-Cl(3)	2.345(3)	N(223)#1-Co(2)-N(223)	178.6(3)
	Co(4)-O(4)	2.146(7)	O(2)-Co(2)-Cl(2)	180.0
	Co(4)-N(423)	2.147(5)	N(123)-Co(2)-Cl(2)	92.09(15)
	Co(4)-N(423)#1	2.147(5)	N(223)-Co(2)-Cl(2)	89.29(15)
	Co(4)-N(323)	2.182(6)	O(3)-Co(3)-N(413)	88.4(2)
	Co(4)-N(323)#1	2.182(6)	N(233)-Co(3)-N(413)	175.6(2)
	Co(4)-Cl(4)	2.367(3)	O(3)-Co(3)-N(333)	91.8(2)
			N(233)-Co(3)-N(333)	89.4(2)
			N(413)-Co(3)-N(333)	88.5(2)
			O(3)-Co(3)-N(133)#1	87.2(2)
			N(413)-Co(3)-N(133)#1	91.3(2)
			N(333)-Co(3)-N(133)#1	178.9(2)
			O(3)-Co(3)-Cl(3)	177.38(17)
			N(233)-Co(3)-Cl(3)	91.99(16)
			N(413)-Co(3)-Cl(3)	91.86(16)
			N(333)-Co(3)-Cl(3)	90.83(16)
		N(133)#1-Co(3)-Cl(3)	90.21(16)	
		O(4)-Co(4)-N(423)	88.63(15)	

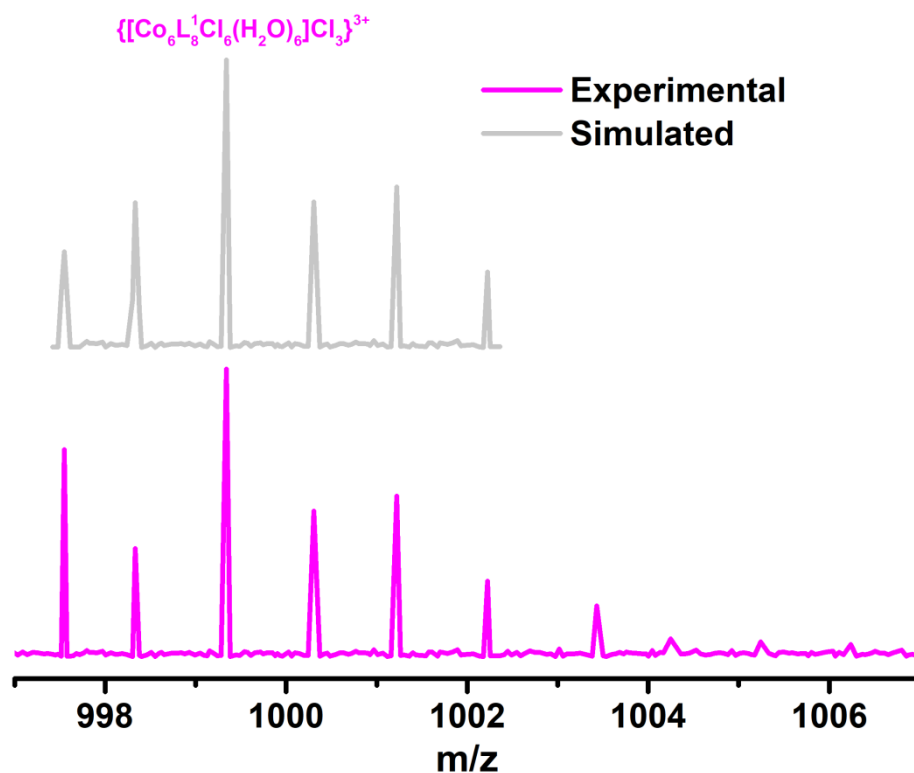


Figure A5.1: The isotope patterns for the cage **14** have been calculated which matches well with the experimental values

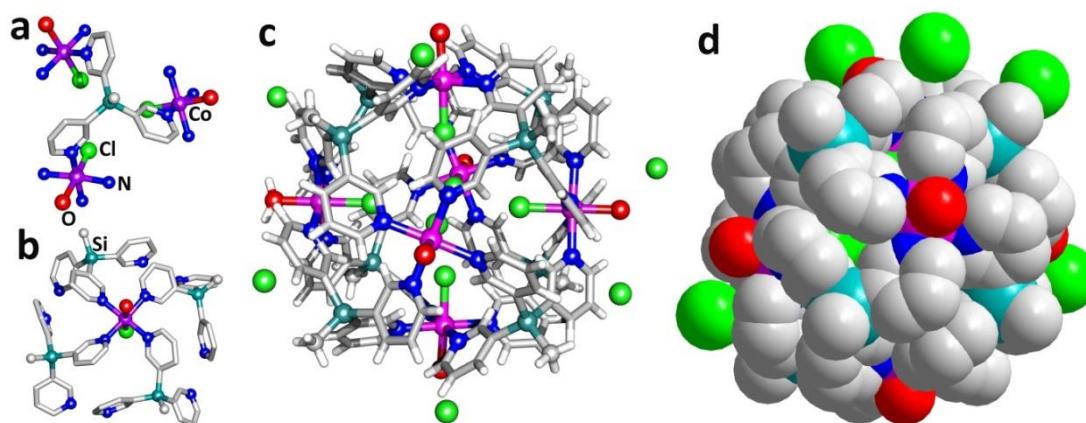


Figure A5.2: Crystal structure of **14** showing (a) the linkage mode of the ligands, (b) the coordination environment around the Co^{II} ions, (c) view of the octahedral cationic cage along with the location of counter chloride ions and (d) space filling model of cage **14** showing the absence of any cage windows and central cavities

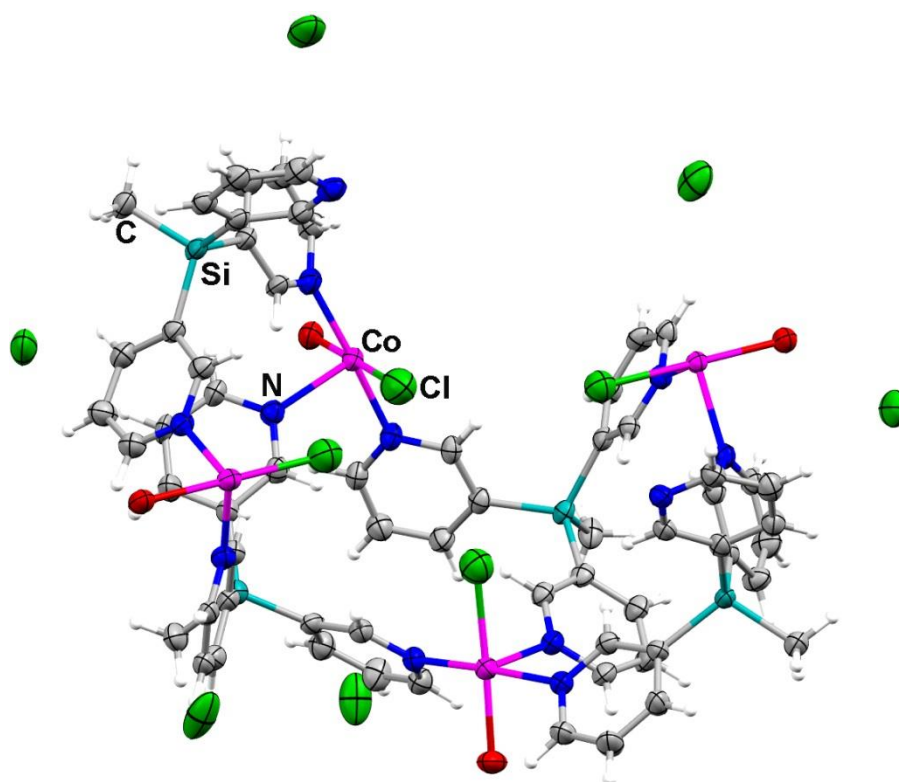


Figure A5.3: Thermal ellipsoid plot at 50% probability for the asymmetric unit of **14**

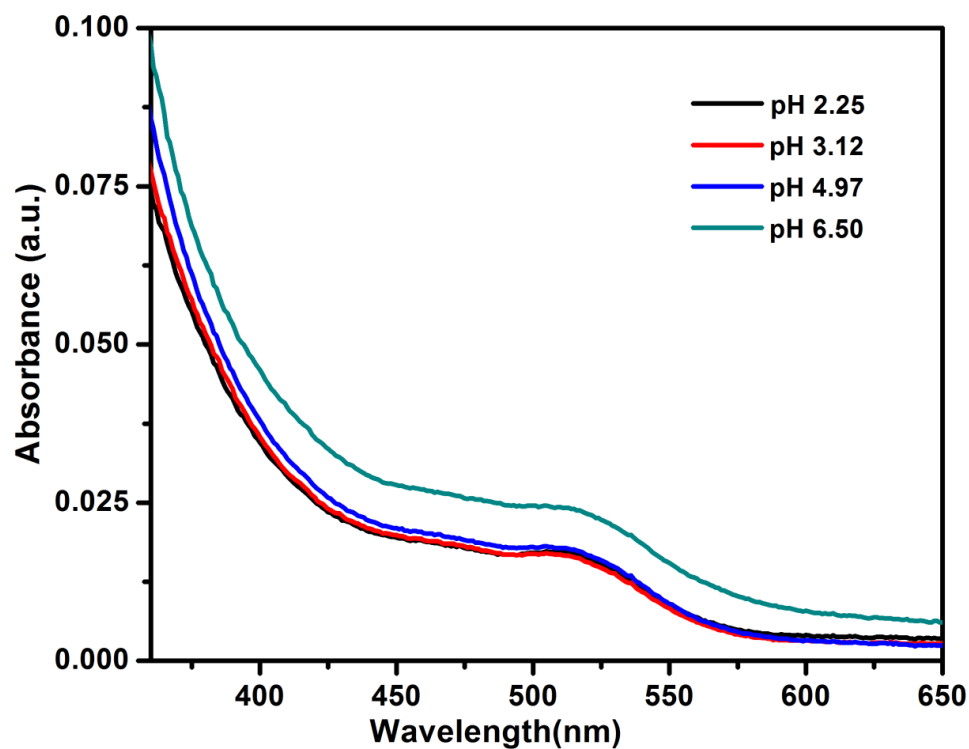


Figure A5.4: UV-Visible spectra of the 0.2 mM solution of cage **14** in B. R. Buffer at various pH at 25 °C

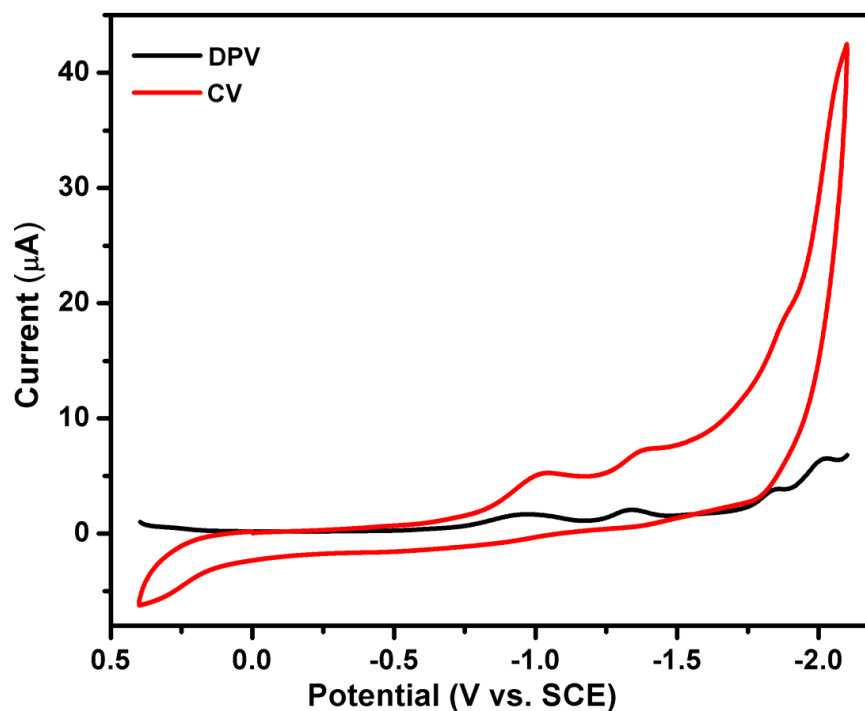


Figure A5.5: CV (red line) and DPV (black line) of 1 mM of ligand L^1 in acetonitrile at a scan rate 100 mV/s, containing 0.1 M ($n\text{-Bu}_4\text{N}$)PF₆) as supporting electrolyte and SCE reference electrode, glassy carbon working electrode and Pt wire auxiliary electrode at 25 °C

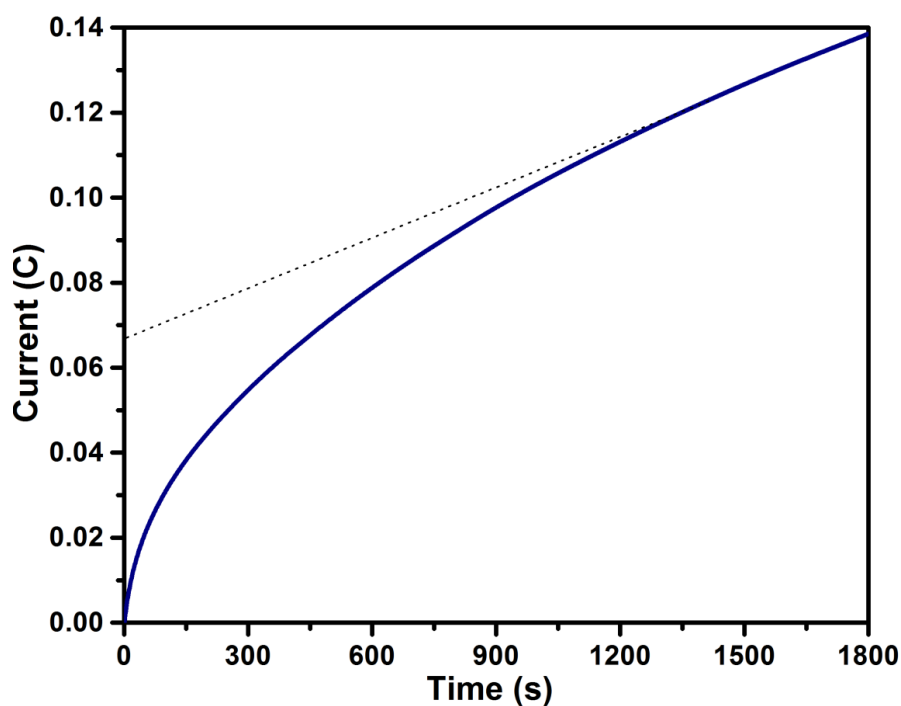


Figure A5.6: Charge vs time curves for bulk electrolysis of a 5 ml sample of 161 μM (cage **14**), at 0.75 V potential in water Supporting electrolyte: KNO₃ (0.1 M); SCE as reference electrode; glassy carbon: working electrode; Pt wire: auxiliary electrode

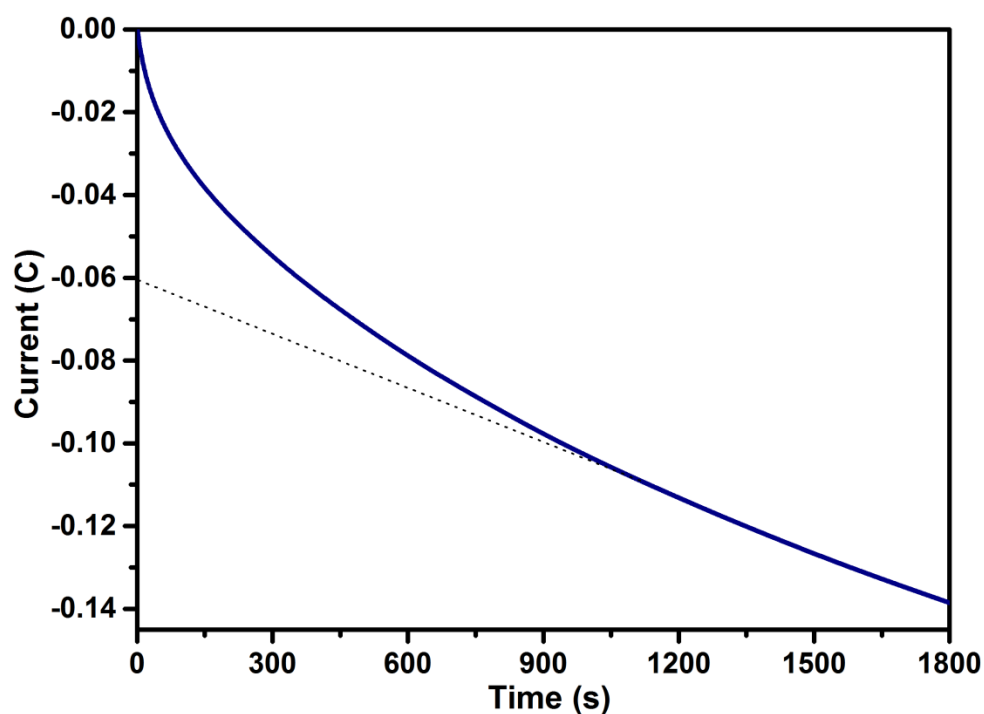


Figure A5.7: Charge-time curves for bulk electrolysis of a 5 ml sample of 161 μM (cage 14), at -0.75 V potential in water Supporting electrolyte: KNO_3 (0.1 M); SCE as reference electrode; glassy carbon: working electrode; Pt wire: auxiliary electrode

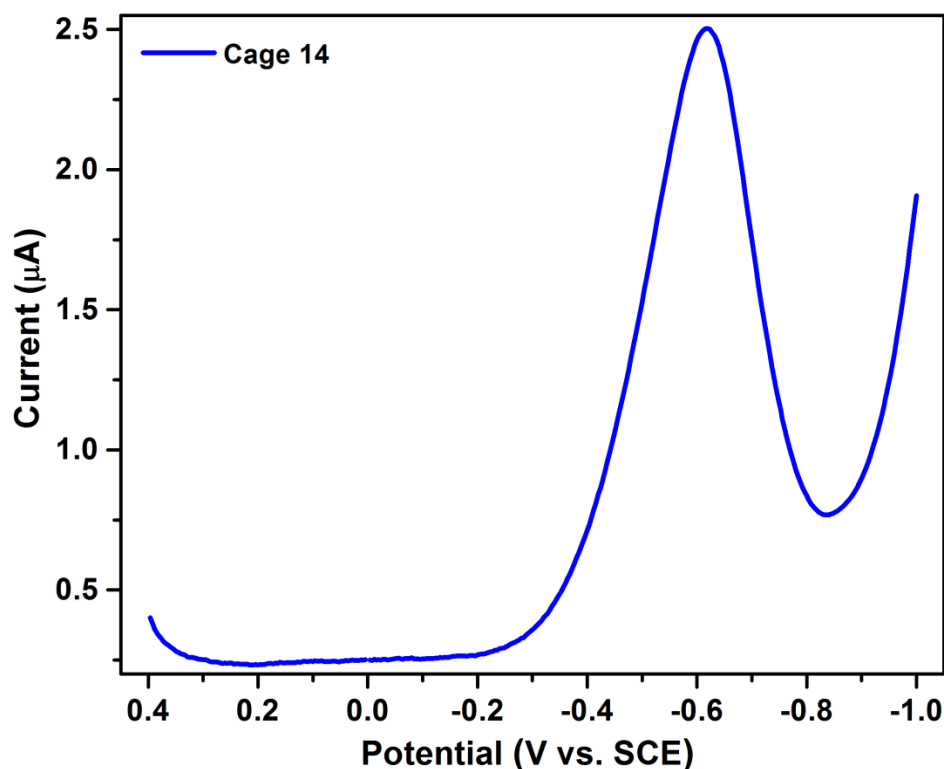


Figure A5.8: DPV of 1 mM 14 in buffer solution (pH 4) at a scan rate of 100 mV/s, containing 0.1 M ($n\text{-Bu}_4\text{N}$) PF_6) as supporting electrolyte and SCE reference electrode, glassy carbon working electrode and Pt wire auxiliary electrode at 25 $^\circ\text{C}$

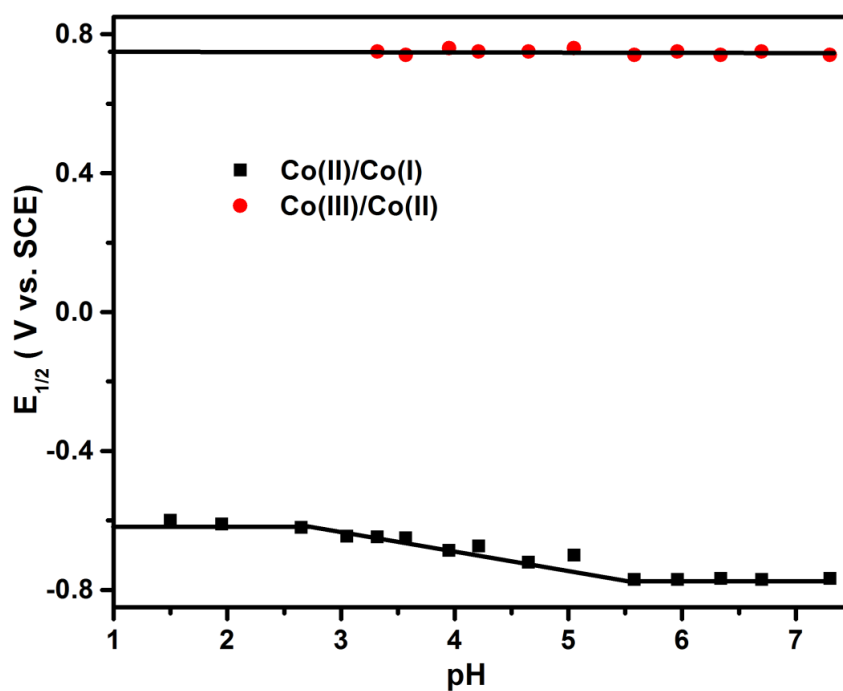


Figure A5.9: The Pourbaix diagram of 1 mM **14** in B.R.buffer by using DPV (Differential Pulse Voltammetry) at 25 °C

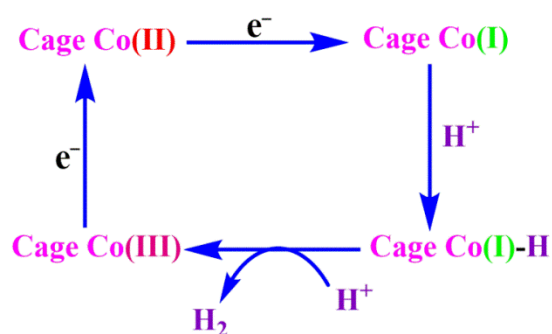


Figure A5.10: Mechanistic representation of hydrogen evolution from water



Figure A5.11: Evolution of hydrogen and oxygen bubbles at glassy carbon disk and Pt wire electrodes, respectively

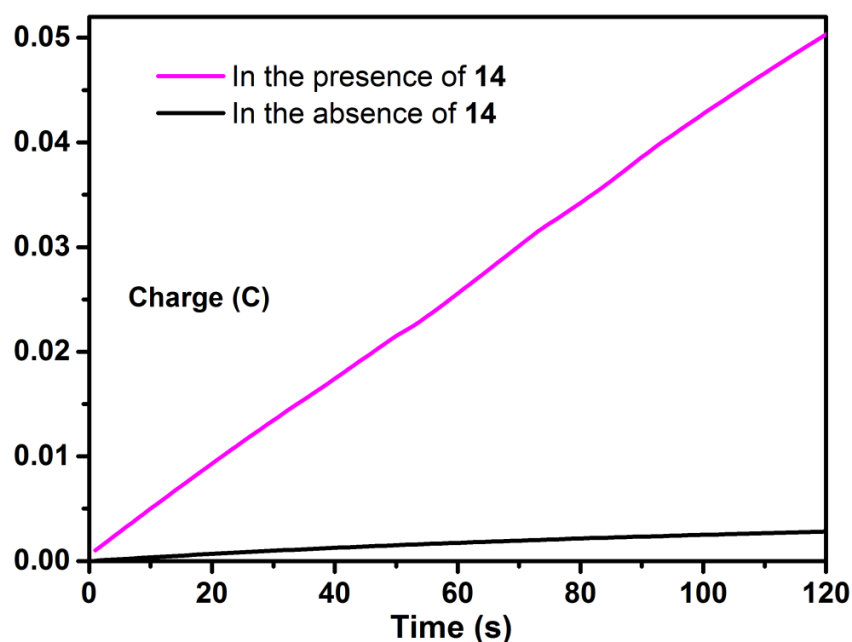


Figure A5.12: Controlled potential electrolysis at -1.4 V (vs SCE); In the presence (pink line) and absence (black line) of 0.5 μM **14** in 1.0 M aqueous phosphate buffer (pH 7.0); Glassy Carbon as working electrode, Pt wire as counter electrode and SCE as the reference electrode.

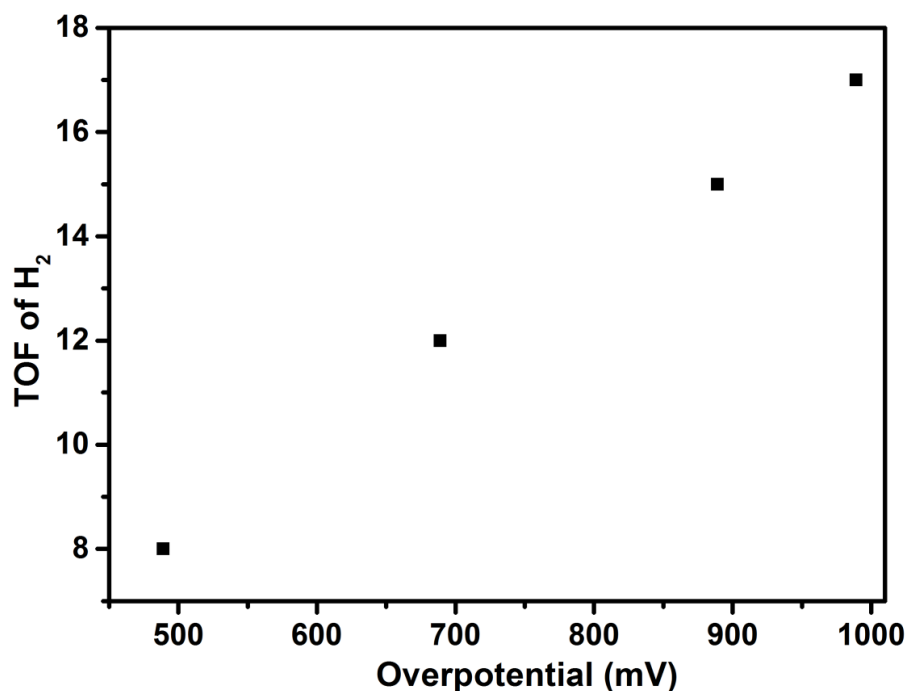


Figure A5.13: Turnover frequency (mol H₂/mol catalysts/h) versus overpotentials (mV) in 1.0 M phosphate buffer (pH 7.0) for the electrocatalytic hydrogen evolution by **14** (0.5 μM). Overpotential = applied potential – E(pH), where E(pH) = 0.059pH

$$\text{TOF} = \Delta C / F n_1 n_2 t \text{ -----} > \text{Eqn. S1}$$

Where,

ΔC = Difference between charge build with and without catalyst

F = Faraday's Constant (96480 mol^{-1})

n_1 = Number electrons involved in the reduction of proton (2)

n_2 = Number of moles of **14**

t = 120 s

Eqn. A5.1: Calculation of Turnover Frequency (TOF)

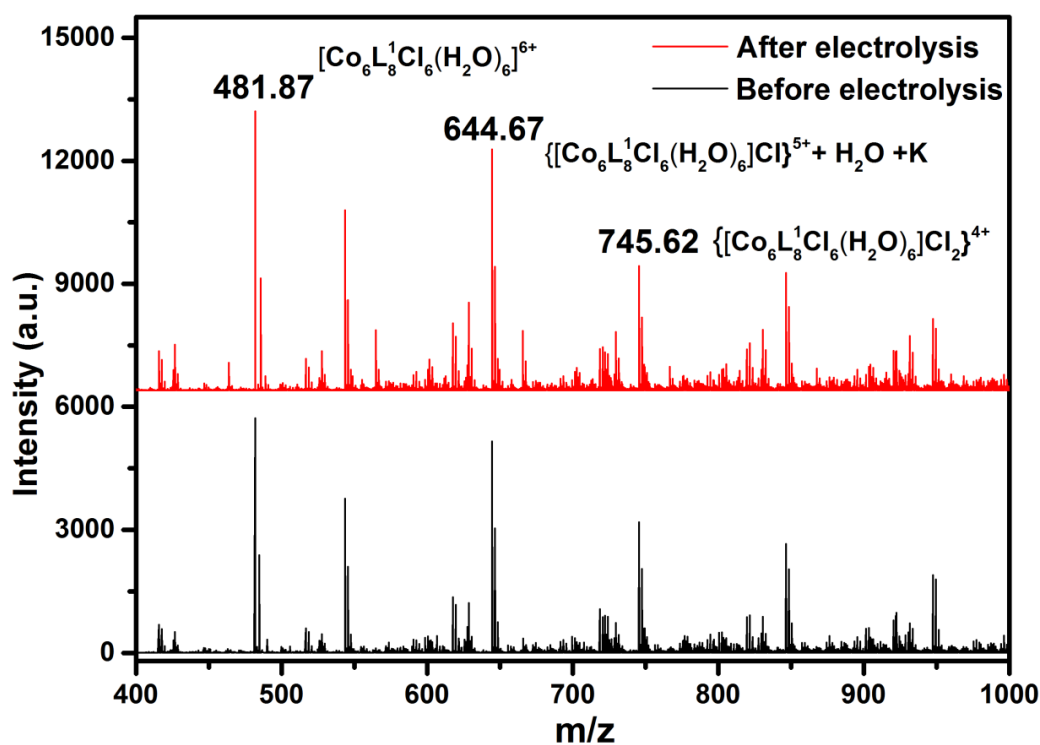


Figure A5.14: ESI mass spectra of **14** before and after the bulk electrolysis

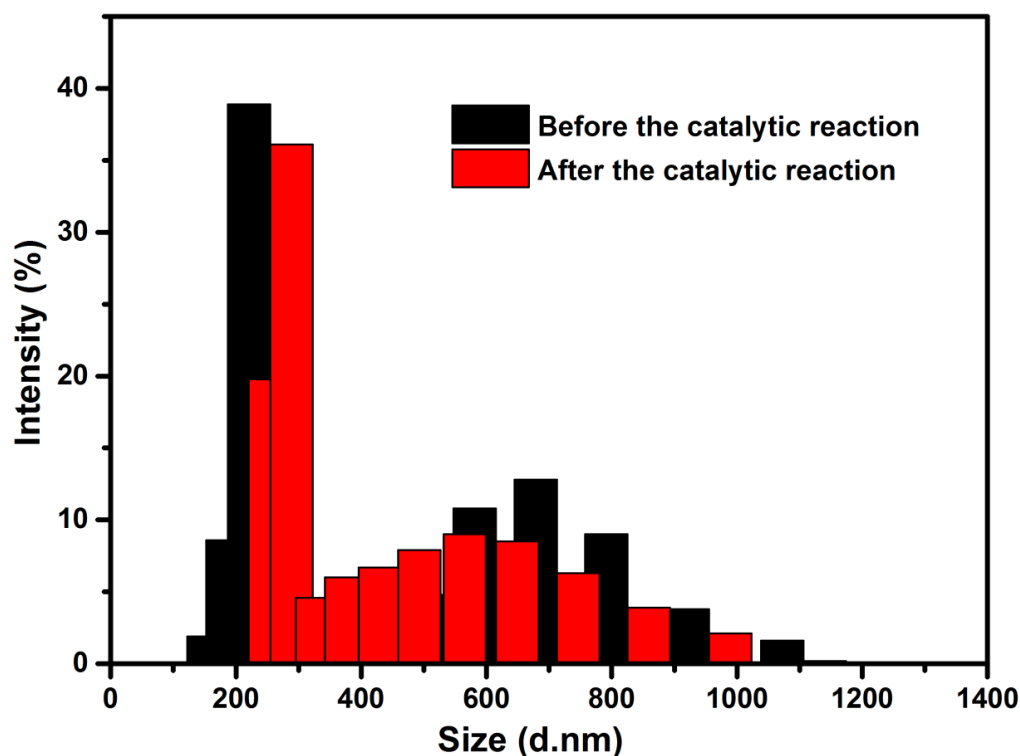


Figure A5.15: DLS analysis of the photocatalytic system; black bar for before and red bar for after the photocatalytic reaction under inert atmosphere

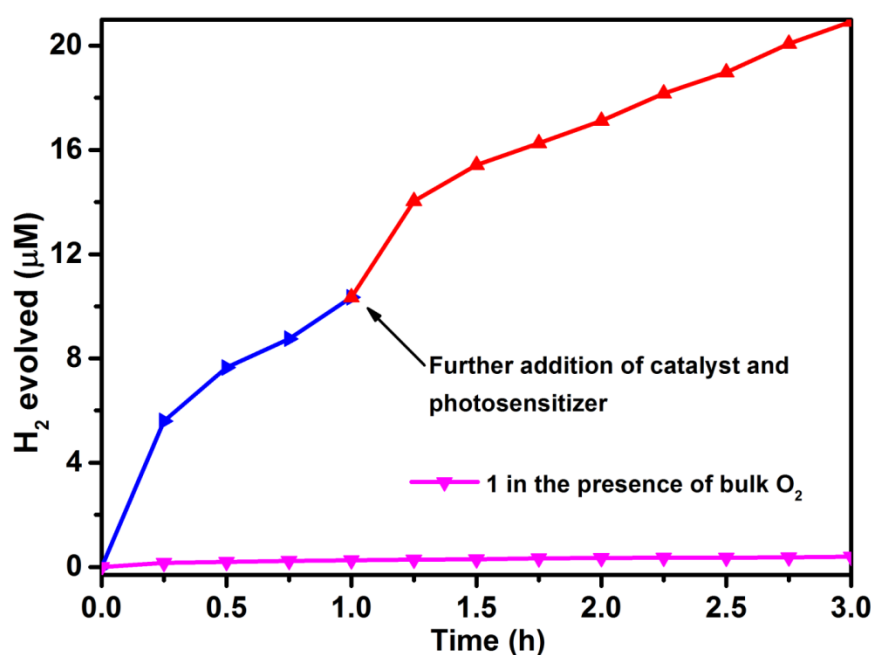


Figure A5.16: Photocatalytic hydrogen evolution over the time. Conditions: 5 mL 1.0 M acetate buffer at pH 4.0, [ascorbic acid] = 0.3 M, [Ru(bpy)₃]²⁺ = 0.5 mM, [**14**] = 200.0 μM, LED light: 469 nm. The arrow indicates addition of **14** (200.0 μM) and [Ru(bpy)₃]²⁺ (0.5 mM) after hydrogen evolution begins to saturate.